Advanced total column ozone retrieval from hyperspectral UV satellite instruments

Dissertation
zur Erlangung des Grades
Dr. rer. nat.
der Universität Bremen

vorgelegt von

Lok Nath Lamsal

Eingereicht am:	09. Mai 2006
Tag des Kolloquiums:	10. Juli 2006
Gutachter der Dissertation:	Prof. Dr. J. P. Burrows Prof. Dr. J. Notholt
Weitere Prüfer:	Prof. Dr. O. Schrems Prof. Dr. S. Bornholdt

Contents

Abstract

This study exploits nadir spectral measurements in 325-335 nm range to infer total column ozone (TCO) from the Global Ozone Monitoring Experiment (GOME) and SCanning Imaging Absorption spectroMeter for Atmospheric CHartographY (SCIAMACHY) instruments. TCO from these two instruments retrieved using the Weighting Function Differential Optical Absorption Spectroscopy (WF-DOAS) are presented. Unlike in standard DOAS where the fitting procedure results in ozone slant column which needs to be converted into vertical column (TCO) by using air mass factor (AMF), in our novel approach direct retrieval of vertical column amounts of ozone is possible by fitting vertically integrated ozone weighting function to the sun-normalized radiances. Other implementations include proper modelling of the Ring effect including Raman correction for ozone absorption, the implicit use of the effective albedo and effective scene height accounting for cloud effects, and an ozone temperature correction. The new algorithm has been extensively validated with ground-based Dobson and Brewer TCO measurements. In general, the agreement between GOME WF-DOAS and ground stations data is very good and the validation shows that the retrieval accuracy of WF-DOAS is within the uncertainty of current ground-based instruments. Better agreements are observed in the comparison with Brewer measurements than with Dobson measurements. This may be explained to a large extent by the neglect of ozone temperature correction in the standard retrieval for Dobson and Brewer. Temperature correction has a larger effect on the Dobson results. The accuracy of WF-DOAS retrievals makes GOME data very attractive for evaluating the ground-based network data. Eight years of GOME data are used to assess the quality of the WOUDC-archived Brewer data. It is shown that monitoring of Brewer data quality and identification of problems in Brewer instruments are possible. This method can also be applied to other ground-based instruments.

Despite improvement with WF-DOAS, somewhat larger differences between satellite TCO and ground based measurements remain at high latitudes under low sun conditions. The persistent TCO differences are due in part to profile shape sensitivity of satellite TCO retrieval algorithms. Improved ozone and temperature profile climatologies, which is prepared and presented in this thesis, will lead to improved satellite ozone measurements. The effect of ozone and temperature profiles on TCO retrievals is explored. The study demonstrates that an improved and updated ozone and temperature climatological profiles can reduce the systematic errors in the retrieved GOME TCO, in particular at high solar zenith angles.

For SCIAMACHY application, the only change of algorithm is for calculating the reference spectra online in each iteration during retrievals rather than using look-up tables. Scaled SCIAMACHY FM ozone cross-section and wavelength pre-shifted by 0.016 nm,

as determined from our comprehensive investigation performed in this thesis, is used for the calculation of reference spectra and the Ring spectra. Improved cloud products and the new ozone and temperature profile climatologies are used. Quality of the retrieved TCO is assessed by correlative measurements from GOME and selected Brewer spectrophotometers. In general a good agreement is achieved apart from a scan angle dependent offset of about -1% to -2%. The reason for the offset is not understood but part of the offset might be related to the calibration errors in the level 1 data. Nevertheless, combined data set from GOME and SCIAMACHY as retrieved from WF-DOAS algorithm presented in this thesis will be valuable for long-term ozone studies.

Publications

The work described in this thesis has been published in various journals as summarised below:

Journal Articles

1. A detailed discussion of the preparation of a new climatology for ozone and temperature profile is done in the following article. This article also provides an evidence of improvement of the GOME ozone profile retrieval by using the climatology. This is the content of Chapter 5.
   Lamsal, L. N., M. Weber, S. Tellmann, and J. P. Burrows (2004), **Ozone column classified climatology of ozone and temperature profiles based on ozonesonde and satellite data**, *J. Geophys. Res.*, 109, D20304, doi:10.1029/2004JD004680.

2. The following paper gives the description of a new total ozone retrieval algorithm. The first half of Chapter 3 is based on this article.
   Coldewey-Egbers, M., M. Weber, L. N. Lamsal, R. de Beek, M. Buchwitz, and J. P. Burrows (2005), **Total ozone retrieval from GOME UV spectral data using the weighting function DOAS approach**, *Atmos. Chem. Phys.*, 5, 1025-1025, SRef-ID: 1680-7324/acp/2005-5-1015.

3. The WF-DOAS algorithm is validated by comparing the retrieved GOME total ozone by using a number of ground based instruments available from WOUDC (World Ozone and Ultraviolet Data Centre). The second half of Chapter 3 is based on this article.
   Weber, M., L. N. Lamsal, M. Coldewey-Egbers, K. Bramsdedt, and J. P. Burrows (2005), **Pole-to-pole validation of GOME WF-DOAS total ozone with ground-based data**, *Atmos. Chem. Phys.*, 5, 1341-1355, SRef-ID: 1680-7324/acp/2005-5-1341.

4. Part of Chapter 7 is based on the following article. A detailed comparison between GOME WF-DOAS and SCIAMACHY operational total ozone product is presented in this article.
   Bracher, A., L. N. Lamsal, M. Weber, K. Bramstedt, M. Coldewey-Egbers, and J. P. Burrows (2005), **Global satellite validation of SCIAMACHY O_3 columns with GOME WF-DOAS**, *Atmos. Chem. Phys.*, 5, 1025-1025, SRef-ID: 1680-7324/acp/2005-5-2357.

5. Stratospheric NO_3 profile retrieval from SCIAMACHY lunar occultation measurements and the comparison of the retrieved profiles with model reults are presented in the following article.
   Amekudzi, L. K., B. -M. Sinnhuber, N. V. Sheode, J. Meyer, A. Rozanov, L. N. Lamsal, H. Bovensmann, and J. P. Burrows (2005), **Retrieval of stratospheric NO_3 vertical profiles from SCIAMACHY lunar occultation measurement over the Antarctic**, *J. Geophys. Res.*, 110, D20304, doi:10.1029/2004JD005748.

6. Impact of choice of ozone and temperature profiles from various climatologies on total ozone retrieval from satellite measurements is investigated in the following article. A practical demonstration of how the climatology from *Lamsal et al.* [2004] could improve the accuracy of the GOME WF-DOAS total ozone especially in polar region is presented in this article. This is the content of Chapter 6.
   Lamsal, L. N., M. Weber, G. Labow, and J. P. Burrows (2006), **Influence of ozone and temperature climatology on the accuracy of satellite total ozone retrieval**, *J. Geophys. Res.*, in press

7. In the following paper, the role of cloud information on total column ozone retrieval has been studied. Part of Chapter 7 is based on this paper.
   Kokhanovsky, A. A., B. Mayer, V. V. Rozanov, K. Wapler, L. N. Lamsal, M. Weber, J. P. Burrows, and U. Shumann (sumbitted 2006), **Satellite ozone retrieval under broken cloud conditions: An error analysis based on Monte-Carlo simulations**, *IEEE Trans. Geosci. Rem. Sens.*

Technical Report

8. M. Weber, K. Bramstedt, L.N. Lamsal, S. Dhomse, A. Darmawan, K. Eichmann, A. Bracher, S. Tellmann, V.V Rozanov and J.P. Burrows (2003), **Ozone profile retrieval from broadband nadir UV/visible satellite spectra: How accurate is the tropospheric profile?**, *in Sounding the troposphere from space: A new era for atmospheric chemistry*, edited by P. Borrell, Springer Verlag.

9. M. Coldewey-Egbers, M. Weber, L.N. Lamsal, R. de Beek, M. Buchwitz, and J.P. Burrows (2003), **GOTOCORD: GOME total ozone column retrieval development**, Algorithm Technical Basis Document, ESRIN *Contract No. 16402/02/l-LG*.

10. M. Weber, L.N. Lamsal, M. Coldewey-Egbers, K. Bramstedt, and K. Vanicek (2003), **GOTOCORD: GOME total ozone column retrieval development**, WF-DOAS V1.0 Validation Report, ESRIN *Contract No. 16402/02/l-LG*.

11. M. Weber, L.N. Lamsal, and M. Coldewey-Egbers (2004), **GOTOCORD: GOME total ozone column retrieval development**, WF-DOAS V1.0 Delta-Validation Report, ESRIN *Contract No. 16402/02/l-LG*.

12. The following report discusses various issues on the selection of various ozone cross-section on total ozone retrieval from SCIAMACHY. This is a content of a section of Chapter 7.
M. Weber and L.N. Lamsal (2005), **Proper choice of ozone cross-sections in SCIAMACHY ozone retrieval** , University of Bremen.

Articles in Conference Proceedings

13. M. Weber, M. Coldewey-Egbers, L.N. Lamsal, R. de Beek, M. Buchwitz, and J.P. Burrows (2004), **Novel total ozone retrieval algorithm for backscatter UV satellite instruments**, *Quadrennial Ozone Symposium*, Greece.

14. M. Weber, L.N. Lamsal, M. Coldewey-Egbers, K. Bramstedt, and K. Vanicek (2004), **Validation of GOME total ozone retrieved using WF-DOAS**, *Quadrennial Ozone Symposium*, Greece.

1 Introduction and Motivation

1.1 Current understanding of atmospheric ozone

The aeronomy and meteorology of atmospheric ozone have been studied for more than one and half century but coordinated research did not start before the 1950s [e.g. *Dobson*, 1968; *Wayne*, 2000]. Substantial progress in the scientific understanding of ozone has been a result from intense research mainly over the last thirty years.

G.M.B. Dobson established the main features of atmospheric total column ozone (TCO) distribution in the first few years of regular observations that were initiated in the 1920s [*Dobson*, 1968]. Global information on the distribution of TCO has been provided by space-based instruments since 1970s. Information on the vertical profile of ozone concentration were derived by Umkehr observations using the ultraviolet spectrophotometer since 1920s, measured in situ by ozonesondes since 1960s, and retrieved from space-based spectrometers since 1970s. Based on the accumulated data sets and their analysis, we now have a reasonable understanding of the global distribution of atmospheric ozone and its long-term behavior. The most important feature of the TCO distribution is a strong latitudinal gradient of total ozone with lower values over the tropics and higher values at mid and high latitudes. The latitudinal gradient of TCO has a pronounced annual cycle, with maximum in spring and minimum in fall. The amplitude of the annual cycle is a function of latitude with a maximum at about 60° north and south and minimum over the tropics. Obvious explanation for this feature is that ozone gets transported from the tropical source region to extra-tropics. Such transport is possible due to a rather long life time of ozone in the lower stratosphere and secondly to the Brewer-Dobson circulation that transports ozone from the photochemical production region in the tropics into higher latitudes [*Randel et al.*, 2002; *Weber et al.*, 2003]. The origin of this circulation and its seasonal cycle are well understood [*Holton et al.*, 1995], however the exact ascent mechanism in the tropics [e.g. *Plumb*, 1996] and dilution of tropical air mass from mid latitudes [*Avallone and Prather*, 1996] are still difficult to quantify.

In addition to the annual cycle, TCO variation occurs on shorter timescales. For example, the TCO variations are highly correlated with synoptic scale meteorological disturbances [*Dobson*, 1968; *Wirth*, 1993]. Ozone at a location is observed to decrease with the passage of cold fronts and increase with the passage of warm fronts. Persistent TCO variability have been related to the quasi-biennial oscillation (QBO) [e.g. *Baldwin et al.*, 2001; *Steinbrecht et al.*, 2003], solar variability [e.g. *Jackman et al.*, 2000; *Zerefos et al.*, 1997], El Niño Southern Oscillation (ENSO) [e.g. *Shiotani*, 1992; *Zerefos et al.*, 1997], and volcanic eruption [e.g. *Chandra*, 1993].

The distribution of ozone is governed by a complex interaction of dynamical, chem-

ical, and radiative processes. Dynamical processes affect ozone abundance firstly, through temperature and secondly, through transport and mixing. These two aspects are however related. Ozone changes are found to be correlated with lower stratospheric temperatures [*Miller et al.*, 1992; *Wirth*, 1993; *Petzoldt et al.*, 1994], with tropopause height [*Hoinka et al.*, 1996; *Steinbrecht et al.*, 1998; *Birner et al.*, 2002], and with isentropic potential vorticity near the tropopause [*Allaart et al.*, 1993]. In the extra-tropical lower stratosphere where the transport timescales is shorter than the chemical lifetime of odd oxygen, the ozone distribution is largely influenced by the residual circulation (Brewer-Dobson circulation) on the one hand and isentropic transport and mixing on the other. Both of these processes are driven by wave activity that is generated in the troposphere [*Fusco and Salby*, 1999; *Randel et al.*, 2002; *Weber et al.*, 2003]. The tropical branch of the residual circulation plays a very important role in determining the global structure of stratospheric transport and mixing. However, it is one of the most poorly understood region of the atmosphere. We have gained sound understanding on latitudinal temperature structure, mean meridional mass circulation, and the hemispheric asymmetry in the strength and variability of the mass circulation. This understanding, however, is more qualitative and the prediction ability of the phenomena still remains poor [*Garcia and Boville*, 1994; *Shepherd et al.*, 1996].

The basic outline of the chemistry controlling atmospheric ozone is known. Oxygen only Chapmann mechanism, ozone loss processes resulting from catalytic O_3 cycles, heterogeneous chemical processes, other various reaction mechanisms relevant to a particular altitude, e.g. the tropospheric ozone formation and loss processes, are well established. Improved laboratory measurements of rate coefficients for various reactions are now available [*DeMore et al.*, 1997]. There are various types of atmospheric chemistry models ranging from box to three-dimensional (3D) [e.g. *Chipperfield*, 1999] that link measurements and theory. Many advanced models do quite well in reproducing the general behavior of ozone in the atmosphere. Nevertheless, there appears to be some discrepancies between model results and measurements, for example, in the stratopause region and in the amount of ozone loss. Models will benefit from more laboratory works and improved representation of transport. The latter can be achieved by incorporating high quality TCO data from ground-based and satellite measurements into the model as feed back.

Besides the natural factors described above, there are also anthropogenic factors that are responsible for global ozone changes. The enhanced levels of anthropogenic chlorine and bromine in the stratosphere perturb the ozone layer. After the discovery of the ozone hole in Antarctica [*Farman et al.*, 1985], many studies have been done on trend analyses and the ozone decline over Antarctica, Arctic, and mid latitudes regions have been observed. No significant trend is evident in the tropics [*WMO*, 2003]. However, in recent years an increase in high latitude ozone has been observed. There is still some debate on if this may be a sign of recovery as a consequence of the reduction in Chlorofluorocarbons (CFCs) or if this is due to circulation changes [*Newchurch et al.*, 2003; *Dhomse et al.*, 2006].

A TCO decline is accompanied by increases in the solar UV irradiance at the earth's surface [*Kerr and McElroy*, 1993, see for example]. The link between ozone decline

and irradiance were studied by various authors [*Stamnes et al.*, 1991; *Eck et al.*, 1995; *Bojkov et al.*, 1995a]. Researches have also intensified on the effects of increased levels of UV radiation on human health and terrestrial and aquatic ecosystems. The importance of exposure to solar UV radiation as a risk factor for melanoma has been confirmed [e.g. *Beitner et al.*, 1990; *White et al.*, 1994]. Besides skin cancer, other UV effects include eye damage, immune suppression, and infectious diseases [e.g. *van der Leun and de Gruijl*, 1993]. Some research have been reported on the impact of increased surface solar UV radiation on terrestrial, freshwater, and marine ecosystems as a result of thinning ozone layer [e.g. *Runeckles and Krupa*, 1994; *Williamson et al.*, 1994]. Forming a serious threat to the global environment lead to a successful collaboration between scientists and policymakers introduced the Montreal protocol with the aim of halting further increases in ambient levels of UV. As a result of the Montreal Protocol and its amendments, atmospheric concentrations of CFCs started to decline. The question remains if a corresponding slow down in the ozone decline has been observed. This requires continued monitoring of the ozone layer in the next decade.

1.2 Total column ozone monitoring instruments

Ozone measuring instruments have played an important role in our current level of understanding of atmospheric ozone. Two principal methods exist that are either based on the chemical method or the spectroscopic method. The chemical method is applicable for in-situ measurements. For example, the vertical distribution of ozone is measured by using the Electrochemical Concentration Cell (ECC) ozonesonde [*Komhyr*, 1969]. In this thesis, the focus will be on UV spectroscopic methods of measuring TCO amount in the atmosphere.

1.2.1 Ground-based measurements

Several ground-based instruments have been devoted to measure TCO. The Dobson spectrophotometer developed by G.M.B Dobson [*Dobson*, 1968] in the 1920s forms the primary standard instruments for ground-based measurements [*Bernhard et al.*, 2005]. About 100 Dobson instruments are in operation worldwide. TCO can be calculated from the direct sun, zenith sky, or focused moon observations. Direct sun measurements are more accurate (accuracy of 1% for well-maintained Dobson instrument). Automated Brewer spectrophotometers [*Kerr et al.*, 1981] are commercially available since 1982. There are about 130 instruments operating worldwide at present. The retrieval accuracy of a properly calibrated Brewer is approximately $\pm$ 1%, and the precision is better than $\pm$ 1%. Brewer spectrophotometers perform simultaneous measurement of SO_2 column amount, which is an important interfering absorber for TCO measurement. The Filter ozonometers [see *Bojkov et al.*, 1994] M-83 and M-124 are another important ozone observing system with about 47 instruments mostly in the Russian Federation. Although less accurate, these filter instruments provide valuable data from a region which occupies almost one third of the landmass in the northern hemisphere. Differential Optical Absorption Spectroscopy (DOAS) [*Noxon*, 1975; *Platt et al.*, 1979] applied

to UV-visible zenith-sky observations performed at twilight allows the measurement of column amounts of ozone and other trace constituents like NO_2, H_2O, OClO, etc. The DOAS retrieval technique consists in studying narrow absorption features after removal of the broad band signal arising for example from scattering processes. Employing these technique, long-term routine measurements are made by Systéme d'Analyse par Observation Zénithale (SAOZ) [*Pommereau and Goutail*, 1988] and other UV-visible DOAS spectrometers since 1980's. These spectrometers have an accuracy of about 3-5% for TCO measurements [*Lambert et al.*, 1999]. The Fourier transform infrared spectrometers, lidars and millimeter-wave radiometers have also been used.

Station TCO data have been used to assess ozone changes at a specific site [e.g. *Staehelin et al.*, 1998]. For example, TCO measurements at Arosa, Switzerland by Dobson spectrophotometer represents the longest record of TCO from ground-based instruments. Time series of TCO smoothed over a month and that smoothed over a year are shown in Figure 1.1. In addition to a strong seasonal cycle, a decreasing trend in TCO is perceptible from the figure. Ground-based TCO data are also used to validate satellite retrievals [e.g. *Weber et al.*, 2005] and to assess long-term calibration stability of satellite measurements. These data, particularly from Dobson and Brewer instruments, are more reliable and stable. These instruments are unevenly distributed with a majority of them being in the northern mid latitude region. Because of uneven distribution with latitude of the ground-based instruments and longitudinal inhomogeneity in the ozone field, long-term global ozone variations and trends estimated exclusively from ground-based data are not sufficient [*Bojkov and Fioletov*, 1995b]. Combining both ground-based and satellite data are therefore required to assess global trends in ozone [*Bojkov and Fioletov*, 1995b; *Fioletov et al.*, 2002]. Since satellite and ground-based measurements have complementary strengths, operation of existing ground-based TCO stations needs to be continued and additional stations should be established. Moreover, a well-established and well-maintained data quality program, as presently carried out by the World Meteorological Organization (WMO) for Dobson instruments [*Staehelin et al.*, 2003], is also required for all kind of instruments.

1.2.2 Satellite measurements

First determinations of ozone from back scattered ultraviolet radiation in 1966 were carried out from the USSR COSMOS satellite [*Rawcliffe and Elliot*, 1966]. Routine and long-term mapping of the global distribution of atmospheric ozone from space began in 1978 with the Total Ozone Mapping Spectrometer (TOMS) and the Solar Backscattered Ultraviolet (SBUV) radiometer [*Heath et al.*, 1975] aboard Nimbus 7. TOMS instruments aboard Nimbus 7 (1979-92), Meteor (1992-94), ADEOS (1996-97), and Earth Probe (1996-present) from the TOMS series, SBUV instruments aboard Nimbus 7 (1979-90), NOAA-9 (1985-97), NOAA-11 (1989-95), NOAA-14 (1995-98), and NOAA-16 (2000-present) from the SBUV series. The intent of the SBUV series is to create a continuous satellite-measured record of both total column and vertical profiles of ozone. The TOMS instruments are dedicated to total column measurement. Launched in April 1995 on board ERS-2 environmental satellite, the hyperspectral Global Ozone Monitoring Exper-

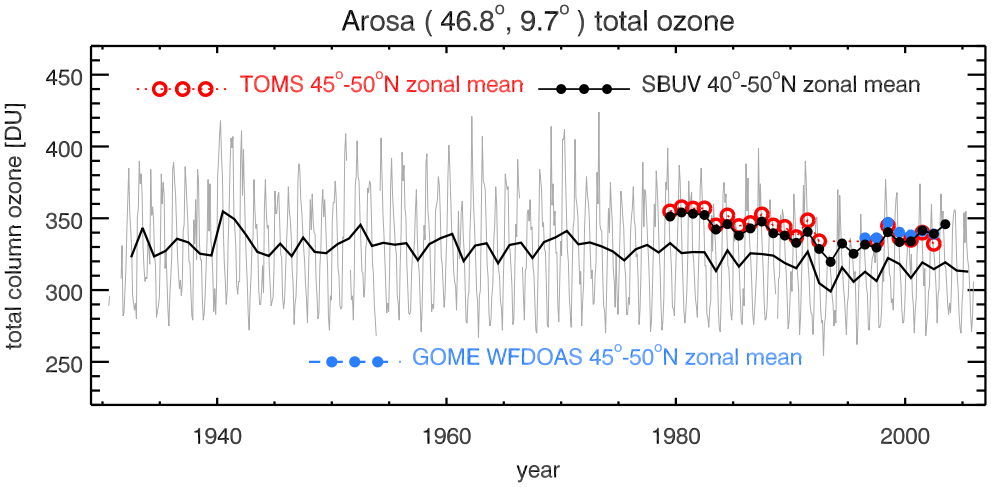

Figure 1.1: Time series of TCO measured by the Dobson instrument at Arosa, Switzerland from 1931 to 2005. Data are given as monthly averaged (gray) and year averaged (black) values. Yearly area weighted zonal mean TCO data from TOMS-series, SBUV-series, and GOME instruments are also shown.

iment (GOME) [*Burrows et al.*, 1999a] provides a global picture of atmospheric ozone and other relevant trace species like NO_2, BrO, OClO, SO_2, and HCHO. The higher spectral resolution (0.2–0.4 nm for wavelengths between 240 nm and 790 nm) and better signal-to-noise ratio of GOME compared to other instruments mentioned above enables ozone profile retrieval down to the upper troposphere [*Munro et al.*, 1998; *Hoogen et al.*, 1999a, b; *Lamsal et al.*, 2004]. It has been followed up by the SCanning Imaging Absorption spectroMeter for Atmospheric CHartographY (SCIAMACHY) [*Burrows et al.*, 1995; *Bovensmann et al.*, 1999; *Kamp and Dobber*, 2000] launched in 2002. It is a unique satellite instrument capable of measuring transmitted, reflected, and scattered sunlight in nadir, limb, and occultation mode. SCIAMACHY observations yield, in addition to TCO information of various tropospheric and stratospheric constituents. The Ozone Monitoring Instrument (OMI) launched in 2004 and other instruments in preparation like GOME-2 (launch in 2006) will be valuable components of the global observing system for atmospheric ozone.

Satellite instruments have a limited lifetime, typically five years. Changes in operational satellites, interruption in the observation record, and data inhomogeneity put major difficulties in assessing long-term global TCO variations. These problems of satellite measurements of TCO is illustrated in Figure 1.1, which shows TCO time series from TOMS-series, SBUV-series, and GOME instruments for a latitude band from mid latitude. It should be noted that part of the discrepancy in satellite TCO is related to the difference in latitude bands considered for zonal averaging. As expected, area weighted zonal mean TCO from satellite instruments do not agree with TCO value from Arosa alone. In order to develop a continuous data record, ozone data from various sensors need to be integrated. A consistent merging of data from different instruments often becomes a

key problem mainly due to uncertainty in instrument calibration and errors in the data reduction algorithm. The data quality is examined through correlative surface, airborne, and satellite measurements on global scale as validation activities, which is the basis of integrating data from various instruments. For instruments having overlap in their observation period, e.g. SBUV instruments, the relative biases during overlap between the instrument records are used to adjust all the data sets and to create a cohesive data set [*Planet et al.*, 2001; *Miller et al.*, 2002]. In another case, the difference between satellite- and ground-based measurements is used to adjust the data from different satellite instruments [*Bodeker et al.*, 2001]. This kind of adjustment may introduce error in the derived data due to possible biases in the ground-based measurements.

Quality of ozone data obtained from multiple satellites will benefit from proper calibration and improved retrieval algorithms for various satellite instruments. An accurate data record results in a reliable ozone trend analysis and improves climate change studies.

1.3 Ground-based total ozone retrieval

In this section only a brief summary of the TCO retrieval from Dobson and Brewer instruments is given. This will be important for characterization of the quality of ground-based and satellite TCO data.

Measurement of both Dobson and Brewer instruments are based on sun photometry. The TCO is derived employing the ozone absorption features of solar light in the Huggins band, in particular in the wavelength region of 305 to 340 nm. For the Dobson instrument the TCO is determined by measurement of the relative intensities, not the absolute ones, at two pairs of wavelengths [*Komhyr*, 1980; *Staehelin et al.*, 2003]. The following wavelength pairs are presently used: A-305.5/325.4 nm, C-311.5/332.4 nm, and D-317.6/339.8 nm. The wavelength pairs are chosen from one wavelength that is relatively unaffected by ozone absorption and another that is strongly absorbed. Standard measurements use AD-pairs. When the sun is lower in the sky the C-pair can be combined with the D-pair.

The basic formula to calculate the TCO using AD-pairs is given by:

$$\mathrm{TCO} = \left(\frac{\mathrm{N_A}}{\mu_\mathrm{A}} - \frac{\mathrm{N_D}}{\mu_\mathrm{D}}\right)\frac{10}{\tilde{\alpha}_\mathrm{AD}} - \mathrm{A_{COR}}\frac{\mathrm{m}}{\mu_\mathrm{AD}}, \tag{1.1}$$

where

$$\mathrm{A_{COR}} = \frac{\tilde{\beta}_\mathrm{AD}}{\tilde{\alpha}_\mathrm{AD}} 1000 \frac{\mathrm{P}}{\mathrm{P_o}}. \tag{1.2}$$

The subscripts in Equations 1.1 and 1.2 indicate the name of wavelength pair. N for example is defined as

$$\log\frac{\mathrm{I_o}}{\mathrm{I'_o}} - \log\frac{\mathrm{I}}{\mathrm{I'}}. \tag{1.3}$$

The ratio (of intensity of shorter and longer wavelengths in a pair) in the first term is determined by the Langley Plot method. Dobson measurement provides the ratio as given by the second term. μ and m represent the optical air mass for ozone layer and the relative optical air mass, respectively. The difference in Rayleigh scattering coefficient for two wavelengths is denoted by $\tilde{\beta}$ and that for ozone absorption coefficient is represented by $\tilde{\alpha}$. P and P_o are the pressures of measuring station and mean sea level, respectively.

The Brewer spectrophotometer determines the TCO by measuring the direct beam, using a prism that points directly to the sun. The spectrophotometer measures routinely at 306.3, 310.1, 313.5, 316.8, and 320.0 nm. The TCO is determined on the basis of relative intensities at these wavelengths.

The TCO can be calculated as follows:

$$\text{TCO} = \frac{\text{MS5} - 0.5\text{MS6} - 1.7\text{MS7} - \text{B1}}{\text{A1} \times \text{M2}}, \tag{1.4}$$

where, MS5 = $\frac{I_{310.1}}{I_{316.8}}$, MS6 = $\frac{I_{313.5}}{I_{316.8}}$, MS7 = $\frac{I_{320.1}}{I_{316.8}}$, A1 = differential ozone absorption coefficient, B1 = extraterrestrial constant, and M2 is the optical air mass. The measurement at 306.3 nm is used for simultaneous determination of SO_2.

$\tilde{\alpha}$ in Equations 1.1 and 1.2 and A1 in Equation 1.4 are assumed to be temperature independent and the absorption cross section at a fixed stratospheric temperature of -46.3° C is employed in the standard algorithm. But, ozone absorption in the Huggins band depends on temperature [*Komhyr et al.*, 1993; *Burrows et al.*, 1999b]. The wavelengths used in the Dobson spectrophotometry, in particular the D-pair, are more temperature sensitive than those used in Brewer. Omission of temperature correction in the operational retrieval algorithm may lead to systematic error of up to 4% in the Dobson data [*Bernhard et al.*, 2005] and to smaller errors in the Brewer data [*Kerr*, 2002].

Filter-based ozonometer is based on the same principle as the Dobson spectrophotometer and the differential absorption of ultraviolet radiation in the 300-350 nm is used. However, the M-83 and M-124 instruments use two broadband filters of 22 nm (291-312 nm) and 15 nm (319-334 nm) and measure the relative attenuation of the solar ultraviolet irradiances either in direct sun or zenith geometry [*Chanin et al.*, 1998].

The zenith-sky UV-visible spectrometry uses the Chappius band of ozone in the visible. The spectrometer exploits the DOAS technique [*Noxon*, 1975; *Platt et al.*, 1979]. The reference spectra are taken at low solar zenith angle. Least-squares fitting of the observed spectra to the reference ozone absorption spectra measured in the laboratory allows the slant column S of ozone to be derived. The vertical column V is then obtained by using the following relationship:

$$\text{V} = \frac{\text{S} + \text{R}}{\text{AMF}}, \tag{1.5}$$

where R is the amount of absorber in the reference spectrum and AMF is the air mass factor. The AMF is calculated by the radiative transfer model [e.g. *Solomon et al.*, 1987]

1.4 Standard DOAS satellite total ozone retrieval

GOME represents the first successful application of the DOAS technique to space-borne passive remote sensing instruments [*Burrows et al.*, 1999a]. DOAS derived column amount of various minor trace gases from the GOME spectral measurements have been successful [*Wagner and Platt*, 1998; *Eisinger and Burrows*, 1998; *Chance et al.*, 2000; *Valks et al.*, 2002; *Richter and Burrows*, 2002].

Details of the DOAS method are given in *Platt* [1994] and its treatment in GOME application is found in *Spurr et al.* [2005]. In brief, the standard DOAS algorithm derives a slant column density S_i by least square fitting a linear combination of reference absorption cross-section spectra σ of trace gases i and a Ring reference spectrum to the measured optical density τ_s, which is the ratio of the earthshine radiance $I(\lambda)$ and solar irradiance $F(\lambda)$. Mathematically,

$$-\ln\frac{I(\lambda)}{F(\lambda)} \simeq \sum \sigma_i(\lambda)\cdot S_i + \sigma_{Ring}(\lambda)\cdot S_{Ring} - \sum_{k=0}^{n} a_k \lambda^k \tag{1.6}$$

The term on the left side of Equation 1.6 is the measured slant optical density. The first term on the right side of the equation defines the absorption of ozone and other interfering gases such as NO_2 and BrO in the spectral region 325-335 nm, the fitting window usually considered for the GOME TCO retrieval. The absorption cross-sections are altitude and temperature dependent. The Ring effect [*Grainger and Ring*, 1962; *Vountas et al.*, 1998] is treated as an effective absorber (second term). It arises from Raman scattering and needs to be accounted for. The last term in Equation 1.6 is a low order polynomial, usually of second order, to be subtracted from the measured optical depth in order to remove the broadband spectral structure resulting from Rayleigh and Mie scattering and the slowly varying components of the molecular absorption. The value of S_i is obtained by a linear least square fit of

$$\| \tau_s(\lambda) - \sum \sigma_i(\lambda)\cdot S_i - \sigma_{Ring}(\lambda)\cdot S_{Ring} + \sum_{k=0}^{n} a_k \lambda^k \|^2. \tag{1.7}$$

Relative spectral alignment is often dealt with by applying shift and squeeze parameters to the wavelength grid of reference $F(\lambda)$ and $I(\lambda)$ spectra. This requires the application of a nonlinear least squares method.

Once the S_i have been determined, the conversion to the desired vertical column densities V_i is the next step. This requires a division of S_i by a suitable air mass factor A_i. Based on the information of measurement geometry, albedo, and profile shape of the desired gas, the air mass factor is determined by radiative transfer calculations. For an optically thin atmosphere, the air mass factor is nearly wavelength independent. However, atmospheric ozone absorption in 325-335 nm range shows significant wavelength dependence. Since a single air mass factor cannot account for the large wavelength dependency, a choice of a suitable reference wavelength is often a serious problem.

For clear sky spectral measurements, the vertical column is a simple ratio of slant column to the air mass factor A_{clear}. For cloudy scenarios, air mass factor computation is based on the independent pixel approximation with

$$V_i = \frac{S_i + f \times GVC \times A_{cloud}}{(1-f)A_{clear} + fA_{cloud}}, \tag{1.8}$$

where A_{cloud} is the air mass factor for the atmosphere down to the cloud-top height. Part of the ozone below cloud that is not detected is called the ghost vertical column (GVC) and is estimated by integrating a climatological profile below retrieved cloud-top height. The cloud information can be derived from the spectral analysis of GOME measurements in the O_2 A-band near 760 nm [e.g. *Koelemeijer et al.*, 2001].

1.5 GOME operational total column ozone: GDP versions

The German Processing and Archiving Facility (D-PAF) has been routinely retrieving GOME TCO with the so-called GOME Data Processor (GDP). Since its first release in 1996 as GDP version 2.0, the level 1 to 2 processing of GDP has undergone three major upgrades, all employing the DOAS-type algorithm. Main motivation after each GDP upgrade was to improve the quality of ozone products. Versions 2.7 and 3.0 were released in 2000 and 2002 after validation campaigns held in 1999 and 2002, respectively. Each upgrade was followed by a set of activities consisting of assessment of data quality, identification of errors, correction of algorithm, and verification of the improvement. These studies concluded that the GDP upgrade from version 2.7 to 3.0 lead to a better agreement of GOME with ground-based TCO data. The improvements were mainly driven by the (1) implementation of the GOME-measured flight model cross-sections [*Burrows et al.*, 1999b], (2) use of two O_3 reference cross-sections at different temperature to retrieve slant column [*Richter and Burrows*, 2002], (3) implementation of pre-shifted O_3 cross-section, (4) use of undersampling correction reference spectrum [*Slijkhuis et al.*, 1999], (5) use of theoretical Ring Fraunhofer spectrum derived from a folding of Raman cross-sections with a high-resolution solar spectrum [*Chance and Spurr*, 1997], (6) implementation of the new AMF, which were determined iteratively using a neural network trained on column-classified ozone profiles [*Wellemeyer et al.*, 1997], and (7) use of cloud database derived from GOME spectra [*Koelemeijer et al.*, 2001].

The performance of the GDP V3.0 TCO product has been characterized by comparison with ground-based measurements, TOMS total ozone, and ozone retrievals from independent DOAS algorithms [*Lambert et al.*, 2002b]. From the comparison, it was evident that the average agreement of GDP V3.0 with ground-based correlative measurements was within -3% to +1% in the tropics, $\pm$3% in mid latitudes, and -3% to 10% in high latitudes. At higher latitudes, the average deviation of GOME from ground-based data did not exceed $\pm$2-4% for SZA (solar zenith angle) below 70°. No long-term drift was observed in the data quality, despite instrumental degradation which were observed

in GDP V2.7 and TOMS V7 total ozone. The GDP V3.0 upgrade resulted in the reductions of 30-50% in amplitude of the GOME TCO dependence on the SZA as compared to its predecessor version. The dependence on TCO amount had almost disappeared.

1.6 Algorithmic problems identified in GDP V3.0

Improvements in GOME total ozone products following the upgrade of GDP from version 2.7 to 3.0 are reported in *Lambert et al.* [2002b]. Validation results also revealed some biases and regional discrepancies, in particular at high latitudes and high SZA, and for high and low ozone amounts. The main conclusions from *Lambert et al.* [1999], *Lambert et al.* [2002b], *Bramstedt et al.* [2003], and *Lambert et al.* [2004] are as following:

1. TCO from GDP V3.0 showed a systematic offsets of about -2% with respect to Brewer and Dobson measurements. The relative difference between GDP V3.0 and ground-based TCO showed meridional dependence. Large differences of up to -6% were observed in the southern polar region.

2. While GDP V3.0 data showed long-term stability, seasonal variation of bias of up to 2% is evident with respect to the ground-based data. Comparison of GDP V3.0 TCO with three Alpine Dobson instruments revealed negligible offset in summertime and an offset of about 3% in late fall and early winter.

3. Although the GDP upgrade from version 2.7 to 3.0 could reduce the amplitude of SZA dependence almost by 50% on average, such dependence, however, was not completely removed.

4. Low ozone values were overestimated by GDP V2.7 by 10-20%. The version 3.0 upgrade reduced this to 5%. Though small, TCO dependence persisted in GDP V3.0.

5. Ground-based TCO is underestimated by GDP V3.0 by 2% to 4% over desert areas with high surface albedo.

6. A large discrepancy existed between GDP V3.0 and TOMS V7 TCO. TOMS V7 TCO overestimated ground-based measurements by about 2% and in the southern hemisphere the bias increased to 6%. This hemispheric bias was removed in the latest version (TOMS V8).

A study carried out as a part of the delta validation exercise identified a number of DOAS-related error sources which may affect the accuracy of the TCO products [*Roozendael et al.*, 2003]. One of the important issues is the inclusion of the molecular Ring. Raman scattered light is not only responsible for the Ring structures, but it also perturbs the molecular absorption features. The neglect of molecular Ring effect in the Ring correction scheme used by GDP V3.0 results in a systematic bias in TCO. Another important issue which is often raised as the limitation of GOME DOAS retrieval in the 325-335 nm

spectral region is the use of a single air mass factor computed at 325 nm in order to convert the slant column density to vertical column density [*Burrows et al.*, 1999a]. According to *Roozendael et al.* [2003], air mass factor calculated at 325.5 nm will reduce the size of this bias at elevated SZA. Also, in GDP V3.0, a shift of 0.012 nm was applied to the GOME Flight Model-98 cross-section. Following the recommendation from *Roozendael et al.* [2003], the shift was reviewed to be 0.017 nm.

1.7 Objectives and Contents

1.7.1 Main goals of the work

The main goals of this work are:

1. To develop and validate a new TCO retrieval algorithm (WF-DOAS) that avoids the assumptions inherent to the standard DOAS approach, with the purpose of creating trend quality (relative accuracy better than 1%) data set for GOME.
2. To prepare an updated and atmospheric dynamics oriented climatology of ozone and temperature profiles with the purpose of improving TCO and ozone profile retrievals from GOME, SCIAMACHY, or any other satellte measurements.
3. To investigate the impact of ozone and temperature climatologies (*a priori*) on TCO and ozone profile retrievals.
4. To adapt the WF-DOAS algorithm to SCIAMACHY and to validate the SCIAMACHY TCO retrievals.

1.7.2 Thesis contents

With the limitations mentioned in Section 1.6, GDP V3.0 clearly does not meet the accuracy requirements of ozone data to be used for long-term ozone trend monitoring. The most critical part of the standard DOAS type GDP algorithm is its assumption that the mean optical path of scattered photons can be considered as independent of the wavelength within the fitting window of 325-335 nm. As such, a constant AMF is used to convert the slant column into vertical column. But, the AMF exhibits dependence on wavelength and solar zenith angle [*Rozanov et al.*, 1998]. To surmount this problem, a new retrieval algorithm, called Weighting Function Differential Optical Absorption Spectroscopy (WF-DOAS), has been developed and is described in Chapter 3. This algorithm is based on approximating the logarithm of the measured sun-normalized radiance by a corresponding linearized model quantity plus a low order polynomial. The fit parameter is TCO and no AMF conversion is needed. Near global validation of WF-DOAS TCO by using various ground based instruments introduced in Section 1.2 is also presented. Consideration of accuracies and uncertainties in ground-based data and discrepancies in data quality from various types of instrument suggests that the accuracy of GOME WF-DOAS TCO lies within the accuracy of a well-maintained ground based instrument. In particular, WF-DOAS results show better agreement with Brewer data.

Following the demonstration of high quality GOME data from WF-DOAS, this data can be used to detect calibration problem and estimate biases in the ground-based data. In particular, this is relevant for Brewer network, which currently lacks a data quality program that the WMO organizes for Dobson. This is the content of Chapter 4. The WF-DOAS TCO data will also be compared with the latest version of TOMS and SBUV/SBUV2 measurements.

Through simulated radiances (in WF-DOAS) or AMF (in standard DOAS) errors in *a priori* (e.g. ozone and temperature profiles) inevitably introduce retrieval errors. Investigation of WF-DOAS related errors has revealed errors of up to 5% due to incorrect climatological ozone and temperature profile shapes [*Coldewey-Egbers et al.*, 2005]. Other independent studies [*Wellemeyer et al.*, 1997; *Lambert et al.*, 2002b; *Bhartia*, 2003] have also reported similar errors from *a priori*. Such errors could be minimized by adopting improved climatologies. A new ozone column classified climatology of ozone and temperature profile has been prepared which is presented in Chapter 5. This chapter also provides evidences on how the new climatology could improve the accuracy of GOME ozone profile retrieved by using the optimal estimation method. Ozone and temperature profile sensitivity of GOME TCO retrieved by WF-DOAS method is discussed in Chapter 6.

The main motivation for the development of the new algorithm WF-DOAS was driven by the requirement of a stable scientific algorithm common to a new generation sensors: GOME, SCIAMACHY, and future GOME instruments on the METOP satellites. Application of WF-DOAS for SCIAMACHY TCO retrieval is presented in Chapter 7 and conclusion is given in Chapter 8.

2 GOME, SCIAMACHY, and SCIATRAN

This chapter introduces briefly the two satellite-based passive remote sensing UV-Vis-NIR spectrometers GOME and SCIAMACHY and a radiative transfer model SCIATRAN that have been used in this study. The SCIATRAN model was developed at the Institute of Remote Sensing (ife), University of Bremen, Germany for fast and accurate simulation of radiance spectra as measured by these spectrometers.

2.1 Spectrometers

2.1.1 GOME

GOME, an ultraviolet/visible nadir viewing spectrometer, is the first of a series of European satellite instruments dedicated to the measurement of global ozone and other relevant trace gases. Launched in April 1995 on board the Second European Remote Sensing Satellite, ERS-2, it is still operational.

High spectral dispersion of light in the GOME instrument is achieved by the combination of a quartz prism and diffraction gratings. The spectra in the range of 240 to 790 nm are recorded simultaneously from four channels at spectral resolution varying between 0.2 nm (UV, channel 1) and 0.4 nm (Vis, channel 4). When light enters GOME via the nadir scan mirror, it is focused into the entrance slit of the spectrometer by a telescope formed by two cylindrical mirrors. Light is first dispersed by a pre-disperser prism creating an intermediate spectrum. The band-separator prism and subsequent mirrors direct the light into the four channels where the light is dispersed by a diffraction grating. The light is sensed by four linear Reticon Si-diode arrays with 1024 spectral elements each. In order to reduce the dark current and improve the signal-to-noise the diode arrays are maintained at 235 K by Peltier coolers that are connected to passive deep space radiators.

The diffraction gratings and pre-disperser prism are polarisation sensitive. In order to correct for the effects, the polarisation fraction of the incoming light is determined by three broadband detectors, the Polarisation Monitoring Devices (PMDs). These measurements are applicable in polarisation correction for the level 1 spectra and also for cloud detection. GOME also has a Pt/Cr/Ne hollow cathode gas discharge lamp for in-flight wavelength calibration and a diffuser plate for daily determination of solar irradiance, which is essential for trace gas retrieval.

The ERS-2 is a sun-synchronous polar orbiting satellite having a local equator crossing time in descending node at 10.30 AM. The satellite moves at a speed of 7 km/s at

Table 2.1: Retrieval of various products from GOME

Product	selected window [nm]	references
Ozone total column	326.6-335	[*Coldewey-Egbers et al.*, 2005]
	325-335	[*Spurr et al.*, 2004]
Ozone profile	290-345	[*Hoogen et al.*, 1999a]
	290-313	[*Hasekamp and Landgraf*, 2001]
Water vapor column	580-605	[*Lang et al.*, 2003]
	585-710	[*Noël et al.*, 1999]
NO_2 column	423-451	[*Martin et al.*, 2002]
	425-450	[*Richter and Burrows*, 2002]
HCHO column	337.35-356.12	[*Chance et al.*, 2000]
SO_2 column	315.5-327.0	[*Eisinger and Burrows*, 1998]
OClO column	357.0-381.5	[*Wittrock et al.*, 1999]

a mean altitude of 785 km and completes an orbit in 100 minutes. During the illuminated part of the orbit, GOME performs across-track nadir observation by scanning the earth surface from east to west. One across-track consists of three forward scans and one backscan with 1.5 s integration time each. Each forward scan has a footprint size of $320 \times 40\,\mathrm{km}^2$ thereby making maximum swath of 960 km width. Such measurement pattern results in a global coverage at the equator in three days. For improved sounding of polar latitudes during springtime, the scan mirror is also positioned at about 47°. ERS-2 is in the night side of the earth for half of the time. During this phase GOME carries out several sequences of dark current and LED measurements (pixel-to-pixel gain). Various temperature sensors spread over the entire focal plane assembly monitor the in-orbit temperature variations. Once a month, the internal calibration lamp is switched on over an entire orbit. During this sequence a series of lamp measurements with and without the solar diffuser permits the investigation of long term degradation of the diffuser and to obtain an update of the wavelength calibration as a function of instrument temperature.

The ground segment of the GDP comprises the Level 0 (raw data) to 1 (calibrated data) and Level 1 to 2 processing. The Level 0 to 1 processing includes a correction for leakage current, stray light, pixel-to-pixel gain followed by the wavelength and radiometric calibrations. The second part of the processing, i.e. Level 2, carries out the geophysical retrieval of atmospheric constituents. The main operational Level 2 data products are the total column ozone and nitrogen dioxide.

The information contained in the backscattered radiances measured by GOME has been exploited and the results have been published in various publications (See Table 2.1). Besides ozone and nitrogen dioxide, the total column amount of BrO, SO_2, HCHO, OClO, and water vapor have been derived. Because of larger spectral range and higher spectral resolution, the retrieval of these trace gases employ the DOAS technique. The height resolved profiles, e.g. O_3 profile, are derived by optimal estimation method

[*Rodgers*, 2000]. Table 2.1 shows a summary of data products derived from GOME spectral measurements. For the trace gas retrieval from these measurements, the presence of cloud should be taken into account. Cloud top height, cloud fraction, and cloud optical thickness (cloud properties) have been derived from the spectral reflectance measurements in the spectral range of 758-778 nm [*Koelemeijer et al.*, 2001; *Rozanov and Kokhanovsky*, 2004]. *Joiner et al.* [2004] has inferred the Lambert-Equivalent Reflectivity (LER) pressure from the measurements in 355-400 nm range. GOME data have also been applied to obtain the aerosol optical thickness by using 1 nm windows centered at 380 nm, 440 nm, 463 nm, 495 nm, 555 nm, 670 nm [*Kusmierczyk-Michulec and de Leeuw*, 2005].

2.1.2 SCIAMACHY

Launched in March 2002, SCIAMACHY, a successor of GOME, is one of the instruments on board European Space Agency's (ESA) ENVIronmental SATellite (ENVISAT). The SCIAMACHY is funded by Germany and the Netherlands with some contribution from Belgium. SCIAMACHY measures the extraterrestrial solar irradiance and the radiance reflected, transmitted and scattered from the earth's atmosphere and surface. The main objective of the mission is to improve our understanding of physical and chemical processes in the atmosphere. More details on mission objectives and measurement strategies can be found in [*Bovensmann et al.*, 1999].

The design of SCIAMACHY instrument is described in detail in *Kamp and Dobber* [2000] and *Burrows et al.* [1995]. Briefly, SCIAMACHY is a UV-Visible-NIR grating spectrometer comprising of eight simultaneously operating spectral channels covering the wavelength range of 240-1750 nm (channels 1-6), 1940-2040 nm (channel 7), and 2260-2400 nm (channel 8). The spectral resolution lies between 0.2 nm and 1.5 nm. Light enters the telescope via two scanner modules. These modules are known as the Elevation Scanner Module (ESM) and Azimuth Scanner Module (ASM). The beam is collimated and directed onto a entrance slit. After the slit, the beam is passed through a pre-dispersing prism thereby forming an intermediate spectrum. Reflective optics are used to separate the spectrum into four parts: 240-314 nm, 314-405 nm, 405-1750 nm, and 1940-2380 nm. The first two parts are directed to the channels 1 and 2, respectively. Light from remaining two parts are further separated into other channels by dichroic mirrors. A grating located in each channel further disperses the light, which is then focused onto eight arrays of detectors consisting of 1024 pixels each.

To minimize dark current noise, the infrared, and UV and visible light detectors are cooled down to 150 K and 200 K, respectively, by a passive radiant cooler. Since the reflecting properties of gratings, which are used to create the spectra, are polarisation-dependent, the intensity calibration of SCIAMACHY has to consider the polarisation effect. Six PMDs measure the polarisation parallel to the spectrometer slit, generated by a Brewster reflection at the back of the pre-dispersing prism. One PMD measures polarisation at 45° direction which is extracted from the part of the light in 405-1750 nm. SCIAMACHY is also equipped with a Pt/Cr/Ne hollow cathode, a UV-optimized tungsten-halogen lamp, a calibrated on-board diffuser, and an extra reference mirror for the pur-

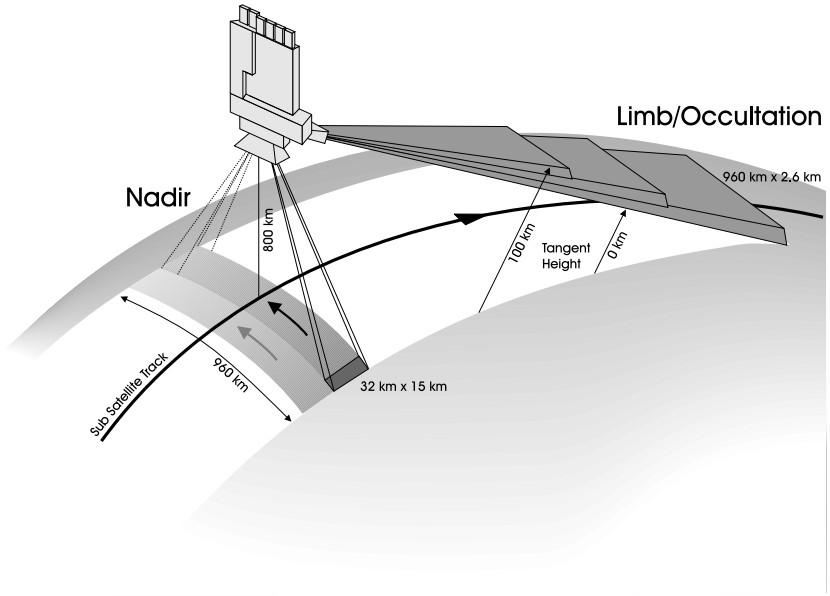

Figure 2.1: Limb/nadir matching of SCIAMACHY. This features enables SCIAMACHY to observe the same atmospheric volume first in limb and then after about 7 minutes in nadir geometry. By using this limb/nadir matching three-dimensional information about the atmosphere can be obtained (*courtesy Stefan Noël, University of Bremen*).

pose of in-flight calibration and instrument performance monitoring.

ENVISAT is also launched in a sun-synchronous near polar orbit (inclination angle of 97.8°). ENVISAT and ERS-2 are flying in the same orbit only 30 minutes apart, but in slightly different altitudes. SCIAMACHY performs measurements in nadir, limb, and solar/lunar occultation viewing geometries. The nadir measurements of SCIAMACHY in the UV-vis are similar to that of GOME. In this mode, the atmospheric volume beneath the spacecraft is observed. The nadir mirror scans a swath of 960 km width from east to west for 4 s in a direction perpendicular to the satellite flight direction. The forward scan is followed by a quick (1 s) backward scan. For major constituents, the forward scan corresponds to 16 ground pixels each of $30 \times 60\,\mathrm{km}^2$ whereas the backward scan comprises of 4 ground pixels. In the limb mode, the instrument observes the atmosphere tangentially to the earth's surface some 3000 km ahead of the sub-satellite nadir point. Both azimuth and nadir mirrors are employed, the azimuth mirror scans in an azimuth direction and the nadir mirror scans through different tangent heights ranging from -3 to 100 km in steps of about 3.3 km. The azimuth mirror scans a swath of size 960 km in 1.5 s in 4 typical limb integration times each (i.e 0.375 s) corresponding to a horizontal resolution of 240 km. A complete limb scan consists of 34 elevation steps. In nominal operation, limb and nadir viewing is alternated in such a way that the same air parcels are first probed in limb and eight minutes later in nadir geometry. These fea-

tures of the SCIAMACHY measurements are depicted in Figure 2.1. This unique feature of SCIAMACHY allows it to monitor trace gases in the troposphere from space for the first time. The tropospheric amount can be derived by subtracting stratospheric column (as retrieved from limb measurements) from total column (as retrieved from nadir measurements), a technique suggested by *Fishman et al.* [1990] who derived tropospheric O_3 by subtracting SAGE stratospheric O_3 columns from TOMS total O_3 columns. Occultation measurements are performed in a similar manner to the limb mode but with the sun/moon in the instrument's field of view. Solar occultation performed once in each orbit during sunrise are limited beyond 65° latitude in the northern hemisphere. Occasionally, there is the additional opportunity for lunar occultation depending on the lunar phase. Lunar occultation is possible for about a week and provides a latitude coverage from 30°S to 90°S. After solar occultation, the full disc solar irradiance measurement above the atmosphere is performed. Besides these measurements, various calibration measurements are performed on a regular basis.

The German Remote Sensing Data Center plays a major role in the design, implementation and operation of the SCIAMACHY ground processors (SGPs). The raw data from the SCIAMACHY instrument are sent from ENVISAT to the receiving stations, where the reformatted data are stored as level 0 data. The SGP comprises the processing of level 0 to 1 and level 1 to 2 data. Level 1 data is further split up in level 1b and level 1c data. Level 1b data is uncalibrated but it contains all necessary information for full calibration. Level 1c data is the data obtained by full or partial calibration. Level 2 data contains the geophysical products like total column or profiles of atmospheric gases. Level 1b to 2 processing is available at Near-Real-Time (NRT) and Offline (OL) levels. At present, the NRT products include the column amount of O_3, NO_2 and BrO, and cloud fraction. The OL products contain O_3 and NO_2 profiles generated from SCIAMACHY limb spectra. Various institutes have developed algorithms for the retrieval of O_3, NO_2, BrO, SO_2, OClO, HCHO, and H_2O columns from SCIAMACHY UV-visible nadir spectra. Columns of H_2O, CO, CH_4, N_2O, and CO_2 are derived from NIR nadir measurements. Other scientific products are the profiles of O_3, NO_2, BrO, OClO, and H_2O utilizing limb measurements. In addition, algorithms have also been developed for the cloud and aerosol products. On going retrieval and validation activities for SCIAMACHY measurements are summarized in *Piters et al.* [2005].

2.2 Radiative transfer model SCIATRAN

Inversion of GOME/SCIAMACHY spectral measurements by an accurate algorithm having a precise radiative transfer model allows the retrieval of the trace gas and aerosol distribution in the atmosphere. The model SCIATRAN is optimised to be applicable to SCIAMACHY measurements and measurements made by any other satellite, air- and balloon-borne, and ground-based sensors operating in the spectral range of 240-2380 nm.

SCIATRAN is the successor of GOMETRAN [*Rozanov et al.*, 1997], which was developed to simulate the solar backscattered radiation in the UV-visible (240-790 nm) as

measured by GOME. SCIATRAN uses the finite difference scheme [*Rozanov et al.*, 1997] for the numerical solution of the monochromatic scalar radiative transfer equation for a plane-parallel and vertically inhomogenous atmosphere as given by,

$$\mu \frac{\mathrm{dI}(\mathrm{z},\mu,\phi)}{\mathrm{dz}} = -\varepsilon(\mathrm{z})\mathrm{I}(\mathrm{z},\mu,\phi) + \frac{\beta(\mathrm{z})}{4\pi} \int_0^{2\pi} \mathrm{d}\phi' \int_{-1}^{1} \mathrm{d}\mu' \mathrm{p}(\mathrm{z},\mu,\mu',\phi,\phi')\mathrm{I}(\mathrm{z},\mu',\phi') \tag{2.1}$$

The radiance I depends on three spatial coordinates: the altitude z in the atmosphere, the solar zenith angle θ, and the relative azimuthe angle with respect to the sun direction ϕ. μ is the cosine of the zenith angle θ. p denotes the scattering phase function; ε and β are the total extinction and scattering coefficients, including contributions from all relevant atmospheric constituents such as molecules, trace gases, aerosols or clouds.

The method is based on an expansion of the radiation field in a Fourier series in azimuth, an expansion of the phase function in combined Fourier-Legendre series, splitting of the Fourier components of I into upward and downward components at each atmospheric layer, their recombination to symmetric and antisymmetric sums, and evaluation of height derivatives of the sum using finite difference scheme. The Fourier components of I are then determined by using LU decomposition of the resulting matrix. The radiance measured by the satellite instrument is the sum of the diffuse radiance, which is obtained by adding all Fourier components, and direct radiance that is reflected at the earth's surface into the instrument's field of view. SCIATRAN enables simultaneous analytical derivation of weighting functions [*Rozanov et al.*, 1998]. Weighting functions are derivatives of the top of atmosphere radiance with respect to atmospheric or surface parameters such as trace gas concentration, albedo, etc. Such altitude resolved weighting functions are important for the retrieval of atmospheric constituents from spectroscopic measurements.

Radiative transfer calculation in a plane-parallel atmosphere is also possible by discrete ordinate and finite element method. Plane-parallel mode leads to larger error for SZA greater than 75° and line of sight (LOS) greater than 20°. For large SZA, the sphericity of the earth's atmosphere is considered in SCIATRAN using a pseudo-spherical approach [*Rozanov et al.*, 2002] whereby the direct radiance is calculated in a spherical atmosphere, while higher order scattering is calculated for a plane-parallel atmosphere. SCIATRAN is also capable of calculating the radiation field in a spherical planetary atmosphere [*Rozanov et al.*, 2000, 2001]

Absorption due to continuum-absorbers such as O_3, NO_2, ClO, OClO, BrO, HCHO, SO_2, NO_3, and O_4 and line-absorbers such as H_2O, CO, CH_4, and N_2O are implemented. These molecular line-absorbers are considered either by using accurate but time consuming line-by-line approach or by faster correlated-k distribution scheme [*Buchwitz et al.*, 2000a]. Scattering by air molecules, aerosols, and clouds and absorption by aerosols and clouds are considered. Parameterization schemes for scattering and

absorption inside the clouds [*Kurosu et al.*, 1997] and aerosols are included. A radiative transfer scheme which accounts for the Ring effect is implemented [*Vountas et al.*, 1998]. This includes the filling-in of solar Fraunhofer and gas absorption lines.

The main quantities that SCIATRAN determines are the top of atmosphere radiance, weighting functions, air mass factors, actinic fluxes, and upwelling and downwelling fluxes. Air mass factor is needed for conversion of slant column into vertical column of trace gases in DOAS type retrieval algorithm. The actinic flux is used for photolysis rate calculation. An improved version of the model PHOTOGT [*Blindauer et al.*, 1996] has been used in SCIATRAN.

3 GOME WF-DOAS total ozone retrieval and validation

3.1 Overview

The GOME instrument together with the TOMS since 1979 provide a valuable long-term data set with near global coverage for ozone trend assessment [*Bodeker et al.*, 2001; *Fioletov et al.*, 2002]. However, differences in algorithm and instrument design (for both satellite and ground instruments) can lead to instrumental artifacts in trend calculation without homogenization of combined data sets [*Bodeker et al.*, 2001]. This will remain an important issue when the current generation of TCO satellite instruments are succeeded by new instruments such as SCIAMACHY/ENVISAT, OMI (launched in July 2004) and the three GOME-2 aboard METOP (first launch 2006) [*Bovensmann et al.*, 1999; *Stammes et al.*, 1999]

Shortcomings of the operational TCO retrieval GDP V3.0 were already discussed in Chapter 1. The approach used by GDP V3.0 assumes that the absorber is weak and the atmosphere optically thin. Ozone in the Huggins band, however, shows significant absorption so that this basic assumption is violated. In the first part of this chapter a more generalized approach, called Weighting Function DOAS (WF-DOAS), will be introduced. It has been first demonstrated to be applicable to trace gas column retrieval in the near infrared region of SCIAMACHY [*Buchwitz et al.*, 2000b]. A direct retrieval of vertical ozone amounts is possible as the slant path wavelength modulation is taken into account. First results seem to indicate its promising potential [*Coldewey-Egbers et al.*, 2004]. The second part describes the validation of WF-DOAS results with ground based data on a global scale. Comparison of operational GDP V3.0 (GOME Data Processor) to ground data are also presented to document the significant improvement achieved by WF-DOAS over prior data versions.

This algorithm introduces several new features that have not been used in prior TCO retrievals from GOME. The variable ozone dependent contribution to the Raman scattering responsible for the filling-in of molecular absorption is summarized in Section 3.2.3. The use of a new cloud scheme in combination with an estimation of effective scene height lead to higher sensitivity to clouds in WF-DOAS. In addition, the GOME retrieved scene albedo is included in the retrieval. This is discussed in Section 3.2.4. Section 3.2.6 gives a summary of the various error sources that contribute to the overall error of the retrieved TCO. In Section 3.3.1 comparisons with simultaneous Brewer and Dobson measurements at Hohenpeissenberg (47.8° N, 11.0° E) and Hradec Kralove (50.2° N, 15.8° E) are presented and discussed. This is a very important comparison since many stations have changed or plan to change from regular Dobson to Brewer observations

and a good characterization of satellite data with respect to both spectrophotometer types is critical for long-term trend assessment from both satellite and ground time series [*Staehelin et al.*, 2003]. The next section shows comparisons with individual WOUDC stations (Section 3.3.2) followed by Section 3.3.3 summarizing the statistical analysis involving all stations selected from low to mid latitudes. Most of the validation statistics at mid latitudes and in tropics rely on ground-based data between 1996 and 1999, but for selected stations the validation has been extended up to 2003 (Lauder and Hohenpeissenberg) for demonstrating the long-term stability of the GOME data. In a separate section (Section 3.3.4) the validation results from comparison with polar station measurements in both hemispheres from 1996 to 2003 are presented. Conclusion is given in Section 3.4.

3.2 WF-DOAS algorithm [1]

3.2.1 Retrieval principle

WF-DOAS is a linear least squares algorithm which extracts the information of TCO amount from its differential absorption features. In this algorithm the logarithm of the measured intensity I_i^{mea} at wavelength λ_i is approximated by a Taylor expansion around a reference intensity I_i^{mod} plus a low-order polynomial P_i (see Eq. 3.1). The polynomial compensates all broadband contributions from, for example, surface albedo and aerosol that affect the radiance.

$$\begin{aligned} \ln I_i^{mea}(V^t,\vec{b}^t) \approx\ & \ln I_i^{mod}(\bar{V},\bar{\vec{b}}) + \frac{\partial \ln I_i^{mod}}{\partial V}|_{\bar{V}} \times (\hat{V}-\bar{V}) + \frac{\partial \ln I_i^{mod}}{\partial T}|_{\bar{T}} \times (\hat{T}-\bar{T}) \\ & + SCD_R \cdot \sigma_{i,R} + SCD_U \cdot \sigma_{i,U} + SCD_{NO_2} \cdot \sigma_{i,NO_2} \\ & + SCD_{BrO} \cdot \sigma_{i,BrO} + P_i \end{aligned} \tag{3.1}$$

Index t, over-bars ($\bar{}$), and hats ($\hat{}$) denote the true atmospheric state, model parameters, and fit parameters, respectively. $\vec{b}$ contains all atmospheric and surface parameters that contribute to the intensity. $\bar{V}$ is the reference ozone column and $\bar{T}$ is the reference surface temperature corresponding to the reference intensity. $\hat{V}$ and $\hat{T}$ are the corresponding fit parameters. Slant column fitting is applied to the Ring effect, $\sigma_{i,R}$, the under-sampling correction, $\sigma_{i,U}$ [*Slijkhuis et al.*, 1999], and for the the minor absorbers NO_2 and BrO. $\frac{\partial \ln I_i^{mod}}{\partial V}$ and $\frac{\partial \ln I_i^{mod}}{\partial T}$ are wavelength dependent ozone and temperature shift weighting functions, respectively. The latter accounts for temperature dependence of the ozone absorption.

This algorithm requires a radiative transfer model for the accurate simulation of the model parameters (i.e. radiance and weighting functions). These parameters are precalculated and stored in a look-up-table (LUT) thereby avoiding time-consuming online

[1] This section is based on the article: Coldewey-Egbers, M., M. Weber, L. N. Lamsal, R. de Beek, M. Buchwitz, and J. P. Burrows (2005), Total ozone retrieval from GOME UV spectral data using the weighting function DOAS approach, *Atmos. Chem. Phys.*, 5, 1025-1025, SRef-ID: 1680-7324/acp/2005-5-1015.

radiative transfer simulation. The unknown fit parameters are determined by a linear least squares minimization.

3.2.2 Look-up-table for reference spectra

In the calculation of WF-DOAS LUT using SCIATRAN (see Section 2.2), the Rayleigh scattering coefficients are based on the *Bates* [1984] values, the ozone absorption coefficients are based on a temperature parameterization of GOME FM ozone cross-section [*Burrows et al.*, 1999b]. A temperature parameterization is commonly used in order to account for the strong temperature dependence of ozone absorption. To deal with wavelength mismatching among cross sections and earthshine, the ozone cross section is pre-shifted by 0.017 nm [*Lambert et al.*, 2002a]. A set of reference spectra, which are calculated using the pseudo-spherical approximation, includes nearly all possible atmospheric states. These spectra are a function of TCO including profile shape, zonal band, SZA, line-of-sight (LOS), relative azimuth angle (RAZ), surface albedo α_s, and altitude. Ozone and temperature profiles are taken from TOMS Version 7 climatology which contains different profile shapes for three latitude belts as a function of the TCO [*Wellemeyer et al.*, 1997]. A total of 26 profiles are available: 6 profiles at low latitude (-25° to 25° N), 10 profiles each at middle (±25° to ±65°) and high latitudes (±65° to ±90°). The profiles cover the range of 225-475 DU at low latitude and 125-575 DU at middle and high latitudes, in steps of 50 DU. Thirty four SZAs with 5° steps in the 15° - 70° range and 1° steps in the 71° - 90° range, 7 LOSs (-34.5°, -23.0°, -11.5°, 0°, 11.5°, 23.0°, 34.5°) for the reference spectra calculation. Azimuth angles are optimised with respect to SZA and LOS. The multi-dimensional LUT has 6 albedos at 0.2 steps and 7 altitudes ranging from 0 to 12 km at 2 km steps. These are not the surface altitudes but rather effective scene heights that account for clouds. It is a weighted sum of surface altitude and cloud top height with cloud fraction as weighting factor.

Because of non-linear variation of intensity and weighting functions in SZA, they are fitted as function of solar zenith angle and wavelength using Chebyshev polynomials. Instead of using one reference spectrum for the whole pixel, mean values are calculated by averaging intensities and weighting functions at three different scan angles (begin, mid, and end of integration) at 1:4:1 ratio.

3.2.3 Ring effect implementation

The Ring effect [*Grainger and Ring*, 1962; *Kattawar et al.*, 1981; *Joiner and Bhartia*, 1995; *Fish and Jones*, 1995; *Vountas et al.*, 1998; *de Beek et al.*, 2001] has to be adequately accounted for in retrieving TCO from UV-visible spectra obtained from spaceborne instrumentations, which includes the filling-in of solar Fraunhofer and gas absorption lines. In particular, the Ring spectrum has large contribution to the differential optical depth in the Huggins band. For the Ring effect, rotational Raman scattering by air (N_2 and O_2) molecules has a dominant role [*Kattawar et al.*, 1981; *Vountas et al.*, 1998]. Provided that the instrument can measure the amounts of parallel and perpendicular polarized light, Ring reference spectra can be derived [*Solomon et al.*, 1987].

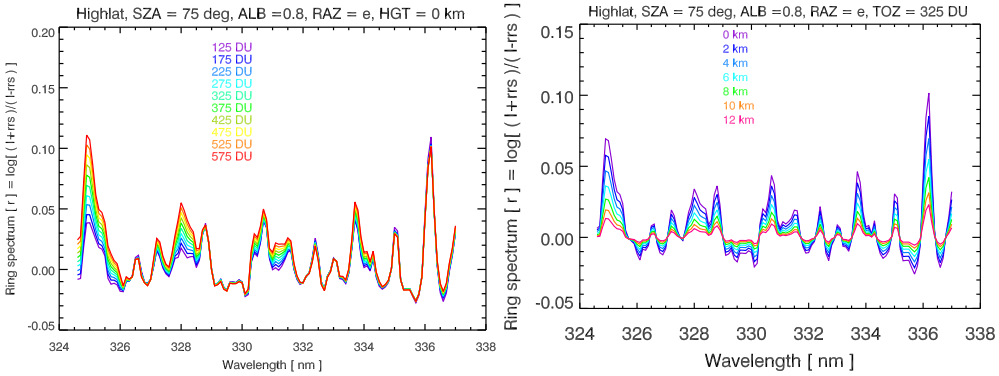

Figure 3.1: SCIATRAN modeled Ring spectra using the high latitude TOMS V7 ozone profile climatology for a given value of SZA of 75°, effective albedo of 0.8, surface altitude of 0 km and different total ozone (and profile shape) (left panel). The right panel is for a given ozone scenario but as a function of altitude/effective height.

GOME and SCIAMACHY instruments do not provide the in-flight cross polarization measurements and hence the method does not apply. *Chance and Spurr* [1997] calculated a Ring spectrum directly from a Fraunhofer spectrum. *Sioris and Evans* [1999] used model radiances to derive Ring spectra. Detailed investigations of the effect of trace gas absorption and particle and cloud scattering requires a radiative transfer model which includes rotational Raman scattering. *Vountas et al.* [1998] introduced a new method to derive Ring spectra from multiple scattering radiative transfer calculations in pseudo spherical mode, using the radiative transfer model GOMETRAN where the Ring reference spectrum is computed as the optical depth difference of calculated intensities with and without the Ring effect.

Derivation of the Ring spectrum from a solar spectrum assumes that the filling-in of telluric absorption lines (molecular Ring effect) is negligible. Raman scattered light is not only responsible for the Ring structures but it also perturbs the molecular absorption features. Since absorption structures also contribute to the Ring spectral signature their variations have to be taken into account. Otherwise the strong correlation of these structures with trace gas cross-sections lead to errors in the retrieval.

The WF-DOAS algorithm employs a sophisticated approach to account for the spectral variability of the Ring effect. A Ring data base containing spectra was generated using SCIATRAN for the same atmospheric scenarios as defined for the reference intensities and weighting functions except that the Ring data base was limited only to nadir viewing mode.

Figure 3.1 demonstrates the variability of the Ring effect caused by the change in TCO (and profile shape). Ozone profiles were taken from the TOMS V7 climatology. The variability is largest near the absorption peaks of ozone. The figure also shows that the largest contribution to the Raman scattering occurs in the Rayleigh layer near the surface. Neglect of the Ring effect can result in TCO retrieval errors of up to 10%

[*Coldewey-Egbers et al.*, 2005].

3.2.4 Auxiliary inputs for WF-DOAS

In WF-DOAS ozone retrieval procedure, subtraction of a smooth polynomial during spectral fit considerably reduces the influence of generally unknown surface, aerosol, and cloud reflectance. However, the retrieval is sensitive to the uncertainty in the state of atmosphere, e.g. cloud, and surface. Therefore, to infer TCO accurately from GOME spectral measurements, the presence and properties of these reflecting surfaces have to be known. The three auxiliary inputs which are explained here are effective albedo, effective height and ghost vertical column.

Including WF-DOAS, various TCO retrieval algorithms assume the reflection of light by a homogeneous surface as Lambertian [for example, *Bhartia*, 2003]. The Lambert Equivalent Reflectivity (LER) [*Herman and Celarier*, 1997], which defines the effective albedo, is obtained from GOME sun-normalized radiance at 377.6 nm. This wavelength was selected since it shows very small variation with respect to the Ring effect that can be easily corrected for. WF-DOAS utilizes a look-up-table of pre-calculated sun-normalized radiances using SCIATRAN/CDI for 26 values of SZA 17 LOSs, 18 RAZs, 7 ground altitudes, and 12 values of surface albedo [*Menkhaus et al.*, 1999]. This LUT allows to determine effective albedo by bi-sectional search for a given set of parameters and radiances. The use of LER in the retrieval represents a first order aerosol correction. Determination of LER requires effective altitude which is obtained from FRESCO (Fast Retrieval Scheme for Clouds from the Oxygen A-Band, [*Koelemeijer et al.*, 2001]). The FRESCO algorithm, as its name suggests, exploits earthshine radiance in and around the oxygen A band from GOME measurements. Due to oxygen absorption, the spectral top of atmosphere reflectance has a deep minimum close to wavelength of 760 nm. For high clouds, for example, this minimum is almost undetectable. These information contained in the reflectivity inside the O_2 A band is used to derive cloud top height, whereas the information of the reflectivity outside the O_2 A band allows us to determine cloud optical thickness and cloud fraction. Since these three cloud parameters cannot be derived uniquely from the measured reflectivity (because cloudy scenes possessing same cloud top height but different cloud optical thicknesses and cloud fractions may give rise to the same reflectivity), FRESCO instead retrieves effective cloud fraction and cloud top height.

The effective height for the GOME ground pixel is a weighted sum of the ground altitude h_o and the retrieved cloud top height h_{cld} weighted by the fractional cloud cover as given by

$$h_{eff} = f \cdot h_{cld} + (1 - f) \cdot h_o. \tag{3.2}$$

The albedo effect of clouds in ozone retrieval is accounted for by the use of LER and effective height. Another effect, often referred as the ghost column effect, is that they shield tropospheric ozone from observation. This effect is corrected by estimating the ghost vertical column (GVC) from climatological vertical ozone profiles. The GVC is computed by integrating the profile $O_3(p)$ from pressure $p(h_o)$ at the surface altitude

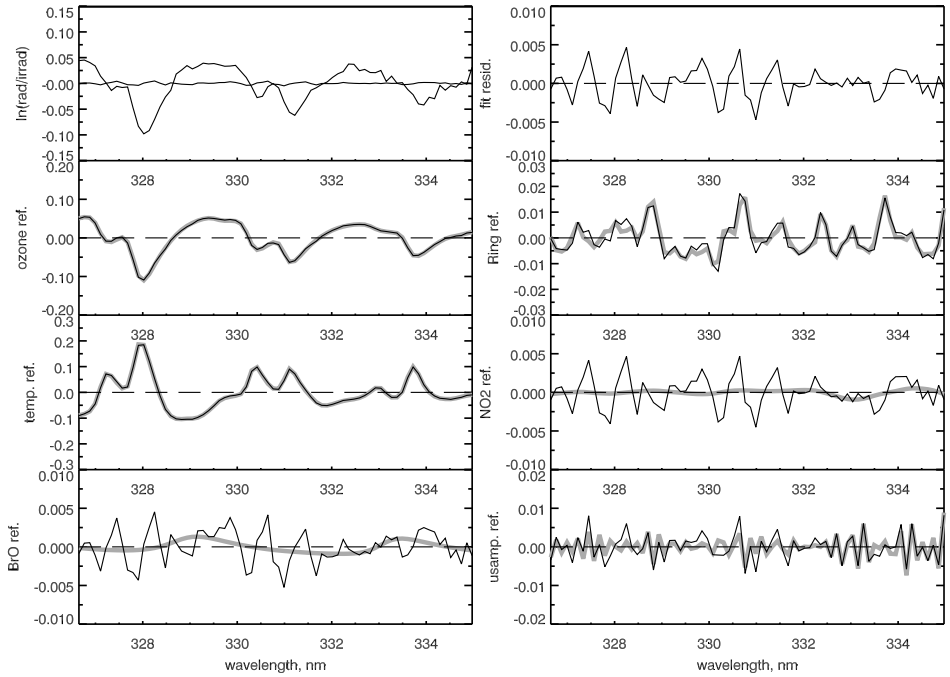

Figure 3.2: Fit results of pixel number 898 in GOME orbit 80706094. The GOME observed differential optical depth (top-left) and fit residual (top-right). The lower panels show the magnitude of various terms in the WF-DOAS equation. Those terms in the decreasing order of their contribution are as following: ozone reference (second left), Ring reference (second right), temperature reference (third left), NO_2 reference (third right), BrO reference (fourth left), and undersampling reference (fourth right). Grey lines show the modeled values and the fit residual has been added to each term to visualize the relative magnitude of the measurement noise.

h_o up to the cloud top pressure $\mathrm{p(h_{cld})}$. Partial cloudiness can be taken into account by multiplying the integrated partial column with effective cloud fraction f as follows:

$$\mathrm{GVC} = \mathrm{f} \cdot \int_{\mathrm{p(h_o)}}^{\mathrm{p(h_{cld})}} \mathrm{O_3(p)\,dp} \tag{3.3}$$

3.2.5 WF-DOAS ozone retrieval

Determination of TCO from WF-DOAS algorithm is based on the linear least squares minimization of Eqn. 3.1. A 8.2 nm wide fit window from 326.6 to 335 nm is selected. To remove the wavelength misregistration, the earthshine spectrum is re-sampled to the wavelength grid of the solar spectrum by carrying out a shift-and-squeeze of wavelength axis. The shift-and-squeeze parameters introduce non-linearity to the least squares procedure which requires an iterative scheme to retrieve TCO. The first step is to find the

nearest neighbor reference scenario. The first guess most closely matches the climatological ozone column. Linear interpolation between effective albedo, effective altitude and relative azimuth angle is performed to obtain the closest reference. The nearest Ring spectrum is selected in the same manner. After the spectral fitting the retrieved TCO is compared with that of the reference scenario and the fit is repeated if a reference scenario can be found which is closer to the retrieved value. After the iterations stops, the ghost vertical column is added to the retrieved column to obtain the final TCO amount.

Typical fitting residuals are shown in Figure 3.2. where the differential optical depth measured and modeled as well as the contribution of the individual terms in the DOAS equation are shown. BrO has in most cases negligible contributions except for those region with enhanced tropospheric BrO. The RMS of the fit residuals is usually on the order of 0.001 which is about half the typical values achieved in GDP V3.0.

3.2.6 A note on errors

Errors in the derived TCO from GOME WF-DOAS may originate from measured radiance, calculated radiance from the radiative transfer model, and retrieval algorithm. These errors could be either systematic or random. In general, an error in the calibration and change with time in instrument sensitivity may lead to systematic error. Errors in the calculated radiance introduce both random and systematic errors in various ways. The calculated radiances are affected by laboratory data and assumed atmospheric properties on which radiative transfer model is based. Errors in, for example, ozone absorption and Rayleigh scattering coefficients will propagate through the algorithm to produce systematic errors in the derived ozone. Ozone absorption cross sections measured in the laboratory are provided at a fixed temperature [*Burrows et al.*, 1999b; *Bogumil et al.*, 2003]. Since the absorptivity of ozone is temperature dependent, the calculated radiance at climatological temperature, which can depart from the real temperature, produces random error in the retrieved ozone. Also, assumed climatological vertical distribution of ozone taken from TOMS V7 profile shape climatology used to compute the look-up tables differ from the actual vertical distribution of ozone. Derived total ozone from WF-DOAS is not significantly dependent at low and moderate SZA but at high SZA it is highly profile sensitive. These *a priori* information are identified as the most important error sources in WF-DOAS which cause the error of 2% for SZA $<$80 and 5% for SZA $>$80. This is discussed in detail in Chapter 6. Random error arises also from ozone variation in troposphere. Simplified assumption in the derivation of auxiliary parameters like effective albedo, effective height, and the correction of TCO in cloudy ground pixels using GVC produces both systematic and random errors which can reach up to 3%.

Linear interpolation between reference spectra from the look-up table is liable to add some error but this error is below 1%. The retrieved total ozone error caused by pseudo-spherical approximation instead of full-spherical radiative transfer modeling is about 0.3%.

Natural and anthropogenic aerosols in the atmosphere produce error in the WF-DOAS TCO by their absorption and scattering of radiation. In particular, absorbing aerosols

absorb Rayleigh scattered radiation and can lead to systematic errors of about -1% while the error due to non-absorbing aerosols is less than 0.3% [*Coldewey-Egbers et al.*, 2005].

3.3 Pole-to-pole validation [2]

3.3.1 GOME, Brewer, and Dobson triple comparison

The majority of the TCO data obtained from the ground are Dobson spectrophotometer measurements. The Dobson spectrophotometer is a double monochromator with the first prism acting as a dispersing element and the second recombining the wavelength pair on to a photomultiplier. A chopper allows the alternating measurements of the wavelength pair with a single detector [*Dobson*, 1931, 1968]. For the standard analysis (World Meteorological Organisation – Global Atmospheric Watch (WMO-GAW), the A (305.5/325.5 nm) and D (317.6/339.8 nm) wavelength pairs are used to derive TCO [*Staehelin et al.*, 2003]. At low solar elevation the D-pair can be combined with the C-pair 311.5/332.4 nm. This instrument can be operated in direct-sun and zenith sky viewing geometry. Most reliable results are obtained in direct-sun (AD pairs) with a precision of 1% using a diffuser plate. Accuracy may be lower due to systematic errors, for instance coming from uncertainties in cross-sections (Bass-Paur are used in the standard retrieval). Under cloudy conditions the error in the zenith-sky results can rise from 3% up to 7% (low clouds) in zenith sky measurements (R. D. Evans, NOAA, personal communication). First measurements with the Dobson instruments have been reported in the twenties [*Dobson*, 1931] and some of the longest time series are provided by the Dobson instruments [*Staehelin et al.*, 1998].

Since the early eighties Brewer grating spectrometers have been installed at several stations [*Kerr et al.*, 1985] and at many stations Dobson instruments have been replaced by Brewer spectrophotometers or are planned to be replaced. The Brewer is a modified Ebert type grating spectrometer which can be operated in single ("single Brewer") or double monochromator ("double Brewer") configuration. This instrument uses five wavelengths in the spectral range 306.3 and 320.1 nm to form several wavelength pairs for the standard ozone retrieval. Besides ozone, NO_2, SO_2, and UV-B radiation can be measured. Particularly SO_2 interferes in the ozone retrieval and has to be corrected for in an urban environment. Particular advantage of the Brewer is its fully automated operation. Both direct-sun and zenith-sky measurements are possible.

In the standard retrieval, for both Brewer and Dobson instruments, the dependence of ozone cross-section on temperature is not accounted for unlike in the satellite retrieval. As discussed by Kerr (2002) atmospheric temperature corrections can be applied to Brewer retrievals, but most of the stations participating in the ground based network still rely on the standard retrieval. Based upon Bass-Paur ozone cross-section spectra [*Bass and Paur*, 1985] convolved to match Brewer spectral resolution, he found a 0.7%/10 K

[2] This section has been published as: Weber, M., L. N. Lamsal, M. Coldewey-Egbers, K. Bramsdedt, and J. P. Burrows (2005), Pole-to-pole validation of GOME WF-DOAS total ozone with groundbased data, *Atmos. Chem. Phys.*, 5, 1341-1355, SRef-ID: 1680-7324/acp/2005-5-1341.

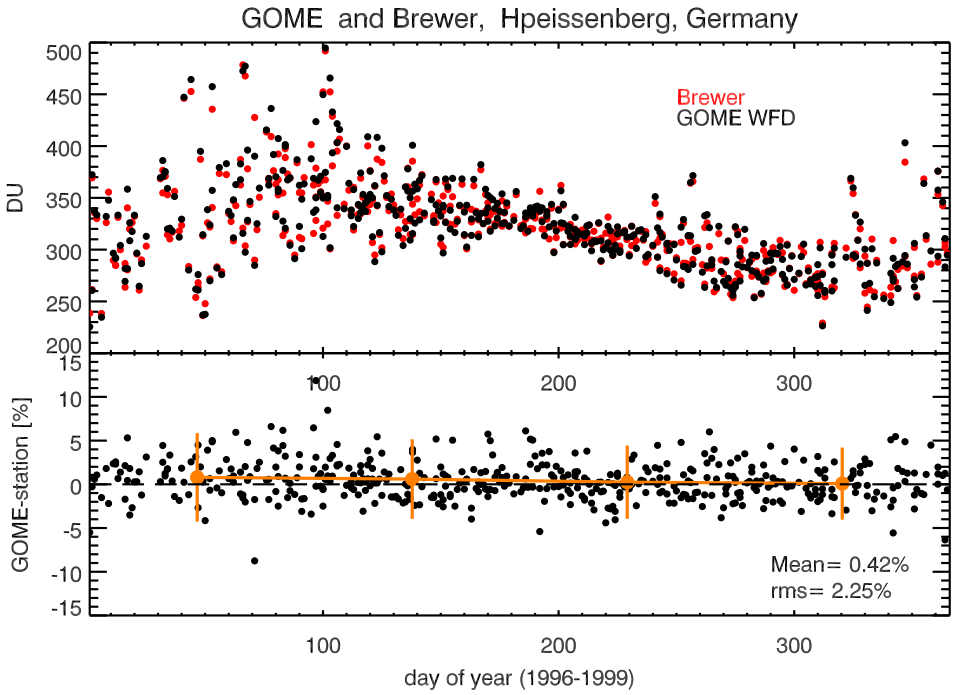

Figure 3.3: Top panel: Collocated GOME WF-DOAS V1.0 and Brewer TCO from Hohenpeissenberg. Bottom panel: Differences in percent. Orange points mark the three month average in the daily differences and bars the 2σ RMS from taking the mean.

temperature dependence for Brewer standard retrieval [*Kerr et al.*, 1988]. This number was revised to 0.94%/ 10 K [*Kerr*, 2002]. Using a different approach based upon Brewer measurements at Toronto that included ozone temperature retrieval, he found that the temperature dependence is rather negligible (-0.05% / 10 K) at standard Brewer wavelengths. For Dobson instruments the temperature dependence is 1.3%/ 10 K [*Komhyr et al.*, 1993]. The temperature sensitivities cited here apply mainly to direct-sun measurements.

Only very few stations provide simultaneous measurements from Brewer and Dobson spectrometers covering an extended period. Two such stations are Hohenpeissenberg (MOHp), Germany, 47.8° N, and Hradec Kralove, Czech Republic, 50.2° N. Both stations in collaboration act as the Regional Dobson Calibration Centre for Europe. They have been operating a single Brewer and Dobson throughout the GOME period 1995–2003 and this data set is very valuable in evaluating the new GOME algorithm. Because of different wavelengths used in all three instruments GOME, Brewer, and Dobson results may differ.

For both stations a maximum collocation radius of 160 km between the centre of the GOME pixel and station location was allowed and measurements had to take place the same day. At a given day only the closest match within that radius was taken. Brewer and Dobson data were provided as daily averages. All Dobson measurements and the

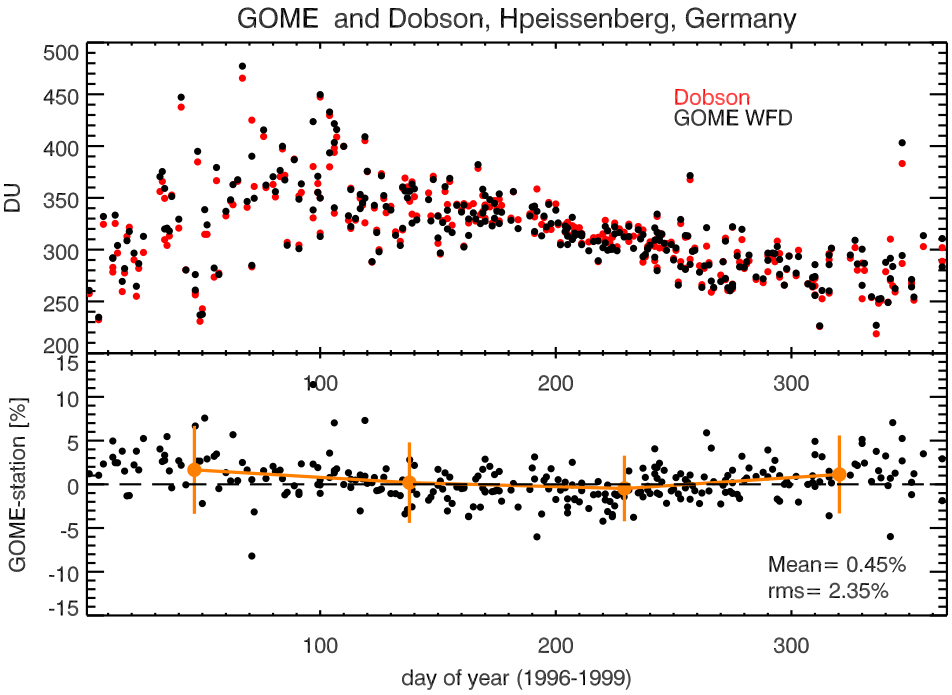

Figure 3.4: Same as Figure 3.3 but shown for collocated WF-DOAS and Dobson measurements at Hohenpeissenberg. Only direct-sun measurements from the Dobson are shown here.

Hradec Kralove Brewer are limited to direct sun measurements that are considered most reliable. Hohenpeissenberg Brewer data also contain zenith-sky measurements.

Figure 3.3 shows the comparison between WF-DOAS V1.0 and Hohenpeissenberg Brewer as a function of the day in the year (1996–1999). The top panels shows the annual cycle of TCO with maximum ozone in spring and minimum in fall, the bottom panel the difference in percent. The WF-DOAS results have a bias of 0.4% and a $\pm$0.5% variability over the annual cycle with slightly higher values in winter (JFM) than in summer/fall.

The comparison of the GOME WF-DOAS V1.0 with the Dobson measurements is shown in Figure 3.4. The RMS scatter in the differences are similar for both Brewer and Dobson data (2.3%). WF-DOAS exhibits a somewhat stronger seasonal cycle of $\pm$1% when compared to Dobson with a maximum of +1.5% during winter and 0% difference in summer. WF-DOAS results appear to exhibit only a very small seasonal variation with respect to the Brewer.

Similar conclusions can be derived from the comparison with the ground-based data from Hradec Kralove. In Figure 3.5 different combinations of differences between satellite and ground-based data are shown. The top two panels show differences of WF-DOAS with respect to Brewer and Dobson, while the lowermost panel depicts the differences between average Dobson and Brewer results from the same day.

The WF-DOAS bias with respect to Brewer is less than 0.2% and a very weak seasonal

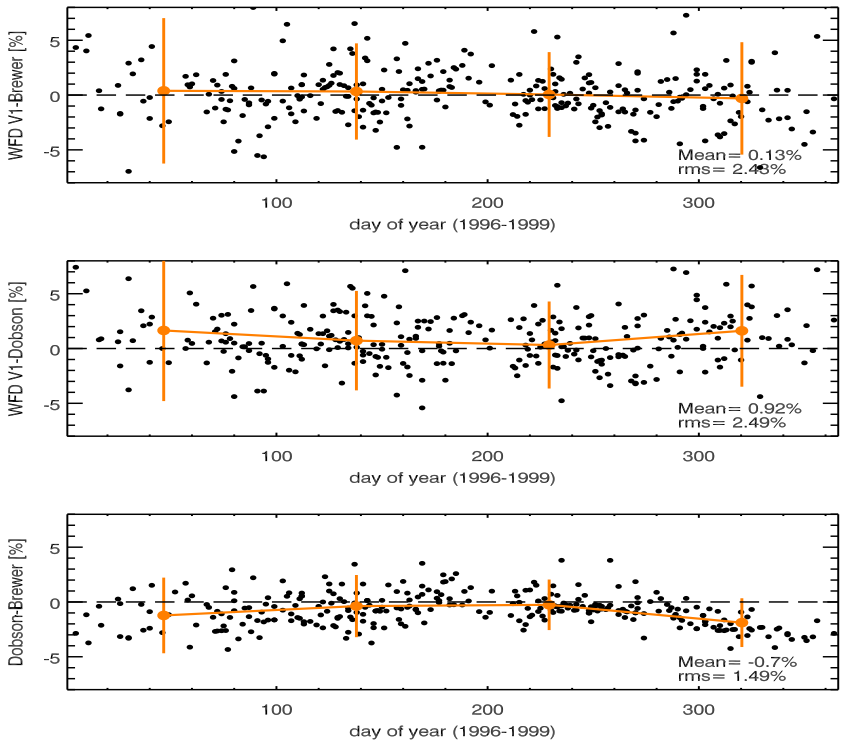

Figure 3.5: Annual course of differences between GOME WF-DOAS V1.0, single Brewer, and Dobson data at Hradec Kralove shown for all possible pair combinations. Top: WF-DOAS minus Brewer. Middle: WF-DOAS minus Dobson, Bottom: Dobson minus Brewer.

cycle of $\pm 0.5\%$ like in the Meteorological Observatory Hohenpeissenberg (MOHp) data is evident here. A somewhat larger seasonal variation is observed if compared to Dobson ($\pm 1\%$). This is in line with the earlier comparison to MOHp. Note that the percentage scale is finer (smaller) in these plots as compared to the MOHp plots; the RMS scatter of the differences remains about the same.

When comparing data from both stations it is noticeable that the Hradec Kralove Dobson is 0.5% lower on average than the same instrument at MOHp. A new set of calibration settings were introduced in Hradec Kralove in 1997 that were not adopted at MOHp [U. Köhler, DWD, personal communication, see also *Staehelin et al.*, 2003] and that may explain this bias. The change in the calibration settings is also noticeable from the long-term times series in the Dobson-Brewer differences at Hradec Kralove that showed less variability in 1996 and earlier [*Staehelin et al.*, 2003, see their Figure 5].

A distinct seasonal cycle in the Dobson-Brewer differences is noticed with maxima in winter and minima (near zero) in summer. The major contribution to this seasonal cycle in Dobson-Brewer differences is due to the use of different wavelength pairs in both instruments to retrieve ozone. Particularly, the D pair ratio of the O_3 cross-sections (317.6/339.8 nm) as used by the Dobson shows the largest temperature dependence of

all ratios used in the standard retrieval by both instruments [*Staehelin et al.*, 2003]. However, a fixed temperature (226.9 K) ozone cross-section is applied in the standard retrieval so that stratospheric temperature variation with season is not accounted for. During winter stratospheric temperatures are well below 226.9 K that may explain the larger differences between Dobson and Brewer. The observed differences between GOME and Dobson are therefore consistent with the expectation from the neglect of temperature corrections in the standard retrieval. Due to the reduced temperature sensitivity of the Brewer wavelengths, it is also not unexpected that GOME WF-DOAS agrees better with Brewer. It should be also noted that the temperature sensitivity is also larger with direct sun than with zenith sky ground-based observations [*Vanicek*, 1998].

3.3.2 Comparison with individual WOUDC stations

Forty-two stations have been selected from the WOUDC data base [*Hare and Fioletov*, 1998; *Fioletov et al.*, 1999] for global validation of WF-DOAS V1.0. The stations are summarized in Table 3.1. Only those stations have been selected that show no larger gaps in time and should not suffer from unreasonable short time jumps and do not have an average bias clearly exceeding 5%. Those excluded were mainly a few Indian stations and Hanoi, Vietnam. Particularly at northern hemispheric mid latitudes, many more stations were available but a fairly even distribution in longitudes were ensured by selecting 19 stations out of this data set. The majority of data are from Dobson measurements. The maximum collocation radius was here set to 300 km (between centre of GOME footprint and station) and only the nearest GOME overpass was used at a given day. The same data set has been used in a recent paper validating the GDP V2.7 data version [*Bramstedt et al.*, 2003]. A change of collocation radius to 300 km rather than 160 km as in the case of the triple comparison presented earlier does not alter the statistics significantly. For each climate zone (in 30° steps) a representative station has been selected and the differences are shown as a function of time from 1996 to 1999 in Figure 3.6. The stations are from north to south; Resolute (Canada, 75° N), Boulder (USA, 40° N), Singapore (1° N), Comodoro Rivadavia (Argentina, 46° S), and Syowa, the Japanese station in Antarctica (69° S). Also shown are the three month mean time series (orange line) in order to visualize possible seasonal variability and a long-term drift in the data. The orange bars indicate the 2σ scatter in the three month mean differences. As with earlier versions of GOME TCO and as shown later for WF-DOAS in Section 3.3.3, the time series of GOME-station differences show no significant long-term drift [*Lambert et al.*, 2002a; *Bramstedt et al.*, 2003].

Both mid latitude stations in both hemispheres as well as the data from Singapore have an average bias over the four year period that is well below $\pm 0.5\%$. Outside the polar regions no significant seasonal signature in the differences is detectable with the exception of Boulder. The Boulder difference series, however, has a distinct seasonal cycle of up to $\pm 1.5\%$ starting in 1997 that is not apparent in 1996. As discussed in the previous section it could be related to the change in calibration settings that many stations introduced to their Dobson spectrophotometers in 1997. The seasonal signature in Boulder is quite similar to that observed with Hradec Kralove and MOHp Dobsons with

Table 3.1: List of WOUDC station data used in the WF-DOAS validation and division into climate zones. The type of instruments are given in the second column: D stands for Dobson, B for Brewer, and F for the M-124 filter instruments.

Station No.	type	Latitude	Longitude	Height[m]	Location
NH polar region					
024	B	74.72° N	94.98° W	65	Resolute
199	D	71.32° N	156.6° W	11	Barrow
105	D	64.82° N	147.87° W	138	Fairbanks
051	D	64.13° N	21.9° W	75	Reykjavik
123	B	62.08° N	129.75° E	98	Yakutsk
043	D	60.13° N	1.18° W	95	Lerwick
NH mid latitude region					
077	B	58.75° N	94.07° W	35	Churchill
143	F	56.00° N	92.88° E	137	Krasnoyarsk
021	B	53.55° N	114.10° W	766	Edmonton
076	B	53.32° N	60.38° W	44	Goose Bay
130	F	52.97° N	158.75° E	78	Petropavlovsk
174	B	52.22° N	14.12° E	112	Lindenberg
053	D	50.80° N	4.35° E	100	Uccle
036	D	50.22° N	5.32° W	88	Camborne
099	D	47.80° N	11.02° E	975	Hohenpeissenberg
277	F	47.73° N	42.25° E	64	Cimljansk
020	D	46.87° N	68.02° W	192	Caribou
119	F	46.48° N	30.63° E	42	Odessa
065	D	43.78° N	79.47° W	198	Toronto
012	D	43.05° N	141.33° E	19	Sapporo
067	D	40.02° N	105.25° W	1390	Boulder
208	D	39.77° N	117.00° E	80	Xianghe
293	D	39.45° N	22.48° E	110	Athens
107	D	37.93° N	75.48° W	13	Wallops Island
158	B	33.57° N	7.67° W	55	Casablanca
Tropics					
031	D	19.53° N	155.57° W	3420	Mauna Loa
187	D	18.53° N	73.85° E	559	Poona
218	D	14.63° N	121.83° E	61	Manila
214	D	1.33° N	103.88° E	14	Singapore
175	D	1.27° S	36.8° E	1745	Nairobi
219	D	5.84° S	35.21° W	32	Natal
084	D	12.42° S	130.88° E	31	Darwin
191	D	14.25° S	170.56° W	82	Samoa
200	D	22.68° S	45.00° W	573	C. Paulista
SH mid latitude					
027	D	27.42° S	153.12° E	18	Brisbane
343	D	31.38° S	57.97° W	31	Salto
091	D	34.58° S	58.48° W	25	Buenos Aires
253	D	37.80° S	144.97° E	125	Melbourne
256	D	45.06° S	169.70° E	370	Lauder
342	D	45.78° S	67.5° W	43	C. Rivadavia
339	D	54.85° S	68.31° W	7	Ushuaia
Antarctica					
233	D	64.23° S	56.72° W	196	Marambio
101	D	69.00° S	39.58° E	21	Syowa
057	D	73.51° S	26.73° W	31	Halley Bay
268	D	77.83° S	166.68° E	250	Arrival Heights

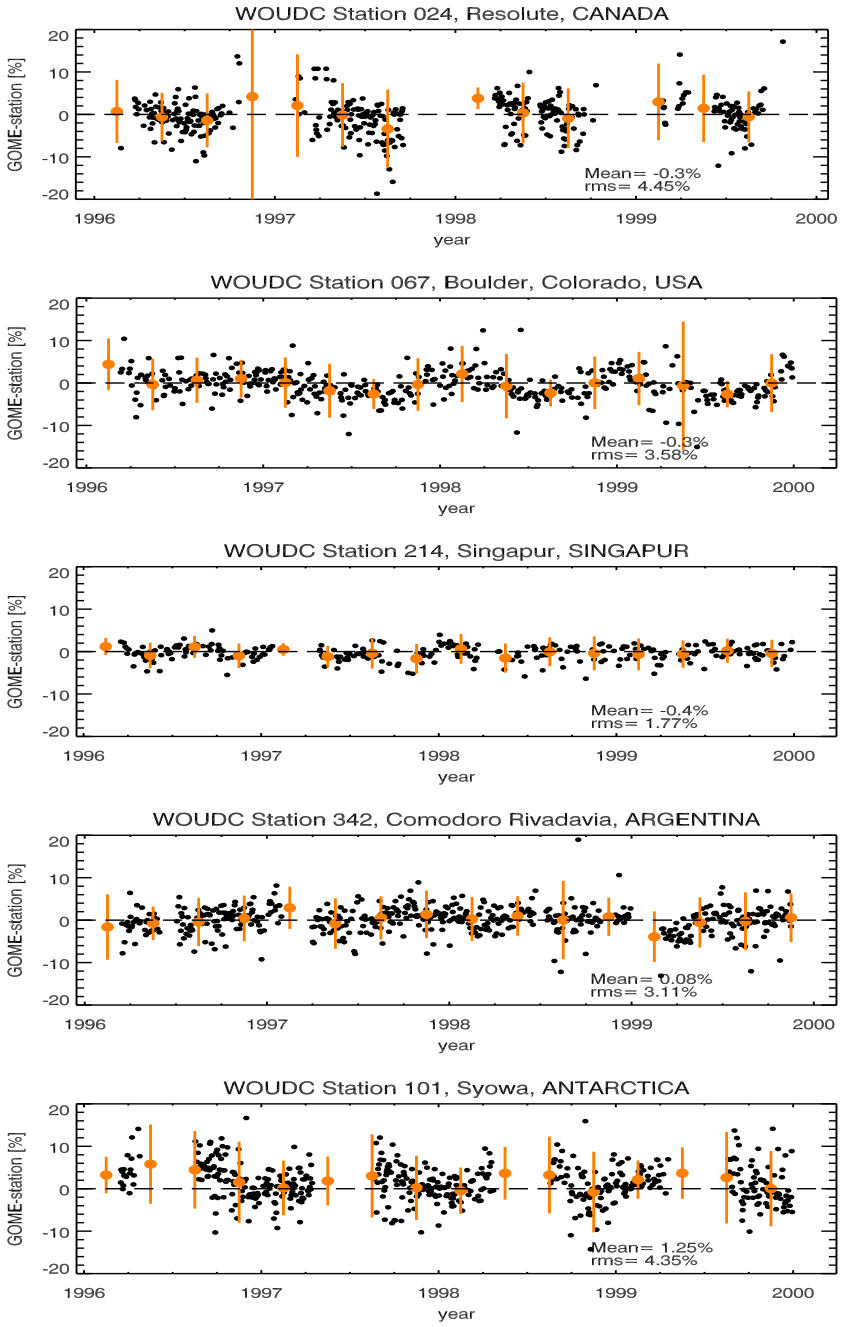

Figure 3.6: Daily differences between collocated GOME WF-DOAS V1.0 and various ground stations distributed from north to south between 1996 and 1999. Orange points mark three month averages and error bars the 2σ RMS in the observed differences. All station data are from Dobsons except for Resolute that are Brewer measurements.

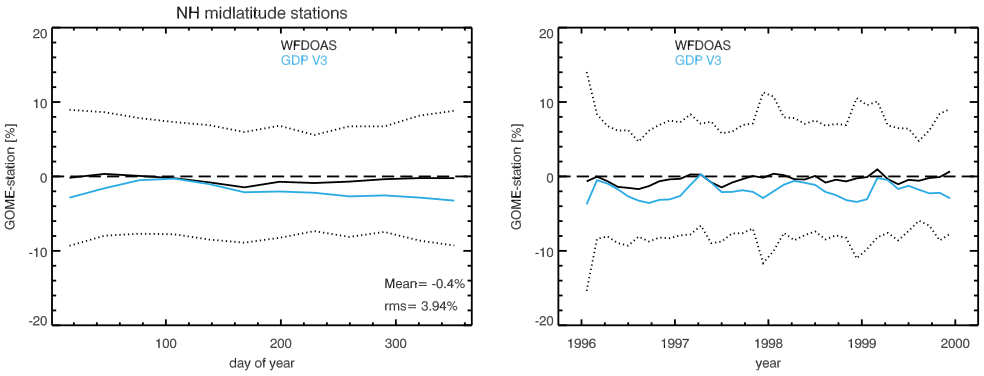

Figure 3.7: Average of WF-DOAS V1.0 and GDP V3.0 differences to nineteen NH mid latitude WOUDC stations: 1996–1999. Left: annual course, right: all years. The dotted lines show the 2σ RMS in the WF-DOAS differences to the ground data from averaging.

maximum in northern hemispheric winter (January, February, March) and minimum in summer (July, August, September).

In Comodoro Rivadavia, Argentina, a seasonal signature is not clearly discernible, except for occasional larger deviations that are not repeated in other years. This is most likely related to interruptions in measurements in southern hemispheric summer (January, February, March), so that only few data contributed to the three month average as in 1997 and 1999.

The two stations in the south and north polar regions, Syowa and Resolute, show a distinct annual cycle in the GOME-ground station differences. Average differences in spring/summer are quite low (below 1%) but can increase to +5% close to the polar night terminator. It is noted that this pattern is symmetric about the polar night period, although TCO under ozone hole conditions in spring is much lower than in fall. The large gradients in ozone observed near the polar vortex edge is responsible for the larger scatter in the southern hemispheric (SH) spring, because both GOME and surface instrument do not look at the same airmass. In fall 1997 the scatter in the differences to the Resolute Brewer data is quite large as expressed by the huge vertical bar in Figure 3.6. This is due to some outliers and due to the fact that close to the polar night period only few data are contributing to the three month mean. In Section 3.3.4 the validation in polar regions and under ozone hole condition is discussed in more detail.

3.3.3 Validation at low to middle latitudes

For a statistical analysis WF-DOAS TCO has been compared with ground based data from 42 stations as listed in Table 3.1. The comparisons have been separated according to climate zones: high latitudes (60° -90°) and mid latitudes (30° -60°) in each hemisphere and tropics (25° S - 25° N) according to the grouping of stations as shown in Table 3.1 . Figures 3.7 to 3.8 show the summary of the comparisons between WF-DOAS and ground based data in each climate zone except for the high latitude results that are presented in

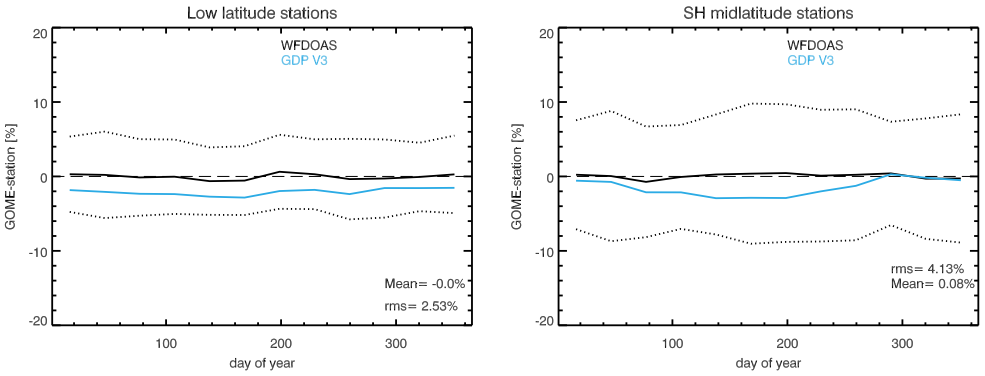

Figure 3.8: Annual course of differences between GOME and ground stations for tropics (left) and SH mid latitudes (right). The dotted lines show the 2σ RMS in the WF-DOAS differences to the ground data from averaging.

the next section. The dotted lines in those figures show the 2σ spread from averaging over all differences between collocated satellite and ground data. For documenting the improvement achieved with WF-DOAS, the same comparison has been made with the operational GOME Data Processor Version 3.0 (short: GDP V3.0) that are shown in blue in Figures 3.7– 3.8. A detailed description of GDP V3.0 can be found in *Lambert et al.* [2002a].

A plot summarizing the comparison between different satellite analyses, WF-DOAS and GDP V3.0 with nineteen mid latitude stations is shown in Figure 3.7. The average annual bias is -0.4% for WF-DOAS. A small seasonal variation of about $\pm 0.5\%$ can be seen, with maximum differences in winter and minimum difference in summer statistically confirming the results from the individual station comparison. The GDP V3.0 shows an annual variability of $\pm 1\%$ with a bias of around -1% with respect to the station data. However, the maximum and minimum in GDP V3.0 differences are shifted towards spring and fall, respectively.

By looking at individual mid latitude stations, it can be noted that for some stations the seasonal variation in the differences is absent (e.g. Dobsons in Uccle, Belgium, and Lauder, New Zealand), while for other stations a weak seasonal cycle is observed with WF-DOAS. In order to see the effect on the statistics by selecting different stations, the comparison has been limited to eight European stations (Arosa, Lindenberg, Potsdam, Hohenpeissenberg, Hradec Kralove, Uccle, Camborne, and Oslo) and Russian stations that mainly operate the so-called M-124 filter spectrometers to measure ozone [*Gushchin et al.*, 1985] have been excluded. Almost no seasonal variation is observed in the WF-DOAS mean differences to the European stations, while the seasonal cycle in the GDP V3.0 differences still remains as shown in Figure 3.9.

The annual course of the GOME differences to the ground-based data for tropical and SH mid latitude stations (see Table 3.1) is shown in Figure 3.8. The SH mid latitude differences show a similar pattern (now shifted by six month) as observed in the northern hemisphere (NH, see Figure 3.7). The WF-DOAS differences like in the NH mid latitudes show no significant annual cycle. The mean bias in low and mid latitudes is less than

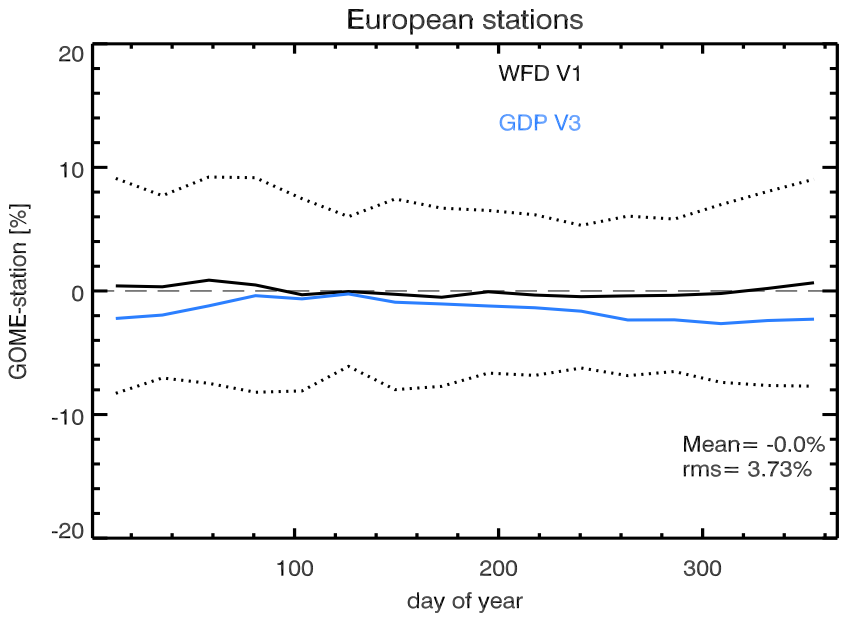

Figure 3.9: Same as Figure 3.7, but for eight European stations (Arosa, Lindenberg, Potsdam, Hohenpeissenberg, Hradec Kralove, Uccle, Camborne, and Oslo), see text for further details.

0.5% for WF-DOAS V1.0.

The insignificant seasonal variation observed in the WF-DOAS differences at mid latitudes is in contrast to the conclusion from the triple intercomparison involving collocated Brewer and Dobson data, where a distinct seasonal cycle signature is expected from the lack of ozone temperature correction in the ground based data retrieval. One should keep in mind that other factors influence Dobson results such as stray light errors (reduces retrieved total ozone) and environmental settings (affecting stray light levels) that may differ from station to station. As pointed out earlier, the ozone temperature correction is more important in direct sun measurements than for zenith sky measurements that are also included in the WOUDC data. An important result from this validation is, nevertheless, that the seasonal dependence in the GOME-ground based data differences is quite small and gets smeared out when averaged over many stations. This is a large improvement compared to GDP V3.0 that shows a distinct seasonal signatures at mid latitudes that does not average out. Both retrievals, WF-DOAS and GDP V3.0, use the TOMS V7 profile shape climatology (GDP V3.0 uses the climatology for airmass factor calculation). The big improvement in WF-DOAS retrieval is that the TOMS V7 ozone profile shape climatology is also used to determine the varying ozone dependent contribution to the rotational Raman correction that is neglected in GDP V3.0.

A long-term comparison has been carried out with Dobson data from Lauder, 45° S, and Brewer data from Hohenpeissenberg, 48° N. The WF-DOAS time series along with the Lauder Dobson data is shown in Figures 3.10 and 3.11. The Hohenpeissenberg time series has been shown in Figure 7 of *Coldewey-Egbers et al.* [2005]. All Lauder

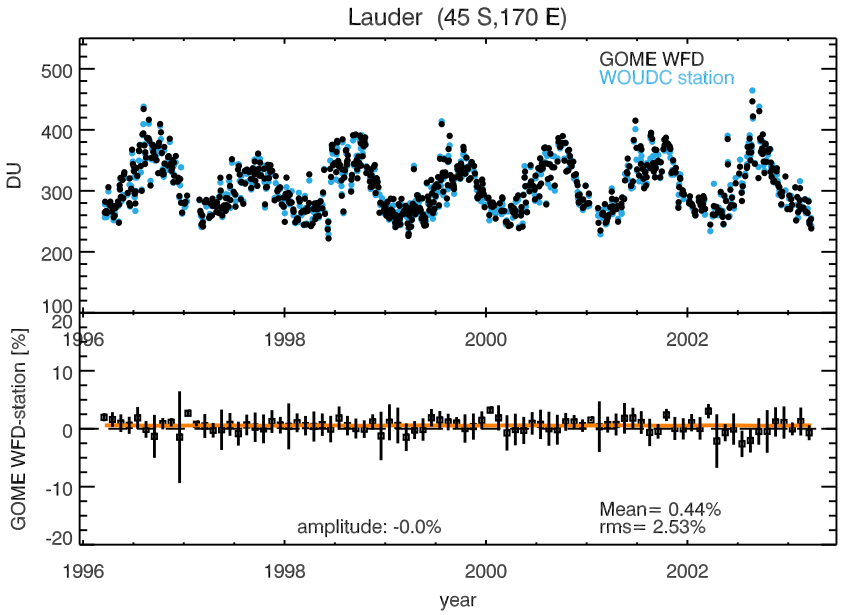

Figure 3.10: Long-term comparison between GOME and Lauder Dobson from 1996 to 2003. Top: daily collocated GOME WF-DOAS (black) and Dobson data (blue) time series. Bottom panel: monthly mean differences between WF-DOAS and Lauder Dobson in percent. Vertical bars indicate the 1σ RMS of the daily differences. Orange lines in bottom two panels show the cosine fit to the data to determine the amplitude of the seasonal variation. The amplitude of the cosine term is about 0% for GOME WF-DOAS.

measurements from zenith-sky and direct-sun ground based data have been included. Apart from a bias of +0.4% for the entire time period (identical to the bias observed in Hohenpeissenberg), no significant seasonal variation, like in the comparison with Hohenpeissenberg, is seen in the comparison with WF-DOAS V1.0. Lower stratospheric temperature seasonal variation is quite small in this region (below 5 K over the course of the year), such that the lack of seasonal variation in the differences between WF-DOAS and Lauder Dobson is not surprising. Figure 3.11 shows the same comparison but with GDP V3.0where a distinct seasonal cycle is evident for all years. The amplitude from fitting a cosine curve (solid orange line) is 1.7%. For Hohenpeissenberg the amplitude was found to be 1.4% for GDP V3.0 (not shown). From this limited comparison (two stations) up to 2003, it can be concluded that the DOAS retrieval in low to middle latitudes does not suffer from the optical degradation that have altered the radiometric accuracy of the GOME instrument particularly in later years [*Tanzi et al.*, 2001].

3.3.4 Validation in polar regions

Six stations in the north polar region and four stations on Antarctica have been selected for validating polar ozone from GOME (see Table 3.1). Figure 3.12 shows the results

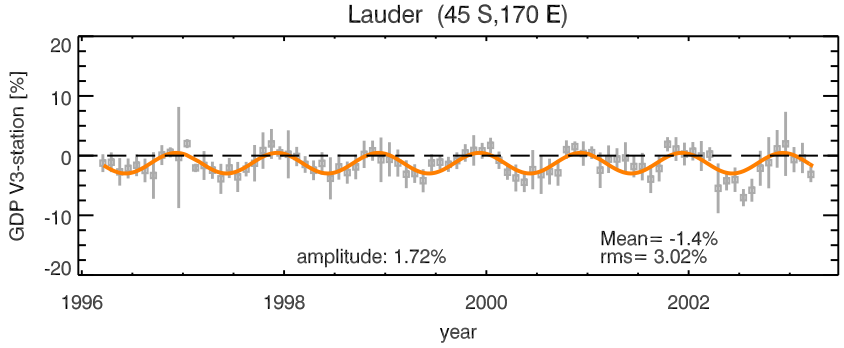

Figure 3.11: Same as Figure 3.10 but for GOME GDP V3.0. The amplitude of the cosine term is 1.7% for GDP V3.0.

from the southern hemispheric polar region. The southern polar data show on average a difference of four percent with respect to ground-based data near the polar night period, in some years it can reach on average 10% like in Antarctic spring 1998. This comparison is difficult since solar elevation angles are low and large ozone gradients near the polar vortex edge, that delineate a cold region where the ozone hole resides, lead to huge scatter in the RMS which can reach a 2σ value of 40% depending on individual stations. Over the annual cycle the average bias is about 0.5%. Comparing these results with GDP V3.0, one notes that the behaviour near the polar night period is similar for both data versions and, on first sight an improvement by WF-DOAS seems only marginal. It is evident that the RMS scatter in the differences is smaller with WF-DOAS during austral summer than with GDP V3.0 and the bias to the station data is lower. Overall, the GDP V3.0 data seem to be lower than WF-DOAS by about 2% throughout the year. From this view point an improvement with WF-DOAS is evident, but the larger discrepancy to ground data near the polar night region (and at high solar zenith angle) remains.

Similar arguments apply to NH polar stations but not as extreme as in the SH (see Figure 3.13) due to the absence of the ozone hole regularly observed in the SH. The seasonal variation in the differences for both WF-DOAS and GDP V3.0 is very similar to the one observed at mid latitudes with minium differences in summer and maximum differences in winter, but enlarged. Like at mid latitudes the minimum differences are shifted from summer to fall for GDP V3.0. It is known that the NH polar ozone shows large interannual variability inside and outside of the polar vortex [see for instance *Weber et al.*, 2002, 2003]. The Arctic winter 1997/1998, 1998/1999, 2000/2001 to 2002/03 have been rather warm stratospheric winters with high ozone well beyond 500 DU, while 1996/1997 and 1999/2000 were cold stratospheric Arctic winters with lower winter TCO levels [*Weber et al.*, 2002]. The differences to the station data during Arctic winter/spring are highly variable, exceeding +10% on average in early 1996 and can be as low as +2% in 1997. A clear trend with time is not observed. It appears that at low solar elevation and higher TCO the winter differences are on average closer to 5% (1998/1999 and 2000/2001) and otherwise in most cases closer to +2 to +3%.

At low solar elevation Dobson instruments suffer from forward scattered stray light

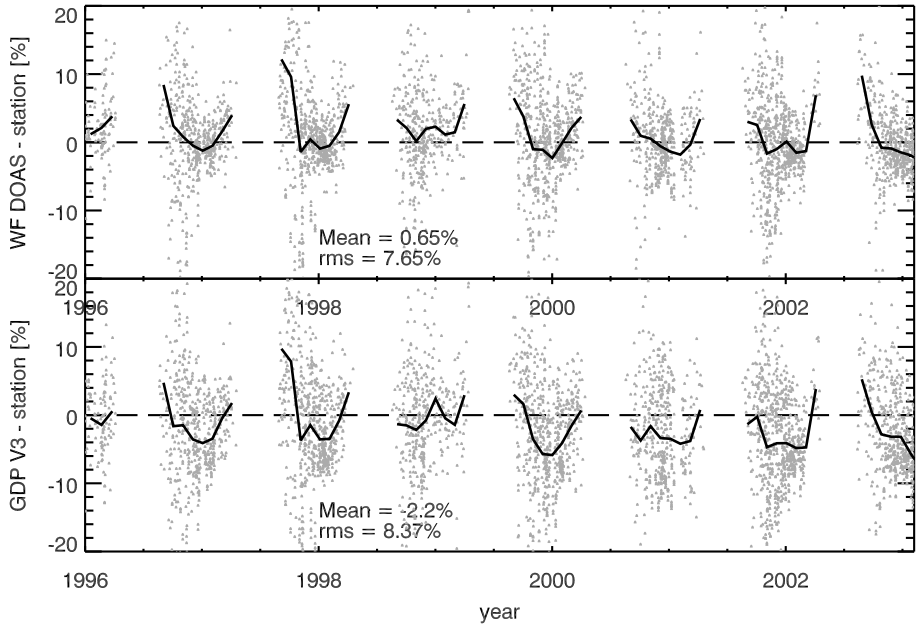

Figure 3.12: WF-DOAS minus Dobson (top) and GDP V3.0 minus Dobson (bottom) from 1996 to 2003 for four SH polar stations: Arrival Heights (78° S), Halley Bay (74° S), Syowa (69° S), and Marambio (64° S). Individual collocations (grey dots) as well as monthly mean differences (solid line) are shown.

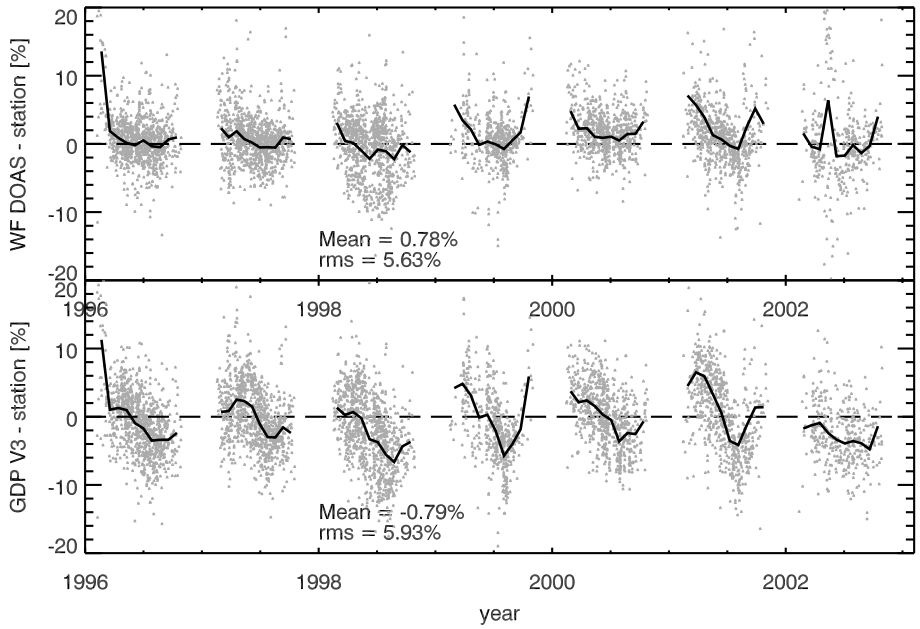

Figure 3.13: WF-DOAS minus Dobson (top) and GDP V3.0 minus Dobson (bottom) from 1996 to 2003 for NH polar stations as listed in Table 3.1. Individual collocations (grey dots) as well as monthly mean differences (solid line) are shown.

and therefore may underestimate the total column. For UV observing satellites like GOME the intensity of the observed scattered light and the signal-to-noise decreases and, therefore, satellite retrieval errors also get larger. Since GOME generally uses larger wavelengths in their retrievals compared to Brewer/Dobsons, the intensity reduction may be lower than for the ground instruments. It is, however, generally difficult for UV/vis instruments to operate in near twilight condition. To reach a better understanding of differences between satellite (TOMS) and ground-based instruments at high-latitudes a measurement campaign involving two Dobson and three Brewer instruments, including single and double Brewers, were carried out in Fairbanks, Alaska, in March/April 2001. Against the travel world standard (Instrument D83, AD pair, direct sun), all Brewer instruments as well as integrated sonde profiles have shown a percent difference of +3 to +4% with respect to the world standard [*Staehelin et al.*, 2003] after careful straylight corrections and ozone temperature corrections applied. The Fairbanks direct-sun Dobson results showed a difference of -1.3% using the AD pair and, when using proper ozone temperature and the CD Pair, a +3.5% difference with respect to D83 was found. From Figure 3.13 it can be seen that in March 2001 the average difference between WF-DOAS for all Arctic stations was on the order of +2 to +4%, that is comparable to the differences observed in the modified Brewer/Dobson retrievals during the TOMS3-F campaign. From a temperature sensitivity of 1.3% /10 K in the Dobson retrieval and a seasonal variation of about 30 K in the lower stratosphere a 3-4% differences could be expected between WF-DOAS and Dobsons and also, possibly, between Brewers and Dobsons at high latitudes. This suggests the missing ozone temperature correction and stray light issues as a possible explanation for the observed positive bias in WF-DOAS differences under low solar elevation condition.

Of particular interest in TCO monitoring is the development of the Antarctic ozone hole from year-to-year. In the WOUDC statistics four stations from Antarctica have been included for the SH polar stations. It was found that close to the polar night period GOME WF-DOAS V1.0 as well as GDP V3.0 can be up to 10% higher on average than ground based Dobson. However the variability of the differences is also very large, so that the differences observed may be also to a large extent depend on the station. In Figures 3.14 and 3.15 the results from GOME WF-DOAS and Dobson comparison for each of the four Antarctic stations, Syowa, Halley Bay, Marambio, and Arrival Heights, are shown as a function of solar zenith angle and GOME TCO, respectively. Also depicted are the results for GDP V3.0 in the bottom panels of each figure. Compared to GDP V3.0 the WF-DOAS differences show a fairly weak dependence to solar zenith angle and total ozone. Looking at the solar zenith angle and TCO dependence in the NH polar regions as shown in Figures 3.16 and 3.17, respectively, the improvement achieved by WF-DOAS becomes even more striking. The reduced dependence on TCO and solar zenith angle also confirms the observation of weaker seasonal variation in WF-DOAS differences to ground data. Nevertheless, both WF-DOAS and GDP V3.0 retrievals are higher than ground based data near the polar night period that may only to some extent be explained by the problems associated with the standard retrieval applied to ground data.

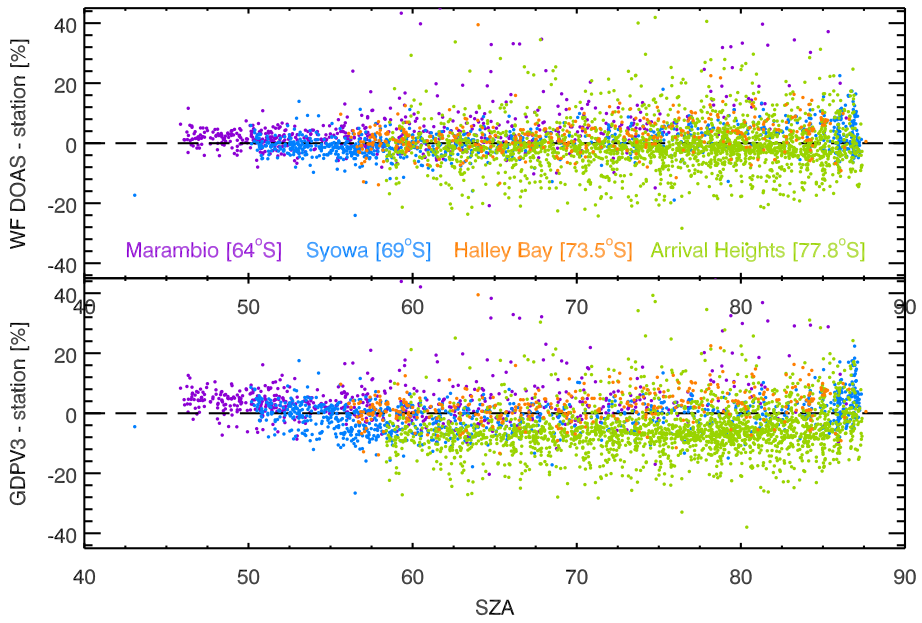

Figure 3.14: WF-DOAS V1.0 minus Dobson (top) and GDP V3.0 minus Dobson (bottom) as a function of solar zenith angle for four SH polar stations: Arrival Heights (78° S), Halley Bay (74° S), Syowa (69° S), and Marambio (64° S).

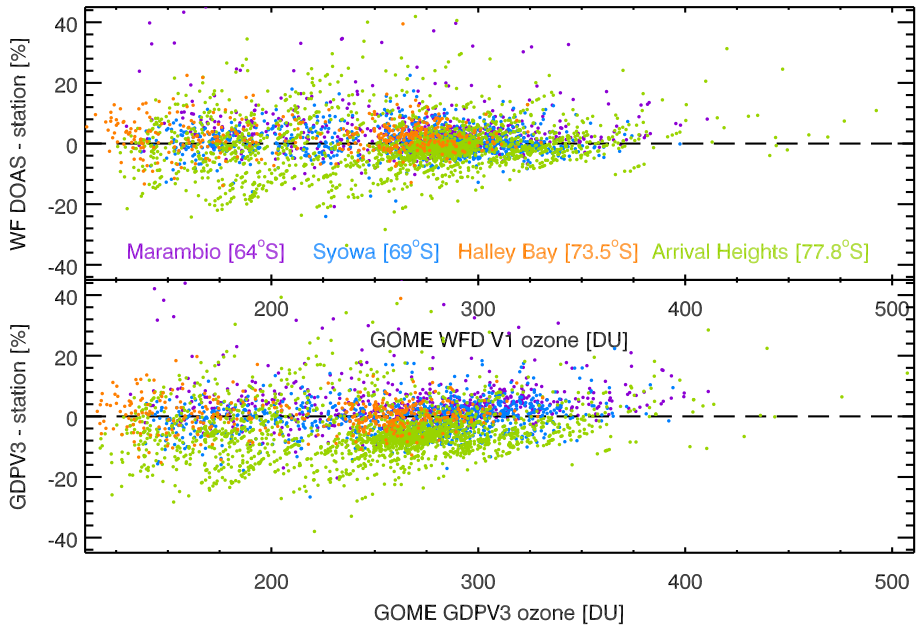

Figure 3.15: same as Figure 3.14 but as a function of retrieved TCO.

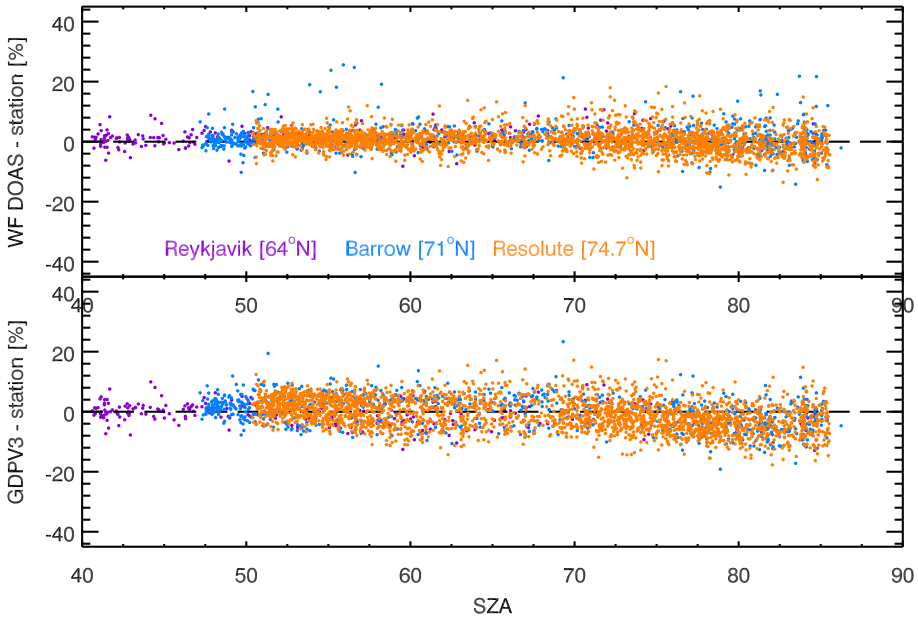

Figure 3.16: WF-DOAS V1.0 minus ground based data (top) and GDP V3.0 - ground based data (bottom) as a function of solar zenith angle for three NH polar stations: Resolute (75° N), Barrow (71° S), and Reykjavik (64° N).

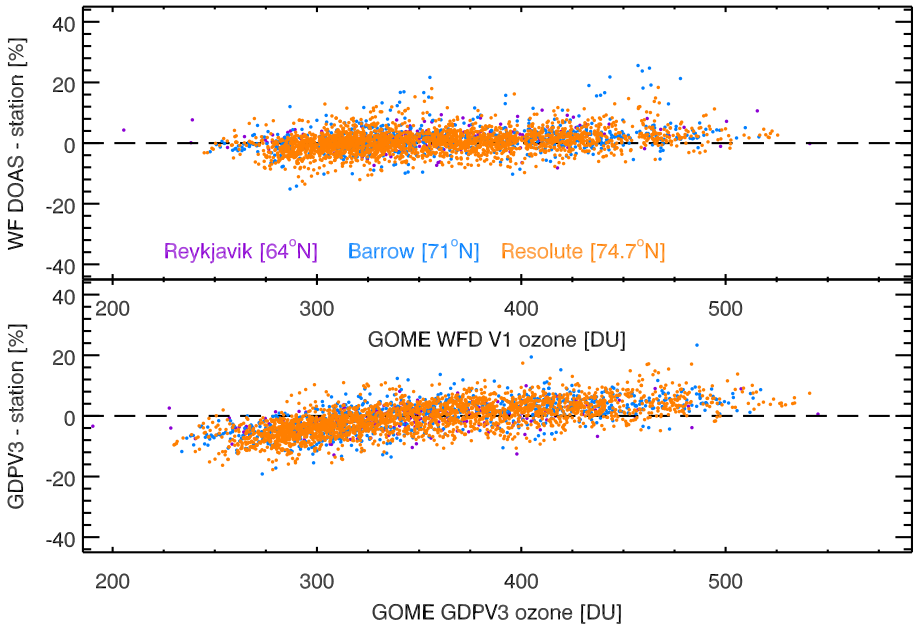

Figure 3.17: same as Figure 3.16 but as a function of retrieved TCO.

3.4 Conclusions

A new TCO retrieval algorithm for backscatter UV satellite instruments, called Weighting Function DOAS, has been developed. The TCO retrieval is based on a comparison between the measured normalised radiance and the radiances derived by radiative transfer calculations. By using wavelength dependent vertically integrated ozone weighting functions, a direct retrieval of vertical column amounts rather than slant columns is possible. Other features of the algorithm include the incorporation of cloud parameter and effective albedo directly derived from GOME measurements. The algorithm accounts for the ozone filling-in as part of the Ring effect, that can lead to systematic underestimation of several percents otherwise.

The new WF-DOAS algorithm for GOME has been extensively compared with globally distributed ground-based data, predominantly Dobson spectrophotometer data. In mid latitudes it agrees on average to within half a percent with WOUDC data. A small negligible seasonal variation of less than $\pm 0.5\%$ is noted, with a maximum in the differences in fall/winter and a minimum in spring/fall. At several mid latitude stations, e.g. Lauder and Uccle, no seasonal variation is observed. GDP V3.0 clearly shows a larger and persistent annual variation ($\pm 1\%$) but the maximum in the differences is shifted towards spring (minimum in fall). No major changes are observed with the new WF-DOAS in the tropics, a constant bias between WF-DOAS (below +1%) and GDP (about -1%) with respect to the ground-based data throughout all years are observed.

In polar regions (both hemispheres) larger positive differences are observed with WF-DOAS close to the polar night period (on average about +4%). If comparisons are made near the polar vortex edge errors can get quite large (up to 40% above Antarctica). If both GOME and the station are well inside the ozone hole it appears that the differences are below 5%. Compared to GDP V3.0, WF-DOAS shows large improvements as evident in weaker solar zenith angle and TCO dependence in the differences to the ground data at high latitudes.

The comparison with Brewer instruments at Hradec Kralove and Hohenpeissenberg has demonstrated excellent agreement with WF-DOAS. The maximum in the differences between GOME and Dobson and to a lesser extent with Brewer is related to the fixed ozone temperature used in the standard retrieval of ground based instruments. Brewer-Dobson differences can be as high as $\pm 2\%$ (generally on the order of 0.5%). This variability gets maximum at high latitudes due to lower solar elevation and the enhanced stray-light problem associated with it. The Fairbanks campaign TOMS3-F, where differences of up to 3–4% between ozone temperature corrected Brewer and standard Dobson were measured in late winter, seems to support this conclusion [*Staehelin et al.*, 2003]. The closer agreement of WF-DOAS with Brewer than simultaneous Dobson data confirms that the temperature shift weighting function appears appropriate to account for the ozone temperature variation.

Overall it can be concluded that the accuracy of the WF-DOAS V1.0 results are now within the uncertainty of the ground-based measurements that make GOME data very attractive for evaluating ground-based network data. The very good agreement with ground based instruments are proof that several issues that has been newly introduced

in WF-DOAS V1.0 have significantly improved TCO retrieval and they are listed here in order of importance: 1) variable ozone filling-in as part of the Ring effect, 2) the introduction of an effective scene height from cloud information and 3) derivation of an effective scene albedo from the GOME spectral measurements. The strong dependence in the GOME-Dobson differences in prior versions [*Bramstedt et al.*, 2003] on cloud cover has been significantly improved (not shown here). These changes are, however, not specific to the type of algorithm that has been used here but can be potentially applied to other retrieval schemes as well. The WF-DOAS theoretical approach by expanding the differential optical depth equation in a Taylor series is a straight forward formulation of the DOAS inversion and is applicable in a more general way than the standard DOAS approach that uses airmass factors to correct for the slant path geometry like in earlier GOME versions. This algorithm can be also applied to other UV/vis backscatter satellite instruments such as SCIAMACHY [*Bovensmann et al.*, 1999] and OMI [*Laan et al.*, 2000] that measure in continuous scan mode. WF-DOAS V1.0 daily gridded TCO data can be obtained from www.iup.physik.uni-bremen.de/gome/wfdoas.

4 Comparison of GOME WF-DOAS total ozone with Brewer and satellite measurements

4.1 Overview

For quantitative understanding of atmospheric ozone, its measurements are needed. The work of Fabry and Buison on atmospheric ozone measurement in 1920 has grown to a worldwide network through the unprecedented work of Dobson and co-workers [*Dobson*, 1968]. Having about 100 instruments in operation worldwide at present, the Dobson instruments have become the primary standard in ground based ozone measurements [*Bernhard et al.*, 2005]. An overview of the instrument, measurement technique, and measurement errors is given in *Staehelin et al.* [2003]. The fast growing Brewer network with about 130 instruments currently in operation around the world forms another independent data source. The instrument and measurement technique are described in several publications [e.g. *Kerr et al.*, 1981; *Kerr*, 2002; *Staehelin et al.*, 2003]. Other ground based instruments devoted to measure TCO are filter ozonometer [*Bojkov et al.*, 1994], SAOZ/UV-visible and FTIR spectrometers, lidar, and millimeter-wave radiometer [*Lambert et al.*, 1999]. Regular ozone monitoring from satellites dates back to 1978 with Total Ozone Mapping Spectrometer (TOMS) and Solar Backscatter Ultraviolet (SBUV). The Global Ozone Monitoring Experiment (GOME) [*Burrows et al.*, 1999a] has been providing information on TCO from space since 1995 and is the first European satellite instrument dedicated to ozone measurements. This task is continued by other instruments like the Scanning Imaging Absorption Spectrometer for Atmospheric ChartograpHY (SCIAMACHY), Ozone Monitoring Instrument (OMI), and GOME-2 [*Callies et al.*, 2000].

Assesment of long-term trends in ozone requires data from multiple instruments. As an example, in Figure 4.1 the TCO data from three widely used satellite instruments, namely, TOMS, SBUV/SBUV2, and GOME are presented. The combined data from the three TOMS instruments span ozone record from 1979 through 2003 with a short interruption in the data, as marked by a data gap, during 1994-1996. The Version 7 algorithm were used to retrieve TCO from TOMS. Another datasets derived using measurements from the SBUV/SBUV2 and TOMS series is also shown in the figure. Here, the SBUV/SBUV2 and TOMS data belong to the Version 6 and Version 7 algorithms, respectively. The original GOME data and the one corrected with the Dobson measurements were retrieved using the GDP Version 3.0 algorithm. Shown in the figure are the seasonal area-weighted average of TCO for the latitude band of 60°S-90°S. Clearly, some

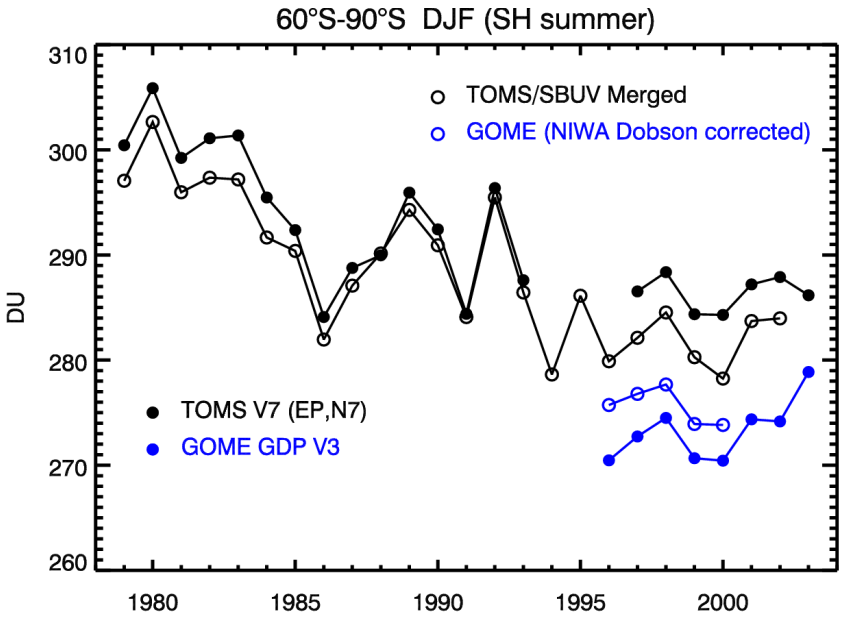

Figure 4.1: Long-term TCO area-averaged over summer months (December, January, and February) for the period 1979-2003 in the southern polar region. Systematic difference is evident among the TOMS V7, the combined datasets from SBUV/SBUV2 and TOMS, the GDP V3.0 TCO data, and the Dobson corrected GOME data.

systematic difference between different datasets are found. A convenient way of estimating and removing such biases is through intercomparison of ozone measurements from various instruments. It follows that comparison of TCO after each algorithm updates is important. This is one of the aims of this chapter. Moreover, the ground-based data might have site- or instrument-specific biases. In particular, having some uncertainty in the calibration of an instrument is not uncommon. Discrepancy exists even between well maintained Brewer and Dobson data. Ozone absorption in Huggins band is temperature dependent but the operational algorithms for ozone retrieval consider a constant stratospheric temperature of -46.3°C [*Staehelin et al.*, 2003]. Higher temperature sensitivity of Dobson measurements, in particular because of wavelength pair D, is one of the important causes for the discrepancy [*Kerr*, 2002; *Staehelin et al.*, 2003; *Weber et al.*, 2005; *Bernhard et al.*, 2005]. Other factors contributing to the difference between Dobson and Brewer measurements are SO_2 interference [*DeMuer and DeBacker*, 1992] and stray light. Brewer spectrophotometer allows simultaneous measurement of SO_2 column amount whereas the Dobson instrument does not. Narrow field of view for Brewer (3° vs. 8° for Dobson) makes it less prone to stray light than the Dobson instrument, that affects the calculated ozone at low solar angles. This effect is more important at mid and high latitude stations. These qualities and its fully automated operation have made the Brewer spectrophotometer valuable. While rapidly

growing, the network of Brewer spectrophotometer lacks transparent and formal calibration procedure and comparable data quality program as that of the Dobson network. The World Meteorological Organization (WMO) organizes calibration and intercomparison for Dobsons but for Brewers such programs are dependent on individual initiative of the operating institutions. Some instruments are known to possess systematic biases due to (a) error in the original calibration and (b) incorrect zenith sky chart [*Fioletov et al.*, 1999] in the Brewer network.

Well-validated ozone products from satellite measurements can be used to identify biased ground-based instruments. Ground-based TCO data archived in WOUDC were reviewed in the past by using TOMS and SBUV data [*Bojkov et al.*, 1988; *Fioletov et al.*, 1999]. In this paper, we will use the GOME TCO derived from Weighting Function Differential Optical Absorption Spectroscopy (WF-DOAS) [*Coldewey-Egbers et al.*, 2005] which is of similar quality as a well-maintained Brewer measurements [*Weber et al.*, 2005] to examine the performance of the Brewer instruments archived in the WOUDC. This work can be considered as the continuation of the work of *Fioletov et al.* [1999] but with data of improved quality. We will also use GOME operational TCO data (version 4.0) [*Roozendael et al.*, 2006; *Balis et al.*, 2006] in our study. Inclusion of additional data set has two-fold purpose. First, similar agreement or disagreement of Brewer data with both GOME TCO will provide more confidence in our evaluation of station data. Second, this will allow us to make a direct comparison of two sets of GOME data retrieved with different algorithms. This kind of quality assessment will be beneficial at improving the accuracy of TCO data.

The structure of this article is as follows. In Section 4.2 various data sets is used in this study are briefly described. Comparison between Brewer and the two GOME algorithms is presented in Section 4.3. This section also shows how the GOME WF-DOAS TCO can be used as a diagnostic tool to monitor Brewer instruments globally. The quality of updated TCO data derived from presently operating satellite instruments namely GOME, TOMS, and SBUV/SBUV2 is evaluated through intercomparison (Section 4.4). The conclusion is given in Section 4.5.

4.2 Data Sets

4.2.1 Brewer

This study uses Brewer data available from the WOUDC where data are reported by the operating institutions. The measurement principle of TCO from the Brewer instrument is already described (see Section 1.3). The measurement principle is same for all three models of the Brewer spectrometer, namely single monochromator MKII, MKIV, and double monochromator MKIII despite having different wavelength coverage and operating procedures. At present, the WOUDC provides daily values of TCO. The TCO can be available as direct sun (DS), zenith sky (ZS), or focused moon (FM) measurements. For cloudy sky conditions TCO is derived from scattered radiation from the zenith direction. DS results are unreliable on cloudy condition and also have larger errors when the sun gets lower. In the present study only DS measurements are considered.

4.2.2 GOME

The GOME TCO data from January 1996 to June 2003 were used for comparison with data from Brewer network. The GOME instrument on board the sun-synchronous polar orbiting satellite ERS-2 having the equator crossing time in descending mode at 10:30 AM has been measuring backscattered radiance of the earth's atmosphere and surface and the solar irradiance, from which atmospheric ozone can be derived. A typical ground pixel size is 320 km $\times$ 40 km and a global coverage was achieved in 3 days until 21 June 2003. The data coverage of GOME is significantly reduced following the failure of the ERS-2 tape recorder on 22 June 2003. For this analysis, the GOME TCO representing a pixel having its center lying within 300 km of a Brewer station for a given day were compared with the daily TCO amount of the station for that day.

The GDP V4.0 TCO data derived by a standard DOAS algorithm are available from the European Space Agency (ESA) web-page at http://earth.esa.int/gome. From validation exercise the GDP V4.0 TCO results lie between -1% and +1.5% of the ground-based values at low and mid latitudes. Another independent algorithm, WF-DOAS which is described in Chapter 3, is shown to provide TCO values with a similar precision to a well maintained ground-based instrument. Both algorithms are reported to have larger biases of up to 5% for high latitudes. The GOME WF-DOAS TCO data are available from the web-page of the University of Bremen at http://www.iup.uni-bremen.de/gome/. Note that for satellite retrievals, a correction is applied to take the effect of cloud into account [e.g. *Coldewey-Egbers et al.*, 2005].

4.2.3 TOMS

This study utilizes the Version 8 TOMS data from Nimbus-7 (October 1978 through May 1993) and Earth Probe (August 1996 through August 2003). Data from Meteor-3 instrument (August 1991 through November 1994) are still only available in Version 7. A comprehensive summary of the new version of the TOMS retrieval algorithm is given in *Bhartia* [2003]. In brief, the Version 8 includes modification from the Version 7 such as inclusion of improved a priori tropospheric ozone, new ozone and temperature profile climatologies, an aerosol and sea glint correction, and off-set correction for the EPTOMS retrievals to remove the scan angle bias.

4.2.4 SBUV

The newly reprocessed Version 8 SBUV combined data set from the SBUV/SBUV2 series of instruments has become available [*Petropavlovskikh et al.*, 2005]. Those instruments flown on the Nimbus-7, NOAA-9, -11, and -16 satellites provide a complete time series between 1979 and 2003. In the new version, the TCO is calculated as the sum of the retrieved profile ozone, unlike from measurements at four wavelengths in its predecessor versions. This makes the TCO less sensitive to variations in surface reflectivity and scattering processes in the troposphere.

4.3 Brewer-GOME comparison

Observations from Brewer instrument were compared with the TCO derived from collocated GOME measurements of the same day. Daily percent differences between GOME overpasses and Brewer observations, defined as $\frac{(\text{GOME}-\text{Brewer})}{\text{GOME}} \times 100\%$, were calculated for both GOME TCO products. The mean bias is calculated from the daily percent differences. The root mean square value of the daily differences is calculated as an indication of variability in the differences. These two terms will be used as a diagnostic tool for quality check of the Brewer data.

4.3.1 Brewer stations

Brewer stations included in this study are summarised in Table 4.1. The stations are sorted according to latitude starting in the northern polar region. Three stations are available from the northern polar region. The northern mid latitude region alone consists of 28 stations. Three stations from the tropics and one from the southern polar region are considered. The majority of the stations (20) use the MKII Brewer spectrophotometer. Fourteen stations use MKIV and MKIII is used only at two stations. The mean bias between the GOME TCO and the Brewer data and the scatter in their differences are presented in the table. Results based on WF-DOAS analysis and GDP V4.0 are shown in separate columns in order to check the performance of two independent retrievals. The bias with respect to both retrieval algorithms are consistent. For about 50% of the stations, the mean bias lies within $\pm 0.5\%$. About 25% stations have somewhat larger bias (i.e. greater than $\pm 1\%$) with respect to the GOME results and remaining 25% of the stations have bias lying between $\pm 0.5\%$ and $\pm 1\%$. The GDP V4.0 results show larger scatter than the WF-DOAS results. The root mean squares (RMS) values based on WF-DOAS analysis are less than 3% for majority of the stations whereas they are less than 4% according to the GDP V4.0 analysis.

The agreement between satellite retrievals and ground-based measurements as shown in the table is very good considering several factors that limit the accuracy of two different observing systems. The quality of satellite retrievals has significantly improved in recent years. The ground based data, in particular from the Dobson and Brewer instruments, can be re-evaluated by comparison with satellite data that may further improve their accuracy. There are several causes that might hamper the quality of ground-based and satellite data. Satellite measurements are less sensitive to the lowest few kilometers in the troposphere and also depend upon the knowledge of true profile shapes of ozone in the entire atmosphere [*Wellemeyer et al.*, 1997; *Lamsal et al.*, 2006]. Cloud effects are another important uncertainty in satellite retrievals. Both WF-DOAS and GDP V4.0 algorithms make similar assumption to deal with its effect. Clouds are treated as a Lambertian surface and the ozone below the surface calculated from a climatology is added in the fitted total ozone results. For this purpose, cloud top height, cloud fraction, and surface altitude need to be accurately known. Inaccuracy in these parameters results in errors in the retrieved TCO. For example, true altitudes of Arosa, J.R.C. Ispra, Sestola, Madrid, and Mt. Waliguan are different than the altitudes that the satellite retrieval

Table 4.1: Results of comparison of Brewer data with GOME TCO. Here WFD and GDP indicate the WF-DOAS and GDP V4.0 results, respectively. Here, topo. indicates the altitude obtained from the topographical data base whereas station means the real altitude of the altitude as obtained from WOUDC.

Stations	lat.	Alt. (km)		difference(%)		RMS(%)		samp.
		topo.	station	WFD	GDP	WFD	GDP	
Resolute	75.25	0.059	0.040	0.21	0.13	3.28	3.52	1196
Sodankyla	67.40	0.261	0.179	-0.39	-1.33	2.80	3.72	844
Vindeln	64.24	0.247	0.225	-0.08	-0.84	3.38	3.83	723
Churchill	58.75	0.076	0.035	-0.06	0.10	3.12	3.44	423
Norrkoeping	58.58	0.061	0.043	-0.51	-0.41	2.96	3.29	644
Edmonton	53.55	0.744	0.766	-0.95	-1.07	3.18	3.42	513
Potsdam	52.22	0.075	o.089	0.50	-0.19	2.91	3.16	526
Lindenberg	52.21	0.077	0.112	0.28	-0.46	2.94	3.02	506
Saskatoon	52.11	0.556	0.530	0.13	0.08	2.54	2.84	402
Debilt	52.10	0.048	0.009	-0.20	-1.18	2.85	2.96	547
Valentia Obs.	51.93	0.010	0.001	-0.15	-0.81	3.09	3.29	545
Belsk	51.84	0.144	0.18	0.94	0.18	2.68	2.73	558
Uccle	50.80	0.138	0.100	2.33	1.24	2.71	2.98	538
Hradec K.	50.18	0.376	0.289	0.24	-0.65	2.49	2.68	586
Winnipeg	49.90	0.309	0.239	0.17	-0.16	2.82	3.14	511
Poprad-Ganovce	49.03	0.446	0.706	1.29	0.75	3.06	3.41	643
Saturna Is.	48.78	0.477	0.178	-0.87	-1.35	2.74	3.18	355
MOHp	47.80	0.977	0.975	0.2	0.05	2.59	3.14	609
Arosa	46.78	1.360	1.840	0.38	0.03	2.31	2.96	627
J.R.C. Ispra	45.80	0.708	0.240	-1.56	-1.86	2.60	3.07	604
Montreal	45.48	0.185	0.031	1.19	0.78	2.94	3.24	337
Longfengshan	44.73	0.374	0.317	0.56	0.13	4.99	5.11	463
Halifax	44.70	0.044	0.050	-0.73	-0.96	3.40	3.38	309
Sestola	44.22	0.370	1.030	0.90	0.30	8.18	8.24	403
Toronto	43.78	0.157	0.158	-0.05	-0.52	2.94	3.25	448
Rome Univ.	40.90	0.233	0.060	-1.59	-1.98	3.55	4.14	581
Thessaloniki	40.52	0.396	0.050	-1.65	-2.31	2.35	2.97	255
Madrid	40.45	0.883	-0.001	-0.96	-1.20	2.55	2.88	407
Murcia	38.00	0.397	0.069	-1.19	-0.25	2.64	2.98	581
Mt. Waliguan	36.29	3.087	3.810	2.47	3.00	3.00	3.28	344
Pohang	36.03	0.109	0.060	-0.60	-0.26	4.88	4.71	306
Funchal	32.64	0.000	0.049	0.09	-0.33	2.23	2.33	500
Delhi	28.65	0.184	0.220	-0.12	-0.36	3.11	3.44	44
Petaling J.	3.10	0.100	0.061	0.39	0.43	1.93	2.59	279
BelgranoII	-77.87	0.275	0.255	1.69	2.25	5.02	5.22	1637

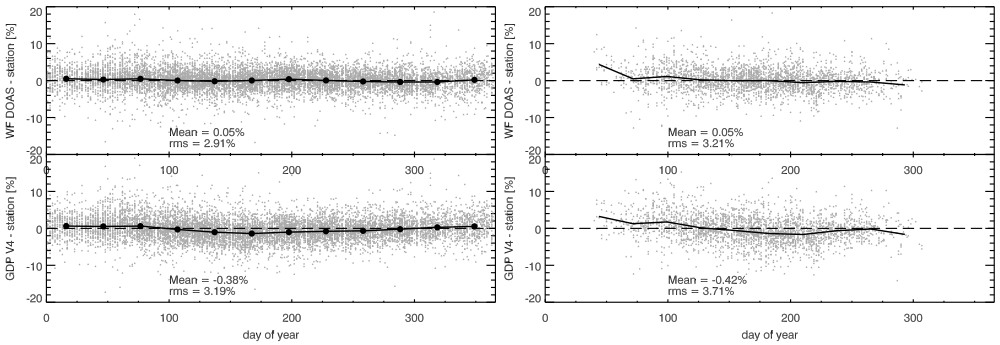

Figure 4.2: Summary plot of the difference between GOME (WF-DOAS and GDP V4.0) and Brewer TCO from northern mid latitude stations (left) and polar stations (right).

algorithms assume (see Table 4.1). The satellite retrieval algorithms use a topographic database for defining the surface altitude. A difference of 0.5 km in the surface can cause a bias of about 1.5 DU in the retrieved TCO. While assessing the Brewer data quality using satellite data these limitations of satellite TCO retrievals need to be considered.

The accuracy of the Brewer data is limited for other reasons. A systematic bias in the Brewer data originates from error in the original calibration. This problem can be resolved through regular calibration against the traveling standard and by comprehensive intercomparison activities with correlative measurements. Another known problem is the use of incorrect zenith sky chart that is used to derive TCO from zenith sky measurements. This, however, is not relevant here since only direct sun measurements are considered. The Brewer data are known to be affected by insufficient treatment of ozone absorption cross-section although to a less extent than the Dobson data [*Bernhard et al.*, 2005]. At high solar zenith angle stray light is another important error source for both satellite and ground-based measurement techniques. The large bias of BelgranoII is related partly to the neglect of temperature dependence of ozone absorption in the standard Brewer algorithm [*Kerr*, 2002] and partly to stray light effect. Another important cause for the difference between satellite and ground based measurements could be the natural difference in altitude seen by the satellite as it looks at a larger area.

4.3.2 Performance of Brewer instruments

Figure 4.2 shows the summary plots of the difference between Brewer and GOME data for 17 mid latitude stations (left panel) and 3 polar stations (right panel) in the northern hemisphere. Those mid latitude stations are: Arosa, Belsk, Churchill, Debilt, Edmonton, Hohenpeissenberg, Hradec Kralove, J.R.C. Ispra, Lindenberg, Montreal, Norrkoeping, Poprad-Ganovce, Potsdam, Saskatoon, Saturna, Toronto, Valentia Observatory, and Winnipeg. The data from these stations are not necessarily agreeing well with the satellite measurements but they do not show sudden jumps in the time series of their differences. The mean offset varies from station to station. These stations have been

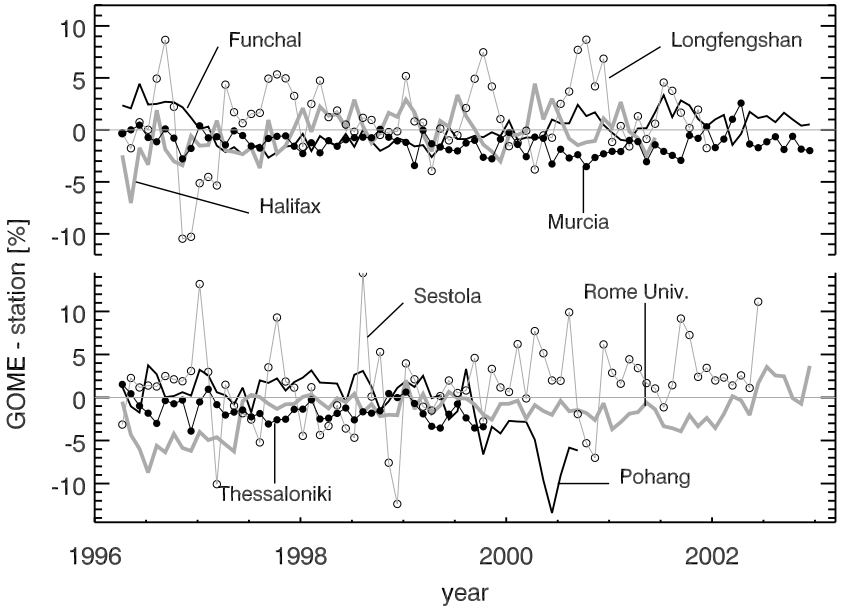

Figure 4.3: Some stations from northern hemisphere which are believed to have some problems in the data quality.

considered in many scientific studies in the past. Resolute, Sodankyla, and Vindeln are the three stations from the northern polar region. In general these stations show good agreement with results from GOME. The summary plots show that the mean offset between Brewer and WF-DOAS data is 0.05% and that between Brewer and GDP V4.0 is about 0.40%. The mean difference smoothed over a month is also shown in the figure. The GDP V4.0 - Brewer differences is characterized by larger RMS and a stronger seasonal cycle of about $\pm$1% for mid latitude stations and $\pm$2% for polar stations. The magnitude of seasonal behaviour is very small with WF-DOAS TCO. Reasons for the stronger seasonal cycle in the difference between the GDP V4.0 and Brewer data is not clear yet but might be related to errors in the treatment of the air mass factor for conversion of the slant column density to the vertical column.

The results presented in Figure 4.2 provide confidence that the two retrieval algorithms for GOME are producing high quality results and indicate that the data quality is sufficient to evaluate the performance of Brewer stations. Eight stations (from the northern mid latitude) with noticeable bias or/and RMS are presented in Figure 4.3. The mean monthly difference is plotted as a function of year. The monthly mean bias for Longfengshan and Sestola is strongly oscillatory and can reach up to $\pm$10% over the entire time period. The Korean station Pohang shows a jump after second half of 1999. The bias increased systematically reaching more than -10% in 2000. Three clear jumps are noticeable for Rome University and Funchal. The reasons for the observed jumps and difference are unclear. The lack of proper documentation of the instrument change or correction methods at each stations makes it difficult to attribute reasons to the ob-

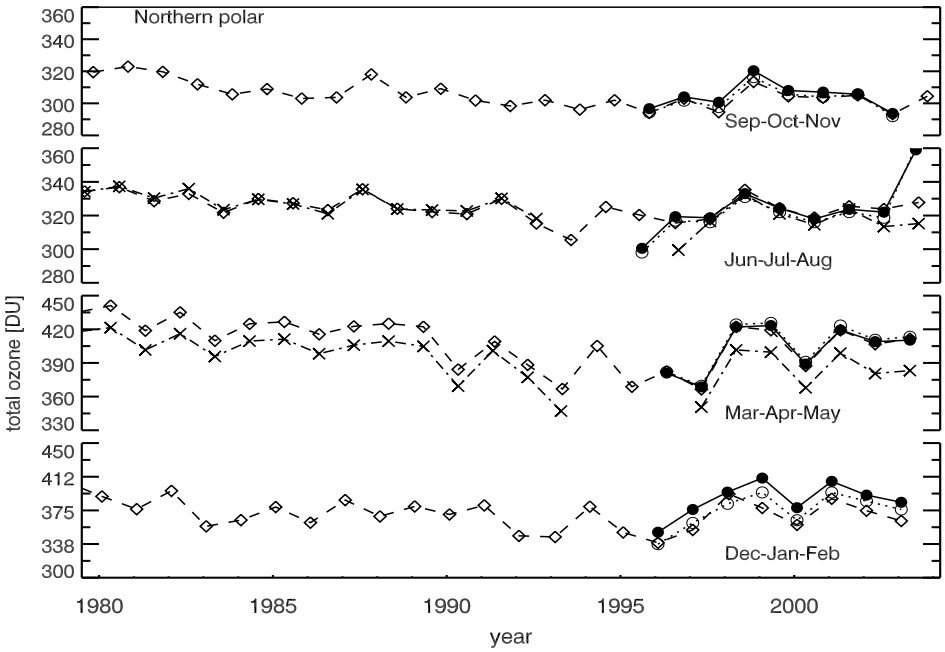

Figure 4.4: Time series of seasonal area weighted TCO for northern polar region (60°N-90°N) obtained from TOMS (dashed-dotted line with x symbols), SBUV/SBUV2 (dashed line with diamond symbols), GOME-WF-DOAS (solid line with filled circles), and GOME-GDP V4.0 (dotted line with open circles). The TOMS data were not available for 1995 and the first half of 1996. The data gaps in SBUV/SBUV2 poleward of 45°S during 1992, 1993, and 1998 are related to the orbital drift of NOAA-9 and NOAA-11

served features.

4.4 Satellite comparison

The objective of this section is to see how the TCO data from TOMS, SBUV/SBUV2, and GOME compare after the recent upgrade of retrieval algorithm for all instruments. This is important because these are the data sets which are going to be used for various scientific studies including trend estimation. A simple way of visualizing this is by plotting time series of TCO from those instruments. The time series are presented for each season of the year. The grouping of month is made as follows: December-January-February, March-April-May, June-July-August, and September-October-November. Such grouping of the months has been used in recent WMO ozone assessments [*WMO,* 1999]. The three month average reflects the seasonal variation in the annual course of TCO.

Figures 4.4, 4.5, 4.6, 4.7, and 4.8 display the area weighted TCO for NH polar (60°N-90°N), NH mid latitude (30°N-60°N), tropics (15°N-15°S), SH mid latitude (30°S-60°S), and SH polar (60°S-90°S) zones in five separate panels. The TOMS time series is affected by periodic data gaps in 1993 and 1994 and absence of data in 1995 and

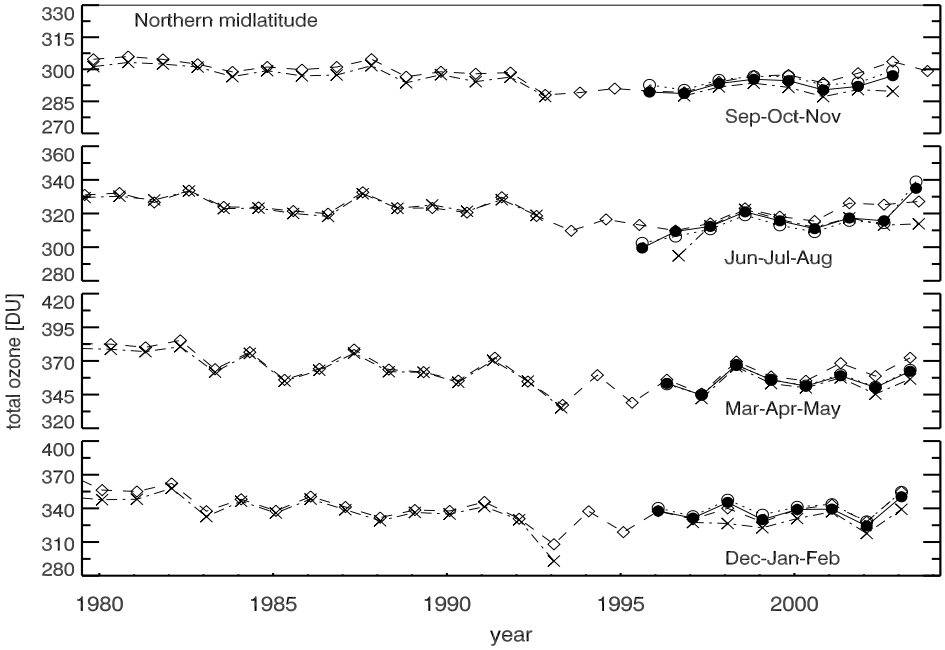

Figure 4.5: Same as Figure 4.4 but for northern mid latitude region (30°N-60°N)

the first half of 1996. It needs to be emphasized that the area weighted GOME TCO for June-July-August of 2003 is in fact the area weighted TCO for June only due to the lack of global coverage after June 2003 and therefore the June-July-August TCO values in the above figure need to be interpreted carefully. The data gaps in the SBUV/SBUV2 time series are associated with SBUV2 data loss poleward of 45°S during 1992, 1993, and 1998 related to the orbital drift of NOAA-9 and NOAA-11. One can observe that the presently available TCO data from various satellite instruments are in good agreement globally except in the winter/spring seasons in high latitudes when the sun is low. There the ozone retrieval is usually complicated [*McPeters and Labow*, 1996; *Weber et al.*, 2005]. Although significantly improved over the earlier data versions (see Figure 4.1), the difference between different data sets seems to have a latitude-dependent systematic bias. The TOMS TCO is too low in most cases. The difference between different data sets, particularly after 2000, can be interpreted as instrumental effects in TOMS [*Bramstedt et al.*, 2003]. Such effect is not observed with GOME WF-DOAS [*Weber et al.*, 2005]. There are uncertainties in instrument calibration. The sensitivity to calibration is reduced in DOAS type retrieval algorithms like for GOME.

In Figures from 4.4 through 4.8 ozone decline can be seen beyond the interannual variability. Usually ozone trends are estimated by eliminating such variability using a statistical model. The variability due to seasonal cycle, QBO, solar cycle related components, and other processes [*Dhomse et al.*, 2006] can be filtered out. All satellite data show a reversal from the long-term downward trend after middle of 1990s at nearly all latitudes.

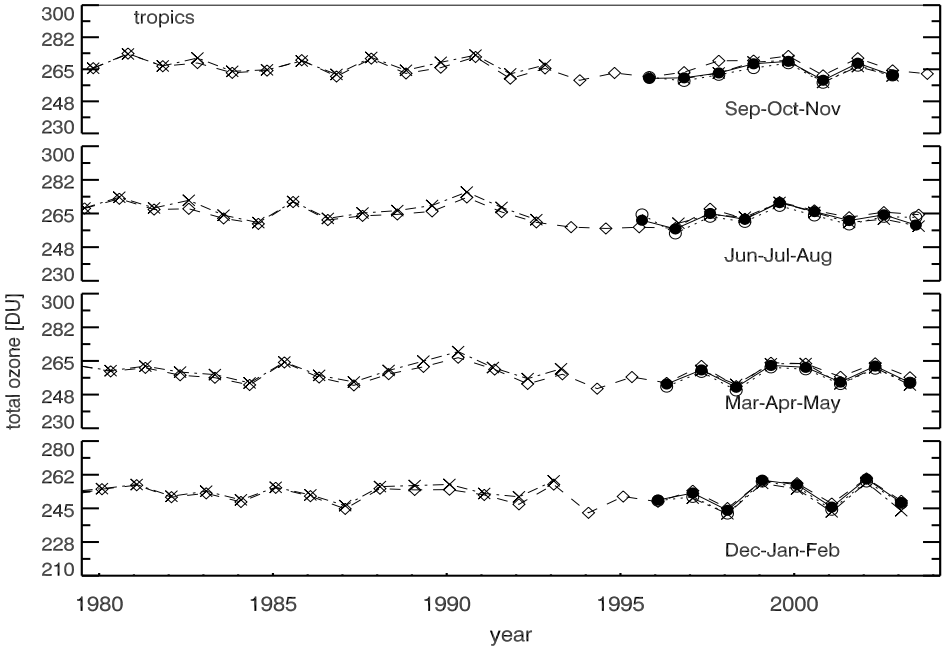

Figure 4.6: Same as Figure 4.4 but for tropics (15°N-15°S)

4.5 Conclusion

25 years of complete ozone data from TOMS and SBUV/SBUV2 reprocessed with their latest version 8 algorithms are now available. Likewise, 10 years of complete GOME data are reprocessed with the latest GDP V4.0 and also with a new and independent algorithm called WF-DOAS. These data sets will be valuable for various scientific studies including upcoming WMO ozone assessment.

This article was devoted to compare the two newly released GOME data sets with the data from Brewer networks, with each other, and with other satellite measurements from TOMS and SBUV/SBUV2. The mean bias between the WF-DOAS TCO and well-maintained Brewer TCO is less than 0.3% and the root mean squares of their difference is less than 3%. The GDP V4.0-Brewer difference shows a stronger seasonal cycle than the WF-DOAS-Brewer difference at mid to high latitudes. With such improved data quality in satellite data, Brewer data quality can be monitored and problems with individual Brewer instruments can be identified. This can also be applied to other ground-based instruments.

Long-term time series of TCO from the last two and a half decade have shown that satellite data from different platforms agree well and are suitable for long-term trend studies. With the recent upgrades the agreement among various data sets has significantly improved. However, further works are still required to improve the quality of satellite and ground-based ozone data from high latitudes.

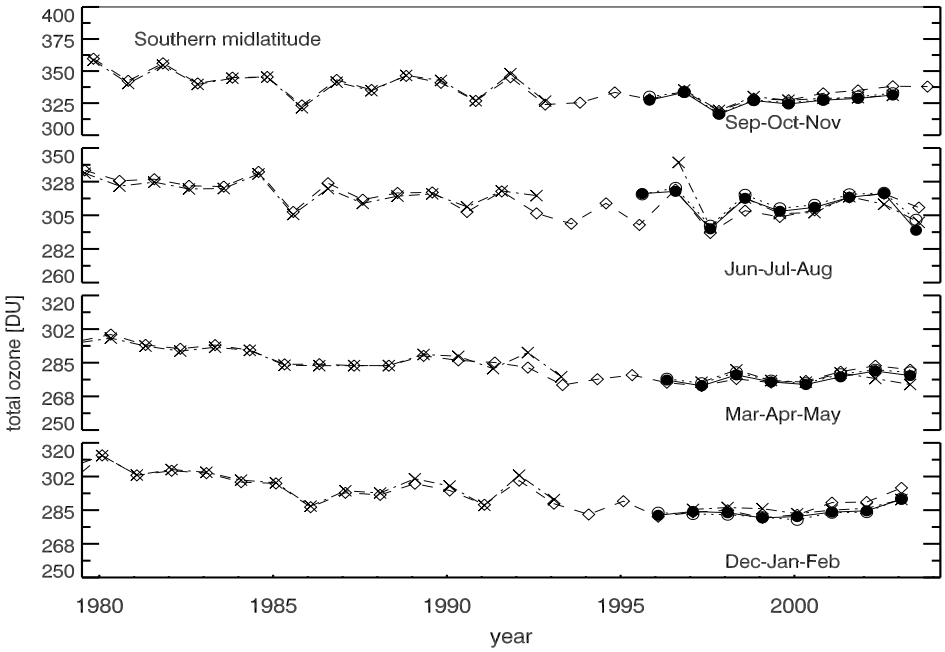

Figure 4.7: Same as Figure 4.4 but for southern mid latitude region (30°S-60°S)

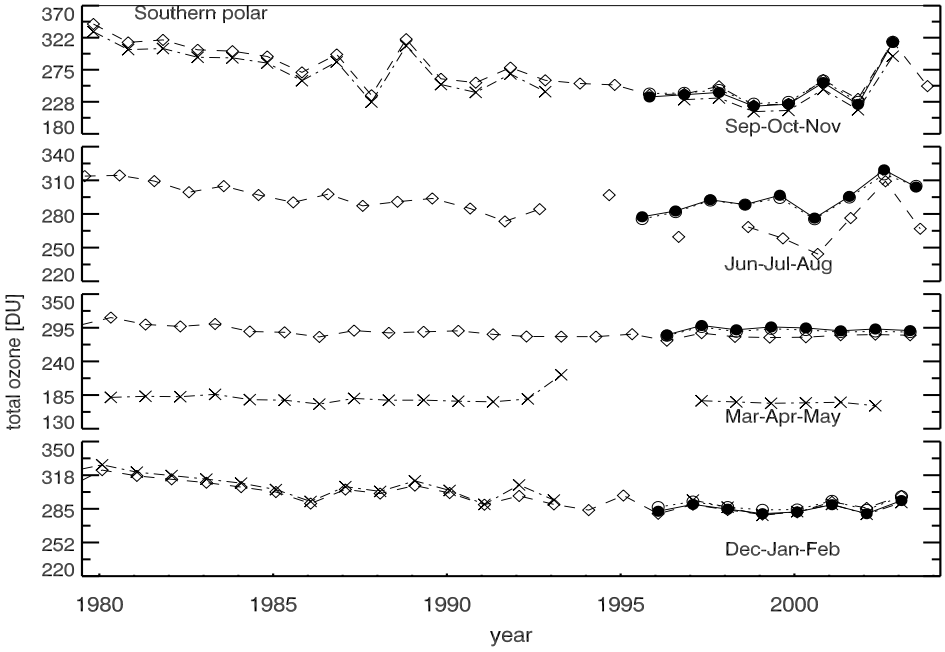

Figure 4.8: Same as Figure 4.4 but for southern polar region (60°S-90°S).

5 Ozone column classified climatology of ozone and temperature profiles based on ozonesonde and satellite data [1]

5.1 Overview

A climatology of ozone is of fundamental importance because it provides information on the mean state and variability (covariance) that can be used either as *a priori* constraint in satellite retrievals or as initial condition for 3-dimensional chemical transport models. In addition, it is a source for comparison with models and retrieved data. Traditionally, climatologies of ozone [e.g. *Fortuin and Kelder*, 1998] and temperature [e.g. *Leblanc et al.*, 1998] are monthly zonal means and in terms of spatial coordinates. Local [e.g. *Yonemura et al.*, 2002], regional, and global climatologies exist. *McPeters et al.* [1997] provided a satellite derived monthly mean zonal mean climatology for the middle and upper stratosphere with the primary purpose of calculating TCOs from balloonsonde measurements. A tropospheric ozone climatology was developed by *Logan* [1999a]. This climatology was based on sonde, surface, and satellite data. It provides the 2-dimensional (latitude and altitude) ozone field at middle and high latitudes, and 3-dimensional (latitude, longitude, and altitude) in the tropics. Aimed for general circulation models, *Fortuin and Kelder* [1998] compiled a 2-dimensional climatology of ozone based on ozonesonde and Solar Backscattered Ultraviolet (SBUV) data over a target period of 1980-1991.

Wang et al. [1995] showed a large longitudinal asymmetry in ozone values. This results in large differences between zonal mean and local values and might cause a bias when zonal mean is used in an atmospheric model or as *a priori* state for inversion. Furthermore, a significant level of information can be lost from zonal averaging in this approach. Thus, the regional and temporal variability in ozone and temperature makes the preparation of a meaningful climatology a challenge. *Wang et al.* [1995] reported a significant improvement in model results by considering longitudinal variation in ozone.

Austin [1998] suggested a climatology in terms of dynamical based coordinates where the author has shown that the small scale features are present in such climatologies. Using TCO as dynamical proxy *Klenk et al.* [1983] derived standard ozone profiles to

[1] This chapter has been published as: Lamsal, L. N., M. Weber, S. Tellmann, and J. P. Burrows (2004), Ozone column classified climatology of ozone and temperature profiles based on ozonesonde and satellite data, *J. Geophys. Res.*, 109, D20304, doi:10.1029/2004JD004680.

use them as *a priori* information for SBUV ozone profile inversion algorithm. For Total Ozone Mapping Spectrometer (TOMS) retrieval, theoretical radiances are computed using standard climatological ozone profiles which were created from Stratospheric Aerosol and Gas Experiment II (SAGE II) and balloonsonde data [*Wellemeyer et al.*, 1997].

Prior knowledge on the state space is an essential part of the optimal estimation method [*Rodgers*, 1976] which is almost exclusively applied for atmospheric observation. Satellite observation that maps the state space into measurement space is an indirect approach of measurement and an inversion process is required for its solution. A finite number of measurements for obtaining a profile (a continuous function) is an underconstrained non-linear problem and standard non-linear least squares methods do not lead to reasonable solutions. The optimal estimation formalism introduced by *Rodgers* [1976] explicitly uses mean and covariance of the *a priori* profile together with the measurement error to constrain a poorly constrained solution space consisting of many possible outcomes. The main aim of an *a priori* constraint is, therefore, to restrict the components of the solution that are in the null space (unmeasurable part of state space) or near null space (e.g. troposphere) of the weighting function matrix. The hidden information of the null space is required to come from the *a priori* information but the components of the state which can be measured well enough are weakly affected by *a priori*. Structures with short vertical scale of variation is not provided by the inverse method but the information at such scales come from *a priori* [*Coe et al.*, 2002]. In order to retain all the information, a fine representation and a realistic *a priori* are needed.

An additional knowledge on the state can also be added as prior information [*Rodgers*, 2000]. Large variances in the *a priori* profile as observed in tropopause region lends no extra information to the inversion. As the monthly mean ozone climatology does not account for interannual variability there is clearly a need to obtain an improved *a priori* climatology, which on one hand represents the large seasonal variability at all altitude levels and, on the other hand, provides variances (and co-variances between altitude levels) which are small enough not to destabilise the retrieval. This can be only achieved by creating a climatology providing extra information about the state, where profile classes are sorted by the information like lower stratospheric potential vorticity (PV) or equivalent latitudes. Strong correlations between TCO and tropopause height [*Appenzeller et al.*, 2000; *Salby and Callaghan*, 1993] and TCO and the height of ozone maximum suggest that TCO, which contains the information of ozone dynamics and chemistry, can also be used as a dynamical proxy. Preliminary studies [*Darmawan*, 2002] have shown a significant reduction in ozone class variances by sorting the profiles by TCO as compared to a monthly zonal mean climatology. Since the use of PV as dynamical proxy can be of problem in the tropics, it is more convenient to use TCO. This has the following advantages: (1) Retrieval process does not require any meteorological data (2) TCO retrieved from the same measurements can be used to select the appropriate *a priori* profile for ozone profile retrieval.

In addition, features like the dramatic ozone loss in Antarctica [*Farman et al.*, 1985], significant negative trend in mid latitude ozone [*Stolarski et al.*, 1991], and potential

sign of ozone recovery [*Newchurch et al.*, 2003] reveal that ozone climatologies should be regularly updated and be based upon recent data sets. The primary goal of the present paper is to provide an updated and atmospheric dynamics oriented ozone and temperature climatologies to be used in ozone retrievals as *a priori* from GOME and SCIAMACHY [*Burrows et al.*, 1999a; *Bovensmann et al.*, 1999] or any other UV backscatter satellite measurements. First, the TCO as retrieved by Differential Optical Absorption Spectroscopy (DOAS) technique can be used to select an appropriate climatological profile to be used as *a priori* information for optimal estimation on ozone profile retrieval [*Munro et al.*, 1998; *Hoogen et al.*, 1999a, b; *van der A et al.*, 2002]. Second, the climatology provides an opportunity to correct for profile shape errors [*Wellemeyer et al.*, 1997] in TCO retrievals, especially at high solar zenith angles. The simultaneous use of matching temperature profiles aids in properly accounting for the temperature dependence of the ozone absorption cross-sections in the retrieval process.

A wide range of data sources is used in the compilation of this new climatology. Description of the data and method of compilation are discussed in Section 5.2. The frequency distribution of ozone is described in Section 5.3. Composite ozone and temperature climatologies are presented in Section 5.4. The correlation between mean ozone and temperature profiles has been studied and is reported in Section 5.5. A climatology of tropopause heights as a function of TCO is presented in Section 5.6. Both features show that the new climatology is truly representative of the ozone profile shapes encountered globally in the atmosphere. Comparison between sonde ozone profiles, the results from the climatology, and GOME ozone profiles retrieved using two different ozone profile climatologies as a priori constraints is presented in Section 5.7. A conclusion is given in Section 5.8.

5.2 Data

5.2.1 Ozonesonde data

Data from ozonesonde stations as listed in Tables 5.1 and 5.2 were used to prepare this climatology. The majority of the data were obtained from the World Ozone and Ultraviolet Data Center (WOUDC), Environment Canada, Downsview, Ontario [*Fioletov et al.*, 1999]. The source of data for the tropics was from the Southern Hemisphere Additional Ozonesondes (SHADOZ) [*Thompson et al.*, 2003a, b]. The geographical distribution of those stations is shown in Figure 5.1. More details about individual stations, seasonal behaviour and trend of ozone can be found in *Logan* [1985, 1999a, b], *Thompson et al.* [2003a, b] and references therein.

The majority of stations included in this study have made regular measurements from 1990 to 2000. Five stations namely, Laverton (from 1989 to 1999), Wallops Island, Sodankylä, Marambio (from 1988 to 1998), and De Bilt (from 1994 to 2001) are from slightly different periods but inclusion of data before 1990 or after 2000 makes them homogeneous in time. Three stations, Lerwick, Eureka, and Praha with ozone observations from 1992 to 2001 and Ny Ålesund from 1990 to 1993 were included to increase the geographical coverage. Tropical stations from WOUDC are not considered reliable

Table 5.1: WOUDC ozonesonde stations used in the compilation of the climatology. Hohenpeissenberg is written in short form. Data are available mainly from four types of ozonesondes, namely Electrochemical Concentration Cell (ECC), Brewer Mast (BM), German Democratic Republic (GDR) sonde, and Japanese sondes (KC). Here the stations are classified into four climate zones: northern polar region (60°N-90°N), northern mid latitude region (30°N-60°N), southern mid latitude region (30°S-60°S), and southern polar region (60°S-90°S). The climatology is based on the data primarily from 1990s.

WMO code	Station	Latitude	Longitude	Type	Data Period
		northern polar region			
018	Alert	82.5°N	64.5°W	ECC	1988 - 1998
315	Eureka	80.0°N	86.2°W	ECC	1992 - 2001
089	Ny Ålesund	78.9°N	11.9°E	ECC	1990 - 1993
024	Resolute	74.7°N	94.9°W	ECC	1990 - 2000
262	Sodankylä	67.3°N	26.5°E	ECC	1988 - 1998
043	Lerwick	60.1°N	1.2°W	ECC	1992 - 2001
		northern mid latitude region			
021	Edmonton	53.5°N	114.1°W	ECC	1990 - 2000
076	Goose Bay	53.3°N	60.4°W	ECC	1990 - 2000
221	Lagionowo	52.4°N	21.0°E	GDR + ECC	1990 - 2000
174	Lindenberg	52.2°N	14.1°E	GDR + ECC	1990 - 2000
316	De Bilt	52.1°N	5.2°E	ECC	1994 - 2001
242	Praha	50.0°N	14.4°E	BM + ECC	1992 - 2001
099	Hohenpeis.	47.8°N	11.0°E	BM	1990 - 2000
156	Payerne	46.5°N	6.6°E	BM	1990 - 2000
012	Sapporo	43.1°N	141.3°E	KC	1990 - 2000
067	Boulder	40.0°N	105.0°W	ECC	1986 - 1996
107	Wallops Is.	37.9°N	75.5°W	ECC	1988 - 1998
014	Tateno	36.1°N	140.1°E	KC	1990 - 2000
007	Kagoshima	31.6°N	130.6°E	KC	1990 - 2000
		southern mid latitude region			
254	Laverton	37.8°S	144.7°E	ECC	1989 - 1999
256	Lauder	45.0°S	169.7°E	ECC	1990 - 2000
		southern polar region			
233	Marambio	64.2°S	56.7°W	ECC	1988 - 1998
101	Syowa	69.0°S	39.6°E	KC	1990 - 2000
323	Neumayer	70.6°S	8.2°W	ECC	1992 - 2002

Table 5.2: SHADOZ (tropical) stations. All of these stations are using ECC except Watukosek which was using Meisei until the instrument type was changed to ECC.

Station	Latitude	Longitude	Data Period
Paramaribo	5.8°N	55.2°W	1999 - 2001
San Christobal	0.9°S	89.6°W	1998 - 2001
Nairobi	1.3°S	36.8°E	1998 - 2002
Malindi	3.0°S	40.2°E	1999 - 2002
Natal	5.4°S	35.4°W	1998 - 2002
Watukosek	7.6°S	112.6°E	1998 - 2002
Ascension Is.	7.9°S	14.4°W	1998 - 2002
Am Samoa	14.2°S	170.6°W	1998 - 2002
Tahiti	18.0°S	149.0°W	1998 - 1999
Fiji	18.1°S	178.4°E	1998 - 2002
La Reunion	21.1°S	55.5°E	1998 - 2002
Irene	25.9°S	28.2°E	1998 - 2002

enough. Their observations are rather irregular and hence were not included. The gap in the tropics was filled by SHADOZ data. Twelve stations were selected, most of them have ozone observations from 1998 to 2002 (see Table 5.2). The use of only five years of data could be one of the limitations of this climatology, particularly in the tropics.

For the climatology to be representative, an extensive geographical coverage is required. In the northern hemisphere (NH), there are many stations to choose from and the geographical coverage is quite satisfactory. The situation has been improved significantly in the tropics, particularly in the southern hemisphere (SH), after the establishment of the SHADOZ network. In the northern tropics and in the southern mid latitude and polar regions, only a limited number of stations are available. More stations in these regions are needed for better understanding of ozone distribution, its variation, and long-term trend. Out of 38 stations used in this climatology, northern mid latitude region (30°N-60°N) alone comprises of 14 stations. Six stations in the northern polar region (60°N-90°N) and 12 stations in the low latitude (30°S-30°N) have been selected. In the southern hemisphere, only two stations in the mid latitude and three stations in the polar region are available with a sufficient 10 year data record. For the frequency of ozone soundings in each of the stations, the reader is referred to *Logan* [1999a, b] and *Thompson et al.* [2003a, b].

Most of the stations used Electrochemical Concentration Cell (ECC) [*Komhyr*, 1969] which has been well validated [*Smit et al.*, 1997; *De Backer et al.*, 1989]. Two European stations, Hohenpeissenberg and Payerne use Brewer Mast (BM) [*Brewer and Milford*, 1960]. Lindenberg and Legionowo changed the instrument type from the German Democratic Republic (GDR) sonde [*Ronnebeck and Milford*, 1976] to ECC sonde in June 1992 and 1993, respectively. The GDR sondes produce larger O_3 mixing ratio than

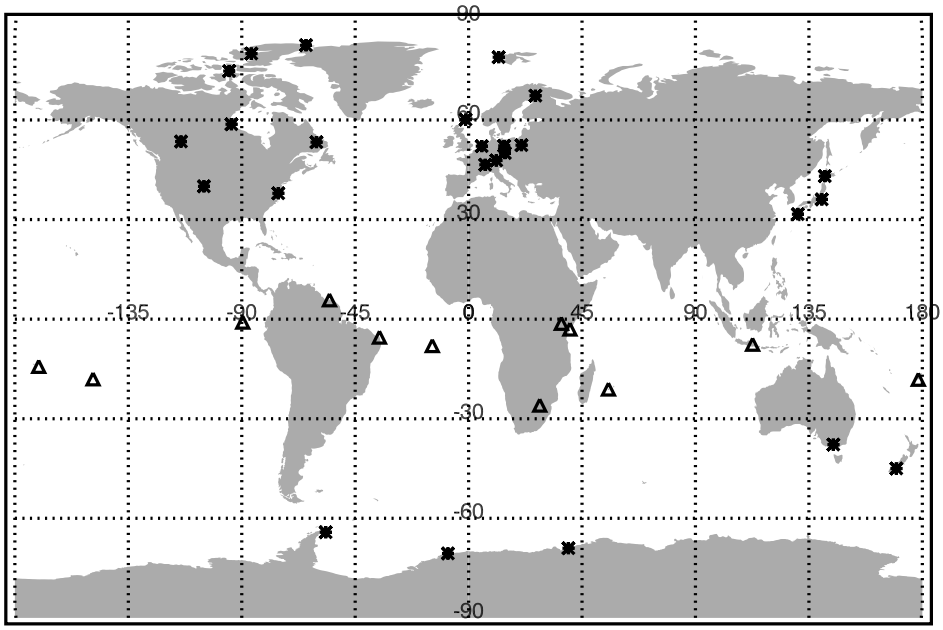

Figure 5.1: Geographical distribution of the ozonesonde stations. Stars and triangles show the location of WOUDC and SHADOZ sonde stations respectively.

either BM or ECC sondes [*Logan*, 1999a]. Four Japanese stations use their own sonde (KC) which is similar to the Carbon Iodide (CI) sonde of [*Komhyr*, 1964]. All these instruments have different precision, accuracy, and different sources of error. A number of comparison campaigns were held to compare the performance of these instruments [*Attmanspracher and Dütsch*, 1970, 1981; *Chanin*, 1983; *Hilsenrath and others*, 1986; *De Backer et al.*, 1995, 1989] but the different campaigns came out with different results. The comparison based on duosounding [*De Backer et al.*, 1989] shows that BM sensors read 10 - 15% higher in the troposphere, almost the same value at the height of ozone maximum, and 5% less at about 10 hPa than ECC sensors. Such differences led to a general practice of correcting the ozonesonde profiles by introducing correction factors (CF). This procedure introduces errors [*Logan*, 1985; *Tiao et al.*, 1986; *McPeters et al.*, 1997] in the so called corrected sonde values and the issue of using correction factors is still ongoing [*WMO*, 1998]. In the current climatology it has not been applied. The temperature and pressure data were obtained from radiosondes flown together with ozonesondes. The radiosonde temperatures form a reliable data set which have a reproducibility of about 0.2 K [*Knudsen et al.*, 1996].

Sonde profiles are classified based on the understanding of spatial and temporal variability of ozone. TCO exhibits a strong annual cycle. The cycle possesses a characteristic late-winter/early-spring maximum and broad late-summer/early-fall minimum [*Eder and LeDuc*, 1999; *Weber et al.*, 2003]. The driving force for the annual cycle in ozone is likely to be dynamical in nature mass transport of ozone from tropical (source) region to higher latitudes [*Bojkov et al.*, 1994; *Holton et al.*, 1995] and seasonal vari-

ance of tropopause height [*Stanford et al.*, 1995]. Photochemistry is another factor for TCO variation which is solar zenith angle dependent. The profile data have been classified with respect to three effective dimensions: latitude e.g. low latitude (30°S-30°N), mid latitude (30°-60°), and polar (60°-90°), season (winter/spring and summer/fall) and TCO amount. Northern winter/spring and summer/fall are defined as being December - May and June - November periods, respectively. A seasonal distinction was not made for low latitude profiles. The individual ozonesonde reading in units of partial pressure at various pressure levels were converted into number density units and volume mixing ratio at various heights. The values at the end points i.e. at 0 km and 27 km were determined by assuming a constant mixing ratio from their nearest values. The 0 to 27 km range was then divided into 18 layers each 1.5 km wide. The mean for each layer was calculated and the missing values in the intermediate layers, if any, were determined by spline interpolation. The same treatment was undertaken for the temperature profiles. The column amount of ozone was calculated by integrating the ozone amount up to 27 km and extending it up to 60 km by using a zonal monthly mean ozone climatology (TOMS V8 climatology, G. Labow, NASA GSFC, personal communication, 2001) that is based on recent ozonesonde and SAGE II data (1990-2000). The ozonesonde profiles were classified by the hybrid (ozonesonde plus climatological extension) ozone column amount in intervals of 30 DU. The mean and standard deviation profiles for ozone (number density and mixing ratio) and temperature were determined for each (ozone amount) class. Note that the climatological profile above 27 km can differ from the true state of ozone and this difference can introduce some error in the hybrid ozone column amount.

5.2.2 Satellite data

SAGE II and Polar Ozone and Aerosol Measurement III (POAM III) ozone profile data were used to construct the stratospheric ozone profiles. SAGE II aboard the Earth Radiation Budget Satellite (ERBS) has been providing high resolution ozone profile data since October 1984 with a short interruption of about three months in July 2002 [*Wang et al.*, 2002]. SAGE II provides 15 sunrise and 15 sunset measurements each day. The SAGE II spatial coverage extends over a latitude range of approximately 70°S to 70°N having month to month variability. The number of the winter/fall profiles in the northern hemisphere and spring/summer profiles in the southern hemisphere beyond 60° latitude are limited. POAM data is a good available extension to prepare stratospheric climatological profiles in the polar region. POAM III instrument [*Lucke et al.*, 1999] on the Pour l'Observation de la Terre (SPOT) 4 satellite makes 14 to 15 measurements per day in each hemisphere. Because of the satellite inclination of 98.7°, the POAM III measurement latitudes vary from 55°N to 73°N in the northern hemisphere and from 63°S to 88°S in the southern hemisphere.

Ten years of SAGE II V6.1 data from 1988 to 1999 were included in the new climatology. SAGE II V6.1 data were not available after middle of 2000 due to an altitude registration problem. The SAGE II ozone retrieval requires the separation of ozone absorption and aerosol extinction [*Steele and Turco*, 1997]. Thus, in spite of improvements in the SAGE II V6.1 retrieval [*Wang et al.*, 2002] algorithm, ozone retrievals from SAGE

II data are biased in the lower stratosphere when aerosol extinction is large e.g. after the eruption of Mount Pinatubo in mid-July, 1991. For this reason the 1991 and 1992 data are not included in the new climatology.

The source of temperature data in the SAGE II operational data is the routine gridded data analyses from the National Meteorological Center (NMC). The temperature data which are based on radiosonde and National Oceanic and Atmospheric Administration (NOAA) operational satellites were used to extend the sonde temperature climatology up to the upper stratosphere. The temperature data as used for the POAM III retrieval were obtained from the UK Meteorological Office (UKMO) which were interpolated to the time and location of the POAM III measurements.

An analysis performed by *Wang et al.* [2002] to assess the SAGE II V6.1 data quality shows that SAGE II and coincident ozonesonde agree in the mean to better than 10% down to the tropopause. SAGE II provides useful data up to 60 km [*Cunnold et al.*, 1989; *Attmanspracher et al.*, 1989] with an expected accuracy of 6% above 25 km altitude. The difference between the sunrise and sunset ozone values are interpreted to be approximately 5%. Validation studies [*Lumpe et al.*, 2002; *Danilin et al.*, 2002; *Randall et al.*, 2003] using ECC sonde data, and aircraft (ER-2) and space-based measurement (SAGE II, HALOE) show that POAM III V3 ozone values agree to within 5 to 7% in the altitude range from 13 to 60 km and a larger disagreement (10 to 15%) is observed below 13 km. The quality of NMC [*Wang et al.*, 1992] and UKMO [*Pullen and Jones*, 1997] temperature data is believed to be poorer at higher altitudes because of the use of satellite data in their data assimilation system.

SAGE II data (for tropics and mid latitude region) were taken from 60 km down to 14 km and POAM III data (for polar region) from 60 to 8 km removing profiles with missing values within the range. The use of satellite data almost down to tropopause is of great significance for the accuracy of climatology because it takes into account the most dynamically sensitive region where short term ozone variations are controlled to a large extent by horizontal and vertical transport [*Salby and Callaghan*, 1993]. SAGE II V6.1 and POAM III V3 ozone profile data sets were extended below 14 km and 8 km respectively by means of the TOMS V8 climatology to evaluate the ozone column amount by integration. The ozone number density, which both data set provide, were converted to volume mixing ratio in order to construct the stratospheric ozone mixing ratio climatology. As in the case of the sonde data, satellite profiles were classified by region (tropics, mid latitude, and polar), season (winter/spring and summer/fall), and TCO (30 DU bins). Mean and standard deviation profiles for ozone and temperature for each of the ozone classes and seasons were calculated.

5.3 Ozone frequency distribution

The frequency distribution of TCO corresponding to the profiles collected in the data set has been determined and evaluated. The distribution function of TCO depends on various atmospheric perturbations such as changes in dynamics, stratospheric chemistry, solar activity, etc. It yields the information about the most probable value and the dis-

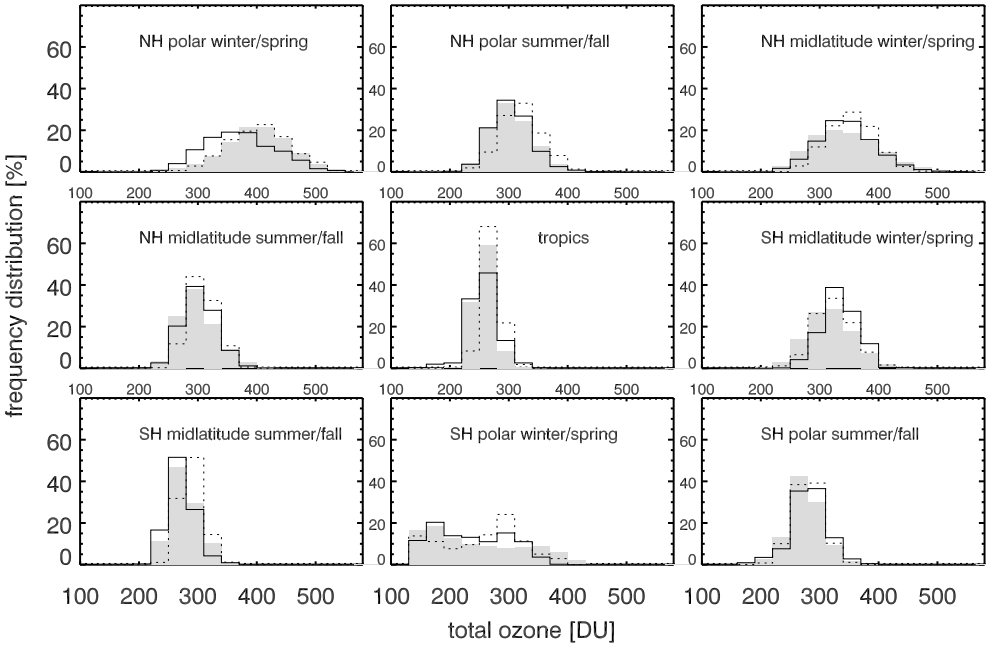

Figure 5.2: Frequency distribution of TCO as obtained by integrating sonde (solid line) and satellite (dotted line) profiles and GOME GDP V3.0 data for GOME-period 1995-2002 (shaded region).

tribution of extreme values [*Reck et al.*, 1996]. The frequency distribution, as shown in Figure 5.2, shows the percentage frequency for a given ozone class of 30 DU width for the satellite and sonde data separately. The frequency distribution of all GOME GDP V3.0 TCO data from middle of 1995 through 2002 are also shown in Figure 5.2 and it approximates the global distribution due to the larger sampling size of GOME as compared to SAGE II, POAM III, and sondes. Effect of different sampling size, interannual variation, and the effect of the instrumental/retrieval differences are expected to affect ozone distribution, but Figure 5.2 shows that sonde and satellite data distributions closely approximate that given by GOME TCO. Integrated ozone values have about the same range of values as given by GOME. The agreement in TCO distribution obtained from two entirely independent sources confirms the good representation of the global ozone field in the new climatology and justifies the methodology with which the climatology was prepared.

The frequency distribution is wider in winter/spring and narrower in summer/fall. Temperature gradients and the resulting short-term TCO variation are stronger in winter than in summer owing to the variation of the solar insulation and variation in planetary activity driving ozone transport into high latitudes [*Fusco and Salby*, 1999; *Randel et al.*, 2002; *Weber et al.*, 2003]. In tropics the distribution is narrow and symmetric around 250-280 DU. Except in SH polar region where maximum frequency lies in the 280-310 DU range in both winter/spring and summer/fall seasons, the winter/spring distribution has a peak that is shifted to higher TCO with respect to the summer/fall dis-

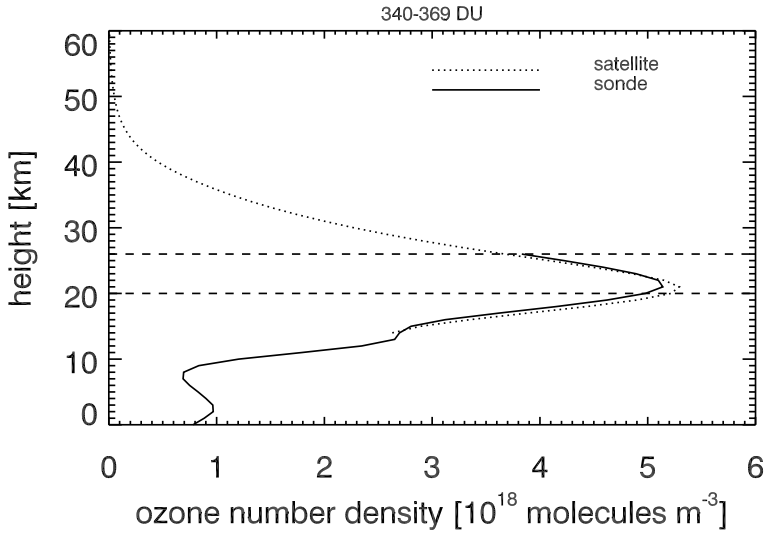

Figure 5.3: Merging of sonde and satellite profiles. This is the mean profile of 340 - 369 DU ozone class for NH mid latitude region during winter/spring. Two horizontal lines at 20 and 26 km show the transition region where the sliding averaging is applied.

tribution. Ozone values in late spring and early winter are reflected in the tails of either side of summer/fall ozone distribution. This is because the separation into different half years (Dec. - May, Jun. - Nov.) is somewhat arbitrary and some of the profile shapes are common to both. Larger differences in profile shape are expected in low TCO classes (ozone hole condition vs. summer/fall profiles).

In SH polar region the asymmetry on the low ozone side is due to chemical depletion of ozone ("ozone hole") in the Antarctic vortex during polar spring. Very low TCO cases are also observed in the SH mid latitude region. Earlier studies [e.g. *Pérez et al.*, 2000; *Callis et al.*, 1997] also reported the events of low TCO. Medium-scale baroclinic disturbances distort the Antarctic vortex and can lead to excursion into mid latitudes. Advection of ozone-poor polar air into the mid latitudes after the final vortex break up has been observed and can also contribute [*Randel and Wu*, 1995]. Particularly in SH mid latitude, the use of satellite data compensates for the lack of suitable stations covering these low ozone cases.

5.4 Composite ozone and temperature profile climatologies

5.4.1 Ozone

The current climatology is compiled by merging the corresponding mean sonde and satellite profiles. Before combining both data sets, sonde values were interpolated into

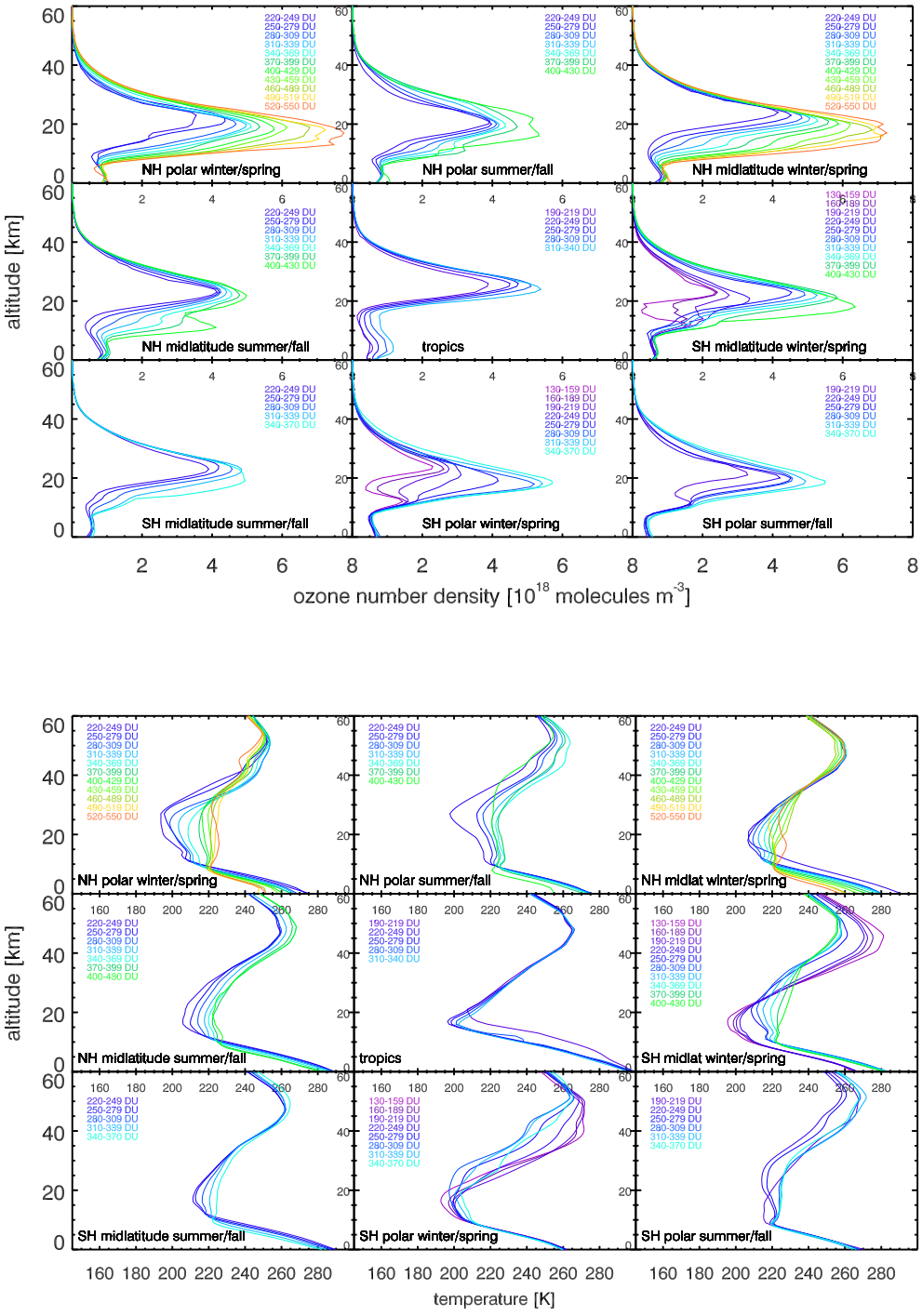

Figure 5.4: TCO classified mean ozone (upper panel) and corresponding temperature profiles (lower panel).

the same altitude grid (1 km) as that of the satellite data. The interpolation was performed for both ozone number density and volume mixing ratio profiles. Mean sonde and satellite ozone profiles for 340 - 369 DU class of NH mid latitude winter/spring are shown in Figure 5.3 as an example. A smooth transition between 20 and 26 km was introduced by applying a sliding average. As can be seen in Figure 5.3, the sonde and satellite climatologies agree well. Some difficulties were encountered at the minimum ozone class for satellite data of SH mid latitude region during winter/spring season where no sonde counterpart was available. Those profiles were extended from 14 km down to 0 km by using the corresponding mean sonde profile from the polar region. The final profiles were scaled, where necessary, to the class mean TCO values. An identical compilation technique was followed for the climatology of standard deviation.

Figure 5.4 shows the results of the new dynamics oriented ozone climatology. NH mid latitude and polar regions both have 11 profiles in winter/spring and 7 profiles in summer/fall seasons. This difference is the result of strong planetary activity which cause the TCO amount vary more strongly in winter/spring. The TCO amounts are higher in the northern than in the southern hemisphere, which appears to be consistent with the greater transport of ozone in NH [*Holton et al.*, 1995]. SH polar winter/spring comprises of 8 profiles which includes the typical ozone hole profiles as well. Including ozone depleted profiles, which were particularly obtained from satellite data, SH mid latitude winter/spring comprises of 10 ozone profiles. In summer/fall, there are 5 profiles in mid latitude and 6 in polar region. In the tropics, five profile classes are identified.

The main features of the ozone distributions are clearly seen in this figure. These features include: decrease in the height of ozone maximum with increase in latitude and TCO, sharp ozone gradients between the vertically stratified lower stratosphere and well mixed troposphere, and Antarctic ozone hole profile in spring in SH polar and ozone depleted profile in SH mid latitude region. Many mid latitude profiles exhibit filamentation or a secondary maximum. This figure clearly shows the hemispheric and seasonal differences in tropospheric ozone which causes profiles of the same ozone class in both hemispheres to differ in the stratosphere. For example, the tropospheric ozone level in the southern hemisphere is, in general, less than in the northern hemisphere. For the same TCO value, southern hemispheric stratospheric ozone level should be higher than in the NH. In the SH, tropospheric ozone levels do not vary as much as in the northern hemisphere. This could be the result of stronger anthropogenic emission in NH, weaker meridional circulation, or underrepresentation of ozonesonde stations in SH. Figure 5.4 also shows that the tropospheric column in tropics are highly variable in line with TCO variation. This result is in agreement with SHADOZ tropospheric ozone climatology [*Thompson et al.*, 2003b] that was based on three years of data.

Figure 5.5 shows the variability defined as (standard deviation)/mean x 100% of ozone. The variability lies below 30% except in the lowermost stratosphere and upper troposphere where the variability is typically up to 60%. This value can increase to 80% during austral spring in southern hemisphere. The large variance in this region is the result of combined contribution from dynamical activity, tropospheric-stratospheric exchange, and the chemical depletion of ozone. The increase in variability in altitude above 40 km may to some extent come from satellite sunrise/sunset differences (sunrise

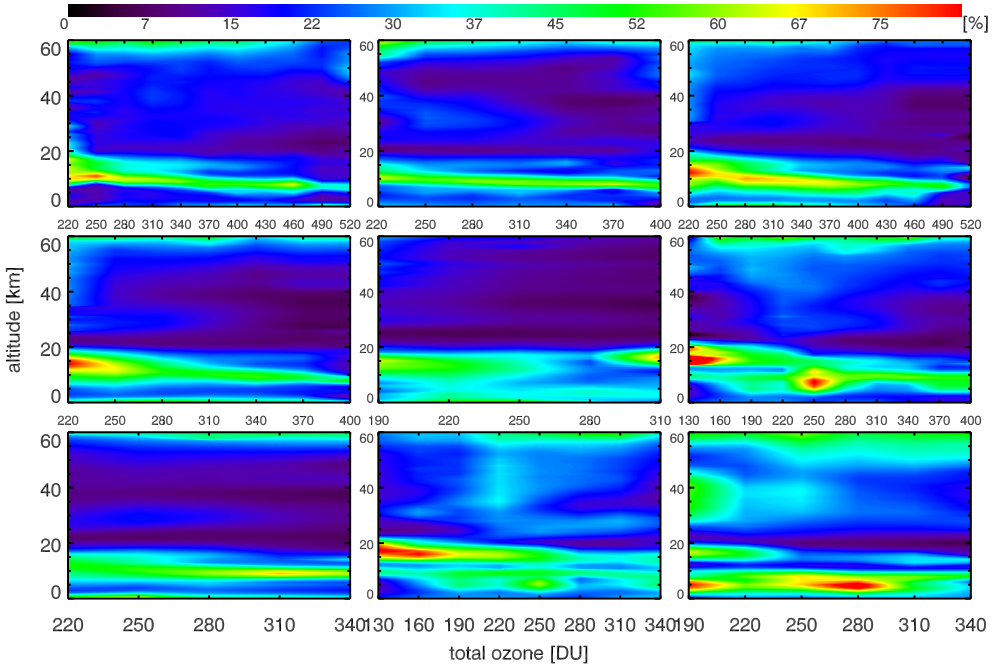

Figure 5.5: Variability of ozone (in %) as a function of altitude and TCO. Variability is highest in the lowermost stratosphere and upper troposphere. The plots are located in the same order as in Figures 5.2 and 5.4 (i.e. first row left to right: NH polar winter/spring, NH polar summer/fall, NH mid latitude winter/spring, second row: NH mid latitude summer/fall, tropics, SH mid latitude winter/spring, third row: SH mid latitude summer/fall, SH polar winter/spring, SH polar summer/fall).

values being higher) and errors in the satellite retrieval algorithm [*Wang et al.*, 1992]. The variability patterns, in general, differ for solstice conditions: low values occurring in summer hemisphere and high in winter hemisphere.

Large ozone variability is observed in the mid latitude region for low ozone cases (220-280 DU, for example). It is likely due to the fact that the high tropopause profile (subtropical origin) and ozone depleted profile (polar origin) can have same TCO amount but different profile shapes. Similar cases are observed in the polar region where early-summer/late-fall profiles and ozone hole profiles belong to the same ozone class.

5.4.2 Temperature

The climatology derived from radiosonde data was combined with the climatology based on meteorological analyses (NMC and UKMO) data set by merging the corresponding ozone class mean temperature profiles using the same sliding average scheme as applied for ozone. The sonde values were spline interpolated to the 1 km altitude grid. For cases when matching sonde profile were missing, the met analyses were extended down to the surface.

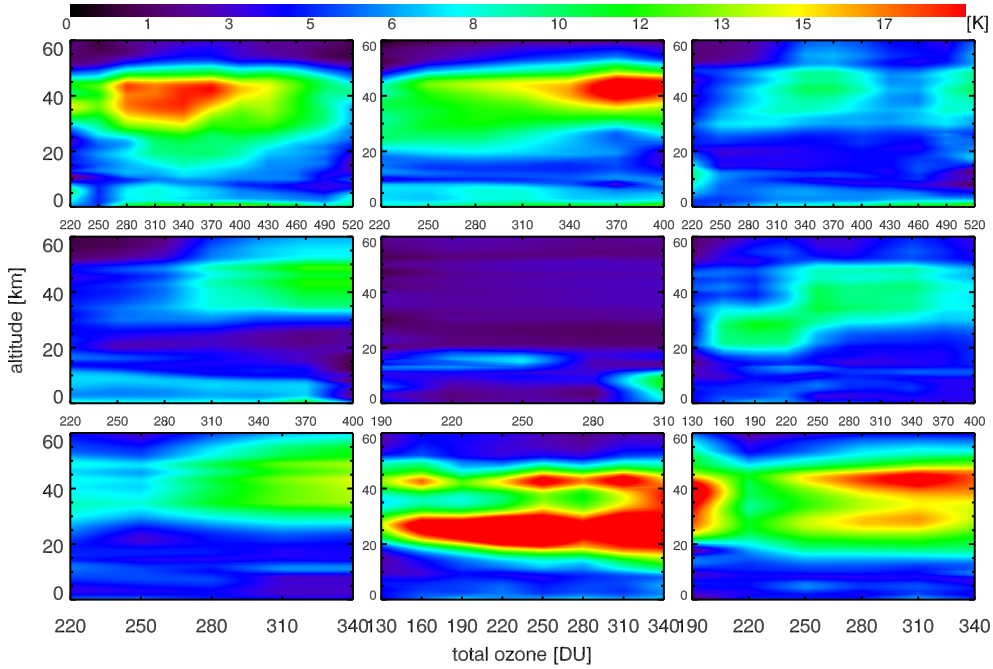

Figure 5.6: Temperature standard deviation (in K) as a function of altitude and TCO. The plots are located in the same order as in Figure 5.5

Mean temperature profiles are shown in Figure 5.4. One of the important features seen in the figure is that the profiles with low tropopause are associated with a cold troposphere, warm lower stratosphere, and high TCO amount. An identical feature, known as stratosphere-troposphere compensation, has been identified by *Steinbrecht et al.* [1998] when the author classified temperature and ozone profiles by tropopause height. In NH mid latitude winter/spring, for example, the temperature for 220-249 DU in troposphere (at surface) is higher than that for 400-429 DU by about 19 K while in the lower stratosphere (19 km) the temperature for 400-429 DU is higher by about 14 K. As seen in this figure, the magnitude of difference differs with seasons, being largest in winter/spring. Furthermore, the difference in temperature between ozone classes decrease with increasing stratospheric altitude and decreasing tropospheric altitude. In the upper stratosphere, no clear pattern of variation could be identified - the reasons for this behaviour are not understood and further investigation is required.

As explained by *Fels* [1982], the Arctic lower stratosphere is warmer than that in the Antarctic. In SH polar region, especially during winter/spring, the lower stratospheric mean temperature falls as low as 193 K leading to severe ozone depletion as shown in Figure 5.4. Figure shows that the low-ozone events in the SH mid latitude region is accompanied by the decrease in the mean temperature of the lower stratosphere as low as 195.5 K. It is likely due to the fact that the fixed latitude of 30°S to 60°S is arbitrary which occasionally samples the vortex air in the mid latitude. The horizontal advection of cold air from Antarctic latitudes could also result in such low-temperature events

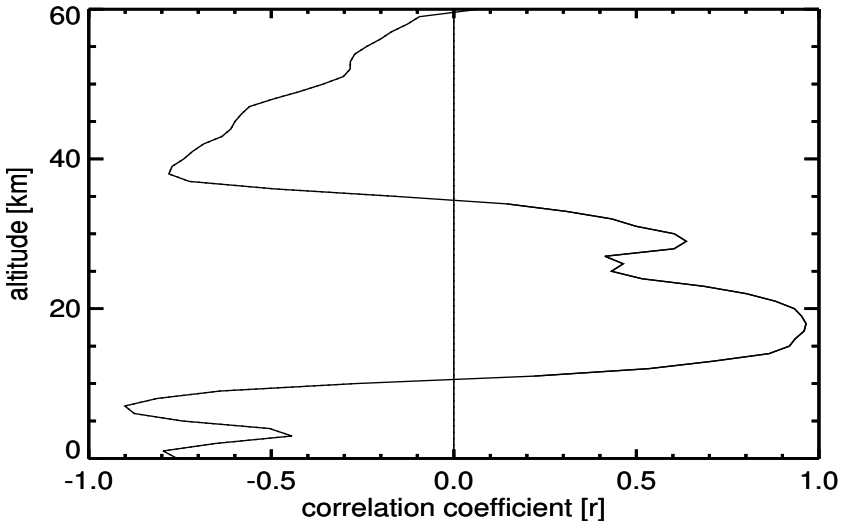

Figure 5.7: Correlation between mean ozone and temperature for NH mid latitude winter/spring as function of altitude.

[*Pérez et al.*, 2000]. Another interesting feature that can be seen in the present climatology is the sharp tropical tropopause temperature minimum which has been pointed out by *Randel et al.* [2003].

The standard deviation for the composite temperature climatology is shown in Figure 5.6. The profiles were obtained from the standard deviation profiles of sonde and met analyses data by the same method as applied to the mean temperature profiles. The standard deviation lies below 14 K in the mid latitude region and becomes as high as 25 K in the polar region during winter/spring. The variance in the upper stratosphere could be explained by the out of phase variation relationship between ozone and temperature [*Smith*, 1995]. In the lower stratosphere, the temperature variation is dominantly controlled by transport [e.g. *Rood and Douglass*, 1985]. The large variability in the polar region could be due to the use of relatively smaller sample size of five years. Note that UKMO data have been used in the polar region and the quality of UKMO temperature decreases with increasing altitude possibly due to the poorer quality of radiosonde temperature and increased use of satellite data. QBO (Quasi-biennial Oscillation), solar cycle, tropopause height variation, etc. also contribute to temperature variability.

5.5 Ozone and temperature correlation

Figure 5.7, as an example, shows the correlation coefficient profile based on the mean ozone and temperature profiles for NH mid latitude winter/spring. The ozone is negatively correlated with temperature above 35 km, positively correlated between 35 and 10 km, and negatively correlated below 10 km. This result is in good agreement with

the model calculated correlation [*Rood and Douglass*, 1985] between ozone and temperature.

The main aim of investigating this type of correlation is to show that the new ozone and temperature climatologies presented here is capable of reproducing the known relationships between ozone and temperature. If these relationships do not hold, it would indicate that either the methodology has faults or the climatology is not a true representation of the global ozone distribution.

The interpretation of the observed correlation is not easy in the kind of studies presented here because the correlation profile shown in Figure 5.7 is based on mean profiles and no other attempts are made to separate the factors which can contribute in the ozone-temperature correlation. Nevertheless, in the upper stratosphere ozone concentration is photochemically controlled. The destruction of odd oxygen (O_3 + O) by various chemical reactions (Chapman chemistry and catalytic cycles) can vary strongly with temperature. An increase in temperature will increase the rate at which ozone is destroyed, so ozone and temperature are negatively correlated. The detail of the explanation on the physical mechanism on ozone temperature relationship in the upper stratosphere can be found in Smith [1995]. In the lower stratosphere, transport dominates over photochemistry [*Brasseur and Solomon*, 1984]. There are two main mechanisms whereby the lower stratospheric ozone and temperature are positively correlated. First, radiative effect: high ozone concentration helps to maintain a persistent temperature through the absorption of solar and terrestrial radiative energy [*Miller et al.*, 1992]. Second, dynamical effect: transport of air parcel and adiabatic compression at high latitudes lead to increase in ozone and temperature [*Wirth*, 1993; *Petzoldt et al.*, 1994; *Fortuin and Kelder*, 1996].

5.6 Climatology of tropopause height

The mean state of tropopause height for each of the ozone classes has been analysed. This provides the mean relationship between TCO and tropopause height. Investigation of the link between TCO and tropopause height itself is a broad field but the basic idea of the present study is to verify if the new climatology of ozone and temperature reproduces the existing knowledge on tropopause height in a climatological sense.

Tropopause marks the location of an abrupt transition in the temperature lapse rate *WMO* [1957], in the values of potential vorticity (PV) [e.g. *Zängl and Wirth*, 2000], and in the concentration of chemical species like ozone [*Bethan et al.*, 1998]. Various tropopause definitions have been identified. *Hoinka* [1998], however, has shown that the tropopause height as evaluated from different definitions provide similar results. In the present study, the tropopause height as provided by NMC data were used for the low and mid latitude regions. It is calculated using the same algorithm as used by National Centers for Environmental Prediction (NCEP) [Joseph M. Zawodny, personal communication, 2003] for the location of SAGE II measurement. Similar to ozone and temperature profiles, corresponding tropopause heights were classified by TCO amount and the mean tropopause heights were calculated for both winter/spring and summer/fall sea-

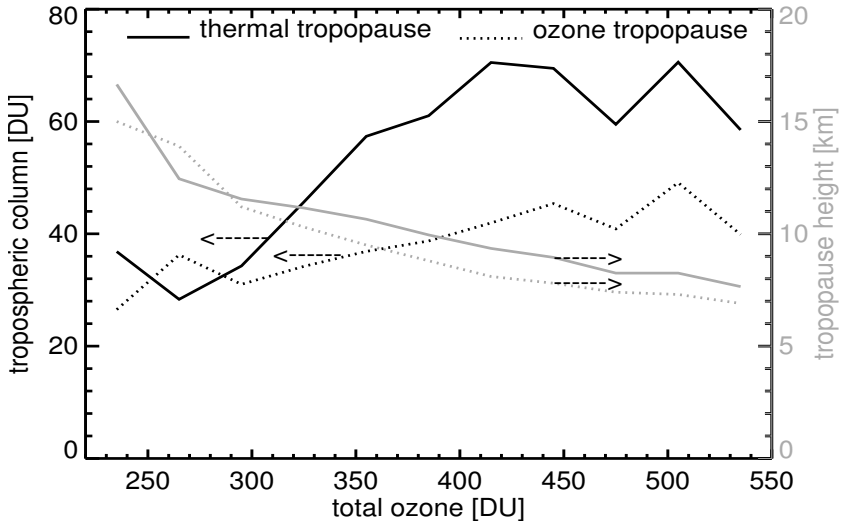

Figure 5.8: Climatology of tropopause height for NH mid latitude winter/spring. It shows the mean relationship between TCO, tropopause height, and tropospheric column.

sons. In the polar region where data come from a different source the position of thermal tropopause was estimated by using *WMO* [1957] definition. Thermal tropopause is the lowest level at which the temperature lapse rate decreases to 2 K per km or less, provided the average lapse rate between this level and all higher levels within 2 km does not exceed 2 K per km. In all cases the location of ozone tropopause was evaluated by applying the criterion developed by *Bethan et al.* [1996]. The threshold value of ozone gradient where ozone tropopause lies is 60 ppb/km at conditions that the ozone mixing ratio exceed 80 ppb and that the values immediately above the tropopause exceed 110 ppb.

Table 5.6 shows how the tropopause (TTP: thermal tropopause, OTP: ozone tropopause) height changes with TCO amount. Figure 5.8, as an example, shows how tropopause height and tropospheric ozone vary with TCO. As apparent in the climatology, various authors [*Hoinka et al.*, 1996; *Steinbrecht et al.*, 1998; *Birner et al.*, 2002] have reported the correlation between the tropopause height and the stratospheric ozone column. Increase in the height of tropopause cause the stratospheric column to decrease. The strength of correlation, however, depends upon the region and season [*Krzyścin et al.*, 1998]. In summer/fall, the increase of TCO for 1 km decrease in tropopause height is larger than in winter/spring. Besides its relation with stratospheric column, the tropopause height is also sensitive to surface temperature [*de F. Forster and Shine*, 1997]. *Santer et al.* [2003] suggested that the increase in the tropopause height is associated with stratospheric cooling due to stratospheric ozone loss.

The tropopause height shows a considerable north south variability but without any clear symmetry between northern and southern hemisphere. The most probable reason for such asymmetry is related to the difference in the distribution of land and ocean in

Table 5.3: Climatology of tropopause height. Tropopause types: TTP (thermal tropopause in kilometer) and OTP (ozone tropopause in kilometer). Regional bins: I: northern hemisphere polar-winter/spring, II: southern hemisphere polar-winter/spring, III: northern hemisphere polar-summer fall, IV: southern hemisphere polar-summer/fall, V: northern hemisphere mid latitude-winter/spring, VI: southern hemisphere mid latitude-winter/spring, VII: northern hemisphere mid latitude-summer/fall, VIII: southern hemisphere mid latitude-summer/fall, IX: low latitude.

Tropopause height

Reg.-sea. → TCO (DU) ↓	Type	I	II	III	IV	V	VI	VII	VIII	IX
145	TTP	-	12.0	-	-	-	12.8	-	-	-
	OTP	-	10.1	-	-	-	10.0	-	-	-
175	TTP	-	11.4	-	-	-	12.2	-	-	-
	OTP	-	9.6	-	-	-	9.6	-	-	-
205	TTP	-	11.3	-	11.6	-	11.6	-	-	17.3
	OTP	-	9.8	-	8.6	-	9.7	-	-	17.0
235	TTP	12.4	10.9	10.9	11.5	14.4	11.5	13.7	13.3	16.5
	OTP	11.5	9.5	12.5	9.1	15.0	9.5	14.9	14.9	16.7
265	TTP	11.6	11.0	10.3	11.5	13.3	12.2	13.0	12.9	16.3
	OTP	11.2	9.6	10.0	8.8	13.9	11.1	14.0	14.5	16.5
295	TTP	11.0	10.5	11.0	11.5	12.0	11.7	12.3	11.2	15.7
	OTP	9.9	9.5	9.4	8.2	11.2	10.9	13.4	13.7	16.3
325	TTP	10.6	10.0	9.4	11.5	11.1	11.1	11.3	9.7	14.5
	OTP	9.3	9.3	8.6	8.2	10.3	10.3	10.6	12.1	15.2
355	TTP	9.7	9.7	9.0	11.4	10.3	10.2	10.7	9.0	-
	OTP	8.6	8.9	8.1	8.1	9.5	9.5	9.2	10.7	-
385	TTP	9.1	-	8.6	-	9.5	9.5	9.6	-	-
	OTP	8.1	-	7.8	-	8.8	9.0	8.2	-	-
415	TTP	8.7	-	7.6	-	9.0	9.1	8.6	-	-
	OTP	7.8	-	7.1	-	8.1	9.0	7.4	-	-
445	TTP	8.3	-	-	-	8.6	-	-	-	-
	OTP	7.5	-	-	-	7.8	-	-	-	-
475	TTP	8.2	-	-	-	8.4	-	-	-	-
	OTP	7.5	-	-	-	7.4	-	-	-	-
505	TTP	7.9	-	-	-	7.8	-	-	-	-
	OTP	7.1	-	-	-	7.3	-	-	-	-
535	TTP	7.6	-	-	-	7.7	-	-	-	-
	OTP	6.7	-	-	-	6.9	-	-	-	-

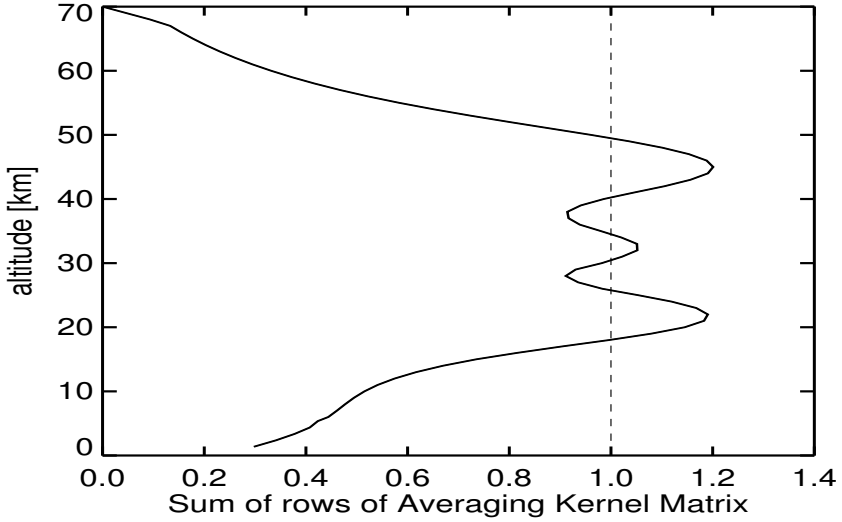

Figure 5.9: Sum of rows of averaging kernel matrix as an indicator for the sensitivity to the measurement. Values larger than about 1 indicate significant contribution from the measurements while lower values indicate stronger weighting towards the a priori value.

the two hemispheres. A sharp and cold tropopause is observed in the tropics which was also observed by *Highwood and Hoskins* [1998]. As expected, the tropopause height is usually higher in summer/fall than in winter/spring in mid latitude region [e.g. *Hoinka*, 1998]. But in polar region, the corresponding summer/fall ozone tropopause is lower than that of winter/spring. This fact is also reported by *Hoinka* [1998]. If the thermal tropopause is considered, the same behaviour is observed in the NH, but not in the SH.

Bethan et al. [1996] evaluated the difference between thermal and ozone tropopause. Based on stations located between 51°N and 79°N, they showed that the ozone tropopause lies about 0.5 km below the thermal tropopause. With few exceptions (e.g. SH polar summer/fall, and extreme ozone cases) this feature is reflected in the climatology.

5.7 Ozone profile retrieval: a case study

FUll Retrieval Method (FURM) [*Hoogen et al.*, 1999a, b] developed for the nadir viewing GOME [*Burrows et al.*, 1999a] has been used to assess the performance of the new climatology. This ozone profile retrieval algorithm is based on the optimal estimation scheme that includes *a priori* profiles in order to stabilize the iterative ozone retrieval [*Rodgers*, 2000]. In the optimal estimation approach, the atmospheric state vector is adjusted in iterative steps in order to minimize the weighted sum of squares between measured and modeled sun-normalized radiances and between the modeled and the *a priori* parameters. In the $(i+1)^{th}$ iteration, the estimate x_{i+1} is given by

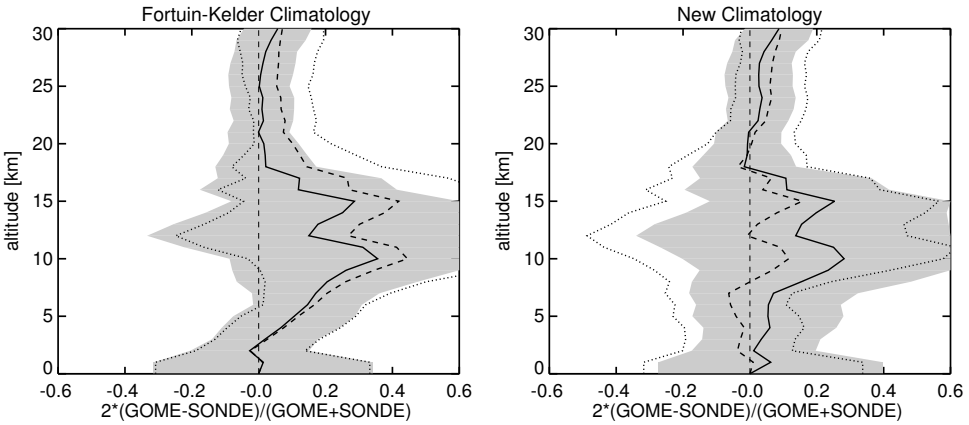

Figure 5.10: Mean relative deviation between retrieved GOME and ozonesonde profiles (solid line) and between climatological and ozonesondes profiles (dashed line), respectively for the year 1997 in Hohenpeissenberg (50 profiles). The profiles were retrieved using zonal monthly mean climatology (left panel) and our climatology (right panel). The shaded region shows the root mean square of mean relative deviation for the retrieval and the dotted line of our climatology.

$$\begin{aligned} x_{i+1} &= x_a + (K_i^T S_y^{-1} K_i + S_a^{-1})^{-1} \\ &\quad \times K_i^T S_y^{-1} [y - y_i + K_i (x_i - x_a)] \end{aligned} \tag{5.1}$$

where x_i and x_{i+1} are the calculated atmospheric state vectors, here the ozone profile, after i^{th} and $(i+1)^{th}$ iterations, respectively, which yield the retrieval solution $\hat{x}$ after the convergence is achieved. The logarithm of sun-normalized radiance as measured by GOME is y. y_i is the same quantity calculated with the radiative transfer model GOMETRAN [*Rozanov et al.*, 1997], x_a is the *a priori* atmospheric state, S_a and S_y are the measurement error covariance and the a priori covariance matrix, respectively, and K_i is the weighting function matrix after i^{th} iteration.

The sum of rows of the averaging kernel matrix,

$$A_i = (K_i^T S_y^{-1} K_i + S_a^{-1})^{-1} K_i^T S_y^{-1} K_i \tag{5.2}$$

is an indicator for the sensitivity of the retrieval to the measurement as shown in Figure 5.9. The information content is low below 15 km and above 50 km and in these altitude ranges climatological ozone information is of critical importance.

Figure 5.10 shows a comparison between GOME vertical ozone profiles derived with the zonal monthly mean ozone climatology from *Fortuin and Kelder* [1998], on one hand, and the new climatology presented in this paper, on the other, with results from

collocated ozonesondes launched in Hohenpeissenberg (47.8°, 11.0°, 50 profiles) during 1997. The mean profile of the new climatology agrees to better than 10% with the mean sonde profile with a root mean square of the mean relative deviation being less than 20% in most cases except in the tropopause. The difference between mean of the zonal monthly mean climatology and averaged sonde results from Hohenpeissenberg in the tropopause region is up to 40% and a factor of four higher compared to result from our climatology. The retrieved mean GOME profile shows a significant improvement in the troposphere by using our updated climatology presented here. Despite the improvement of the GOME retrieval using the new climatology a positive bias in the GOME-sonde mean differences in the lowermost stratosphere remain. This can be explained by the asymmetric averaging kernels that smooth the GOME profiles. In the lowermost stratosphere contribution from the ozone maximum increases the retrieved ozone down to the tropopause region [*Hoogen et al.*, 1999a; *Meijer et al.*, 2003].

5.8 Concluding remarks

Ozone column classified ozone and temperature climatologies at six month long seasonal and 30° wide latitude bins have been derived using large volume of recent ground-based and satellite data. The resulting set of ozone profiles is presented in Figure 5.4 and their variances are shown in Figure 5.5 and 5.6.

The climatologies were developed with the aim of improving the quality of *a priori* information. They are intended to be used for the ozone column and profile retrieval from GOME, SCIAMACHY, and their future generation like GOME-2. Separation of ozone profiles by column amount, what is used as a proxy for an atmospheric dynamics, has been proven to reduce the variances in the tropopause region compared to the traditional zonal monthly mean climatology. This helps to stabilize the fit results in the profile retrieval. A case study pursued at Hohenpeissenberg has demonstrated a good use of our climatology. Profile shape and matching temperature profile as additional information may also improve the accuracy of the retrieved TCO [*Wellemeyer et al.*, 1997].

The strong point of this climatology is the separation into hemispheres and semi-annual cycles. The semi-annual cycle allows a better distinction of profiles associated with low TCO that is dominated by chemically depleted ozone in winter/spring while in summer/fall it is related to the photochemical decay resulting in different profile shapes for the same TCO class. The use of POAM III data in the polar region and SHADOZ sonde data in the tropics has significantly improved the global representation of the ozone field. Nevertheless, the climatology needs to be regularly updated as the maturity of data sets in polar (satellite data), SH mid latitude regions and northern tropics (both ground-based) increases in order to account for the long-term changes in the ozone field. This climatology can be downloaded from http://www.iup.physik.uni-bremen.de/gome/o3climatology.

6 Influence of ozone and temperature climatology on the accuracy of satellite total ozone retrieval [1]

6.1 Overview

Ground and space based instruments have been measuring TCO for a significant number of years. These measurements do not only provide a unique record of ozone variability on local and global scale but also permit estimation of long-term ozone trends [*Bojkov et al.*, 1995a; *WMO*, 1998; *Staehelin et al.*, 2001; *Bodeker et al.*, 2001; *Fioletov et al.*, 2002]. Precise TCO observations from ground and space are a prerequisite for reliable long-term trend assessments. Ground-based measurements can provide trends at a single site and importantly serve as a control of possible long-term instrumental drifts of satellite instruments. Regular ground-based and satellite measurement comparisons are, thus, needed to ensure that the near global data coverage offered by satellite instruments is of as high quality as possible. Satellite TCO retrievals often have shown larger disagreement in high latitudes which may complicate trend studies in polar regions.

In addition to the long total ozone record by TOMS and Solar Backscatter UltraViolet (SBUV) starting in 1978 [*Heath and Park*, 1978], the Global Ozone Monitoring Experiment (GOME) [*Burrows et al.*, 1999a] has been providing global distribution of ozone for the last ten years. A long continuous data record length from a single instrument is desirable for long-term trend studies, however, due to the limited lifetime of satellites, a stable and consistent data record has to be derived from multiple instruments [*Bodeker et al.*, 2001].

GOME data is routinely retrieved with the off-line GOME Data Processor (GDP), which has undergone several years of progressive refinements since its first release in 1995. Various validation activities [*Lambert et al.*, 1999, 2002a] helped identify many limitations of the earlier versions of GDP and reduced the large discrepancies with a 2%–5% bias at SZA $<70^\circ$ and 10% at SZA $>70^\circ$ for GDP V2.7 to better than 1% in the current version GDP V4.0 [*Roozendael et al.*, 2006] for most part of globe except in polar regions [*Balis et al.*, 2006]. GDP V4.0 is a standard Differential Optical Absorption Spectroscopy (DOAS) retrieval where slant columns retrieved from a spectral fit are converted to vertical columns using air mass factors (AMFs) calculated at a single wavelength. However, ozone absorption in the Huggins band is wavelength dependent.

[1] This chapter is taken from the article "Lamsal, L. N., M. Weber, G. Labow, and J. P. Burrows (under revision 2006), Influence of ozone and temperature climatology on the accuracy of satellite total ozone retrieval, *J. Geophys. Res.*" with minor modification.

Wavelength dependence of ozone air mass factors become important, in particular at high SZA. This is taken into account by the WF-DOAS retrieval [*Coldewey-Egbers et al.*, 2004, 2005] that uses wavelength dependent weighting functions. In this approach vertical ozone column density is directly determined in the spectral fitting. Near global validation of the WF-DOAS results has shown that the WF-DOAS ozone retrievals are of comparable quality to the ground-based data [*Weber et al.*, 2005]. At polar latitudes, WF-DOAS results are improved with respect to GDP V3.0 but the discrepancy with respect to ground-based data still persists. In order to minimise the impact of the wavelength dependent AMF one can select a representative wavelength for the AMF in the standard DOAS approach [*Burrows et al.*, 1999a; *Lambert et al.*, 2002a].

GOME WF-DOAS ozone retrieval error studies [*Coldewey-Egbers et al.*, 2005] have identified the assumed ozone and temperature shapes as an important source of error which could lead to errors of up to 5% in the retrieved TCO at high SZA. Past GDP validation and delta-validation teams have also pointed out the ozone profile shape, which is used in the AMF calculation, as a cause of ozone retrieval errors. Following recommendations of the validation team, the TOMS V7 ozone profile climatology [*Wellemeyer et al.*, 1997] was implemented in GDP V3.0 to compute off-line AMFs. The current version GDP V4.0 uses the TOMS V7 ozone profile climatology [*Roozendael et al.*, 2006]. The most recent version of TOMS TCO retrieval algorithm (TOMS version 8) [*Bhartia*, 2003] has corrected several errors that were discovered in its predecessor version 7 [*McPeters et al.*, 1998]. One of the major upgrades to version 8 is the implementation of the improved TOMS V8 ozone climatology.

The choice of climatological ozone profile shapes for radiance calculations as in the case of WF-DOAS or TOMS retrievals or in the computation of AMF as in the case of GDP V4.0 is important. The accuracy of satellite TCO retrievals rely on our ability to model the propagation of radiation in the atmosphere and the resultant energy measured by the satellite instruments. The back-scattered radiance at a wavelength as measured by the instrument depends upon the actual atmospheric state (e.g. the entire ozone profile shape) from top of the atmosphere to surface. Deviation of assumed atmospheric properties from the real atmosphere (e.g. the standard ozone profiles) considered in radiative transfer calculations results in random errors in derived TCO. *Caudill et al.* [1997] pointed out that the incorrect simulated radiances at high SZA can result in TCO differences of up to 6%. *Wellemeyer et al.* [1997] showed that day-to-day variability in profile shapes gives rise to a standard deviation of 10% in TOMS TCO retrieval. Ozone retrieval errors associated with the assumed profile shape do not only affect the ozone retrieval accuracy but also propagate into subsequent data products which are derived from TCO.

It is clear that a proper choice of ozone profile climatology is important, especially at high latitudes where profile shape sensitivity of simulated radiance (and weighting functions) and/or AMF is high. One of the important aspects for improving TCO retrievals from satellite measurements is the proper use of representative ozone and temperature profiles. In this paper, we will analyse TCO retrieved by using some of the more recent climatologies that are commonly used in the TCO retrievals. Those climatologies are introduced in Section 6.2. The impact of the climatologies on TCO retrievals at some

selected stations of various climate zones are discussed in Section 6.3. A detailed study has been carried out at one of the high latitude stations (i.e. Syowa) where the choice of climatology is more important and is presented in Section 6.4. The conclusions are given in Section 6.5.

6.2 Climatologies under study

6.2.1 IUP climatology

IUP climatology [*Lamsal et al.*, 2004] provides a total ozone column dependent climatology of ozone and temperature profiles in 1 km steps up to 60 km. This climatology provides a separate set of profiles for both winter/spring and summer/fall seasons in high and mid latitudes of each hemisphere. No seasonal distinction is made for low latitude profiles. The ozone climatology was based on ozonesondes (mid and high latitudes), Southern Hemisphere Additional Ozonesondes (SHADOZ) [*Thompson et al.*, 2003a, b] (low latitude), Stratospheric Aerosol and Gas Experiment II (SAGE) II [e.g. *McCormick*, 1987; *Chu et al.*, 1989] (low and mid latitudes) and Polar Ozone and Aerosol Measurement III (POAM III) [*Lucke et al.*, 1999](high latitude) ozone profile data set primarily from 1990 to 2000. National Meteorological Center (NMC) and UKMet Office (UKMO) temperature profile data, which are used in SAGE II and POAM III ozone profile retrievals, respectively, and radiosonde (flown together with ozonesonde) data contributed to the associated temperature profile climatology.

6.2.2 TOMS V7 climatology

TOMS V7 profile shape climatology [*Wellemeyer et al.*, 1997] was derived by applying a Principal Component Analysis using balloon measurements and data from SAGE II. The climatology comprises of 26 standard profiles of ozone and temperatures: ten for high and mid latitudes and six for the low latitude. No distinction was made between hemispheres. These profiles span TCO values between 125 and 575 Dobson unit (DU) in 50 DU bins. For each ozone profile, a climatological temperature profile is supplied which was derived from SAGE II coincident NMC data. TOMS V7 standard profiles are expressed in Umkehr layers.

6.2.3 GSFC climatology

An updated monthly zonal mean ozone profile climatology has been prepared by NASA Goddard Space and Flight Centre [Ozone climatological profiles for satellite retrieval algorithms, Submitted to Journal of Geophysical Research, 2005, hereinafter referred to as McPeters et al., Submitted manuscript, 2005]. This climatology consists of monthly mean zonal mean ozone values for 18 bands (90 degree south to 90 degree north), each 10 degree wide and at altitude intervals of 1 km extending up to 60 km. It was compiled from ozonesonde data from 0 to 24 km, SAGE or Microwave Limb Sounder (MLS) from 29 km to 60 km and a weighted average in between. This climatology was based

on ozone observations from 1988–2001. The latest version called LLM (Labow, Logan, McPeters) climatology with an improved merging of the sonde and satellite data is available at (ftp@toms.gsfc.nasa.gov/pub/LLM_climatology).

6.2.4 TOMS V8 climatology

This is a recent update of the TOMS V7 ozone profile climatology. It provides total ozone classified ozone profiles for each 10 degree wide latitude bands and for each month. It is an extension of the NASA Goddard Space Flight Center (GSFC) climatology. This climatology, however, does not provide corresponding temperature profiles like TOMS V7.

6.2.5 KNMI climatology

The monthly mean ozone climatology developed at the Royal Netherlands Meteorological Institute (KNMI) consists of zonal mean ozone values and standard deviations for 17 zonal bands extending from 85 degree south to 85 degree north each of 10 degree wide and at 19 pressure levels (1000 hPa - 0.3 hPa) [*Fortuin and Kelder*, 1998]. This climatology was prepared from ozonesonde of 30 ozonesonde stations from 1000 to 30 hPa and SBUV satellite measurements from 30 to 0.3 hPa. Data from 1980 to 1990 were included in this climatology.

6.3 GOME total ozone retrieval

6.3.1 Forward Model: SCIATRAN 2.0

SCIATRAN is a 1-D radiative transfer code designed to allow fast and accurate simulation of radiance as measured by the space-based, air-borne, and ground-based instruments. SCIATRAN has become a widely applicable and valuable tool for the retrieval of atmospheric constituents from remote radiance measurements. A new generation of SCIATRAN (version 2.0) has been recently released [*Rozanov et al.*, 2005a].

The SCIATRAN radiative transfer model (RTM) [*Rozanov et al.*, 2002] is the successor to GOMETRAN [*Rozanov et al.*, 1997] that was developed to simulate back-scattered intensities and weighting functions to retrieve atmospheric parameters from GOME measurements. It covers the spectral range 240–2385 nm comprising the 8 spectral channels of SCIAMACHY [*Burrows et al.*, 1999a; *Bovensmann et al.*, 1999] and uses a spherical approximation to arbitrary order that is important for UV limb geometry [*Rozanov et al.*, 2004]. For nadir application pseudo-spherical approximation suffices. Rotational Raman scattering by air molecules has been included [*Vountas et al.*, 1998]. In particular for ozone retrievals, the Raman scattering also depends on the ozone profile shape and must be accounted for [*Coldewey-Egbers et al.*, 2005]. The Ring effect is significant for polarisation sensitive spectrometers like GOME and SCIAMACHY.

The different ozone and temperature climatologies have been included in SCIATRAN V2.0. In the radiative transfer calculation, ozone and temperature profiles have to be

specified. The new upgrade of the RTM facilitates the choice of following sets of ozone and temperature profile climatologies.

- IUP-Bremen climatology (ozone and temperature)
- TOMS V7 (ozone and temperature)
- TOMS V8 (ozone) and COSPAR International Reference Atmosphere 1986 (CIRA) zonal monthly mean (temperature) [*Fleming et al.*, 1988]
- GSFC zonal monthly mean (ozone) and CIRA (temperature)
- KNMI zonal monthly mean (ozone) and CIRA (temperature)
- Max Planck Institute (MPI) model based ozone and temperature profiles

The MPI trace gas climatology was derived from 2D chemical transport model calculations [*Crutzen and Brühl*, 1993] and was originally used for all trace gas retrievals from GOME [*Burrows et al.*, 1999a]. Selection of proper ozone and temperature profiles from GSFC, KNMI and CIRA climatologies requires as input information on latitude and month. If the total ozone amount is specified, the selected ozone profile is scaled. *A priori* TCO information is required for selecting TCO based climatologies (IUP, TOMS V7, TOMS V8). Using this information the ozone profile from IUP, TOMS V7, and TOMS V8 climatologies is generated as follows:

$$L(T) = \frac{(T - T^{(1)})}{(T^{(2)} - T^{(1)})} \times L^{(2)} + \frac{(T^{(2)} - T)}{(T^{(2)} - T^{(1)})} \times L^{(1)},$$

where adjacent climatological profiles with total column $T^{(1)}$ and $T^{(2)}$ corresponding to the profiles $L^{(1)}$ and $L^{(2)}$, respectively, that brackets the ozone profile L with TCO amount of T. In case of GSFC and KNMI climatologies, the monthly mean profile can optionally be scaled to the station TCO amount.

In IUP climatology, profiles are further classified according to season. TOMS V8 climatology provides such profiles for each 10 degree wide latitude bands whereas in the IUP and TOMS V7 climatologies, the bands are in accordance with climate zones, for example tropics, mid latitude and polar region. As in many other studies, the climate zones are specified by a fixed latitude. But, the meteorological regimes defined by the subtropical and polar frontal positions are not bounded to specific latitudes [*Hudson et al.*, 2003]. A large variation in ozone profiles along the frontal position and a significant jump in profile characteristics across it can result in a profile shape related error of 1% in the low to mid latitudes and 2% in the mid to high latitude [*Coldewey-Egbers et al.*, 2005]. Most of the climatologies use a smooth transition between different regions and seasons. The IUP climatology is separated in five zones: two polar regions ($>60^\circ$), two mid-latitude regions (30°–60°), and the tropics ($<30^\circ$) with two seasons winter/spring and summer/fall. Linear interpolation of profile shapes are done in ten degree wide bands centered at the boundaries and between seasons, here 15th November

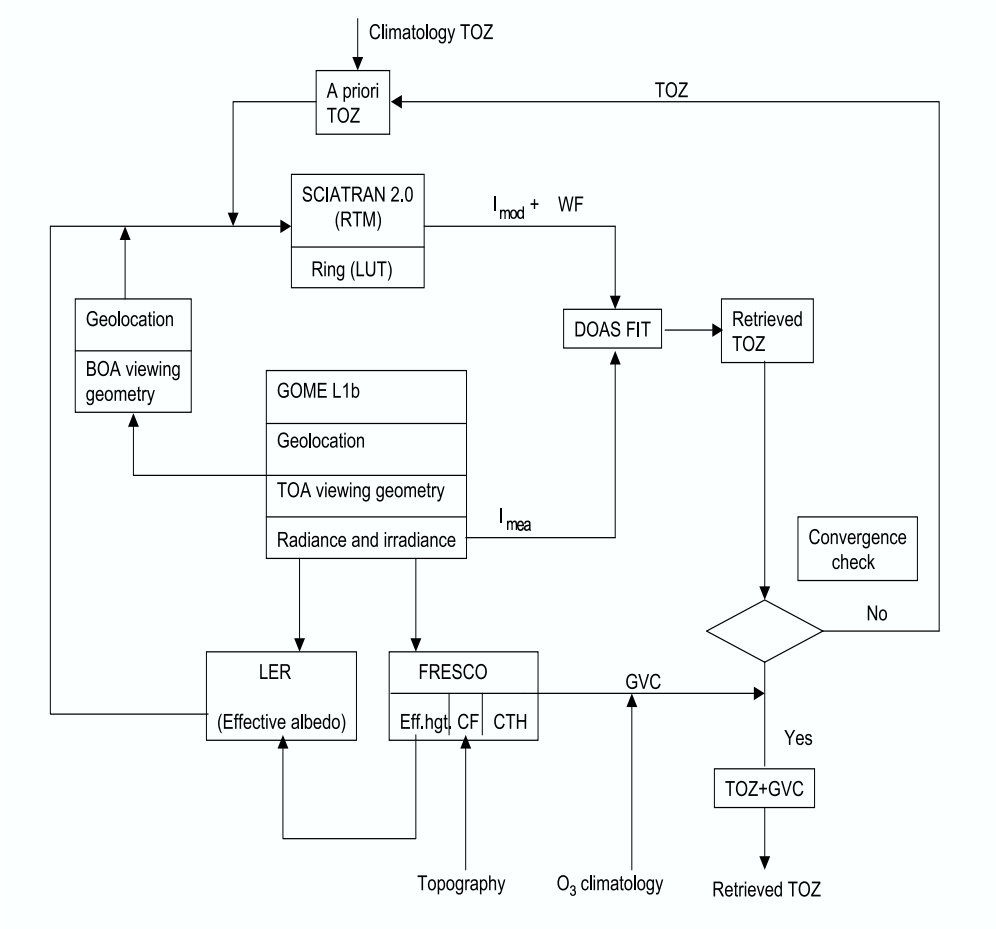

Figure 6.1: Scheme of the iterative online WF-DOAS TCO retrieval. I_{mod} is the modeled intensity and I_{mea} is the measured intensity. Meaning of acronyms: radiative transfer model (RTM), bottom of atmosphere (BOA), top of atmosphere (TOA), weighting function (WF), look-up-table (LUT), Lambert equivalent reflectivity (LER), effective height (Eff.hgt), cloud fraction (CF), cloud top height (CTH), ghost vertical column (GVC), and total ozone (TOZ). See the text for detail.

to 15th December (fall to winter) and 15th May to 15th June (spring to summer). TOMS V7 climatology is treated in a similar way. This climatology does not make seasonal distinctions in the profile shapes.

6.3.2 Retrieval: Online WF-DOAS

Weighting functions are the derivative of the radiation field with respect to the atmospheric parameters and they are used in the retrieval of absorbing species [*Rozanov et al.*, 1998]. *Buchwitz et al.* [2000b] introduced the WF-DOAS for trace gas retrievals in the near-infrared spectral region of SCIAMACHY. WF-DOAS has been applied for the first time to TCO retrievals from GOME UV spectral measurements [*Coldewey-Egbers et al.*, 2004, 2005] and validation using a large number of ground based measurements indicated an excellent agreement of WF-DOAS ozone results with ground based measurements to within 1% for most part of the globe [*Weber et al.*, 2005].

The principle behind this retrieval method is that the measured atmospheric optical depth can be approximated by a Taylor expansion around a reference intensity. A low order polynomial is added to account for all broadband contributions from surface albedo and aerosol. The Ring effect and the undersampling spectra are treated as an effective absorber. For interfering gases NO_2 and BrO, slant column fitting is applied. This algorithm makes use of wavelength dependent trace gas weighting functions. This overcomes one of the important limitations of the standard DOAS approach of computing air mass factor for the conversion of slant column into vertical column at a single wavelength of 325 nm. The standard DOAS approach assumes that the absorber is weak and the atmosphere is optically thin. In the original version 1 of WF-DOAS, the RTM quantities were pre-calculated and are read from look-up tables (LUT) [*Coldewey-Egbers et al.*, 2005]. The online version of WF-DOAS integrates the SCIATRAN RTM into the inversion scheme to retrieve TCO.

Figure 6.1 shows a schematic of the online algorithm. The retrieval scheme includes the extraction of GOME level 1b data including geolocation information and viewing geometry, and the preparation of additional data like effective albedo, ghost vertical column, etc., which are required by the retrieval procedure. Cloud top height, cloud fraction, and effective scene height are obtained from Fast Retrieval Scheme for Clouds from the Oxygen A-band (FRESCO) [*Koelemeijer et al.*, 2001]. Effective height is the weighted sum of ground altitude and cloud top height by the fractional cloud cover. Effective albedo is obtained from GOME sun-normalised radiance at 377.6 nm. The reader is referred to *Coldewey-Egbers et al.* [2005] for further detail.

The algorithm uses non-linear least squares fitting that includes wavelength shifts and squeeze [*Coldewey-Egbers et al.*, 2005] for the nadir earthshine spectrum to make the direct comparison between measured and modeled backscattered radiances. The modeled radiance, ozone and temperature weighting functions are computed as a function of solar zenith angle, line of sight, relative azimuth angle, surface height and effective albedo by using the radiative transfer model SCIATRAN V2.0 in the pseudo-spherical approximation.

A 8.2 nm wide fit window from 326.6 to 335.0 nm was selected. Iteration begins with

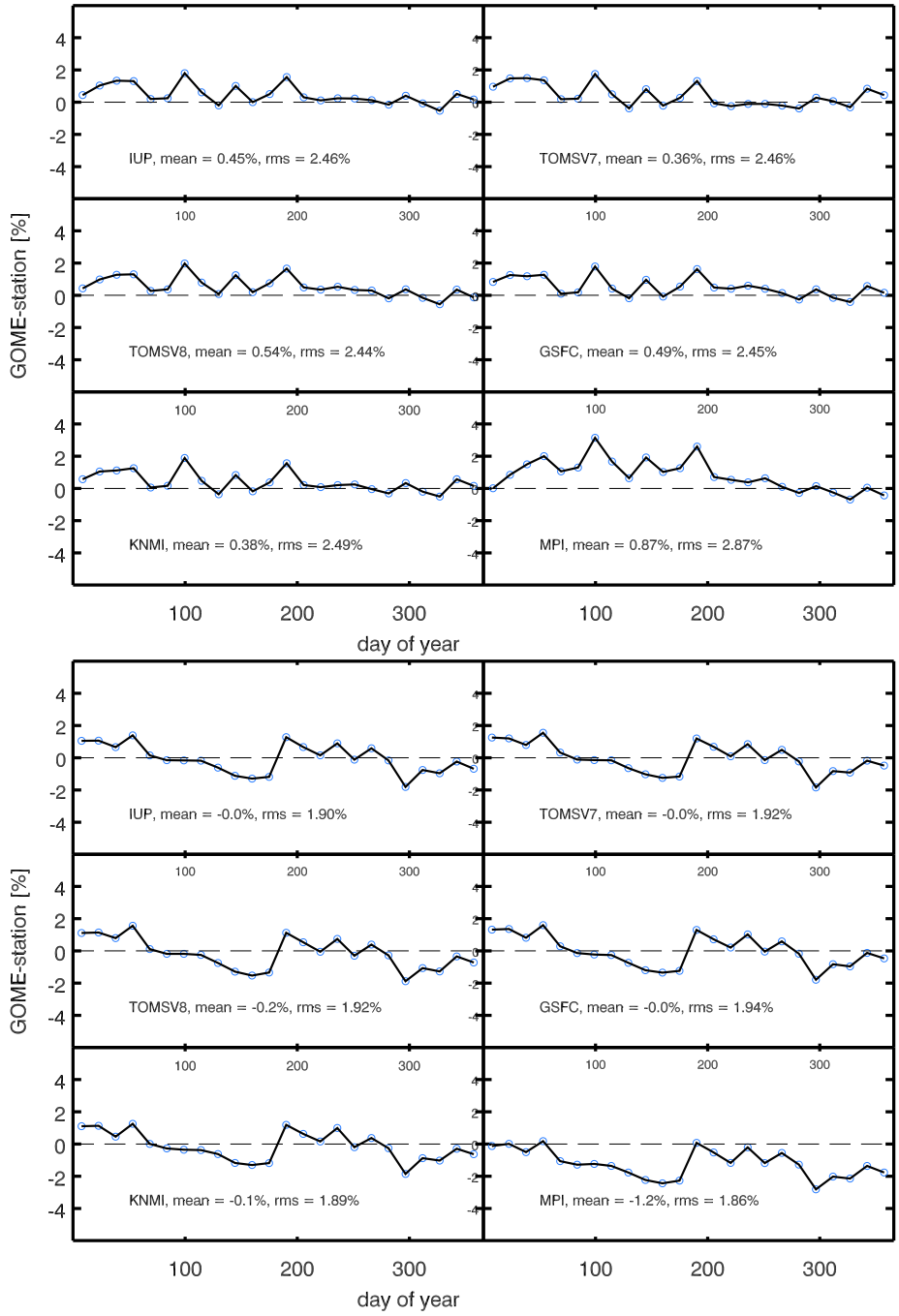

Figure 6.2: Difference in retrieved TCO utilising different ozone and temperature profile climatologies as indicated and Brewer data plotted as a function of day of year at Hohenpeissenberg (upper) and at Singapore (lower). The solid circles are the mean difference averaged over 15 days. The comparison was based on data from 1996 to 2003 for Hohenpeissenberg and from 1996 to 2000 for Singapore.

the online simulation of radiance and weighting functions leading to the direct fitting of vertical ozone column. The correct profile shape is chosen from climatology based on the geographical information, day of year, and optionally the TCO first guess. In order to account for the Ring effect a proper Ring data suited to the atmospheric scenario is selected from a LUT. The LUT was prepared for various atmospheric scenarios and viewing geometries. The impact of cloud in the retrieved TCO is accounted for by adding a so-called ghost vertical column (GVC) derived from zonal monthly mean ozone climatology, here the GSFC climatology. GVC is the amount of hidden ozone below cloud top pressure assuming an optically thick cloud and is weighted by cloud fraction before adding to the retrieved column. Zonal monthly mean climatologies generally are better suited for tropospheric ozone.

The various climatological ozone and temperature profiles were used in the GOME retrieval. Retrievals were performed at 6 stations: two each from Arctic and Antarctic and one each from mid and low latitude region. Those stations are Resolute (75.2°N, 74.7°E), Sodankylä (67.4°N, 26.6°E), Halley Bay (73.5°S, 26.7°W), Syowa (69.0°S, 39.6°E), Hohenpeissenberg (47.8°N, 11.0°E), and Singapore (1.3°N, 103.9°E). For this comparison, only those GOME pixels were considered whose footprint centre lay within 300 km collocation radius from the station, except for Hohenpeissenberg where the collocation radius was reduced to 160 km. This change was intended only for allowing more data in the comparison for other stations. Since the GOME footprint for most part is 320 km across track, the dependence on the collocation radius is not a critical issue. For all stations, the measurement had to take place on the same day of the satellite overpass.

The comparison at Resolute, Sodankylä, and Hohenpeissenberg was done with Brewer measurements. A properly calibrated Brewer instrument provides TCO values at an accuracy of $\pm$ 2.5% and its precision is estimated to be $\pm$ 0.25% [*Kerr and McElroy*, 1995]. The TCO amount derived from the standard algorithm results in some systematic errors, for instance, coming from uncertainties in the cross-sections [*Kerr*, 2002]. Syowa, Halley Bay, and Singapore TCO observations were from Dobson instruments. The Dobson instrument has performance similar to a Brewer spectrophotometer. Brewer measurements have the advantage over Dobson that they are less sensitive to ozone temperature variation [*Kerr*, 2002; *Weber et al.*, 2005; *Bernhard et al.*, 2005]. In the WMO standard retrieval the ozone cross-section is fixed at -46°C that can lead to systematic errors in the Dobson retrieval [*Bernhard et al.*, 2005].

Figure 6.2 (left panel) shows the difference between GOME WF-DOAS and Hohenpeissenberg daily averaged Brewer TCO data (in percent) plotted as a function of day in the year 1996–2003. During the period Brewer TCO ranged from 219 DU to 466 DU and the GOME SZA was in the range 25°–73°. Except for the MPI profile for June and 20°-30°N latitude band, WF-DOAS results show mean biases of less than 0.5% and a small seasonal signature irrespective of which climatology was used. Tropical ozone profiles in June might differ significantly from the profiles at Hohenpeissenberg (mid latitude) and consequently resulted in somewhat larger biases. The motivation for using MPI profile was to elucidate the error in the retrieved TCO caused by the application of a single arbitrary profile. These comparisons have indicated that the ozone and temper-

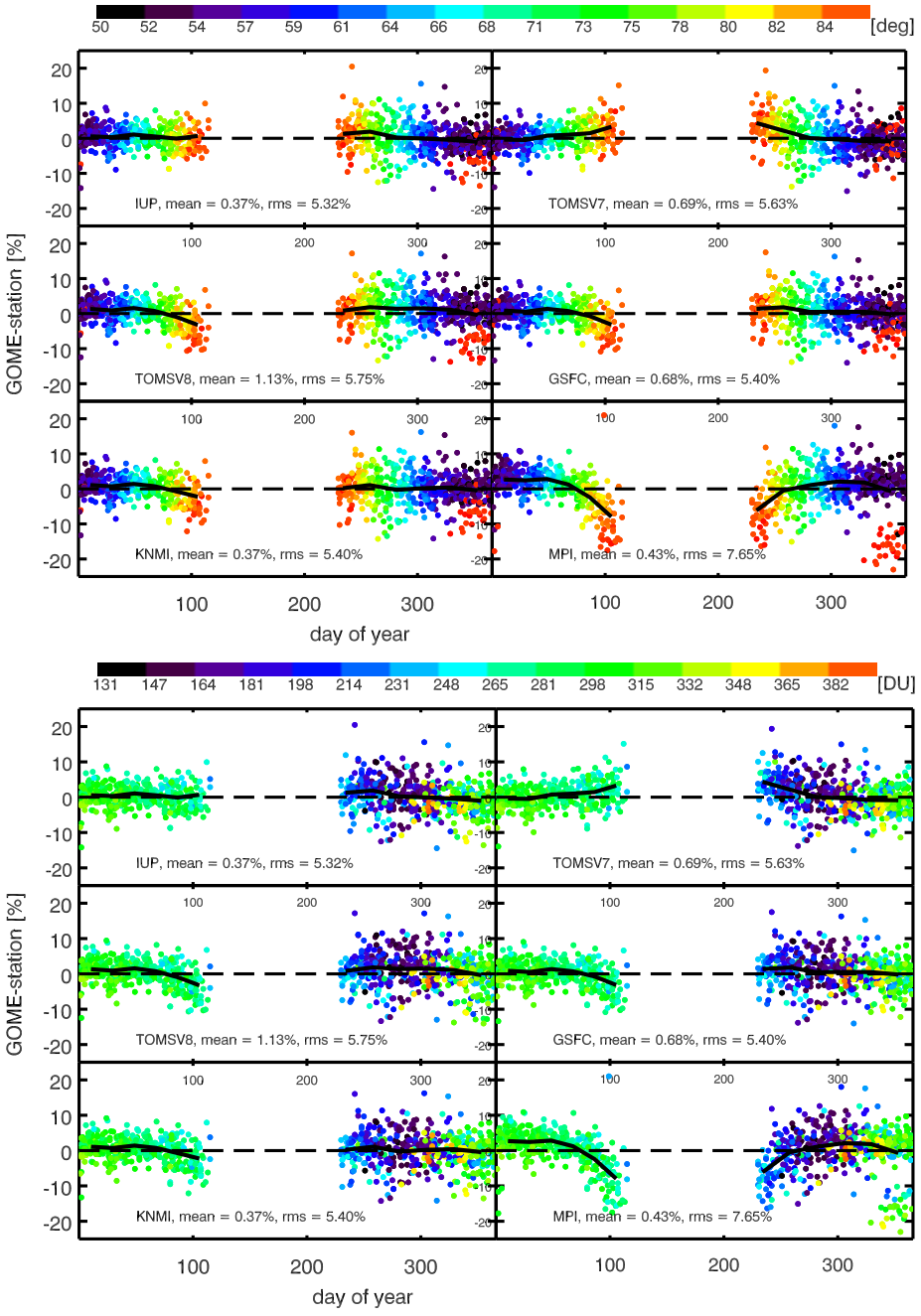

Figure 6.3: Difference in retrieved TCO and Dobson data plotted as a function of day of year at Syowa. Ground based TCO data was obtained from a Dobson spectrometer. The data points are color coded by GOME SZA (upper) and Dobson TCO (lower) through the use of colors.

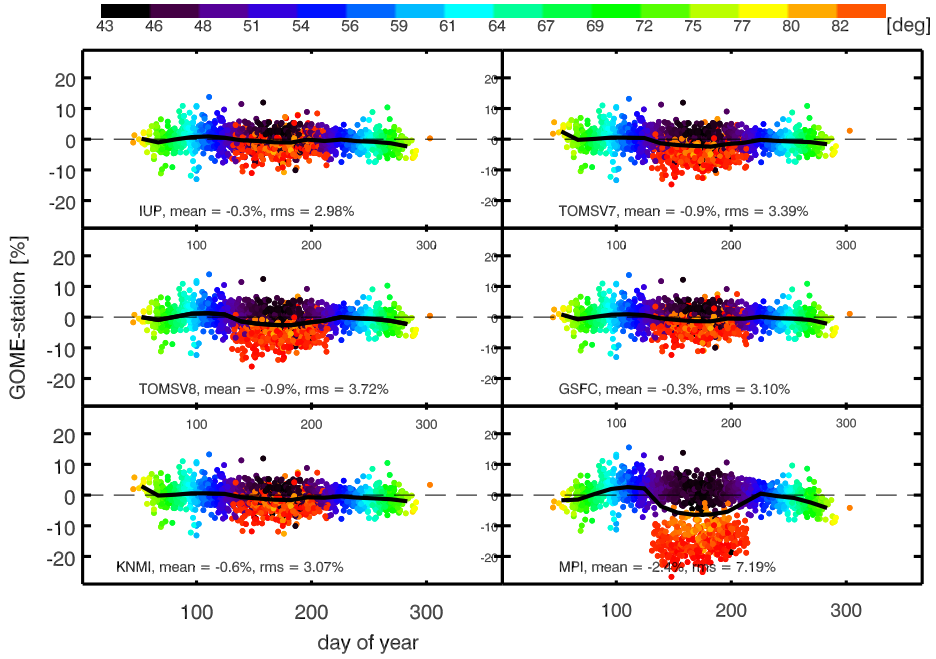

Figure 6.4: Same as Figure 6.3 but for Sodankylä.

ature profiles that are used in forward models to compute the radiance and weighting functions have a minor error contribution to TCO retrieval at mid latitudes. Similar results are observed in Singapore (Figure 6.2 right panel), a low latitude station. The comparison for this station is limited to the period 1996–2000 because of the problem in the station data quality (Vitali Fioletov, Meteorological Service of Canada, 2005, personal communication). GOME total ozone retrieved using the MPI profile is slightly lower than by using other climatologies. Note that the effect at Singapore is opposite to that at Hohenpeissenberg. The MPI profile peaks at higher altitude than ozone profile at Hohenpeissenberg. Its use in the retrieval results in higher TCO. The MPI profile peaks at lower altitude than ozone profile at Singapore and its use causes lower TCO.

Unlike at Hohenpeissenberg and Singapore, WF-DOAS results obtained by using different climatologies at high latitude stations are highly sensitive to the choice of climatological profiles. The difference (in percent) between WF-DOAS and the ground-based data from Syowa as a function of day of year (1996–2003) is shown in Figure 6.3. Each panel corresponds to a retrieval using the indicated climatology. The third dimension is introduced through colors to identify the GOME TCO dependence by GOME SZA and Dobson TCO. Each colored circle represents a collocated single measurement and the solid black line the monthly mean of the difference. In Figure 6.3, the austral polar night as indicated by the GOME data gap separates two distinct seasonal feature: (1) summer/early fall with low scatter pattern and (2) late winter/spring with high scatter pattern. Large standard deviation in the spring months is due to the large day to day vari-

ability in the atmospheric profile shapes and hence results in larger error in the satellite retrieval. This error is termed as random error and can be as large as 10%. We also identified some systematic errors which are specific to a given climatology application in the respective TCO retrievals. As can be seen in the figure, this error is SZA dependent which is positive for TOMS V7, negative for MPI and almost zero for IUP climatology. Based on these data, a clear dependency on TCO is not evident. Results from another Antarctic station Halley Bay are fairly similar.

Comparison of retrievals at one of the Arctic stations Sodankylä is shown in Figure 6.4. Effect of climatology in the retrieval is not noticeable for GOME SZA up to about 75°. Differences are observed for higher SZA, in particular for TOMS V7, TOMS V8, and MPI (June, 20°-30°N) profile. Large bias of the order of 20% is observed with the MPI profile at high SZA. This result is consistent with that observed at Syowa. The difference for the TOMS V7 climatology is not as high as at Syowa. Results from another Arctic station Resolute are also similar. Zonal monthly mean climatologies (GSFC and KNMI) result in very good retrievals at both of these Arctic stations.

In both examples presented above, it is interesting to note that GOME observations at high solar zenith angles are occuring near the polar night terminator (winter) and during polar summer. Near the northern polar nights GOME observations over Sodankylä did not exceed 80° SZA and therefore the SZA dependent bias is not very prominent for all climatologies. For all zonal monthly mean climatologies including the single MPI profile, the retrieved TCO at high SZA is negatively biased at both stations (polar night and summer). Near the polar night terminator the TCO retrieved with the TOMS V7 climatology shows no significant bias at Sodankylä (northern hemisphere), but positive bias at Syowa (southern hemisphere). A weak negative bias at Sodankylä and no significant bias at Syowa are evident at high SZA during polar summer. These inconsistencies could be due to the difference in ozone and temperature profiles between two hemispheres and/or seasons, which the TOMS V7 climatology does not distinguish.

6.4 Analysis of retrievals at Syowa

6.4.1 Direct comparison of sonde measurements with climatologies

Four years of ozonesonde data (1996–1999) from Syowa, Antarctica, were used in order to check if the climatologies presented in Section 6.2 can reproduce the measurements. Syowa uses Japanese sonde KC which is similar to the Carbon Iodide (CI) sonde of *Komhyr* [1969]. KC ozonesondes give less consistent results than Electrochemical Concentration Cell (ECC) [*Komhyr*, 1969; *Smit et al.*, 1997], however, this station continues using the sensor for reasons of homogeneity of long-term ozone profile time series. Dobson spectrophotometer stationed at Syowa provide matching total ozone values to ozonesonding profiles. TCO measurements from Dobson spectrophotometer have the relative uncertainty of 2% [*Basher*, 1985; *Hare and Fioletov*, 1998]. Both of these data sets were available from the World Ozone and Ultraviolet Radiation Data Center (WOUDC). In order to compare ozone concentration from ozone column classified climatologies (IUP, TOMS V7, and TOMS V8) with that from ozonesonde measurements,

TCO information obtained from Dobson instrument is required. Linear interpolation in TCO is essentially performed using the equation given in Section 6.3.1. TOMS V8 climatology requires additional information on month and latitude. For the zonal monthly mean climatologies (KNMI and GSFC), month and latitude information suffice. In case of GSFC and KNMI climatologies, the monthly mean profile can optionally be scaled to the station TCO amount. Given these variables (TCO, month, latitude), climatological ozone concentration at any altitude level can be compared with regular ozonesonde measurements.

For ozonesonde-climatology comparison, we ensure that ozone concentrations are expressed in the same units and the values are on a common grid. Both IUP and GSFC climatologies provide ozone values at 1 km altitude steps. KNMI climatology expressed in pressure levels was converted to the same altitude levels by using the US standard atmosphere and spline interpolation. Special care was taken to express the TOMS V7 and TOMS V8 ozone values in Dobson units given for Umkehr layers into the same altitude intervals as IUP climatology. Ozone number density at layer midpoints were calculated from the ozone values at consecutive layers which were finally interpolated to the 1 km altitude grid. Between 60 km and 98.6 km the volume mixing ratio at 60 km was linearly interpolated to 0.0521105 ppmv at 98.6 km from *Liang et al.* [1997]. The individual ozonesonde readings in units of partial pressure were converted into number density.

Figure 6.5 gives the ozone number density reproduced by the climatologies at different altitudes as a function of TCO amount measured at Syowa. Sonde data interpolated to those altitude levels are also shown in the figure. Shown are the mean and 2σ variance of ozone from averaging in 25 DU wide TCO bins. The selected altitudes cover a broad range from the tropopause to the height of ozone peak. It consists of dynamically highly sensitive region (around tropopause) where short-term ozone variation is controlled to a large extent by horizontal and vertical transport [*Salby and Callaghan*, 1993] as well as altitudes where the chemical destruction of ozone is rapid and severe. Higher variability in ozone is observed in this altitude range.

Climatological ozone number density is less than ozonesonde values at 10.5 km. IUP climatology shows better agreement than others but it also underestimates winter/spring ozone values. All updated and recent climatologies reproduce ozonesonde values at 15 km and 19.5 km very well. KNMI climatology overestimates observations mainly in the lower stratosphere. This climatology is based on data from 80's and the dramatic ozone loss seen mostly in the 90's is not captured. TOMS V7 climatology appears to be too low around and below 15 km. Simple scalar scaling of the monthly mean climatologies slightly improves their agreement with ozonesondes.

The reproducibility of the climatologies for ozone number density presented here only at selected altitude levels should not be understood as the general feature at all levels. A climatology performing well at a certain altitude level may not behave as well at other levels. Additionally, the test was limited to the altitude below 24 km. Although the altitude region of ozone number density peak contributes most strongly to the total column amount, TCO retrieval accuracy rely on the accuracy of a climatological profile over the entire altitude range. Therefore it is difficult to draw any firm conclusion regarding

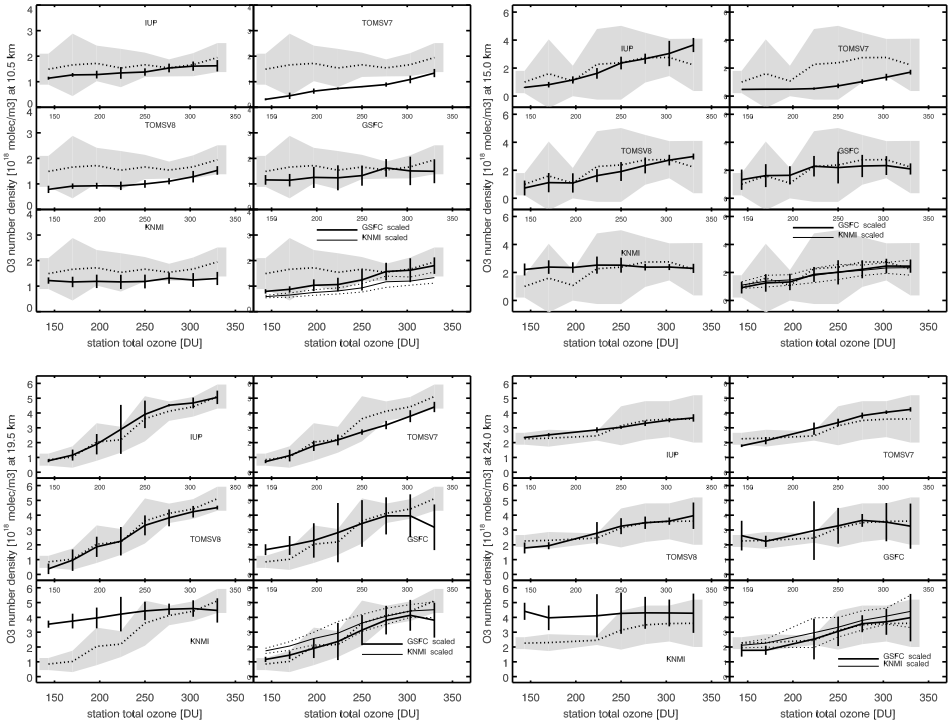

Figure 6.5: Ozone number density at 10.5 km (upper left panel), 15 km (upper right panel), 19.5 km (lower left panel), and 24 km (lower right panel) plotted as a function of ground based TCO measurements at Syowa (69°S, 39°E). The dotted line represents the mean and the shaded region indicates 2σ level of ozonesonde measurements. The black line and the bar represent the mean and 2σ level of ozone values reproduced by the climatologies. In case of GSFC and KNMI climatologies, the profiles scaled to the station TCO amount are also shown in a separate plot (sixth figure in each panel). Here the 2σ level of ozone values for the KNMI scaled are shown by two thin dotted lines.

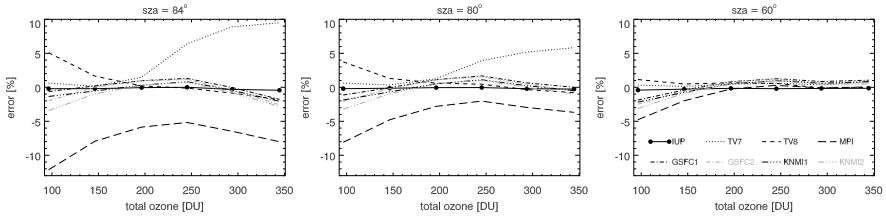

Figure 6.6: Error in the retrieved TCO caused by the differences in TCO amount or/and distribution of ozone and temperature in the above mentioned climatologies using the IUP climatology as a reference. Three columns correspond to solar zenith angle of 84°, 80°, and 60°. GSFC2 and KNMI2 represent the original profiles and GSFC1 and KNMI1 are the profiles which are obtained by scaling the original profiles with a given ozone column.

the accuracy of a particular climatology and its impact on TCO retrievals. Nevertheless, for the purpose of identifying the profile shape related errors in TCO retrieval this kind of test might be helpful to some extent. In general the agreement is satisfactory at the ozone number density peak height for all climatologies, with the exception of the KNMI and TOMS V7 climatologies. This could be the reason for such larger errors observed in the case of TOMS V7 climatology during high solar zenith angle conditions (Figure 6.3). Despite the large discrepancies in ozone number density between ozonesonde and KNMI climatology, the TCO retrievals with it is hardly any worse. This could primarily be due to the fact that the GOME SZA is moderate when there is extremely low ozone and consequently larger ozonesonde-KNMI difference (see Figure 6.3). Relatively good ozonesonde-climatology agreement at those selected altitudes for IUP climatology is suggestive of improved retrievals upon its use.

6.4.2 Retrieval studies using modeled radiance

For further investigation of the influence of ozone and temperature profiles of various climatologies on TCO retrievals, we also retrieved total ozone from synthetic radiances. The main motivation here is that all the input quantities which produce the spectra will be known and the role of each of the inputs on the retrieved TCO can be investigated.

The radiances were computed using SCIATRAN V2.0 at TCO 100 DU, 150 DU, 200 DU, 250 DU, 300 DU, and 350 DU, SZA 84°, 80°, and 60°, relative azimuth angle 0°, line of sight 0°, surface height 2 km, effective albedo 0.1, and latitude and longitude that of Syowa. A clear sky scenario was assumed. Ozone and temperature profiles were taken from IUP climatology. These radiance were used to retrieve TCO using the online WF-DOAS algorithm. The main purpose of taking the same radiative transfer model is to avoid any retrieval error from model bias. We retrieved TCO from the synthetic radiances by altering the climatologies but keeping all other input parameters identical. For zonal monthly mean climatologies GSFC and KNMI, two retrievals were performed: (1) with and (2) without scaling ozone profiles to the retrieved TCO during each iteration.

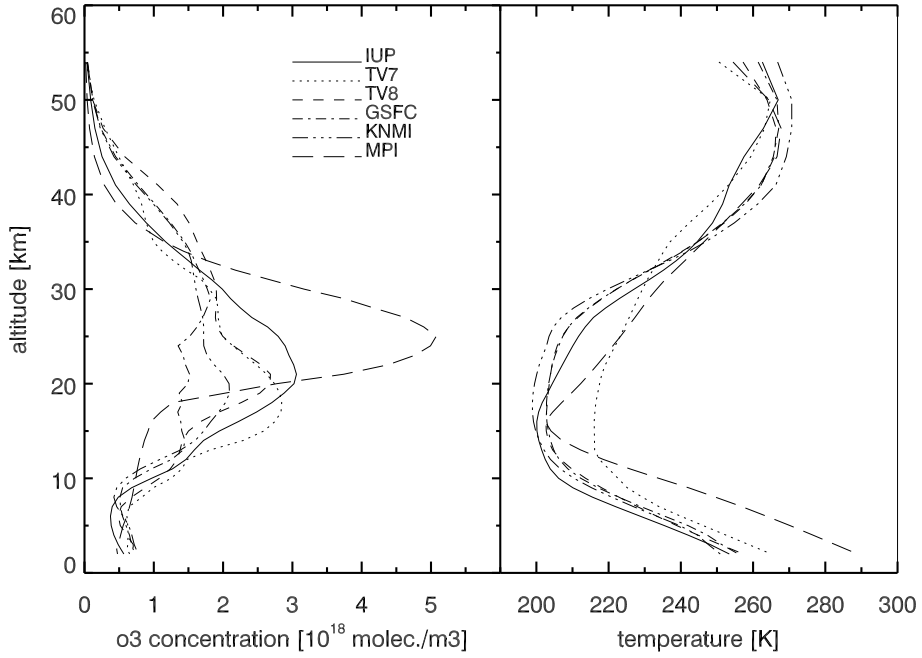

Figure 6.7: Ozone (left) and temperature (right) profiles in September at Syowa from various climatologies. For TCO classified climatologies, the profile corresponds to 250 DU.

Figure 6.6 shows the error in retrieved TCO plotted as a function of total ozone. Results are presented for three SZA 84°, 80°, and 60°. As expected, the retrieval using IUP climatology reproduced TCO (i.e. almost zero bias). TCO using TOMS V7 climatology shows systematic bias beyond 200 DU and is SZA dependent. The error can be as high as 10% at 350 DU and SZA of 84°. Retrieved TCO using TOMS V8 climatology is biased for low ozone cases and the error can reach up to 5% at 100 DU and SZA of 84°. Errors from zonal monthly mean climatologies range from -2% to 2% depending upon the TCO amount. They tend to underestimate at low and high ozone cases. The method of scaling zonal monthly mean ozone profiles to total ozone can improve the retrieved TCO by up to 1% in those cases. Retrieved TCO using MPI profiles largely underestimates and the error enhances with SZA.

The observed discrepancies in the TCO retrieved by using different climatologies have indicated that the distribution of ozone with altitude can be different despite having the same ozone column amount. The top of atmosphere (TOA) earth shine radiance responds differently to changes in ozone concentration and temperature by ozone absorption at various altitude levels [*Rozanov et al.*, 1998]. As an example, we further analysed the TCO retrieval at 250 DU of Figure 6.6. Figure 6.7 shows the ozone and temperature profiles in September at 69°S from various climatologies. IUP, TOMS V7 and TOMS V8 ozone profiles correspond to the ozone column amount of 250 DU. Both IUP and TOMS V8 profile peak at around 20 km, TOMS V7 around 17 km, and MPI profile at 25 km.

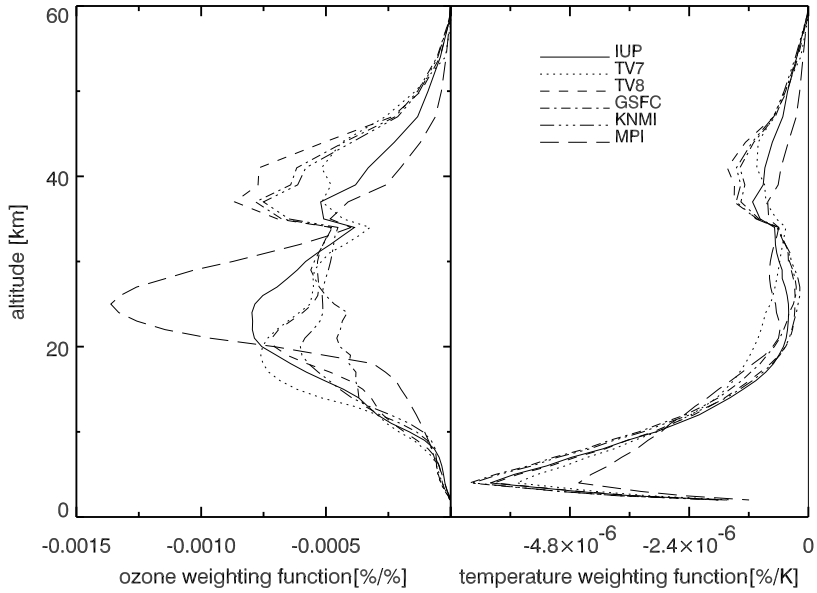

Figure 6.8: Ozone (left) and temperature weighting functions at 327.9 nm in the Hartley-Huggins band of ozone. These weighting functions correspond to the TCO retrievals using simulated radiance based on the 250 DU profile of the IUP climatology.

Zonal monthly mean profiles from GSFC and KNMI show ozone depletion near 20 km as might be expected from simple averaging of all profiles in September, which consists of ozone hole profiles as well. Moreover, some ozone profiles are flatter than others. Temperature profiles also vary significantly, particularly the TOMS V7 temperature profile which is warmer than others up to 35 km and colder above. This difference might be due to the fact that TOMS V7 climatology provides a set of temperature profiles common to warmer northern and colder southern hemispheres. The tropical MPI profile is warmer and is characterized by a sharp tropopause [*Randel et al.*, 2003].

Figure 6.8 shows the ozone and temperature weighting functions at 327.9 nm, which corresponds to the retrieved TCO as following: IUP 245.2 DU, TOMS V7 254.9 DU, TOMS V8 246.4 DU, GSFC 249.1 DU, KNMI 247.9 DU, and MPI 240.0 DU. Ozone profile corresponding to the 250 DU TCO (input) spans from 0 km to 60 km. The difference between input 250 DU and TCO retrieved with the IUP climatology is mainly due to the fact that the surface altitude is assumed to be 2 km for TCO retrievals. Integrated ozone from 0 km to 2 km turns out to be about 4.7 DU. The TOMS V7 profile thus can cause an overestimation of about 3.9% (254.9 DU vs 245.3 DU), the MPI profile causes underestimation by about 2.2% (240.0 DU vs 245.3 DU) and all other show better agreement.

The ozone weighting function indicates the percent change of the radiance field due to a 1% change in the vertically integrated ozone profile. Likewise the temperature weighting function represents the change of radiance field due to a change of 1 K at all

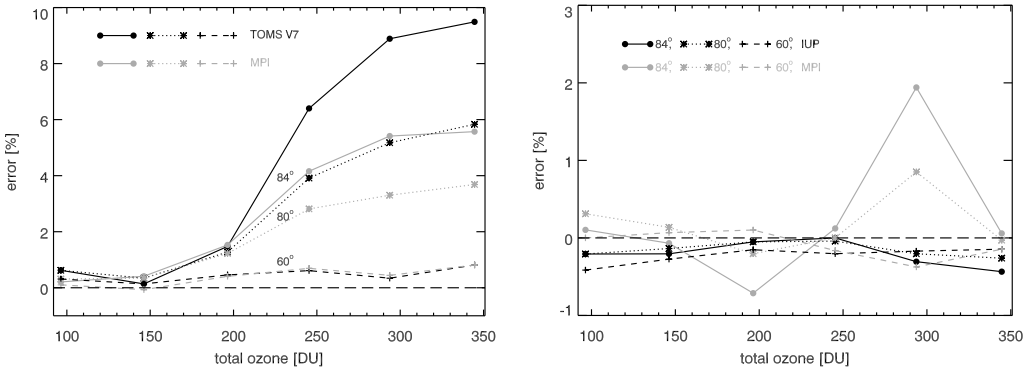

Figure 6.9: Error in retrieved TCO associated with TOMS V7 temperature profile (left). Error in retrieved TCO using the TOMS V7 ozone and temperature profiles are shown in black lines and the grey lines represent the errors while using TOMS V7 ozone climatology in combination with the MPI temperature profile (of 60–70°S, September). Similar results but for the IUP climatology is shown in right. Reference scenarios were calculated using the IUP climatology (at the location of Syowa, winter/spring seasons).

altitudes. The shape of these weighting functions might differ significantly depending on the climatology as presented in Figure 6.7. Ozone weighting functions from various climatologies resemble their respective ozone profile shapes. TOMS V7 TOA radiance is associated with broad high response altitude range peaking at about 17 km. For MPI, the response is mainly coming from 20 to 35 km with maximum response from about 25 km. TOMS V8, GSFC, and KNMI climatologies have a similar peak response altitude around 23 km. These monthly mean climatologies have a stronger secondary maxima that peaks around 37 km. Their lower response at lower altitudes might be compensated at higher altitudes. Despite the fact that the temperature weighting functions from different climatologies also vary from each other, most significantly for TOMS V7 and MPI, the relative shapes are quite similar. Influence of temperature on molecular scattering and ozone absorption coefficient are the cause for the larger values in lower altitude and higher altitude respectively. Here it is important to point out that the weighting functions on which the TOA radiance depends is shown only for 327.9 nm. The WF-DOAS TCO retrieval uses spectral fitting over entire wavelength window from 326.5 nm to 335 nm. It is therefore difficult to completely associate the observed difference in the ozone and temperature weighting functions to the retrieved TCO.

These investigations have indicated that the larger errors from TOMS V7 profile shape climatology might also be related to its temperature profile. To confirm this, we retrieved total ozone from the same synthetic radiance as explained above using ozone profiles from various climatologies but in combination with a single temperature profile from a zonal monthly mean MPI profile of September and 60–70°S latitude band. This provides an opportunity to isolate TCO error from temperature and from ozone of various climatologies. No significant difference is found in the case of zonal monthly mean climatologies (GSFC, KNMI, and TOMS V8), some discrepancy is found in the case of

IUP climatology, and a substantial difference is evident for TOMS V7 climatology (Figure 6.9). As discussed in Section 6.3.1, the CIRA zonal monthly mean temperature climatology has been used in combination with GSFC, KNMI, or TOMS V8 ozone climatology. Similar results for these climatologies would mean that the MPI profile agrees with the CIRA profile. Retrieval using IUP ozone climatology and MPI temperature profiles also shows an increased error around 300 DU and the error is SZA dependent reaching up to 2% for SZA of 84°. It could be that the IUP SH (southern hemisphere) polar winter/spring temperature profiles for certain ozone class have some errors due to the use of limited data sets in the polar regions [*Lamsal et al.*, 2004]. Retrieval errors with TOMS V7 ozone and temperature climatologies as shown in Figure 6.9 is consistent with the one shown in Figure 6.3. The TCO error, which is both SZA and TCO dependent, can reach up to 10% for SZA of 84° and TCO of about 350 DU. Interestingly, using TOMS V7 ozone and MPI temperature profile the error in the retrieved TCO is lowered systematically by almost 50% and as such the TCO error for SZA of 84° and TCO of about 350 DU decreases to about 5.5%. Thus it appears that the TOMS V7 temperature is responsible for 50% of the observed error in Figure 6.3. Note that at lower SZA the error in retrieved TCO is less than 0.5% irrespective of whether the temperature profile is taken from the TOMS V7 climatology or the MPI model-based climatology.

6.5 Conclusion

Good *a priori* knowledge of vertical profiles of ozone and temperature are essential for the calculation of back-scattered UV radiances used in the total ozone retrieval. The temperature profile is needed because ozone cross-sections are weakly temperature dependent. Error in assumed profiles propagates into simulated radiances, AMF, etc. thereby finally affecting the accuracy of retrieved TCO. In order to investigate the profile related TCO retrieval error, TCO retrievals were analysed at 6 stations that represent Antarctic (Syowa and Halley Bay), Arctic (Sodankylä and Resolute), mid latitude (Hohenpeissenberg) and low latitude (Singapore). More stations were included in the polar region because the profile sensitivity of TCO retrieval is significantly larger in this region. GOME TCO retrieved by using WF-DOAS shows negligible effect of climatological profiles at Singapore and Hohenpeissenberg but considerable systematic differences are observed at high latitude stations, specially for SZA larger than 70°. Our studies based on the GOME spectral measurements and synthetic radiances that were used for TCO retrievals using the WF-DOAS algorithm, have identified both random and systematic errors in the retrieved TCO originating from the climatological ozone and temperature profiles. The systematic errors can be up to 10% (e.g. TOMS V7 climatology) at high SZA. Profile sensitivity of TOA radiance is strong when the SZA gets large. By using the IUP climatology an improvement in the retrieved TCO at high SZA was observed. The TOMS V8 climatology shows improvements over its predecessor TOMS V7. Zonal monthly mean ozone climatologies scaled by TCO result in similar retrievals as the updated column classified IUP climatology, with the exception in southern polar region (e.g. Syowa) where the chemical loss of ozone is severe. The investigation carried

out in this paper provides a clear message that regular updates of ozone and temperature climatologies can remove some of the discrepancies observed in the current satellite ozone products.

7 Retrieval and validation of WF-DOAS total ozone from SCIAMACHY

7.1 Overview

Satellite-based ozone observations are important for detecting, verifying, and understanding ozone depletion. Such activities require an international effort on launching satellite instruments, improving retrieval algorithms, validating and refining the ozone data. Both the NASA and NOAA series of instruments, TOMS [*Bhartia and Wellemeyer*, 2004] and SBUV [*Bhartia et al.*, 1996], have made a major contribution by providing ozone data from space since 1979. Currently there are three European satellite instruments as part of the European contribution in this respect: GOME on ERS-2 [*Burrows et al.*, 1999a] operating since April 1995, SCIAMACHY as part of the atmospheric chemistry payload of the third ESA Earth observation satellite platform called ENVISAT which was launched in March 2002 [*Bovensmann et al.*, 1999] and OMI on-board EOS-AURA [*Veefkind and Haan*, 2002] operating since July 2004. Many other advanced instruments are planned for future satellite missions. The satellite total ozone retrieval algorithms are also matured and are able to produce high quality long-term ozone data sets [*Bhartia*, 2003; *Coldewey-Egbers et al.*, 2005; *Weber et al.*, 2005; *Petropavlovskikh et al.*, 2005; *Roozendael et al.*, 2006; *Balis et al.*, 2006].

Since satellite instruments have limited lifetime, it is necessary to obtain ozone data from multiple satellites/instruments for studying long-term trends. This emphasizes the need to develop an approach to produce a globally harmonized data set of known quality. Significant work has been done in developing a merged data set from SBUV and TOMS series of instruments. For this, the major efforts have been on identification and correction of calibration and algorithm problems [*Hilsenrath et al.*, 1998]. Similar efforts are also required for GOME and SCIAMACHY which are providing a wealth of data for the last 11 years. Global total ozone data from GOME and SCIAMACHY overlap for a period of 16 months which will be very helpful to compare and combine the two data sets.

The work presented here is an attempt to make an effort of creating a combined trend-quality data set from GOME and SCIAMACHY. The data set will be continued by OMI, and GOME-2 series of instruments [*Callies et al.*, 2000]. In this context, the necessity of developing a high-quality retrieval algorithm has a high priority. The present operational ESA algorithm for SCIAMACHY which will be described in Section 7.2, is known to have several shortcomings because the algorithm is based on outdated GDP V2.4 of GOME. Those limitations will be highlighted in Sections 7.2.2, 7.2.3, and 7.2.4 by comparing its results with the GOME WF-DOAS total ozone. Our motivation for adapting the WF-

DOAS algorithm for SCIAMACHY was, on one hand, its good performance for GOME and, on the other hand, the known problems with the current SCIAMACHY operational ozone data.

7.2 SCIAMACHY operational total ozone product [1]

Vertical column densities of ozone are retrieved from SCIAMACHY and GOME UV-VIS nadir measurements by using the Differential Optical Absorption Spectroscopy (DOAS, Platt 1994) in the 325-335 nm (UV) spectral window. It is also possible to retrieve ozone slant columns in the 425-450 nm (VIS) spectral window from SCIAMACHY. The SCIAMACHY VIS ozone product still shows major errors [e. g. *Bracher et al.*, 2002]. After generation of four versions of SCIAMACHY operational data products from the near real time processor (SCI_NL) during commissioning phase, the SCI_NL processor was upgraded to the newly operational V5.01 in March 2004. Compared to previous versions, the main changes are an updated radiometric calibration of radiance (level-1 data) and the use of ozone cross-section measured with the SCIAMACHY flight model (FM) by *Bogumil et al.* [2003]. In August 2004 one part of the SCIAMACHY 2003 level-2 data set was processed with V5.04, which improves mainly the (re)processing capabilities. Except for the time period from 01 Jan 2003 to 21 March 2003 where V5.01 had been affected by an incorrect handling of a season index, the level-2 product of V5.01 and V5.04 are equal. All versions of the SCIAMACHY operational ozone column product are an adaptation of an outdated version 2.4 of the GOME Data Processor that are three versions behind the current GOME GDP V4.0. The shortcomings of the GDP Version 2.4 have been attributed to the following: lack of temperature correction in the ozone cross sections, AMF calculations which use a ozone climatology based on an outdated two-dimensional coupled climate model, a lack of iterations to match total ozone of climatological ozone profiles used in the AMF calculations to the retrieved total ozone, the limited treatment of the atmospheric profile shape effect, and the partial unsuitability of the particular spectral analysis when the atmosphere becomes optically thick [*Lambert et al.*, 1999]. In addition, ozone filling-in as part of the overall Ring effect was not included as it is in the new generations of total ozone algorithms like the GOME WF-DOAS algorithm [*Coldewey-Egbers et al.*, 2005], TOSOMI [*Eskes et al.*, 2005] and GDP V4.0 [*Lambert et al.*, 2004].

A validation reference data set of SCIAMACHY data V5.01 has been compared to ground-based [*Lambert et al.*, 2004b] and satellite measurements [*Bracher et al.*, 2004; *Hilsenrath et al.*, 2004], models, and assimilation data [*Eskes and Dethof*, 2004] to verify the improvement upon the previous SCIAMACHY versions 3.5x and assess the geophysical consistency of the latest operational SCIAMACHY data version. These validations concluded that SCIAMACHY V5.01 improved upon previous versions, but known

[1] This section has been taken from the article "Bracher, A., L. N. Lamsal, M. Weber, K. Bramstedt, M. Coldewey-Egbers, and J. P. Burrows (2005), Global satellite validation of SCIAMACHY O_3 columns with GOME WF-DOAS, *Atmos. Chem. Phys.*, 5, 1025-1025, SRef-ID: 1680-7324/acp/2005-5-2357" with some modifications.

errors, e.g. dependence on solar elevation and on ozone column, inherited from GOME GDP V2.4 remained. An overall agreement of about 1% of SCIAMACHY V5.01 to assimilated GOME TOGOMI [*Eskes and Dethof*, 2004], a negative bias around 1% to ground stations [*Lambert et al.*, 2004b] and GOME GDP V3.0 [*Bracher et al.*, 2004], and up to 3% to SBUV2 V7 [*Hilsenrath et al.*, 2004] were found. However, the result has to be considered with some suspicion since ground-based validation showed a solar zenith angle dependence of 8 to 10% at high latitudes, an overestimation of low ozone columns recorded during springtime ozone depletion events, and a fractional cloud cover dependence at about one third of the stations. The poor space/time sampling (the data were only sparsely available from the second half of 2002 and the majority were measured above Europe and the south polar region) might have biased these results. In order to derive firm conclusions on the data quality of SCIAMACHY a global validation of a consolidated long-term SCIAMACHY data set versions V5.01/V5.04 (differences are negligible between both versions with regard to total ozone) with GOME WF-DOAS V1.0 ozone columns from the first half a year of 2003 was performed. Only for this time period a large set of collocation can be found where ozone columns derived from both instruments are globally available in the latest versions. After June 2003 GOME has a reduced coverage because of a tape recorder failure.

7.2.1 Comparison with GOME WF-DOAS

As stated above, complete data sets with near global coverage from both instruments were available for the first half of 2003. For all data sets (SCIAMACHY V5.01/V5.04), and GOME (WF-DOAS V1.0) measurements taken at solar zenith angles below 88° were included in the comparisons because at solar zenith angles above 88° the signal to noise ratio is too low. Since GOME/ERS-2 and SCIAMACHY/ENVISAT are flying in the same orbit only 30 minutes apart, numerous collocated measurements can be found (up to 10000 a day). In order to quickly compare collocations of a day up to a month period, and to overcome the difference in ground pixel sizes of SCIAMACHY and GOME, the following method was applied. Daily TCO data were binned into 2.5° × 2.5° wide cells and then compared. The center coordinate of the satellite footpath was used to locate the bin. We tested the binning with several grid resolutions and compared the results of the comparisons to the direct comparisons where the mean value of all SCIAMACHY total ozone measurements within a GOME pixel was compared. Using 2.5° by 2.5° bins provided similar results compared to the direct comparison as will be shown later. This grid resolution seems also to roughly approximate the GOME ground pixel size in across-track direction.

When both instruments had measurements in the same grid, the mean of one instrument was compared to the mean of the other instrument as follows:

$$100 \times (\mathrm{tO_3 \text{ of SCIAMACHY}} - \mathrm{tO_3 \text{ of GOME}})/\mathrm{tO_3 \text{ of GOME}} \tag{7.1}$$

The daily comparisons were analyzed in five zonal bands (90°S to 60°S, 60°S to 23°S, 23°S to 23°N, 23°N to 60°N, 60°N to 90°N) and as a function of solar zenith angle and total ozone. In addition to that, means and root mean square (RMS) values of the mean

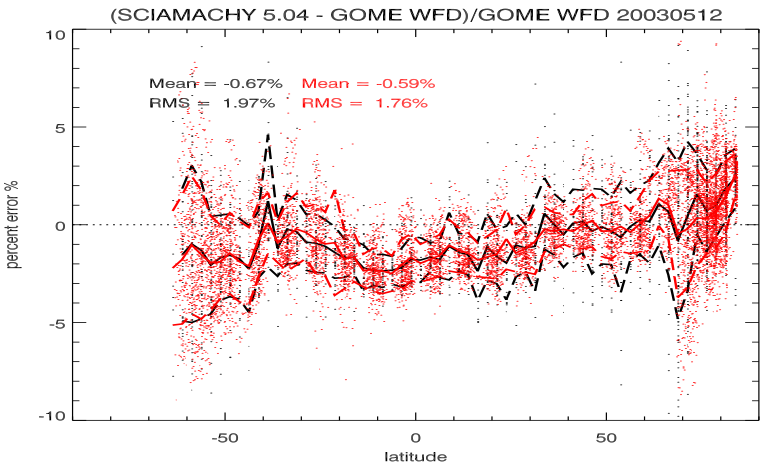

Figure 7.1: Mean values of mean relative deviations (straight line) and root mean squares of the mean relative deviation (dotted line) between data sets binned in 2.5°× 2.5° grids as a function of latitude. The results of the direct comparison of SCIAMACHY V5.01 to GOME WF-DOAS V1.0 total ozone is shown in red.

relative deviations as a function of solar zenith angle and total ozone combining all days were determined.

GOME WF-DOAS V1.0 and SCIAMACHY V5.01/V5.04 retrieval results and the differences between them are shown in Fig. 7.1 for May 12, 2003, and summary plots in Figs. 7.2, 7.3 and 7.4 for first half of 2003. [*Lambert et al.*, 1999, see Fig. 4] observed dependencies on TCO amount, solar zenith angle, and latitudes in GDP V2.4 TCO products from comparison with data from ground-based sensors. For both GOME GDP V2.4 and GDP V2.7 this dependence was within 4%. Similar results are also expected from SCIAMACHY V5.01/V5.04 TCO retrievals.

7.2.2 Latitude dependence

The relative deviations between the binned data sets of both SCIAMACHY retrievals (V5.04) to GOME WF-DOAS from May 12, 2003 are shown as a function of latitude (Fig. 7.1). As an example, results of direct comparisons of SCIAMACHY V5.04 to GOME are also added. Here, the mean of the TCOs from V5.04 of all SCIAMACHY pixels to the corresponding GOME WF-DOAS value are compared. Note that the SCIAMACHY pixels were sampled 30 minutes before GOME pixels. Both comparison methods agree to within 0.5% for relative deviations and within 0.08% for the mean and 0.2% for the RMS for the relative deviations. SCIAMACHY V5.04 compared to GOME WF-DOAS V1.0 shows a clear latitudinal dependence. From 63°S to 30°N (except for 40°S) SCIAMACHY V5.04 has a bias of between -3.5% and 0% (±1-3%) and from 30°N to 80°N between -0.5% and 2% (±1-3%) to GOME WF-DOAS. At higher latitudes (>50°S and >65°N) with higher solar zenith angles (>75°) the relative deviations are larger and

show more scatter. The overall bias of SCIAMACHY to GOME WF-DOAS for SCIAMACHY V5.04 (operational product) a negative bias of 0.7% (or -0.6% for direct comparisons) was found.

Figure 7.2 is summarizing the results from all daily comparisons of SCIAMACHY V5.01/V5.04 to GOME WF-DOAS between January and June 2003 based upon the binning method. The results have been grouped into various zonal bands and the number of data bins within each zonal band is also shown. If all data of one day have been available from both instruments around 3200 data bins were available for comparisons. At mid latitudes and in the tropics (Figs. 7.2, upper right, middle left, and middle right panels) number of bins vary between 20 and 700 per day. No significant differences in mean deviations and RMS can be observed in relation to the number of available bins. Similar conclusions can be drawn from the global comparison (90°S to 90°N, Fig. 7.2 lower right panel). Here, the number of bins varies between 200 and 3200. In the polar regions, the number of binned data decreases from 1200 to 0 by changing from summer to winter (Fig. 7.2, lower left panel). For both polar regions, a significant increase in scatter of mean relative deviation and a significant increase of RMS is observed when number of data within each bins falls below 300 (in winter season) and also for both regions the negative bias of SCIAMACHY V5.01/V5.04 to GOME WF-DOAS becomes significantly larger than in other seasons. During Antarctic summer (Fig. 7.2, upper left panel) the mean relative deviation and RMS are very stable between -1.5 and 0%, and 2%, respectively. From March until May, when the number of binned data falls below 300, both mean relative deviation and RMS are increasing to between -4.5 and 0.5% and between 2 and 4%, respectively. A similar picture is observed in the Arctic (Fig. 7.2, lower left panel): During winter mean relative deviation and RMS are high with -6 to 0% and 3 to 5%, respectively; in spring and early summer (March to June) the mean deviation gets smaller with a mean relative deviation of between -1 and 4.5% and a RMS of 3%. At mid latitudes a very weak seasonal signal in the differences can be observed; in the northern hemisphere (Fig. 7.2 middle right panel) SCIAMACHY is within 1.5% of GOME and the RMS decreases slightly from values of 2 to 3% in winter to 1.5 to 2% in spring and summer. At southern mid latitudes (Fig. 7.2 upper right panel) SCIAMACHY has a mean relative deviation of -2 to 0% with RMS of 1 to 2% compared to GOME for the whole investigated time period in 2003 with no seasonal effect, but the RMS increases slightly from 1 to 1.5% in summer to 2 to 3% in winter. In the tropics, SCIAMACHY V5.01/V5.04 total ozone compared to GOME WF-DOAS shows very little variation throughout the half year time period. A negative bias of 0.5 to 2.5% with RMS of 1% is observed between SCIAMACHY and GOME. Similar conclusions are drawn from results containing all data (90°S to 90°N), where SCIAMACHY total ozone compared to GOME shows very little variation throughout the investigated time period with a mean relative deviation of between -2 and 0.5% and a RMS on the order of 2%.

In summary, there is generally an underestimation around 1% (RMS around 2%) of SCIAMACHY V5.01/V5.04 total ozone with respect to GOME WF-DOAS except for the northern mid and polar latitudes where larger variation in the differences are observed. As seen in the single day comparison (Fig. 7.1), SCIAMACHY V5.01/V5.04 shows a clear negative bias as compared to GOME WF-DOAS in the southern latitudes and tropics,

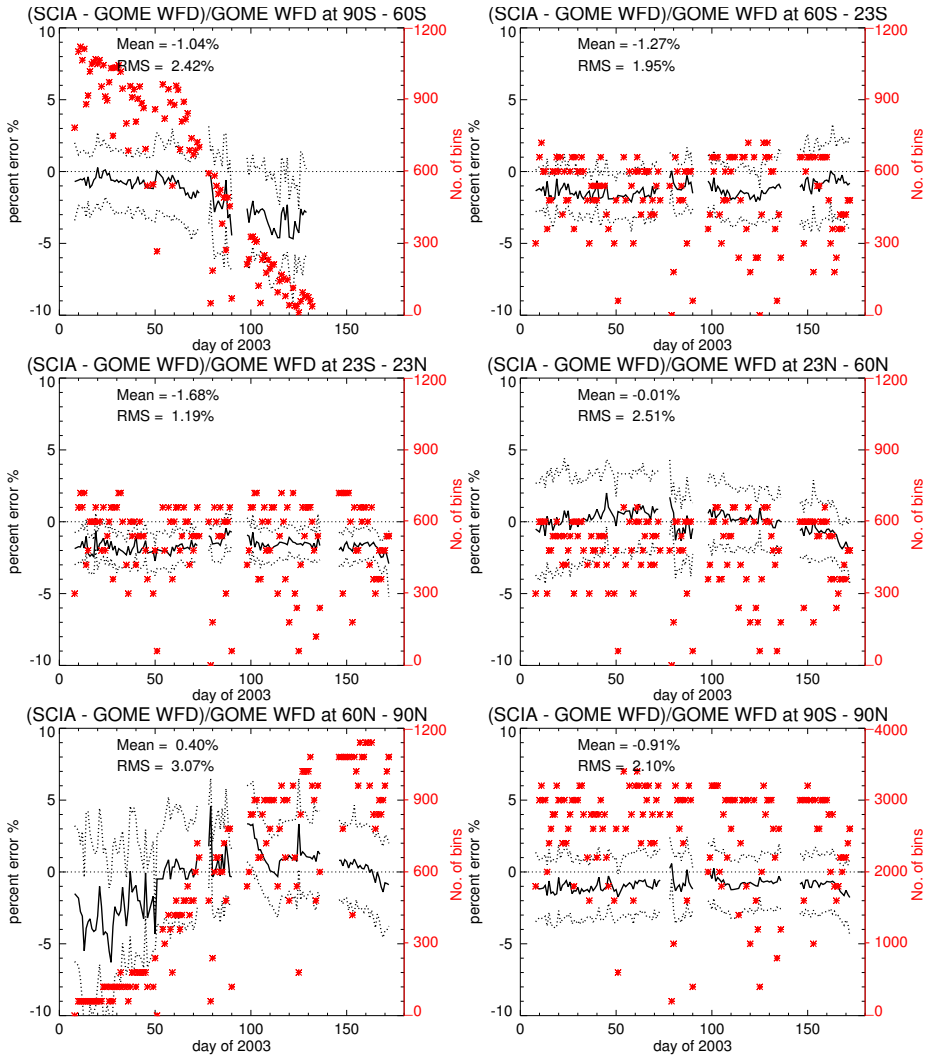

Figure 7.2: Mean relative deviation (black solid line), root mean square of daily mean relative deviation (black dotted line) and number of data bins (red stars) of all comparisons between SCIAMACHY V5.01/V5.04 and GOME WF-DOAS V1.0 total ozone during first half of 2003 in various zonal bands: Antarctic latitudes (upper left panel), mid southern latitudes (upper right panel), tropics (middle left panel), mid northern latitudes (middle right panel), arctic latitudes (lower left panel), and globally (lower right panel).

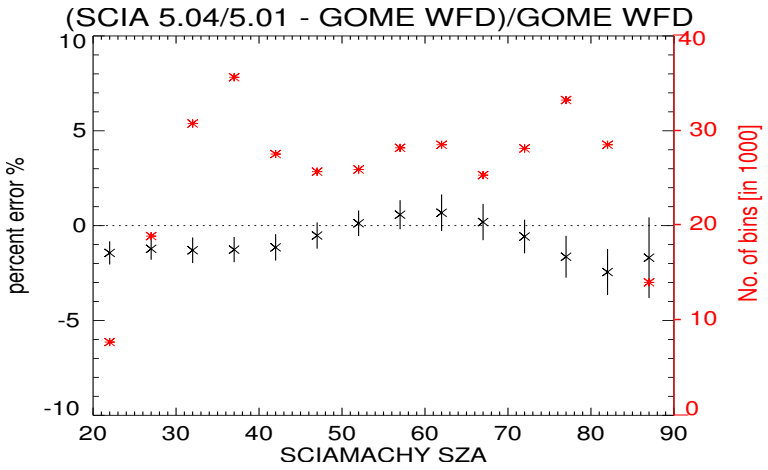

Figure 7.3: Summary plot of comparisons of all (i.e. data from the first half of 2003) binned SCIAMACHY V5.04 with GOME WF-DOAS V1.0 total ozone as a function of SCIAMACHY solar zenith angle in 5° steps. The number of data bins is given in red stars.

while in the northern latitudes SCIAMACHY V5.01/V5.04 total ozone columns shows on average a positive bias to GOME WF-DOAS (polar region) or the bias disappears (mid latitudes). This is in agreement with earlier validation results of GOME GDP V2.7 (about the same as GDP V2.4 regarding ozone) by *Bramstedt et al.* [2003] where a negative bias during summer/fall (as is here the case for southern latitudes) and a reduced bias during spring/winter (as is here the case for northern latitudes) were observed. Although the time period of half a year is rather short, we can conclude that a seasonal bias is clearly observed in both polar regions, while in the mid latitudes this signal is weaker and comparisons of a longer time period need to be looked at.

7.2.3 Solar zenith angle dependence

In order to evaluate the results, the validation results are investigated as a function of solar zenith angle. Fig. 7.3 shows the results of the comparison for the SCIAMACHY V5.01/V5.04 validation with GOME WF-DOAS the results including all days. The operational SCIAMACHY V5.04 shows a SZA dependency in the differences to GOME WF-DOAS retrievals. The bias of the mean relative deviation to GOME becomes more positive (from -1.5% to 1%) between 20° and 75° SZA and more negative at higher SZA (down to -2.5%), and increases again above 85% SZA (around -0.5%). Above 85% SZA the RMS becomes significantly larger in all analyses as compared to lower SZAs. GOME WF-DOAS mean total ozone agree to within 1% (RMS $\pm$1 to 2.5%). Above 80° the scatter of the results becomes somewhat larger (RMS of 2-3%). In this case the number of bins is significantly lower (i.e. 50 bins) than for other comparisons (between 140 and 340 bins).

It should be noted that a larger negative bias between SCIAMACHY V5.01 and GOME

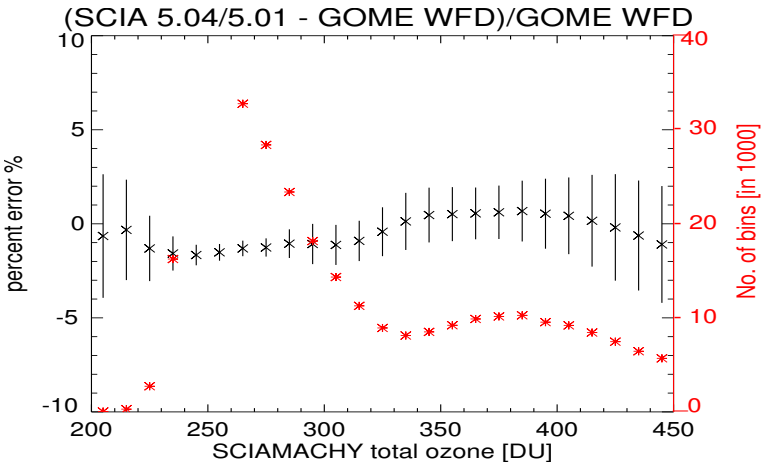

Figure 7.4: Same as Figure 7.2.3 but as a function of SCIAMACHY total ozone in 10 DU steps. The stars in red show the frequency distribution of TCO amounts.

WF-DOAS could be related to the difference in sampling time (30 minutes) for the two instruments. SCIAMACHY measurements at high northern latitudes during sunrise are taken at higher solar zenith angles than GOME measurements and therefore may probably show a larger error than collocated GOME data. This effect seemed to be more pronounced in the Arctic region than in the Antarctic, because Antarctic winter season observations were not covered in our study.

7.2.4 Total ozone dependence

Fig. 7.4 shows now the difference as a function of SCIAMACHY total ozone. The plot summarizing all days shows that RMS is becoming larger when number of data bins is decreasing. The bias increases from -2% during low TCO to about 1% at about 400 DU and then decreases again. The frequency distribution of total ozone peaking around 270 DU is also shown in the figure.

7.3 Adaptation of GOME WF-DOAS algorithm to SCIAMACHY

A brief account of the WF-DOAS algorithm is given in Chapter 3. For detailed description the reader is referred to *Coldewey-Egbers et al.* [2004, 2005], and *Weber et al.* [2005]. In the WF-DOAS algorithm the measured atmospheric optical depth is approximated by a Taylor expansion around a reference intensity plus a low-order polynomial. For interfering gases in the ozone fitting window of 326.8-335.0 nm a slant column fitting is applied. All fit parameters are then derived using a linear least squares minimization. The modeled intensity and weighting functions are calculated online as a function of ozone and temperature profiles, solar zenith angle, line of sight, relative

azimuth angle, and bottom of atmosphere altitude and albedo using the multiple scattering SCIATRAN radiative transfer model in the pseudo-spherical approximation. The ozone and temperature profiles are taken from IUP climatology [*Lamsal et al.*, 2004] which provides total ozone column dependent profile shapes for 5 latitude belts (low latitude, northern midlatitude, southern midlatitude, northern polar, and southern polar) and two seasonal bins each of six months (winter/spring and summer/fall) duration. For the calculation of intensity and weighting functions proper choice of ozone absorption cross-section is important. This issue is discussed in a separate section (see Section 7.4).

For ozone retrieval with WF-DOAS the following data and information are required: Calibrated level 1 radiance and solar spectrum from the same day, *a priori* value for total ozone which for convenience is the climatological one, effective scene height, and effective albedo. SACURA (Semi-Analytical CloUd Retrieval Algorithm) [*Kokhanovsky et al.*, 2003] or FRESCO [*Koelemeijer et al.*, 2001] provides information of cloud fraction (CF) and cloud top height (CTH) to determine the effective altitude. These two algorithms are described in detail in Section 7.6. Determination of the effective scene height requires a topography database. Considering smaller ground pixel size of SCIAMACHY compared to that of GOME, a new topography database of size 20 km$\times$20 km was derived from the 2' gridded global relief dataset ETOPO2 from the World Data Center for Marine Geology & Geophysics [*Smith and Sandwell*, 1997]. The effective albedo is defined by the Lambert Equivalent Reflectivity (LER) [*Herman and Celarier*, 1997] obtained from GOME sun-normalized radiance at 377.6 nm. The LER are retrieved by finding the best match between measured and calculated top of atmosphere (TOA) reflectance by inverse search in the multidimensional look up table prepared using SCIATRAN. The use of the LER approach also represents a first order correction for clouds and non-absorbing aerosol effects.

One of the most important aspects of total ozone retrieval algorithms is the treatment of the Ring effect [*Vountas et al.*, 1998]. The most significant improvement with WF-DOAS in comparison to current SCIAMACHY operational retrieval is the proper modeling of the varying ozone dependent contribution to the molecular filling-in as part of the rotational Raman scattering. This is discussed in detail in Section 7.5.

7.4 Choice of ozone cross-sections [2]

Currently available DOAS ozone retrieval algorithms for GOME measurements [*Coldewey-Egbers et al.*, 2005; *Weber et al.*, 2005; *Eskes et al.*, 2005; *Roozendael et al.*, 2006; *Balis et al.*, 2006] are using ozone cross-sections from *Burrows et al.* [1999b] that were measured with the GOME flight model and are also known as the GOME FM ozone cross-sections. In the retrieval from Dobson and Brewer instruments the Bass-Paur cross-sections are standard [*Bass and Paur*, 1985; *Paur and Bass*, 1985; *Staehelin et al.*, 2003]. After proper adjustments to the spectral resolutions of GOME, the Bass-Paur data yield total ozone that are 2% higher than that retrieved with the GOME FM

[2] This section has been taken from the article "M. Weber and L.N. Lamsal (2005), Proper choice of ozone cross-sections in SCIAMACHY ozone retrieval, Technical Note, University of Bremen".

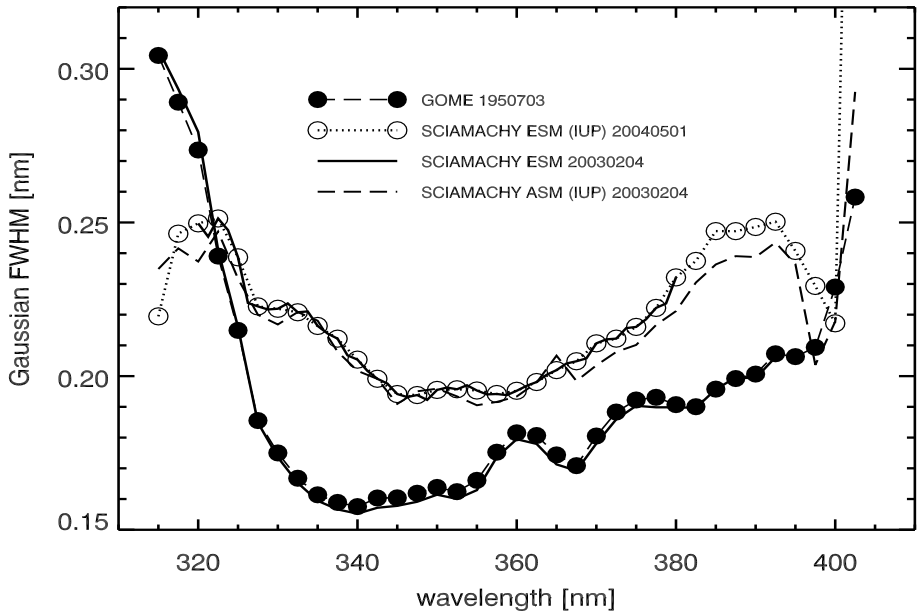

Figure 7.5: Gaussian FWHM from a instrument line shape fitting using the Kurucz solar spectrum and applied to ESM and ASM diffuser solar spectra from SCIAMACHY and GOME following the procedure by *Casper and Chance* [1997]

spectra [*Roozendael et al.*, 2003]. The idea of using GOME FM cross-sections in the GOME retrieval is the advantage that the instrument slit function does not need to be known. It is, therefore, obvious to use the SCIAMACHY FM cross-sections as reported by *Bogumil et al.* [2003] for SCIAMACHY. First results indicate that the use of the Bogumil data leads to a rather high bias on the order of +5% with respect to the ground based measurements [*Eskes et al.*, 2005]. In a preliminary analysis the use of the GOME FM cross-section in the WF-DOAS retrieval showed good agreement with collocated GOME results [*Bracher et al.*, 2005]. *Bracher et al.* [2005] also reported a high bias when using the SCIAMACHY cross-sections in the retrieval.

This study deals in more detail with the question which cross-sections should be recommended for SCIAMACHY ozone retrieval.

7.4.1 Spectral resolution and wavelength calibration

Before dealing with retrieval issues it is important to investigate the spectral resolution of Channel 2 spectra from SCIAMACHY (310 nm-400 nm). For GOME it was shown that the instrumental slit width varies across channel 2 [*Casper and Chance*, 1997]. In addition, an increasing asymmetry of the instrumental line shape (ILS) was found towards the GOME channel boundaries [*Roozendael et al.*, 2003].

A similar analysis has been carried out for SCIAMACHY. Following the procedure from *Casper and Chance* [1997], a high resolution solar spectrum, measured with the

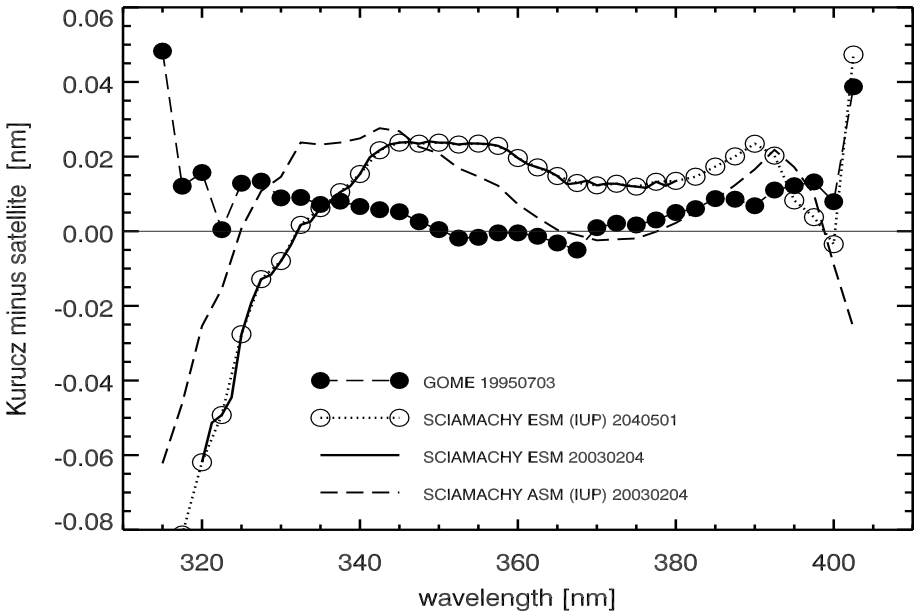

Figure 7.6: Same as Fig. 7.5 but for shifts between Kurucz and satellite data.

Fourier transform spectrometer at the McMath solar telescope at Kitt Peak, Arizona [*Kurucz et al.*, 1984], is convolved with a Gaussian ILS and matched to the SCIAMACHY solar spectrum. From a non-linear least squares fit the Gaussian FWHM, a wavelength shift, and a third degree polynomial (differential fitting) are determined. The results for the Gaussian FWHM and wavelength shifts are shown in Figs. 7.5 and 7.6, respectively. The spectral fitting was done in 5 nm wide spectral windows across the channel. For comparison the GOME results from solar data recorded on 3 July 1995 are shown as well.

For SCIAMACHY a fully IUP calibrated ESM diffuser spectrum from 1 March 2004 [*Skupin*, 2005] and a IUP partially calibrated ASM diffuser spectrum from 4 February 2003 were selected. The partial calibration of the ASM diffuser spectrum includes pre-flight wavelength calibration and subtraction of night time dark current measurements (Richter, 2004, private communication). The ASM diffuser plate has been added to SCIAMACHY to further reduce the differential spectral features that are observed with the ESM diffuser that strongly perturb minor trace gas retrieval [*Richter and Wagner*, 2001; *de Beek et al.*, 2004]. The absolute radiometric calibration of the ESM diffuser spectra by IUP goes beyond the current operational procedure and is described in detail by *Skupin* [2005]. Also shown are the results for a regular ESM spectrum from 2003 as provided by the recent DLR extraction software (V5.04). The spectral window of 325-335 nm is the preferred choice for total ozone retrieval for both GOME and SCIAMACHY [*Burrows et al.*, 1999a; *Spurr et al.*, 2005]. Since the focus lies in that spectral window well away from the channel boundaries, no further attempts were made to determine the asymmetry in the ILS.

Table 7.1: Gaussian widths and wavelength shifts in ozone retrieval window 325-335 nm. The errors are given for 2σ. Two different results are shown: fits with a scaling factor of 1 and with a scaling factor included (see Appendix A for details)

Solar data	Scaling factor (-)	ILS FWHM (nm)	Kurucz-satellite Shift (nm)
SCIAMACHY ESM (IUP)	- 0.947(62)	0.222(15) 0.213(18)	0.012(7)
SCIAMACHY ESM (V5.04)	- 0.933(64)	0.224(16) 0.213(19)	0.000(8)
SCIAMACHY ASM (IUP)	- 0.935(59)	0.218(14) 0.206(16)	0.017(7)
SCIAMACHY preflight [*Dobber*, 1999]	-	0.209(11)	-
GOME	- 0.961(63)	0.174(11) 0.171(14)	0.008(6)

In the ozone window the average Gaussian width for SCIAMACHY is 0.22 nm. With a sampling rate of 0.11 nm in Channel 2, this spectral region is roughly sampled at the Nyquist criterion. Between 335 nm and 380 nm the Gaussian widths, however, fall below 0.22 nm and this spectral region becomes mildly undersampled. For comparison the average spectral resolution for GOME in the ozone window is 0.17 nm and nearly the entire GOME Channel 2 is strongly undersampled. As expected, for most part of Channel 2 the spectral resolution does not differ between ESM and ASM diffuser spectrum.

The wavelength shifts between SCIAMACHY/GOME and Kurucz solar data are shown in Figure 7.6. The GOME and SCIAMACHY ASM solar spectrum have not been corrected for the Doppler shift, while SCIAMACHY ESM has been. For the central part of Channel 2 the shifts vary between 0.0 nm and 0.025 nm for both SCIAMACHY solar data. Differences in shifts for the SCIAMACHY spectra are either due to differences in pre-flight (ASM) and on board calibration (ESM) as well as due to the Doppler correction. In Table 7.1 the average ILS FWHM and wavelength shifts are summarized for the 325-335 nm ozone window. The results for SCIAMACHY ILS FWHM agree well with the values obtained during preflight calibration [*Dobber*, 1999].

7.4.2 Spectral resolution information from SCIAMACHY and GOME FM cross-section spectra

Similar to the procedure outlined in the previous section, ILS information were retrieved for various available ozone cross-sections using the FTS spectrometer data from *Voigt et al.* [2001] and Bass-Paur data [*Bass and Paur*, 1985; *Paur and Bass*, 1985] as a reference. Such an analysis were carried out by *Orphal* [2002, 2003] for various O_3

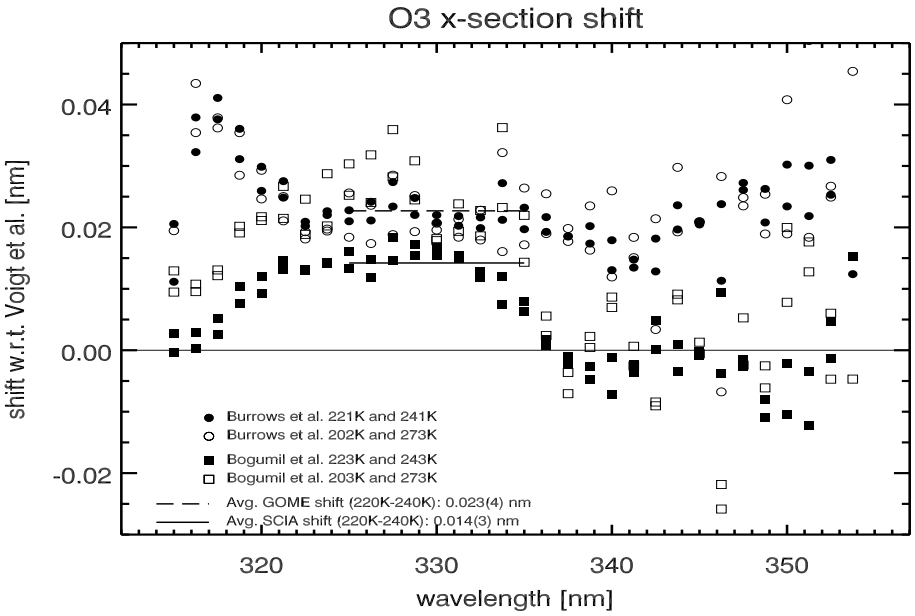

Figure 7.7: Wavelength shifts between *Voigt et al.* [2001] data and flight model data from SCIAMACHY and GOME [*Burrows et al.*, 1999b; *Bogumil et al.*, 2003]. Within the ozone fitting window from 325 to 335 nm an average shift of 0.014(3) nm was found for SCIAMACHY FM in the temperature range 223-243 K.

cross-sections but for a larger spectral window (323-343 nm). The Voigt data were recorded at 5 cm^{-1} spectral resolution with a Fourier transform spectrometer which corresponds to about 0.055 nm near wavelength 330 nm. Wavelength uncertainties for the *Voigt et al.* [2001] data are cited to be better than 0.0001 nm (0.01 cm^{-1}). Bass-Paur spectra were recorded at a spectral resolution of better than 0.025 nm. For all cross-sections here a Bass-Paur parameterization as a function of temperature was applied before the ILS retrieval [*Orphal*, 2002].

Results for the comparison with *Voigt et al.* [2001] data are summarized in Table 7.2. The retrieved Gaussian FWHM and scaling factors that have been obtained varies with temperature of the cross-section measurements. The same is true for the retrieved wavelength shifts. This temperature dependences has been also noted by *Orphal* [2002, 2003] and is at the moment not understood, but could be related to differences in ILS fittings that are directly applied to the cross-section data (as done here) and, on the other hand, from transmission spectra with ozone absorption that are more representative of the laboratory measurements (see Appendix B). On average a shift of 0.016 nm is obtained for the *Bogumil et al.* [2003] data in the WF-DOAS fitting window (326.6-335 nm, [*Coldewey-Egbers et al.*, 2005]. This is in agreement with the shift retrieved from the comparison of the ASM solar spectrum with Kurucz (see Table 7.1). Both ASM solar data and *Bogumil et al.* [2003] data were based upon pre-flight wavelength cal-

Table 7.2: Gaussian ILS fits using *Voigt et al.* [2001] FTS cross-sections in the WF-DOAS fitting window (326.6-335 nm) as reference. For the *Bogumil et al.* [2003] spectra the FWHM is given by the squared sum of widths from the ILS retrieval and FTS spectral FWHM of 0.055 nm. All errors are 2σ, except for the errors of the means which are derived from a weighted averaging of the temperature data.

Voigt et al. Temp (K)	Scaling Factor (-)	Bogumil et al. FWHM(nm)	Shift Voigt-Bogumil(nm)
205	1.091(9)	0.201(11)	0.024(2)
220	1.030(5)	0.209(7)	0.019(1)
240	0.978(3)	0.218(4)	0.013(1)
270	0.949(3)	0.222(5)	0.012(1)
Mean	0.992(46)	0.215(7)	0.016(4)
SCIAMACHY ESM	-	0.221(11)	0.001(5)
	0.915(42)	0.207(12)	

ibrations. The average FWHM obtained for the SCIAMACHY FM is slightly below the solar value, but agrees to within the uncertainties.

Figure 7.7 shows the required wavelength shifts that should be applied to the SCIAMACHY FM and GOME FM spectra to match the FTS data in Channel 2. For the larger ozone window of 325-335 nm a mean shift of 0.014(3) nm and 0.023(4) nm was found for SCIAMACHY FM and GOME FM, respectively. Between 315 and 335 nm the SCIAMACHY FM show a parabola in the wavelength shift as a function of wavelength. This could point at the lack of reference lines from the Pt/Ne/Cr hallow cathode lamp that were used for the wavelength calibration.

ILS fitting was also applied by using Bass Paur cross-sections as a reference and the results are summarized in Table 3. This analysis has been also extended to the *Burrows et al.* [1999b] cross-sections. Both solar and FM cross-section data provide consistent estimates for the SCIAMACHY spectral resolution, while the GOME FM analysis indicate a significant higher spectral resolution than that derived from the GOME solar data.

In contrast to the comparison with the FTS cross-section, the various instrumental widths and scaling factors are nearly independent of the cross-section temperature when Bass-Paur data are used as reference data. The scaling factors indicate that the differential SCIAMACHY cross-sections have to be scaled by +3.6%, while GOME FM data have to be scaled by -0.8% with respect to Bass Paur data. It was found that the differential scaling, after adjustments for the differences in spectral resolution, is -3.7% when comparing GOME FM directly to SCIAMACHY FM. This is in agreement with the observed bias of the SCIAMACHY total ozone retrieval when using *Bogumil et al.* [2003] data (SCIAMACHY FM) instead of *Burrows et al.* [1999a] data (GOME FM) as reported by *Eskes et al.* [2005] and *Bracher et al.* [2005] on one hand and the bias between the use of Bass-Paur and GOME FM data in the GOME retrieval [*Roozendael et al.*, 2003].

Table 7.3: Gaussian ILS fits with Bass-Paur cross-sections in the WF-DOAS fitting window (326.6-335 nm) as reference. For the GOME FM and SCIAMACHY FM, the FWHM is given by the squared sum of widths from the ILS retrieval and Bass-Paur spectral resolution of 0.025 nm FWHM. Errors for ILS fittings are 2σ, while errors for the means are from weighted averaging of the temperature data.

BP Temp (K)	SF (-)	Bogumil FWHM (nm)	BP-Bogumil shift (nm)	SF (-)	Burrows FWHM (nm)	BP-Burrows shift (nm)
205	0.967(7)	0.199(6)	-0.017(2)	1.010(9)	0.131(16)	-0.012(2)
220	0.964(5)	0.198(8)	-0.015(2)	1.009(7)	0.132(12)	-0.007(2)
240	0.963(5)	0.198(7)	-0.012(1)	1.007(6)	0.135(10)	-0.003(2)
270	0.967(5)	0.196(9)	-0.008(2)	1.007(5)	0.137(10)	-0.001(1)
Mean	0.965(2)	0.198(1)	-0.013(3)	1.008(1)	0.134(2)	-0.005(4)
solar	- 0.92(4)	0.221(11) 0.207(12)	0.001(7)	- 0.949(3)	0.171(7) 0.165(7)	0.009(3)

A surprising result here is that the GOME FM cross section, that works so well for the GOME retrieval appear to have a significantly different spectral resolution than indicated from the analysis of the GOME solar data.

7.4.3 Wavelength shift from WF-DOAS analysis

The WF-DOAS total ozone setup for SCIAMACHY is nearly identical to the one described in *Coldewey-Egbers et al.* [2005]. One major change is that in an online version of WF-DOAS the radiative transfer calculations for calculating reference intensities and weighting functions are included in the iterative retrieval process. The difference between the online and look-up-table versions were found to be less than 0.2% as tested by application to GOME. The cross-section shifts have been both tested in the GOME and SCIAMACHY retrieval. The use of proper shifts in the cross-section improves the fit residual RMS as shown for GOME in Figure 7.8. The optimum shift for the cross-sections agree with those obtained from comparisons with the *Voigt et al.* [2001] cross-sections in the previous section. In the WF-DOAS retrieval the wavelength axis are adjusted to the Kurucz spectrum by Fraunhofer fitting the solar data before retrieving ozone. There seems to be indirect evidence that both Kurucz and *Voigt et al.* [2001] FTS data are in good agreement regarding the wavelength calibration. The question still remains how the use of GOME FM and SCIAMACHY FM cross-sections with optimized wavelength shifts impact the accuracy of SCIAMACHY ozone retrieval.

For a given SCIAMACHY ground pixel the various ozone cross-sections were tested in the WF-DOAS retrieval. Systematic wavelength shifts were applied and the results are summarized in Fig. 7.9. Shifting the SCIAMACHY FM cross-section by 0.015 nm

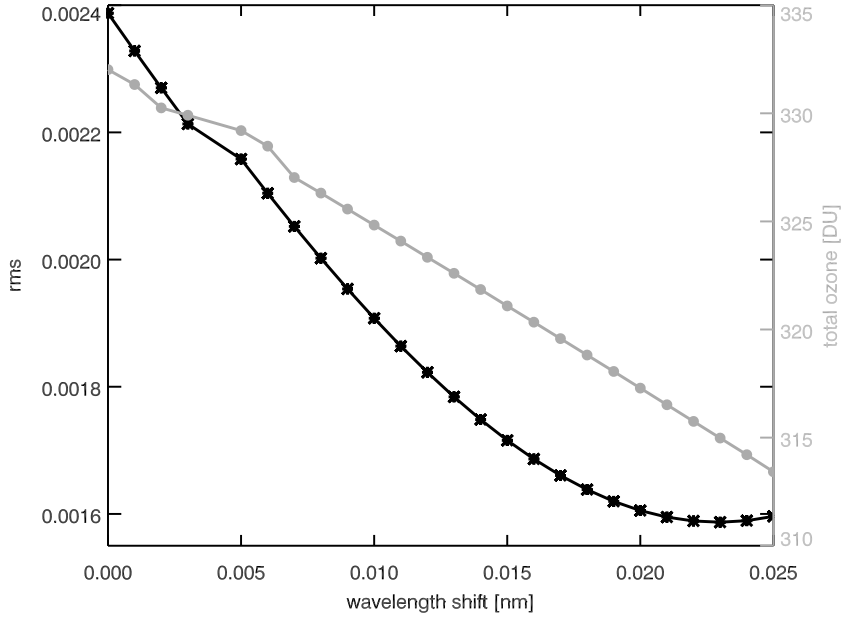

Figure 7.8: Dependence of fit residual RMS and retrieved GOME total ozone as a function of the applied wavelength shifts to GOME FM cross-sections. Minimum RMS were found at shifts of 0.023 nm for GOME.

reduces total ozone by roughly 9 DU (-3.6%). Comparing SCIAMACHY FM (shift of 0.016 nm) and GOME FM (shift of 0.017 nm) a difference of 8 DU (-3.3%) is found. The minimum in rms of the residuals is achieved at a wavelength shift of 0.017 nm for unadjusted GOME FM and 0.016 nm for SCIAMACHY FM, respectively. However, in the cases of the transformed GOME cross-sections (BP and BP-S) the minimum rms is reached at 0.021-0.023 nm in agreement with Fig. 7.7. The BP and BP-S cross-sections are the SCIAMACHY adjusted GOME FM spectra via the Bass-Paur reference data (Table 7.3) with and without additional differential scaling.

The scaling of the differential SCIAMACHY cross-section (SCIA-S) by +3.8% (with a shift of 0.015 nm) as derived from the direct comparison of GOME FM with SCIAMACHY FM leads to the same results when using the GOME FM cross-section with a shift of 0.017 nm. A small bias of about 3 DU is found when the GOME FM cross-section would be further shifted to +0.023 nm that was the optimized value found from the comparison with the *Voigt et al.* [2001] data (Section 7.4.2, Figure 7.7). The combination of proper wavelength shifts and differential scaling is important to make the use of the SCIAMACHY FM data in the SCIAMACHY retrieval consistent with the use of GOME FM spectra in the GOME satellite retrieval.

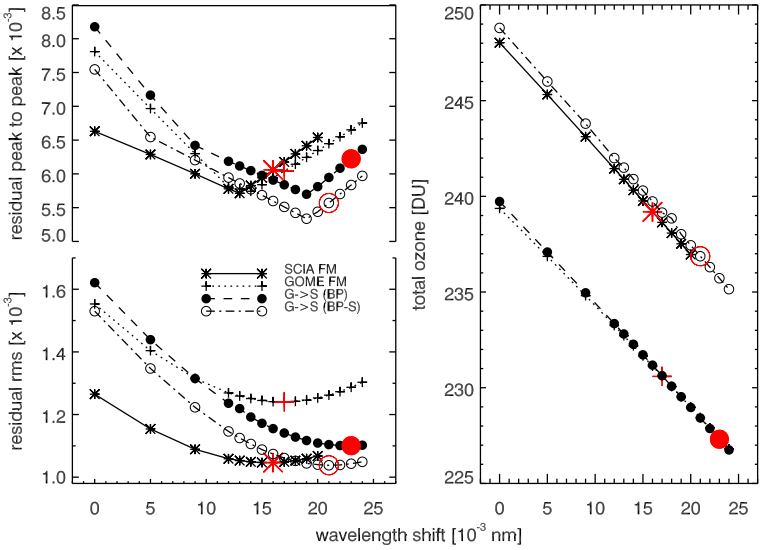

Figure 7.9: WF-DOAS SCIAMACHY retrieval with different cross-sections as a function of applied wavelength shifts for ground pixel 1994 of orbit 04868 on the day of 4 Feb 2003. Left: RMS and maximum peak-to-peak residual from the spectral fitting. Right: retrieved SCIAMACHY total ozone. SCIAMACHY FM and GOME FM are the *Bogumil et al.* [2003] and *Burrows et al.* [1999b] data, respectively. The Bass-Paur adjusted GOME FM cross-section (matching SCIAMACHY FM spectral resolution) without and with scaling are marked BP and BP-S, respectively (see Table 7.3). The red symbols indicate the results for which the rms error in the fit residuals were minimum. The wavelength shifts in the cross-sections was also accounted for in the Ring calculations.

7.5 Ring database

In order to account for the dependence of the Ring effect on various atmospheric parameters like ozone column column, altitude, solar zenith angle, and albedo, a Ring database as a function of these parameters was created using SCIATRAN V1.0. The Ring database was calculated at an equidistant wavelength grid of 0.055281 nm which is about half of the sampling grid of the SCIAMACHY solar reference spectrum. The fit RMS in the WF-DOAS total ozone retrieval was observed to be reduced by calculating the Ring spectra at the smaller wavelength grid. Moreover, the retrieval results were also found to be sensitive to the wavelength step size of the Ring spectra.

Table 7.4 gives an overview of the parameter space. As noted in Section 7.3 the ozone and temperature profiles were taken from IUP climatology. Based on our earlier studies presented in Section 7.4 the SCIAMACHY FM cross-section [*Bogumil et al.*, 2003] differentially scaled by 1.038 and wavelength shifted by +0.016 nm were used. The Ring spectra were computed for discrete solar zenith angle with 5° step below 70° and

Table 7.4: Parameter space of the look-up-table. The acronym used for total ozone are as follows: TROP (tropics), NMWS (northern midlatitude winter/spring), NMSF (northern midlatitude summer/fall), SMWS (southern midlatitude winter/spring), SMSF (southern midlatitude summer/fall), NPWS (northern polar winter/spring), NPSF (northern polar summer/fall), SPWS (southern polar winter/spring), SPSF (southern polar summer/fall).

Atmospheric parameter	Min	Max	Δ	N
Total ozone (TROP)	205 DU	340 DU	30 DU	5
Total ozone (NMWS)	235 DU	535 DU	30 DU	11
Total ozone (NMSF)	235 DU	415 DU	30 DU	7
Total ozone (SMWS)	145 DU	415 DU	30 DU	10
Total ozone (SMSF)	235 DU	355 DU	30 DU	5
Total ozone (NPWS)	235 DU	535 DU	30 DU	11
Total ozone (NPSF)	235 DU	415 DU	30 DU	7
Total ozone (SPWS)	145 DU	355 DU	30 DU	8
Total ozone (SPSF)	205 DU	355 DU	30 DU	6
Solar zenith angle	15°	92°	5° if SZA $\leq 70°$ 1° if SZA $> 70°$	34
Surface albedo	0.02	0.98	~ 0.2	6
Altitude	0 km	12 km	2 km	7

1° above. Altitude of the boundary in the lower atmosphere ranged 0 km - 12 km. In the actual retrieval this altitude is identified with the effective height. Surface albedo was taken between 0.02 and 0.98 at 0.2 step. The Ring database was limited to nadir viewing and consists of 99960 Ring spectra.

7.6 SCIAMACHY cloud product for use in WF-DOAS [3]

For an accurate determination of trace gases in the atmosphere knowledge on the cloud properties is essential. Several algorithms have been developed to extract cloud properties from SCIAMACHY measurements [*Kuze and Chance*, 1994; *Loyola*, 1999; *Koelemeijer et al.*, 2001; *Rozanov and Kokhanovsky*, 2004]. The algorithms either use the Polarization Measurement Devices (PMDs) reflectance or the top of atmosphere reflection having deep minimum at 760 nm of O_2 A-band [e.g. *Koelemeijer et al.*, 2001; *Rozanov and Kokhanovsky*, 2004], 680 nm of O_2 B-band, or 477 nm of collision complex of O_2-O_2. The depth of minimum is characterized by cloud altitude because the chance of

[3]This section has been taken from the article "Kokhanovsky, A. A., B. Mayer, V. V. Rozanov, K. Wapler, L. N. Lamsal, M. Weber, J. P. Burrows, and U. Shumann (sumbitted 2006), Satellite ozone retrieval under broken cloud conditions: An error analysis based on Monte-carlo simulations, *Rem. Sens. of Env.*" with some modification.

photon absorption by oxygen is large for low clouds and less for higher ones.

The Optical Cloud Recognition Algorithm (OCRA) [*Loyola*, 1999] analyses the color of PMD images and retrieves CF. The Heidelberg Iterative Cloud Retrieval Utilities (HICRU) also uses PMDs [*Grzegorski*, 2003]. Utilizing the O_2 A-band the Initial Cloud Fitting Algorithm (ICFA) derives CF [*Kuze and Chance*, 1994]. *Koelemeijer and Stammes* [1999] noted that the ICFA produces inaccurate CFs. In FRESCO [*Koelemeijer et al.*, 2001] algorithm, the effective CF and CTH are derived by comparing the measured and modeled reflectivities in three 1 nm wide windows- 758-759 nm, 760-761 nm, and 765-766 nm of O_2 A-band. Here, the cloud is assumed to be a Lambertian reflector with albedo of 0.8 below a clear atmosphere. An algorithm with an improved physical description of radiative transfer within the atmosphere is SACURA [*Rozanov and Kokhanovsky*, 2004], which uses the measurements of the cloud reflection functions in order to retrieve CTH and cloud geometrical thickness.

7.6.1 The influence of clouds on the total ozone retrieval

In the WF-DOAS retrieval procedure, a smooth polynomial is subtracted from the logarithm of the measured top of atmosphere reflectivity before the spectral fit to the radiative transfer model is performed. The polynomial takes into account, to some extent, generally unknown broad-band spectral signatures arising from surface, aerosol, and cloud reflectances. However, there exists non-negligible uncertainty in the retrieval of TCO arising from inadequate treatment of cloud properties. Improved knowledge on cloud parameters is required for the estimation of TCO in a cloudy atmosphere. The relevant cloud properties that are needed for correct TCO retrievals are the cloud optical thickness(τ) or cloud albedo (A), CF(c), cloud top height (h_{top}), and cloud bottom height (h_{bot}).

WF-DOAS TCO error analyses have suggested an accuracy of better than 3% for solar zenith angle lying below 80° [*Coldewey-Egbers et al.*, 2005]. Comparisons between GOME WF-DOAS TCO and that from a reliable ground-based direct sun measurements have shown a mean deviation less than 1% with typical RMS scatter of less than 4% [*Weber et al.*, 2005]. Such scatter in the satellite measurements is likely to come from cloud and surface assumptions in the radiative transfer and limited treatment of cloud in the retrieval process.

Clouds can affect the ozone retrieval mainly in three ways. First, clouds act as a reflecting boundary below the ozone layer and enhance the depth of the ozone absorption bands. Second, clouds shield tropospheric ozone from being observed by satellite instruments. This effect is often termed as the ghost column effect. Third effect arises from the enhancement of the photon path inside the clouds causing an enhancement of the absorption line depth of ozone inside clouds. In order to account the albedo effect of clouds on ozone retrieval, we require the information of CF and cloud albedo. Alternatively, the product of these quantities, often referred to as effective CF, can be used. For the correction of the ghost column effect we require both the effective CF and the CTH.

Homogeneous cloud field

In current satellite ozone column retrieval procedures, for example TOMS V8 [*Bhartia*, 2003], WF-DOAS [*Coldewey-Egbers et al.*, 2005], a cloud is replaced by a impenetrable lambertian surface. Such a technique allows fast TCO retrievals while its accuracy will not be significantly compromised. The lambertian surface with albedo of 80% is positioned at height(h_L); the h_L is retrieved by fitting a modeled signal at O_2A absorption band with the measured one. [The influence of clouds on total ozone concentration retrieval using the backscattered solar light in the Huggins band, Submitted to J. Quant. Spectroscopy and rad. Transfer, 2005, hereinafter referred to as Kokhanovsky and Rozanov, Submitted manuscript, 2005] investigated the influence of such assumptions on the total ozone retrieval from space-borne measurements. The study covered an idealized case of cloud where the cloud field is assumed to be horizontally and vertically homogeneous. The authors note that if the CTH is chosen correctly, the error in the retrieved TCO is $\pm$3% for solar zenith angle of 60° depending on the cloud optical thickness. If the h_L and τ are incorrect, the error in the derived TCO can range from -4% to 9% depending upon assumed h_L and τ. For cloud optical thickness of 40 which roughly corresponds to the cloud albedo of 80%, the bias of 1% in the cloud top height introduces an error in TCO of less than 1%. The Lambertian surface determined by fitting corresponding O_2 A-band simulated spectra and measured spectra is usually lower than the true cloud-top height by 0.47 to 1.17 km depending on the value of τ and SZA. Such differences further reduce the error in the TCO retrieval [*Rozanov and Kokhanovsky*, 2004] and ranges -2.5% to 4.5% for SZA of 60° and -0.5% to 3% for SZA of 30°. Therefore, the Lambertian surface model could perform quite well in the ozone retrieval algorithms like WF-DOAS and TOMS V8. However, the accuracy is uncertain and depends on the cloud characteristics for a given atmospheric state.

Broken cloud

The studies of the influence of cloudiness on the ozone retrieval algorithms are usually performed assuming horizontally homogeneous cloudiness [*Coldewey-Egbers et al.*, 2005; *Kokhanovsky and Rozanov*, 2004]. In reality, clouds are inhomogeneous on all spatial scales. Therefore, it is of importance to understand how the broken cloud conditions influence the ozone retrievals made in the assumption of the independent pixel approximation (IPA) whereby the top-of-atmosphere reflected light intensity can be presented as a linear combination of clear sky and cloud contributions. The reflection function R at a given wavelength λ is written as follows:

$$R(\lambda) = cR_c(\lambda) + (1-c)R_a(\lambda) \tag{7.2}$$

Here, c is the CF, R_c (λ) and R_a (λ) are the reflection functions for cloudy and clear sky conditions, respectively. The CF along with CTH are used in the WF-DOAS TCO retrieval.

The Monte-Carlo technique offers an opportunity to investigate the influence of IPA assumption on TCO retrieval. The technique allows for a solution of the forward prob-

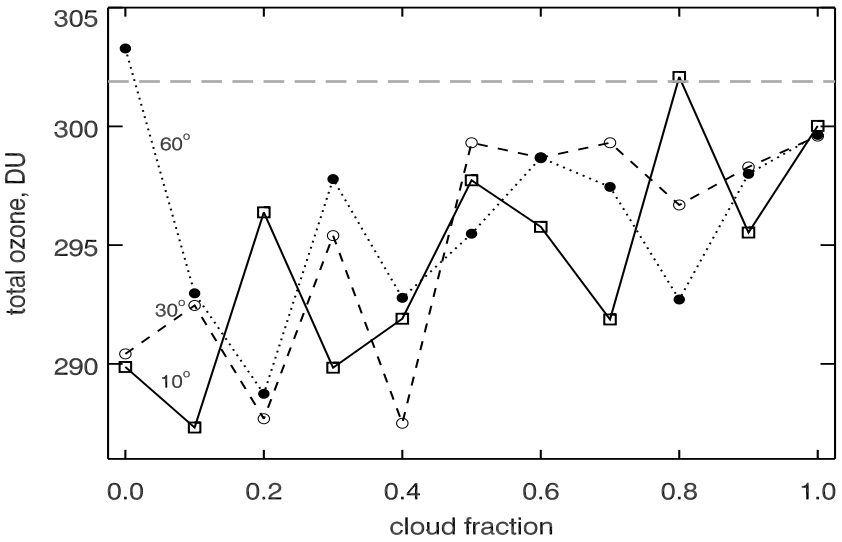

Figure 7.10: Dependence of the retrieved total ozone concentration TCO on the CF for several solar zenith angles and the nadir observation. The true value of TCO is equal to 302 DU.

lem using conceptually simple model of photon paths tracing in arbitrary inhomogeneous atmosphere-underlying surface system. The synthetic top-of-atmosphere (TOA) radiances obtained can be used in any of currently used ozone retrieval schemes for the sensitivity study.

[Satellite ozone retrieval under broken cloud conditions: An error analysis based on Monte-Carlo simulations, submitted to Rem. Sens. of Env., 2006, hereinafter referred to as Kokhanovsky et al., submitted manuscript, 2006] evaluated the accuracy of Eq. 7.2 for the calculation of the spectral top-of-atmosphere reflectance by using the 3D Monte Carlo code for the phYSically correct Tracing of photons In Cloudy atmospheres, MYSTIC [*Mayer*, 1999, 2000]. MYSTIC is a forward Monte Carlo code which traces photons on their individual paths through a vertically and horizontally inhomogeneous atmosphere. The main conclusion of the work is that the spectrally averaged relative error of IPA δ = 1- R_{IPA}/R_{MYSTIC} is found to be solar zenith angle dependent. The error is smaller for larger solar zenith angles. However, it could reach -6% for the solar zenith angle 10 degrees. Results for 10 and 30 degrees are close to each other because in this problem not angles but their cosines are of the most importance. Generally, the IPA overestimates the reflectance as compared to the full 3-D radiative transfer model. It follows that the error is generally larger for the intermediate values of c.

Such errors of IPA lead to errors in the retrieved values of the total ozone concentration TCO as derived using backscattered UV light techniques. It is of importance to understand the possible range of errors ε = TCO_{retr}/TCO_{true} - 1 due to the error of IPA and also due to uncertainties in the forward modeling (e.g. inaccurate information on the CTH and CF).

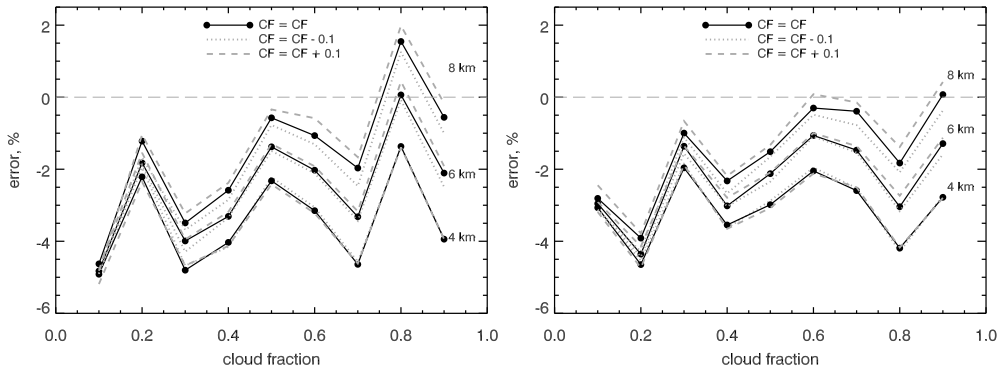

Figure 7.11: Dependence of the total ozone concentration retrieval error on the CF for various values of the CTH and the cloud fraction bias at SZA = 10° (left) and SZA = 60° (right)

To study correspondent errors, the GOME total ozone column WF-DOAS retrieval algorithm (see the description of the algorithm in the paper by *Coldewey-Egbers et al.* [2004]) was applied. Synthetic spectral reflectances calculated with MYSTIC were used in the retrieval procedure. Because the total column concentration is exactly known for the MYSTIC run, ozone profile of June in northern hemisphere at 45° having TCO of 302 DU (MPI model [*Crutzen and Brühl*, 1993]), in this case, it is a straight forward matter to investigate correspondent errors. WF-DOAS algorithm uses SCIATRAN 2.0 for the online simulation of intensities and relavent weighting functions. The same set of ozone and temperature profiles were considered for SCIATRAN as for MYSTIC.

Fig. 7.10 shows the difference in TCO plotted as a function of CF for various solar zenith angles. The CTH is assumed to be at 6 km. Apparently, the algorithm gives too small values of TCO (2-12 DU, on average). The errors are CF dependent: larger errors for low CFs. In Figure 7.11, the percent error in the retrieved TCO is presented for the two values of SZA. It follows that the error is generally smaller than 4% (and positive) for inaccurate assumptions on CTH ($\pm$2 km). The error in the CF does not influence results significantly. Note the solar position-dependent error in Figure 7.11 (left and right). In WF-DOAS algorithm, the effect of cloud is corrected by the concept of the ghost column, which helps reducing the error in the retrieved TCO. This also explains the larger errors for low value of CF because the ghost vertical column is the climatological integrated ozone concentration below CTH weighted by CF. Errors increase considerably if the concept is not used.

The CTH information needed for the concept of the ghost column is obtained from measurements of reflected light in O_2 A-band. It is of importance to understand how large errors of the retrieved values of TCO are. This is illustrated in Fig 7.12 at c =0.1, 0.5, 1.0. It follows that correspondent errors are in the range [-4%, 7%] depending on c. They are only weakly dependent on the solar zenith angle.

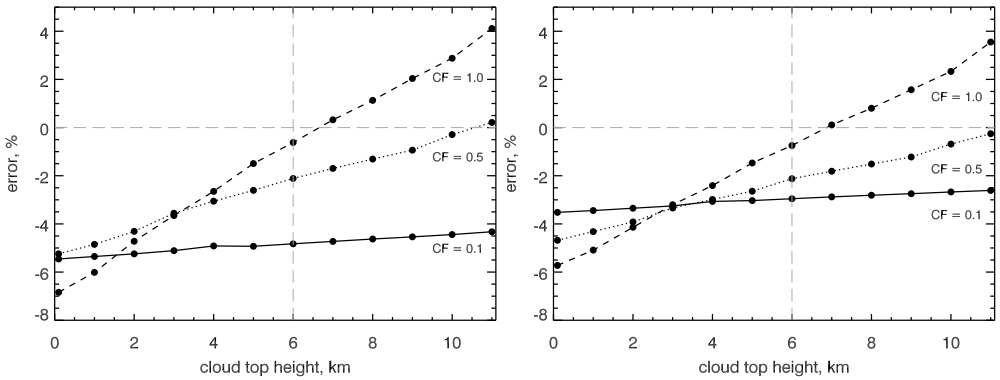

Figure 7.12: Dependence of the total ozone concentration retrieval error on the CTH for various values of the CF bias at SZA = 10° (left) and SZA = 60° (right)

7.6.2 Selection of cloud products

FRESCO determines both the effective CF and the CTH that are required for ozone retrievals. Since the SACURA algorithm considers single scattering above clouds and the cloud bi-directional reflection distribution functions unlike a Lambertian surface in FRESCO, the cloud top height determined by SACURA is considered to be more accurate particularly to completely cloudy pixels. For broken clouds, the determination of cloud top height by SACURA requires an additional information on the cloud fraction. This information is taken from the operational SCIAMACHY cloud fraction product (OCRA). OCRA uses the red, green and blue PMDs for cloud fraction determination.

FRESCO results have been compared with that derived from thermal infrared technique of the Along Track Scanning Radiometer-2 (ATSR-2). The comparison indicated a reasonable agreement between them. FRESCO overestimates cloud top pressure by about 65 hPa on average as compared to infrared techniques [*Koelemeijer et al.*, 2001]. Using GOME spectral measurements *Rozanov et al.* [2004] also reported an underestimation of CTH by about 1.88 km by FRESCO as compared to ATSR-2 for several cases. The difference is likely to come from neglect of photon absorption inside clouds [*Koelemeijer et al.*, 2001]. FRESCO overestimates the effective CF over desert areas. This overestimation is caused by the surface albedo considered in FRESCO. Correction of surface albedo allows the retrieval of the effective CF to be improved over deserts [*Fournier et al.*, 2005]. FRESCO effective CF and CTH are sensitive to the type of landcover through the use of its surface albedo database. However, due to simultaneous retrieval of CTH and cloud fraction, the FRESCO cloud retrieval algorithm gives consistent results [*Tuinder et al.*, 2004].

OCRA CF retrievals have been have been validated by comparing with the results from FRESCO and collocated measurements from Moderate Resolution Imaging Spectroradiometer (MODIS) [*Salomonson et al.*, 2002] aboard the Terra and Aqua satellites [*Fournier et al.*, 2005]. A good agreement between OCRA and FRESCO, and OCRA and collocated MODIS results has been reported [*Fournier et al.*, 2005]. However, the

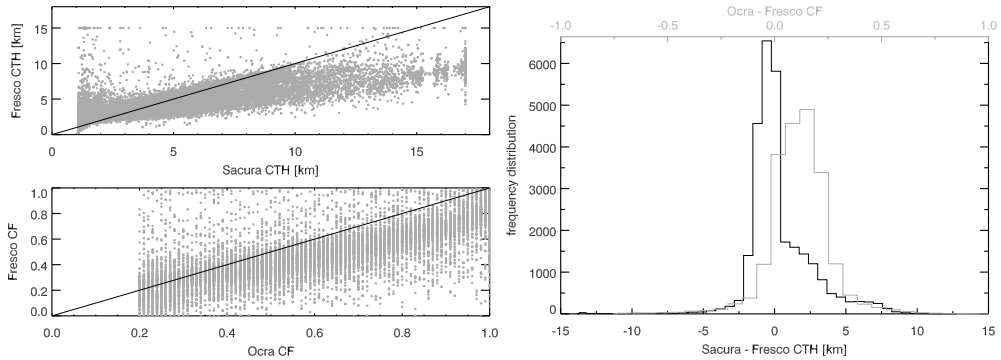

Figure 7.13: Comparison of CTH from FRESCO and SACURA, and CF from FRESCO and OCRA. The analysis is based on the SCIAMACHY measurements on 20 June 2003.

CF difference between OCRA and FRESCO plotted as a function of viewing zenith angle produces a parabolic response. This dependency is believed to come from OCRA due to an inadequate definition of reflectances, which takes the cosine of the angle into account.

Rozanov et al. [2004] have compared the CTH retrievals from GOME (SACURA) and collocated measurements from ATSR-2. The authors reported similar results (deviations are inside error bars of SACURA) from the two instruments. They reported somewhat larger difference between SACURA and FRESCO CTHs, with FRESCO underestimating the cloud top heights by about 2 km. In a separate study on 931 GOME pixels *Rozanov et al.* [2005] observed that the CTH from SACURA as applied to GOME differ from the CTH from ATSR-2 by 0.6 km on average.

The left upper panel of Figure 7.13 shows the CTH retrieved from FRESCO and SACURA from SCIAMACHY on 20 June 2003. Retrieved CFs from FRESCO and OCRA are presented in the left lower panel. Frequency distributions of the difference are shown in the right panel of Figure 7.13. We observe significant discrepancies in the CTH from FRESCO and SACURA. The lower limit of CTH fixed at 1.5 km is clearly evident in the SACURA retrievals when FRESCO CTHs vary by up to 13 km. In other cases, the FRESCO CTHs are lower than that from SACURA. In majority of the cases, the difference in CTHs is about 2 km as reported by *Rozanov et al.* [2004]. CFs from FRESCO and OCRA show good correlation but in many cases the CF from FRESCO underestimates by up to 0.2. It follows that according to earlier investigation presented in Section 7.6.1, the quality of retrieved total ozone from SCIAMACHY is influenced by the choice of cloud data either from FRESCO or SACURA-OCRA.

7.7 Iterative online WF-DOAS retrieval

Settings and databases as outlined in previous sections have been implemented in the online WF-DOAS algorithm for retrieving total ozone column from SCIAMACHY. A flow

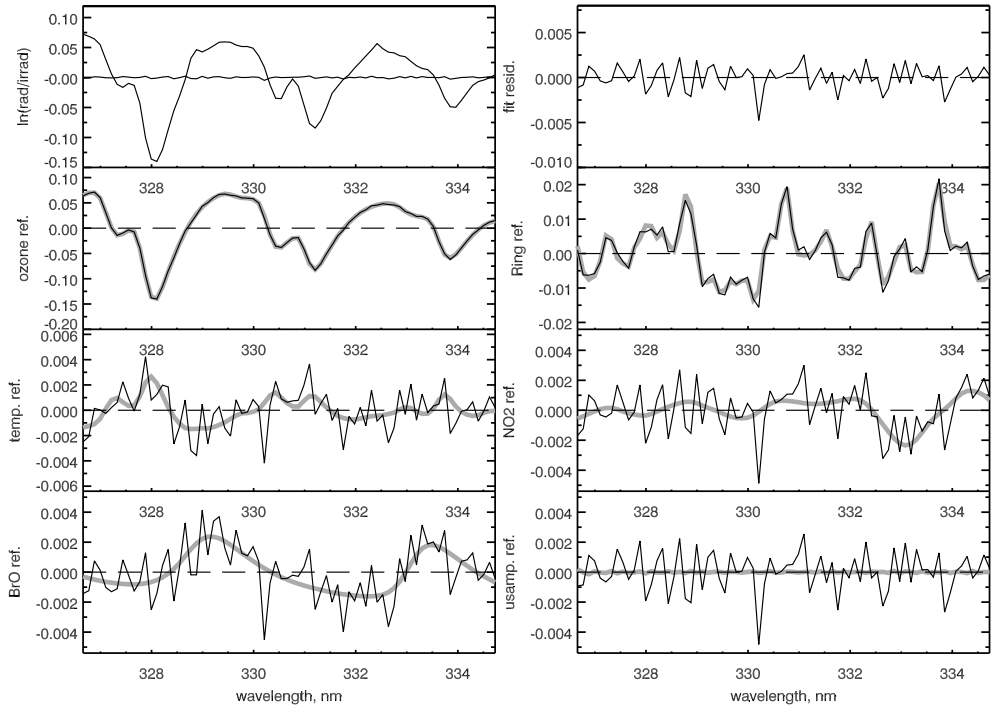

Figure 7.14: Fit results for pixel number 804 having its center at 50.16°N latitude and 19.63°E longitude of SCIAMACHY orbit 5587. The top left panel shows the optical depth observed by SCIAMACHY and the top right panel shows the fit residual. The lower panels show the contributed part by various terms in the WF-DOAS equation. Grey line show the sum of the modeled values and the fit residual plotted separately for each terms. Those terms (from top to bottom and left to right) are ozone, Ring, temperature shift, NO_2, BrO, and undersampling correction.

diagram of the online WF-DOAS algorithm has been given in Figure 6.1 of Section 6.3.2. The algorithm couples simulation and retrieval parts. In the first step, simulated intensity is calculated for the given geometry of a measurement, a first-guess total ozone, ozone and temperature profiles from the IUP climatology that correspond to the total ozone, and other information on surface and cloud parameters. The retrieval part computes total ozone by spectral fitting of simulated intensity and weighting functions and measured intensities taking the impact of the Ring effect, and other interfering gases such as NO_2, BrO into account. The first iteration updates the first-guess total ozone, simulates intensity and weighting functions, updates the Ring spectrum, and finally retrieves total ozone. The retrieved total ozone is compared with the earlier total ozone scenario and the fitting process is repeated until the convergence criteria is met. After the iteration stops the ghost vertical column is added to the retrieved column to obtain the final total ozone column amount.

Typical fit results of WF-DOAS retrievals are shown in Figure 7.14. The Figure shows the differential optical depth measured, fit residual, and the contribution of each of the terms in the WF-DOAS equation. BrO, NO_2, and temperature shift have small contribution. The contribution of the undersampling correction is so small that it is not required to be included in the DOAS equation. The RMS of the fit residuals is usually of the order of 0.002 which is similar to the GOME results.

7.8 Validation of SCIAMACHY WF-DOAS total ozone

7.8.1 Comparison with GOME WF-DOAS total ozone

Comparing a thoroughly validated satellite TCO data with a new satellite data is an effective approach of validation [*Hilsenrath et al.*, 2004; *Bracher et al.*, 2005]. This approach allows comparison of more data covering a wide range of viewing conditions and TCO amounts. Such comparisons cover larger geographical area. With ground based measurements, results of comparisons are often hampered by instrumental bias from one station to the next. These difficulties are avoided in satellite comparisons. GOME data serving this purpose of validation for SCIAMACHY has an additional advantage that the measurement time of these two instruments are just 30 minutes apart. In the following sections the GOME TCO retrievals with WF-DOAS will be used to analyse the WF-DOAS TCO retrievals from SCIAMACHY. For majority of the studies presented below the level 0-1b processing of SCIAMACHY data was done with software version 5.04.

Total ozone and level 1b data versions

A study was performed to investigate if the upgrades of the operational level 0-1b processing software of SCIAMACHY have improved TCO retrievals. Such investigation will provide essential input to the level 0-1b data processing team.

Software of SCIAMACHY operational level 0-1b processor has been upgraded several times since the launch of ENVISAT. The 0-1b reprocessing of SCIAMACHY data has been continued with software version 5.04 since August 2004. These data are the basis for the retrieval of various geophysical parameters.

For TCO retrievals, the level 1b data were calibrated to level 1c using ESA's SciaL1C program (v2.2.9). All calibration options were applied which include memory effect, dark current, stray light, pixel-to-pixel gain, etalon, and polarisation corrections and wavelength and radiometric calibrations. TCO retrievals for selected orbits that were processed with different software versions of level 0-1b processor are documented in Figure 7.15. Here the SCIAMACHY retrievals are done using the SCIAMACHY FM cross-section with a scaling of +3.7% and a shift of +0.016 nm. GOME WF-DOAS TCO data measured 30 minutes later are also shown in the figure. Accuracy of GOME TCO is 1% except at high latitudes. Details of GOME WF-DOAS TCO data quality is given in *Weber et al.* [2005]. Use of scaled SCIAMACHY FM data leads to small negative bias in SCIAMACHY TCO of -1 to -2% with respect to GOME WF-DOAS TCO. Higher biases of up to 5% are observed with the unscaled SCIAMACHY FM data. Similar results

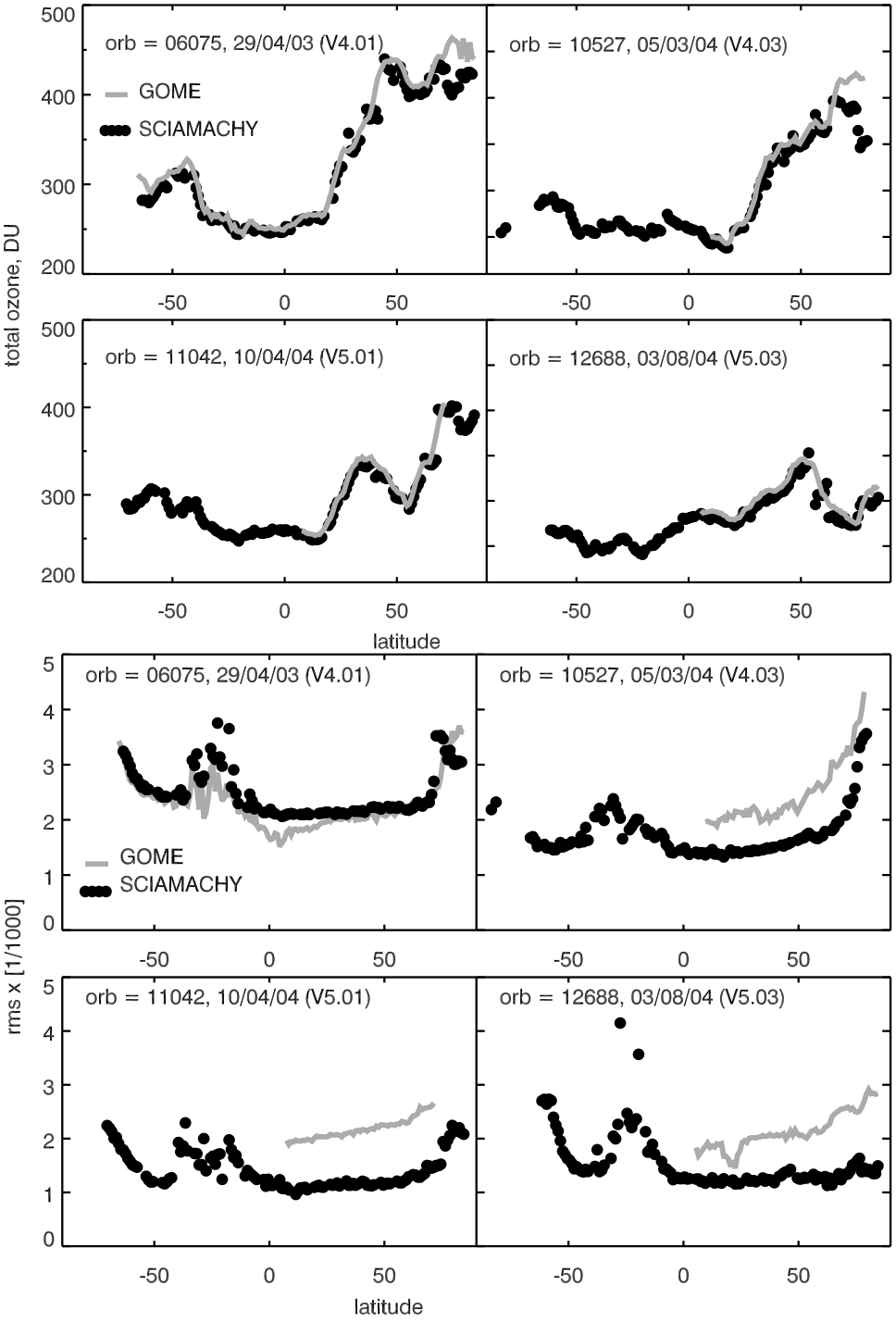

Figure 7.15: Analysis of four selected SCIAMACHY orbits processed with various versions (V4.01, V4.03, V5.01, V5.03) of software for level 0-1b processor. Shown are the TCO retrieval results from GOME (grey solid line), and SCIAMACHY using the scaled SCIA FM (+3.7%) with a wavelength shift of 0.016 nm (solid symbol). Upper two rows: retrieved TCO, lower two rows: fit residual RMS. Data are binned in 1° latitude steps

are also reported by *Eskes et al.* [2005] and *Bracher et al.* [2005]. The more recent SCIAMACHY level 1b version (v5.01 and v5.03) data show a significant improvement in the residual rms and are generally lower than for the GOME retrieval. The overall absolute radiometric calibration is critical for the SCIAMACHY retrieval. In particular the memory effect, dark current determination, and the polarization correction needs to be further improved [*Frerick*, 2005].

Total ozone and solar data

For TCO retrievals, DOAS-type algorithms need the ratio of Earth shine to solar irradiation. The solar irradiation can be measured using the ESM and the ASM diffusers. Investigations revealed that the sun-over-ESM-diffuser produce large spectral features to which are the DOAS retrievals sensitive [*de Beek and Bovensmann*, 2000]. With the sun-over-ASM-diffuser, which was installed at the later stage, the spectral features were minimised. But an absolute calibration cannot be performed with the sun-over-ASM-diffuser. For minor trace gas retrievals the partially calibrated irradiance data from the sun-over-ASM-diffuser and radiance spectra are recommended [*Lichtenberg et al.*, 2005].

In order to investigate the impact of choice of solar spectra (sun-over-ESM-diffuser or sun-over-ASM-diffuser) on TCO retrievals, a few orbits were analysed using the sun-over-ESM-diffuser and the sun-over-ASM-diffuser irradiance data separately. Operational processing of SCIAMACHY level 1b data products provides fully calibrated spectra for the sun-over-ESM-diffuser but for the sun-over-ASM-diffuser it is only partially calibrated. In the latter case, an equivalent calibration steps i.e. memory effect, leakage current, and stray light corrections and wagelength calibration need to be applied for the earth shine radiance for the DOAS fitting. Fully calibrated solar irradiance and earth shine radiance are still required to determine the effective albedo.

In Figure 7.16, an example of retrievals for SCIAMACHY using these solar data is shown for the orbit 05583 on 28 March 2003. Figures demonstrate retrieved TCO (left upper panel) and RMS value of the fit residuals (right upper panel). The change in TCO (left lower panel) and RMS (right lower panel) illustrate the impact of different solar data in TCO retrievals. The difference in TCO does not exceed $\pm 2\%$ but it shows a clear dependency on latitude. The reason for this latitude dependence could be polarisation related. TCO retrievals with the sun-over-ASM-diffuser solar spectrum is without a polarisation correction in the earth shine radiance. For the fully calibrated radiance, the polarisation correction is accurate to up to 2% (S. Slijkhuis, DLR, personal communication, 2006). For improved TCO retrievals, further improvements in polarisation correction is necessary. The reason for the persistent cyclic offsets in each SCIAMACHY state observed particularly in the northern hemisphere is not clear. With the use of ASM-diffuser solar data, the RMS value of the fit residuals are usually larger by up to 20%.

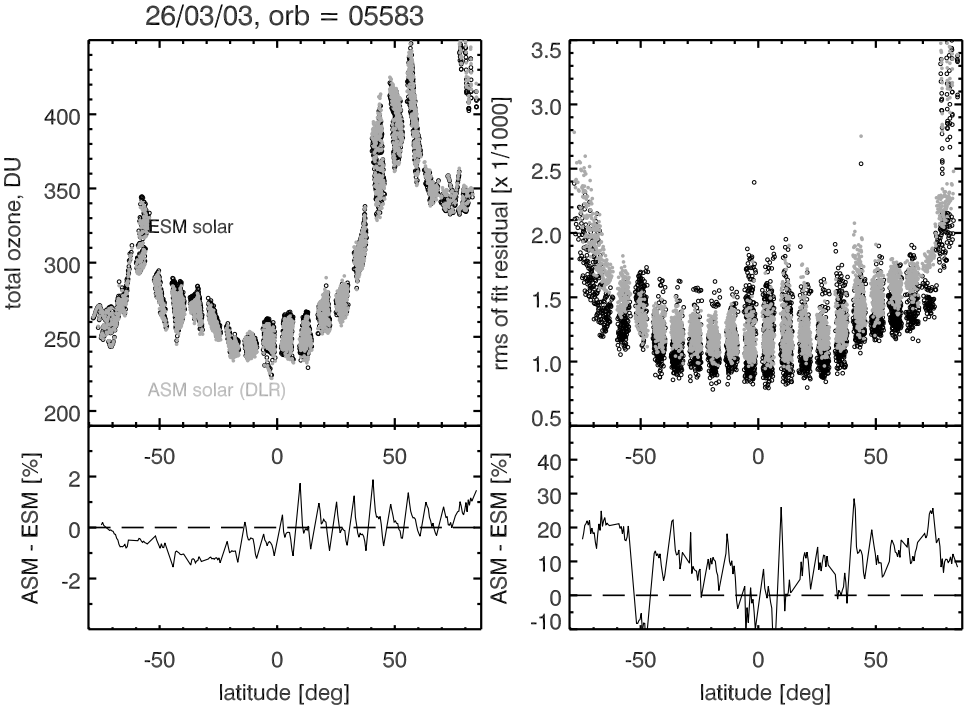

Figure 7.16: TCO (left) and fit residuals (right) from SCIAMACHY WF-DOAS retrievals using the sun-over-ESM-diffuser (black) and the sun-over-ASM-diffuser (grey) irradiance data for one selected orbit (orbit number 05583 on 28 March 2003). The difference expressed in % for TCO (left) and rms (right) are shown in the lower panels.

Scan angle dependent bias

TCO differences between the retrievals based on the sun-over-ASM-diffuser and the sun-over-ESM-diffuser solar data is shown in Figure 7.17. Shown here are the results only for one SCIAMACHY state from orbit 05587. Numerals along abscissa indicate the ground pixel indices that follow the scan from east (1 representing the eastmost pixel) to west (16 representing the westmost pixel) comprising 16 forward scans. Each pixel having the size 30 km$\times$60 km corresponds to an integration time of 0.25 s. The forward scan is followed by four backscans (numbered 17 to 20 in the figure) with a lower spatial resolution (ground pixel size of 30 km$\times$240 km). For east pixels, TCO using the sun-over-ASM-diffuser solar data are usually higher than that using the sun-over-ESM-diffuser solar data. The opposite is the case for west pixels. The bias is not constant for all pixels but appears to be parabolic in shape. The difference lies in the range +3% to -1% going from east to west. This means that the choice of solar data results in differences in the retrieved TCO. Retrievals with the sun-over-ESM-diffuser solar data apply polarisation correction but the current correction is not sufficient on one hand and on the other hand the retrievals with the sun-over-ASM-diffuser solar data do not apply any

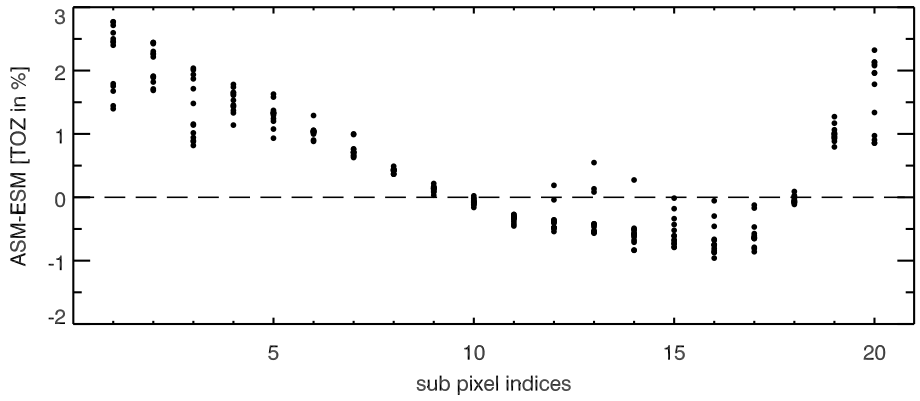

Figure 7.17: Difference in TCO retrieved using the sun-over-ASM-diffuser and the sun-over-ESM-diffuser solar measurements. Results are shown here only for one state of SCIAMACHY orbit 05587 on 26 March 2003. Numerals along abscissa stand for the ground pixel indices.

polarisation correction. This makes interpretation of the observed scan angle dependent bias very difficult.

Either the sun-over-ESM-diffuser or the sun-over-ASM-diffuser or both solar data could be the cause for scan angle dependent bias in retrieved TCO. In order to investigate this, the SCIAMACHY TCO were compared with the GOME WF-DOAS TCO for a few selected days. The GOME data from WF-DOAS algorithm are suitable because they do not show any significant scan angle bias with respect to ground based measurements.

Since SCIAMACHY and GOME footprints are of different size, SCIAMACHY ground pixels were combined to match GOME resolution. Figure 7.18 shows the percent difference in TCO between SCIAMACHY and GOME. Shown are the results based on one SCIAMACHY orbit (orbit number 05591) on 26 March 2003. For retrievals with the sun-over-ASM-diffuser, the average SCIAMACHY TCO biases are about 0%, -2%, and -4% for east, nadir, and west pixels respectively. With the sun-over-ESM-diffuser the biases are somewhat smaller. Summarising, the retrievals with both the sun-over-ASM-diffuser and the sun-over-ESM-diffuser show scan angle dependence, but the scan angle dependence is more severe for retrievals with the sun-over-ASM-diffuser. Reflectance comparison also revealed such east west bias [*van Soest et al.*, 2005]. In addition to the scan angle dependency, the use of the sun-over-ASM-diffuser solar data are observed to result in the latitudinal dependence (north-south bias). This effect is likely to come from the polarisation effect (S. Slijkhuis, DLR, personal communication, 2006), which is not accouted for in the latter case.

Comparison of TCO measurements from SCIAMACHY and GOME were done for several days. The software version 5.04 was used for level 0-1b processing and the sun-over-ESM-diffuser solar data were used for TCO retrievals for SCIAMACHY. For the comparison with correlative measurements, all GOME and SCIAMACHY data have been gridded to $1^\circ \times 1^\circ$. The difference was then calculated from the corresponding gridded

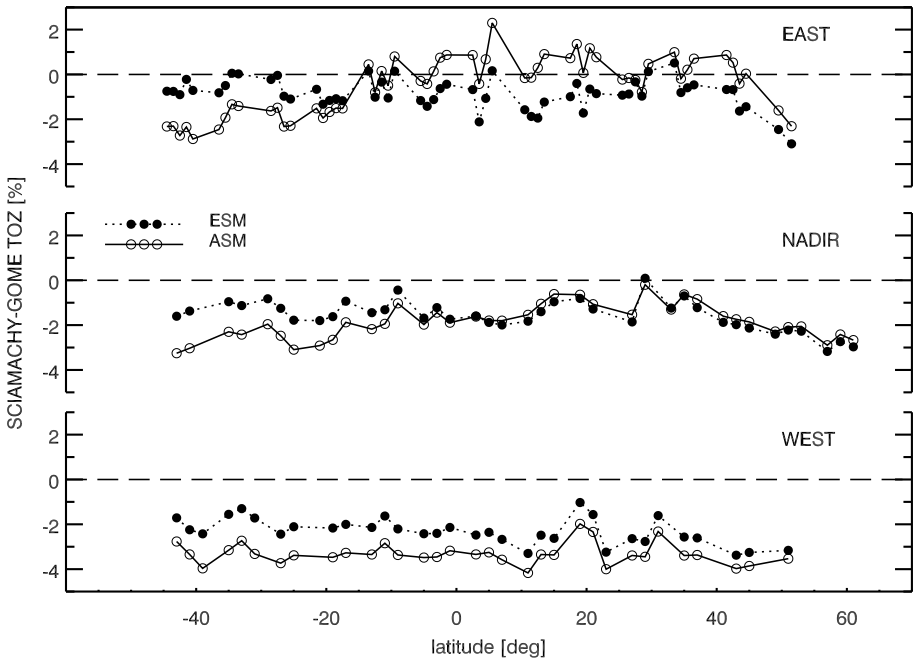

Figure 7.18: Comparison between SCIAMACHY WF-DOAS and collocated GOME WF-DOAS results separated by retrievals with the sun-over-ASM-diffuser (ASM) and the sun-over-ESM-diffuser (ESM). These results are based on measurements of TCO by SCIAMACHY on 26 March 2003 from orbit 05591.

values. As discussed above, in several cases the difference shows a clear scan angle dependence. West pixels are about 2% too low than the east pixels. Typical difference plot is shown in the left panel of Figure 7.19. In the right panel an example is shown where such biases between east and west pixels are not observed. In those cases the overall agreement between SCIAMACHY WF-DOAS TCO and GOME results is very good. The question remains why the difference between correlative SCIAMACHY and GOME TCO shows scan angle dependency for some orbits while such dependency is not always observed. The reason for this is not understood at this moment. This could partly be related to the level 1 calibration problems.

Overall agreement

Figure 7.20 summarises the monthly mean of the difference between SCIAMACHY and GOME TCO averaged over the 960 km-wide swath. About 5 orbits per month were selected. Most of the selected orbits correspond to ERS-2 and ENVISAT satellites passing over Europe. The main idea for selecting these orbits is to make comparison of SCIAMACHY TCO with GOME and ground-based measurements. Note that the WOUDC monitoring network has higher spatial station density in Europe.

SCIAMACHY-GOME WF-DOAS monthly mean TCO difference for 2003 is shown in

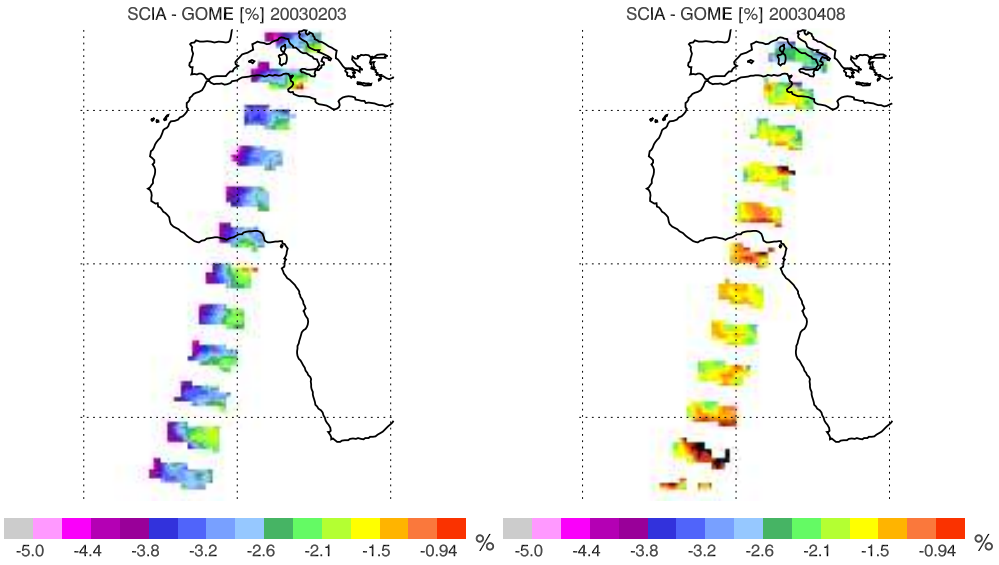

Figure 7.19: Difference in TCO amount between SCIAMACHY and GOME for two selected SCIAMACHY orbits 04857 (on 3 February 2003) and 05773 (on 8 April 2003). The level 0-1b processing for both of these orbits were done with software version 5.04.

Figure 7.20. The SCIAMACHY WF-DOAS results have a latitude dependent bias ranging from -2% at low and midlatitudes to -10% at high latitudes. Dispersion of the difference increases significantly beyond 70° of both hemispheres. Except at high latitudes, month-to-month variation is not observed.

7.8.2 Comparison with ground based measurements

For comparison with ground based data the same set of orbits (63 orbits) as reported in Section 7.8.1 were processed. These include mainly data from various months of 2003. The orbits were selected seeking suitable coincidences and appropriate sampling during 2003 with the ground based measurements. Since global coverage can be achieved in six days with SCIAMACHY, about 5 correlative measurements could be expected in a month. Undoubtedly, these limited orbits are not sufficient for complete validation, but it should at least be important to check the consistency between SCIAMACHY-GOME and SCIAMACHY-ground based comparisons.

Primary reason for using this limited orbits was that the study intended to include only the data set reprocessed by software version 5.04 of the level 0-1b processor. As shown earlier, the level 0-1b processor upgrade has an impact on TCO retrievals.

The validation of TCO measured by SCIAMACHY and retrieved by WF-DOAS algorithm was carried out by comparing with ground based observations from Brewer spectrophotometers operating at selected sites at midlatitude. The stations are listed in Table 7.5. The Brewer instrument is designed for near simultaneous measurements of

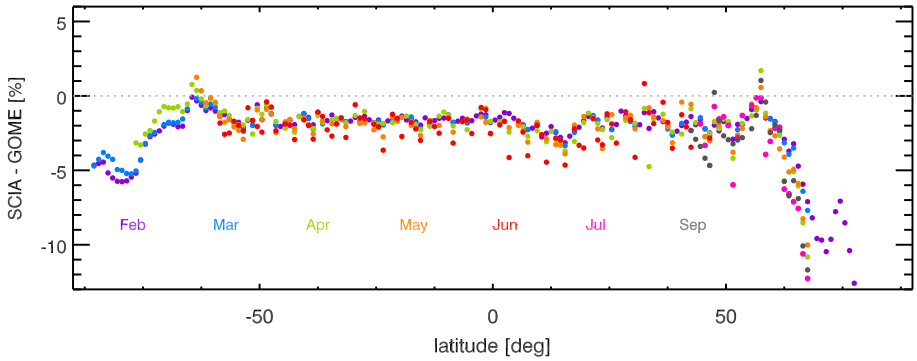

Figure 7.20: Longitude averaged difference between SCIAMACHY WF-DOAS and collocated GOME WF-DOAS for various months of 2003. Total of 63 orbits, about 5 orbits per month, were taken.

Table 7.5: Ground stations used in the present study.

station	WMO code	lat.	lon.	collocations
Arosa	035	46.78	9.68	50
Belsk	068	51.84	20.79	41
Debilt	316	52.10	5.18	43
Hohenpeissenberg	099	47.80	11.02	48
Hradec Kralove	096	50.18	15.83	57
J.R.C. Ispra	301	45.80	8.63	53
Lindenberg	174	52.21	14.12	54
Norrkoeping	279	58.58	16.15	58
Potsdam	050	52.22	13.05	22
Uccle	053	50.80	4.35	40

TCO, SO_2, and global spectral irradiance in the wavelength range 290-372 nm. An important advantage with the Brewer measurements is that the wavelengths that is used in the Brewer spectrophotometers are less temperature dependent [*Kerr*, 2002; *Staehelin et al.*, 2003; *Weber et al.*, 2005]. All these station data were available from WOUDC.

In the present study, a distance of 300 km and measurements taken on the same day were chosen as coincidence criterion. From earlier studies it is observed that the result is not changed by selecting lower collocation criteria up to 500 km [*Bramstedt et al.*, 2003; *Weber et al.*, 2005]. Only direct sun measurements have been used. The accuracy of the direct sun ozone retrieval in Brewer is reported to be $\pm 1\%$ [*Staehelin et al.*, 2003].

Figure 7.21 displays the individual relative difference for each station, plotted all together as a function of day of year. In general a good agreement is achieved apart from the constant bias of about -1 to -2%. This implies that for most of the stations SCIAMACHY WF-DOAS underestimates the ground based values. No significant seasonal dependence is observed. Although the available data set are not sufficient to separate clearly a possible SZA dependence, this comparison indicates that a clear SZA dependency is not seen. Note that such dependency were reported for the SCIAMACHY operational TCO product [*Hilsenrath et al.*, 2004; *Lambert et al.*, 2004b; *Bracher et al.*, 2004, 2005].

The comparison of SCIAMACHY WF-DOAS TCO with two independent measurements, namely GOME and Brewer, shows consistent results that the SCIAMACHY WF-DOAS TCO is 2% too low. The reason for such systematic bias is not clear yet but likely due to calibration errors. The reported negative bias for the southern midlatitude and tropics and the positive bias for northern latitudes in the operational TCO [*Bracher et al.*, 2005] are not observed with the WF-DOAS retrievals.

More comparisons between SCIAMACHY and ground based measurements globally are needed to cover the entire SCIAMACHY period to verify the conclusions drawn here. A more extensive validation is planned.

7.9 Conclusion

A combined TCO data set from GOME and SCIAMACHY instruments is important for ozone studies, in particular for long-term trend determination. Comparative studies of the current operational SCIAMACHY TCO (V5.01/V5.04) with correlative GOME WF-DOAS V1.0 results have concluded that the operational TCO shows a mean relative bias of about -2% and a strong dependence on latitudes, solar zenith angle, and TCO amounts. These problems are inherited from GDP V2.7 in the operational product and are accompanied by the quality of level 1 data and auxiliary data like ozone cross-section, atmospheric parameters, etc. that are essential for TCO retrievals. Part of the problems are resolved by the application of the new generation of algorithms for GOME such as WF-DOAS. This article gave an overview of the WF-DOAS set up for SCIAMACHY which is nearly identical to that for GOME (see Chapter 3 for further details).

Modifications in the WF-DOAS set up for SCIAMACHY are primarily for auxiliary parameters, in particular, ozone cross-section and cloud parameters. A detailed investiga-

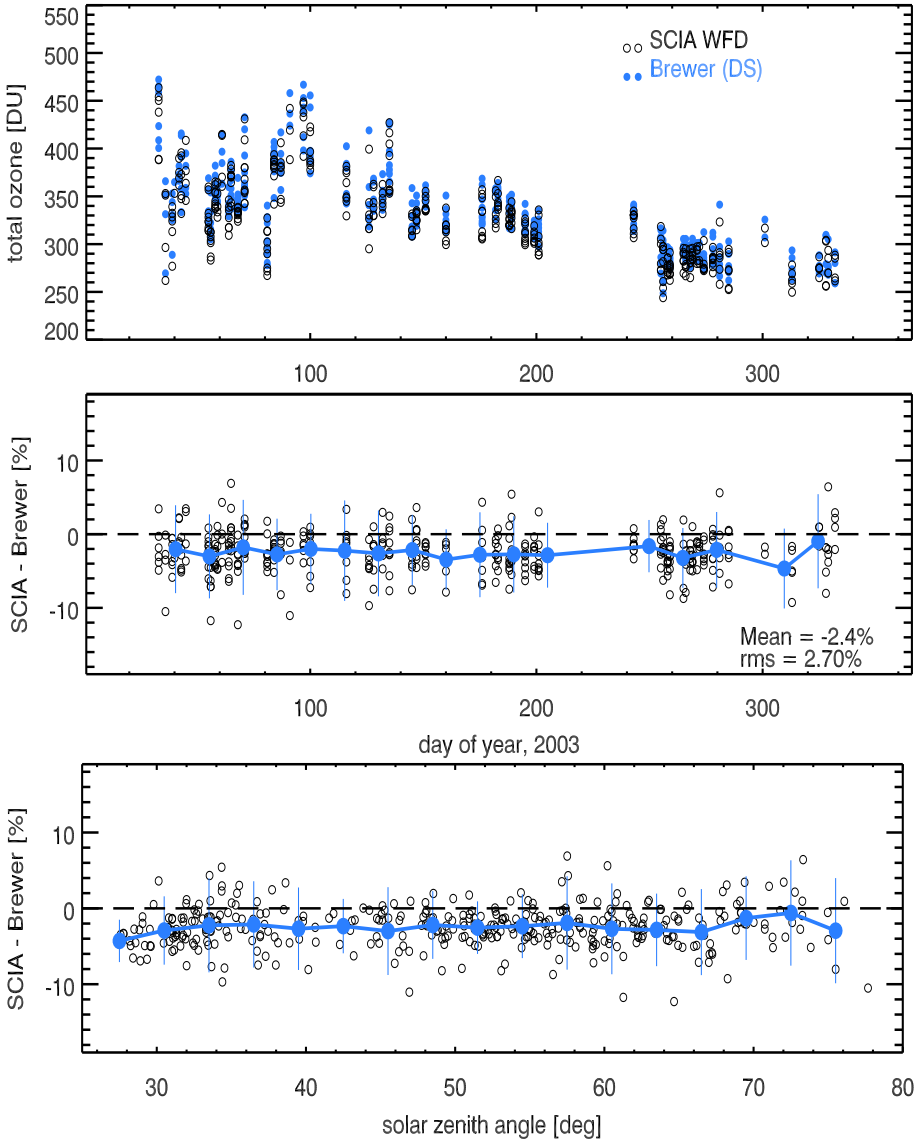

Figure 7.21: Comparison of SCIAMACHY WF-DOAS with collocated European mid latitude Brewer stations in 2003. Top Panel: SCIAMACHY (open circle) and Brewer total ozone (solid circle). Middle panel: SCIAMACHY Brewer differences in percent. Bigger solid circles are bi-weekly averages with 2σ variability. Bottom panel: Same as middle panel but as a function of solar zenith angle. Here, the bigger solid circles represent the 5°-bin averages.

tions of the influences of the auxiliary parameters have been carried out. Moreover, the SCIAMACHY WF-DOAS implementation makes use of the improved climatology [*Lamsal et al.*, 2004] and a high resolution topographic data base. The only modification in the algorithm is that the new implementation employs online iterative retrieval process instead of a look-up-table as for GOME.

The main conclusions of the investigation with regard to the proper use of ozone cross-sections in the SCIAMACHY TCO retrievals are itemized below:

- From the ILS fitting of solar and cross-section data it was found that the optimised wavelength shift for GOME FM and SCIAMACHY FM cross-sections are +0.023 nm and +0.016 nm, respectively, in the ozone window of 325-335 nm. These shifts are particularly recommended in DOAS retrievals that use the Kurucz solar data to wavelength calibrate the solar reference data as done, for instance, in the WF-DOAS retrieval.

- After careful adjustments of the differences in spectral resolution between GOME and SCIAMACHY a differential scaling factor from GOME FM to SCIAMACHY FM of 0.963(2) on average was found in the 326.6-335 nm window. Small changes in the spectral windows may change the scaling by several tenths of a percent.

- If no differential scaling between GOME FM and SCIAMACHY FM is done, a bias of about +4% in the SCIAMACHY retrieval between SCIAMACHY FM and GOME FM is to be expected. This adjustment would be needed to homogenise the GOME and SCIAMACHY retrieval under the condition that the radiometric calibration has the same level of accuracy for both instruments.

- For SCIAMACHY WF-DOAS TCO retrieval that uses the spectral window of 326.6-335 nm, the SCIAMACHY FM cross-section needs to be differentially scaled by 1.037 and wavelength shifted by +0.016 nm.

Additionally, the influence of inhomogeneous clouds on TCO retrievals from space based measurements has been studied. It is confirmed that a 2 km error in cloud top height results in more than 1% error in TCO and that a 0.2 error in cloud fraction results in about 1 DU error in the retrieved TCO. Comparisons of cloud top heights retrieved from FRESCO and SACURA and cloud fractions retrieved from FRESCO and OCRA suggest that the FRESCO algorithm underestimates the cloud top heights by about 2 km and the cloud fraction by about 0.2. It follows that the quality of retrieved TCO from SCIAMACHY is influenced by the choice of cloud data either from FRESCO or SACURA-OCRA. Moreover, IPA used in ozone satellite retrievals may bias results significantly depending on the type of cloudiness.

Comparison/validation of the ozone products has been carried out with other satellite-based measurements (GOME WF-DOAS TCO) as well as measurements from ground-based instrument (Brewer). The validation exercises show an offset of -1% to -2% as compared to GOME retrievals and ground-based observations. Part of the offset is related to the quality of the level 1 data. The difference in the viewing angle given in the

level 1 files and that corresponding to the read out time for ozone window (325-335 nm) explains only a small part of the observed offset. Problems with the radiometric calibration and polarisation correction are believed to be the main contribution. In addition, a clear scan angle dependence in the observed biases was found, with larger biases for west pixels. The reason for this effect is not understood at the moment.

Apart from this offset, a good agreement between SCIAMACHY and GOME WF-DOAS was found. A clear dependency of TCO on latitude, solar zenith angle, and TCO amounts was not observed. However, further validation exercises need to be carried out for longer time period in order to verify these conclusions.

8 Overall summary, conclusions and future perspectives

8.1 Overall summary

The main focus of this thesis has been on the development, validation, and improvement of a retrieval algorithm for deriving TCO amounts from backscatter hyperspectral UV satellite instruments. The new WF-DOAS algorithm has been successfully applied to GOME and SCIAMACHY. It can be also adapted to other currently operating and future instruments such as OMI(2004-) and GOME-2 (launch in 2006). The updated TCO data have become valuable for various scientific investigations.

TCO retrieval from the traditional DOAS-type operational GDP algorithm consists of three steps: (1) derivation of the slant column density by fitting the reference differential absorption spectrum of ozone to the measured earth radiance spectrum and solar irradiance spectrum, (2) conversion of the slant column density to the vertical column density using the air mass factor, and (3) correction for the screening of ozone below clouds. Although the algorithm has yielded good results for TCO abundances, there are some unresolved issues, mainly concerning the air mass factor. The major problem lies with the use of an air mass factor calculated at an appropriate wavelength. Additionally, the air mass factor shows sensitivity to the assumed ozone profile shape. Given the motivation for this study, the aim was to develop a robust algorithm where vertical column density of ozone is retrieved without requiring air mass factor calculation.

The WF-DOAS TCO retrieval as presented in Chapter 3 is based on a comparison between the measured normalised radiance and the radiances derived by radiative transfer calculations. By using wavelength dependent vertically integrated ozone weighting functions, a direct retrieval of vertical column amounts is possible. Proper modeling of the Ring effect including Raman correction for ozone absorption have been implemented. Neglect or insufficient treatment of the Ring effect can lead to errors in TCO of several percent. The algorithm uses cloud parameter and effective albedo directly derived from GOME measurements. Other implementations include the use of effective scene height accounting for cloud effects, an ozone temperature correction, and the use of TOMS V7 climatology.

The new WF-DOAS algorithm for GOME has been extensively compared with globally distributed ground-based data, predominantly Dobson spectrophotometer data. In mid and low latitudes it agrees on average to within half a percent with WOUDC data. The observed bias shows small seasonal variation of up to $\pm 0.5\%$. Such seasonal variation is however not persistent at all stations. The predecessor version GDP V3.0 clearly shows a larger and persistent annual variation ($\pm 1\%$) at mid latitude stations and in the

tropics it shows a constant bias of about -1% with respect to the ground-based data. In polar regions somewhat larger differences are still observed with WF-DOAS although the errors in the retrieved TCO is reduced as compared to GDP V3.0. WF-DOAS shows weaker solar zenith angle and TCO dependence in the differences to the ground data.

A detailed study was carried out to assess the comparison between simultaneous WF-DOAS and ground-based Dobson and Brewer measurements. The comparison with Brewer measurements at Hradec Kralove and Hohenpeissenberg has demonstrated excellent agreement with WF-DOAS. The larger differences between GOME and Dobson is related to the fixed ozone temperature used in the standard retrieval of ground based instruments. Brewer wavelengths have a much weaker temperature dependence and this explains the agreement of WF-DOAS with Brewer data. Brewer-Dobson differences can be as high as $\pm 2\%$ (generally on the order of 0.5%). This variability gets maximum at high latitudes during winter due to lower solar elevation and the enhanced stray-light problem associated with it. The better agreement of WF-DOAS with Brewer than simultaneous Dobson data confirms that the temperature shift weighting function appears appropriate to account for the ozone temperature variation.

The validation of WF-DOAS as presented in Chapter 3 suggest that the GOME WF-DOAS data is very attractive for evaluating ground-based network data as presented in Chapter 4, where Brewer measurements from 35 stations archived in WOUDC are examined. We focused on Brewer instruments because these instruments currently lack transparent calibration procedure and data quality program.

About 50% of the stations have mean WF-DOAS-station TCO bias of less than 0.5%, about 25% have mean bias in the range 0.5% - 1% and the remaining stations are found to have a bias of 1% to 2%. For the majority of stations, the root mean squares (RMS) of the difference between WF-DOAS and Brewer data have been observed to be less than 3%. The operational GDP V4.0 TCO data have shown similar results but with somewhat larger bias and RMS. Time series of difference between WF-DOAS and Brewer TCO can help identify problems in Brewer instruments and operation. Sudden jumps in the time series were observed, for instance, in Pohang, Longfengshan, and Sestola.

In Chapter 4, we have also compared GOME TCO (reprocessed with WF-DOAS and GDP V4.0) with the recent updates of TOMS and SBUV/SBUV2 data. These data sets will be valuable for various scientific studies including the upcoming WMO Ozone Assessment. Long-term time series of TCO from the last two and a half decade have shown good agreement among these data sets. However, further works are still required to improve the quality of satellite and ground-based ozone data from high latitudes.

Updated and atmospheric dynamics oriented ozone and temperature climatologies are presented in Chapter 5. The new climatology was developed with the aim of improving the quality of *a priori* information in ozone retrievals. They are intended to be used for ozone column and profile retrieval from GOME, SCIAMACHY, or any other backscatter satellite measurements. Since TCO retrievals by GDP-like, WF-DOAS, TOMS-like algorithms are sensitive to the profile shape of atmospheric ozone, this climatology provides an opportunity to correct the profile shape errors in the retrieved TCO. These climatological profiles can also be used to improve the ozone profile retrieval using the optimal estimation technique, provided that TCO is known from TCO retrieval algorithm.

Chapter 5 presents the methodology of preparation of the climatologies. The climatologies are classified by TCO and are based on semi-annual intervals and 30° wide latitude bins using recent ground-based and satellite data. Total column dependent profile shapes have advantage that they better represent the dynamical variability of ozone with respect to tropopause lifting and horizontal advection. In particular, the tropopause variance of the classified profiles was successfully reduced compared to a traditional zonal monthly mean climatology. This helps to stabilize the fit results in the profile retrieval. A case study pursued at Hohenpeissenberg has demonstrated the usefulness of an updated climatology like IUP climatology. The ozone profile retrieval has been significantly improved, in particular in the lower part of the atmosphere. Some additional analyses carried out in order to evaluate the IUP climatology suggest that they are reliable and can represent the global ozone field. In particular, the use of POAM III data and SHADOZ sonde data have improved the ozone climatology in polar region and tropics.

In Chapter 6 we investigate how TCO retrievals are influenced by the choice of ozone and temperature profiles from various currently available climatologies. In order to investigate the profile related TCO retrieval error various ozone and temperature profile climatologies were analysed with the help of ozonesonde, lidar, and radiosonde data of Hohenpeissenberg in mid latitude and Syowa in polar region. GOME TCO retrieved by using WF-DOAS shows negligible effect of climatological profiles at Hohenpeissenberg but considerable systematic differences are observed at Syowa for SZA larger than 70°. Our studies based on the GOME spectral measurements and synthetic radiances that were used for TCO retrievals using WF-DOAS algorithm, have identified both random and systematic errors in the retrieved TCO originating from the climatological ozone and temperature profiles. The systematic errors can be up to 10% (e.g. TOMS V7 climatology) at high SZA. Profile sensitivity of TOA radiance is strong when the SZA gets large. By using the IUP or TOMS V8 climatology a significant improvement in the retrieved TCO at high SZA was observed. Such demonstration at Syowa does not necessarily prove that the IUP or TOMS V8 climatology is the best but provides a clear message that regular updates of ozone and temperature climatologies can remove some of the discrepancies observed in the current satellite ozone products.

A combined TCO data set from GOME and SCIAMACHY instruments signifies high importance for long-term trend assessment. Comparative studies of the current operational SCIAMACHY TCO (V5.01/V5.04) with correlative GOME WF-DOAS V1.0 results have concluded that the operational TCO shows a mean relative bias of about -2% and a dependence of the difference on latitudes, solar zenith angle, and TCO amounts. These problems were inherited from GDP V2.7 that was adapted for SCIAMACHY operational retrieval. In addition the quality of level 1 data and auxiliary data like ozone cross-section, atmospheric parameters, etc. that are essential for TCO retrievals were not optimized. Part of the problems could be resolved by the application of the new generation of algorithms such as WF-DOAS. Chapter 7 gives an overview of the WF-DOAS set up for SCIAMACHY which is nearly identical with that for GOME as described in Chapter 3.

A detailed investigation of the spectral resolution of Channel 2 spectra from SCIAMACHY (310 nm-400 nm) was carried out using a high resolution solar spectrum mea-

sured with the Fourier transform spectrometer. Similar investigation was carried out for SCIAMACHY FM cross-section using the FTS spectrometer data from *Voigt et al.* [2001] and Bass and Paur data. From the ILS fitting of solar and cross-section data it was found that the optimised wavelength shift for SCIAMACHY FM is 0.016 nm in the ozone window of 325 nm-335 nm. The study also showed that for WF-DOAS TCO retrievals the SCIAMACHY FM cross-section spectra needs to be differentially scaled by 1.037.

The influence of inhomogeneous clouds on TCO retrievals from space based measurements has been studied. It is confirmed that a 2 km error in cloud top height results in more than 1% error in TCO and that a 0.2 error in cloud fraction results in about 1 DU error in the retrieved TCO. Comparisons of cloud top heights retrieved from FRESCO and SACURA and cloud fractions retrieved from FRESCO and OCRA suggest that the FRESCO algorithm underestimates the cloud top heights by about 2 km and the cloud fraction by about 0.2. The study concluded that the quality of retrieved TCO from SCIAMACHY is influenced by the choice of cloud data either from FRESCO or SACURA-OCRA.

The SCIAMACHY implementation of the WF-DOAS uses the scaled SCIAMACHY FM cross-section and wavelength pre-shifted by 0.016 nm for the calculation of reference spectra and the Ring spectra. Cloud data either from FRESCO or SACURA-OCRA, an improved climatology [*Lamsal et al.*, 2004] and high resolution topographic data base are other implementations. The only modification in the algorithm is that the new implementation employs online iterative retrieval process instead of look-up-tables like for GOME.

Comparison/validation of the SCIAMACHY WF-DOAS has been carried out with GOME WF-DOAS as well as measurements from ground-based instrument (Brewer). The validation exercises show an offset of -1% to -2% as compared to GOME retrievals and ground-based observations. Part of the bias is related to the quality of the level 1 data. The difference in the viewing angle given in the level 1 files and that corresponding to the read out time for the ozone window (325-335 nm) explains only a small part of the observed bias. Problems with the radiometric calibration and polarisation correction are believed to be the main contribution. In addition, a clear scan angle dependence in the observed biases was found, with larger biases for the west pixels. The reason for this effect is not understood at the moment.

Apart from this offset, good agreement between SCIAMACHY and GOME WF-DOAS was found. A clear dependency of TCO on latitude, solar zenith angle, and TCO amounts was not observed. However, further validation exercises need to be carried out for longer time periods in order to verify these conclusions.

8.2 Main conclusions of this work

The main conclusions from this work are:

1. A new algorithm (WF-DOAS) for TCO retrieval from hyperspectral UV satellite instrument, GOME, has been developed and the algorithm has been carefully validated using ground-based TCO measurements.

2. A new climatology (IUP climatology) has been prepared with the primary aim of improving TCO and ozone profile retrievals from satellite (e.g. GOME, SCIAMACHY) measurements.

3. TCO retrievals at high solar zenith angle show a large profile shape sensitivity. In such condition, the use of recent and updated *a priori* ozone and temperature profile, for example from the IUP climatology, can improve TCO retrievals. Also, with the use of improved *a priori* profile from the IUP climatology a significant improvement in the retrieved GOME ozone profile at and around tropopause can be achieved.

4. The WF-DOAS algorithm was successfully adapted for SCIAMACHY and the SCIAMACHY WF-DOAS has been validated using correlative GOME and ground-based Brewer measurements.

8.3 Future perspectives

Total column ozone retrievals at high latitudes:

Near global validation of the WF-DOAS retrievals has shown that the accuracy of WF-DOAS TCO is similar to that of a well maintained Brewer or Dobson instrument for low and mid latitudes where the solar zenith angles during satellite measurements are lower. This is usually the case for UV nadir satellite instruments like GOME and SCIAMACHY that are flying in a sun-synchronous orbit with a fixed local time (around noon). At polar latitudes the measurements are made at high solar zenith angles when the profile effects are most prominent. Then the WF-DOAS-Brewer differences increase on average to 2% to 5%. Under ozone hole condition the difference can be as high as 8%. The work presented here has demonstrated that the difference can be reduced to some extent by the use of improved ozone and temperature climatologies. This suggests the need of regularly updating the IUP climatology presented in this thesis as the maturity of data sets increases and in order to account for the long-term changes in the ozone field.

As with GOME WF-DOAS, GDP V4.0 and TOMS V8 also show a strong bias with respect to ground-based measurements at high solar zenith angle in polar region. Further assessment of retrievals should be carried out in order to improve the absolute accuracy of TCO observations made under the extreme conditions of high ozone and large solar zenith angles.

SCIAMACHY WF-DOAS total column ozone:

The SCIAMACHY WF-DOAS TCO retrievals are 1% to 2% lower as compared to TCO measurements from GOME WF-DOAS and Brewer spectrometer. This conclusion is based on comparison using a subset of data mainly from 2003. A more extensive validation with many ground stations and for entire SCIAMACHY period should be carried out in order to verify the conclusions drawn here.

From the comparison between SCIAMACHY and GOME WF-DOAS retrievals, it is evident that there often exists a systematic scan angle dependent bias in SCIAMACHY TCO. The west pixels show larger bias of about 2% than the east pixels. The difference between viewing angle as given in level 1 file and that corrsponds to the readout time for ozone fitting window amounts to about 0.4°. Change in viewing angle due to spacecraft attitude errors does not exceed 0.1° (Christian von Savigny, IUP Bremen, personal communication, 2006). These cannot explain the observed scan angle dependent bias of about 2%. Moreover, occasionally such biases are completely absent. Therefore, the observed mean bias of 1% to 2% and the scan angle dependent bias might be related to level 1 calibration problems. When resolving these issues it is believed that the SCIAMACHY WF-DOAS TCO will be of the same quality as GOME WF-DOAS.

Current SCIAMACHY WF-DOAS algorithm makes iterative calls to SCIATRAN to compute RTM quantities during retrieval. The online retrieval is better suited for sensitivity studies in particular to adapt the algorithm for new instruments. For operational processing the look-up-table approach is preferred since it is computationally faster. The look-up-table approach should be followed in order to process/reprocess SCIAMACHY data over the full instrument lifetime.

SCIAMACHY has a great potential for improving our understanding of tropospheric ozone mainly due to its limb/nadir matching capibilities and better spatial resolution. Improved retrievals of TCO from nadir observation and ozone profiles from limb observation will enable us to obtain a global picture of tropospheric column ozone. Better separation of the stratospheric and the tropospheric ozone is of critical importance to our overall understanding of atmospheric ozone.

Acknowledgements

I sincerely thank Dr. Mark Weber and Prof. Dr. John P. Burrows for accepting me in the UV Satellite Data and Science Group and entrusting me with interesting projects. My thesis advisor Mark has been a constant source of motivation and new research ideas. I greatfully acknowledge his support, excellent guidance, encouragement, and freedom. His impact on this work is immeasurable. I am grateful to Prof. John P. Burrows for his guidence, encouragement, valuable advice, and useful comments throughout the period of this study. The experiences I gained working with him, in particular as his teaching assistant, proved invaluable.

I would like to take this opportunity to express my deep gratitude to Prof. Dr. Jörn Bleck-Neuhaus for his great support until I was enrolled in the Ph.D program and also his constant encouragement and best wishes through out the period.

I wish to express my debt to all present and former colleagues at Institute of Environmental Physics and Remote Sensing (IUP/IFE), University of Bremen, who have so generously shared their knowledge and technical expertise with me. Many thanks to Melanie Coldewey-Egbers for her effort to make me acquianted with GOME WF-DOAS algorithm, Dr. Andreas Richter for useful discussions related to DOAS retrievals. I enjoyed working with Dr. Astrid Bracher in the validation of SCIAMACHY TCO, I am grateful. Thanks to Dr. Silvia Tellmann for her contribution in the study of the impact of ozone climatology in the ozone profile retrievals, Dr. Vladimir Rozanov, Dr. Alexei Rozanov, and Dr. Rüdiger de Beek for discussions related to radiative transfer model SCIATRAN, Dr. Alexander Kokhanovsky and Dr. Heinrich Bovensmann for their co-operation and discussions concerned with the effect of clouds in TCO retrievals, and Dr. Stefan Noël and Dr. Jochen Skupin who were helpful on issues related to the SCIAMACHY level 1 data quality. Many thanks are owed to Dr. Klaus Bramstedt, Wolfhardt Lotz, Dr. Marco Vountas, Dr. Viju Oomen John for their programming related assistance, Dr. Leonard Amekudzi, Dr. Astrid Bracher, and Ninad Sheode for proofreading different parts of the thesis, and Dr. Mark Weber and Rupa Devkota for tirelessly proofreading and giving valuable comments for the entire thesis.

Thanks to the many friends, Sandip Dhomse, Ninad Sheode, T.R. Sreerekha, Viju O. John, Leonard Amekudzi, Ram Krishna Dulal, and many others, with whom I enjoyed a number of fun and intellectual exchanges during my stay in Bremen. I appreciate the co-operation of Stefanie Bühler. I wish to thank the secreteries, especially Sabine Packeiser, and other members of IUP for their assistance.

I would like to express my deepest thanks to my parents, brothers, sisters, and their families for their constant love and supports. Finally, I wish to thank Rupa for her patience, sacrifices, and love.

I would like to acknowledge the financial support from the GSF-National Research Center for Environment and Health for GOMSTRAT (Grants 07ATF42) and the European projects SCILOV (ENVI-CL-EOPG-SW-04-0017) and CANDIDOZ (EVK2-CT-2001-00133).

Bibliography

Allaart, M. A., H. Kelder, and L. C. Heijboer, On the relation between ozone and potential vorticity, *Geophys. Res. Lett., 20*, 811–814, 1993.

Appenzeller, C., A. K. Weiss, and J. Staehelin, North atlantic oscillation modulates total ozone winter trends, *Geophys. Res. Lett., 102*, 1131–1134, 2000.

Attmanspracher, W., and H. U. Dütsch, International ozonesonde intercomparison at the observatory Hohenpensenberg, *Ber. Dtsch. Wetterdienstes, 16*, 1970.

Attmanspracher, W., and H. U. Dütsch, Second international ozonesonde intercomparison at the observatory Hohenpensenberg, *Ber. Dtsch. Wetterdienstes, 18*, 1981.

Attmanspracher, W., J. De La Noe, D. De Muer, J. Lenoble, G. Megie, J. Pelon, P. Pruvost, and R. Reiter, European validation of SAGE II ozone profiles, *J. Geophys. Res., 94*, 1989.

Austin, J., Some ideas on the further development of a stratospheric ozone climatology, *Adv. Space Res., 21*, 1393–1402, 1998.

Avallone, L. M., and M. J. Prather, Photochemical evolution of ozone in the lower tropical stratosphere, *J. Geophys. Res., 101*, 1457–1461, 1996.

Baldwin, M. P., et al., The Quasi-Biennial Oscillation, *J. Geophys. Res., 39*, 179–229, 2001.

Balis, D., et al., Reprocessing the 10-year GOME/ERS-2 total ozone record: the new GOME Data Processor Version 4.0, Paper 2: Product Validation, *J. Geophys. Res.*, in press, 2006.

Basher, R. E., Review of the Dobson spectrophotometer and its accuracy, in *Atmospheric Ozone*, edited by C. S. Zerefos and A. Ghazi, Reidel and Dordrect, 1985.

Bass, A. M., and R. J. Paur, The ultraviolet cross-sections of ozone, I, The measurements, in *Atmospheric Ozone Proc. Quadr. Ozone Symp. Halkidiki, Greece*, edited by C. Zerefos and A. Ghazi, pp. 606–610, 1985.

Bates, D. R., Rayleigh scattering by air, *Planetary and Space Science, 32*, 785–790, 1984.

Beitner, H., S. E. Norell, U. Ringborg, G. Wennerstin, and B. Maston, Malignant melanoma: aetiological importance of individual pigmentation and sun exposure, *Br. J. Dermatol.*, *122*, 43–51, 1990.

Bernhard, G., R. D. Evans, G. J. Labow, and S. J. Oltmans, Bias in Dobson total ozone measurements at high latitudes due to approximations in calculations of ozone absorption coefficients and air mass, *J. Geophys. Res.*, *110*, doi:10.1029/2004JD005559, 2005.

Bethan, S., G. Vaugham, and S. J. Reid, A comparison of ozone and thermal tropopause heights and the impact of tropopause definition on quantifying the ozone content of the troposphere, *Quart. J. Roy. Meteorol. Soc.*, *122*, 929–944, 1996.

Bethan, S., G. Vaugham, C. Gerbig, A. V.-Thomas, H. Richer, and D. A. Tiddeman, Chemical air mass differences near fronts, *J. Geophys. Res.*, *103*, 13,413–13,434, 1998.

Bhartia, P., Algorithm theoretical baseline document, TOMS V8 total ozone algorithm, http://toms.gsfc.nasa.gov, 2003.

Bhartia, P., and C. W. Wellemeyer, TOMS V8 Algorithm Theoretical Basis Document, http://toms.gsfc.nasa.gov/version8/v8toms atbd.pdf, 2004.

Bhartia, P. K., R. D. McPeters, C. L. Mateer, L. E. Flynn, and C. Wellemeyer, Algorithm for the estimation of vertical ozone profile from the backscatter ultraviolet (BUV) technique, *J. Geophys. Res.*, *101*, 18,793–18,806, 1996.

Birner, T., A. Dörnbrack, and U. Schumann, How sharp is the tropopause at mid latitude?, *Geophys. Res. Lett.*, *29*, doi:10.1029/2002GL015142, 2002.

Blindauer, C., V. V. Rozanov, and J. P. Burrows, Actinic flux and photolysis frequency comparison computations using the model photogt, *J. Atmos. Chem.*, *24*, 1996.

Bodeker, G. E., J. C. Scott, K. Kreher, and R. L. McKenzie, Global ozone trends in potential vorticity coordinates using TOMS and GOME intercompared against the Dobson network: 1978-1998, *J. Geophys. Res.*, *106*, 23,029–23,042, 2001.

Bogumil, K., et al., Measurements of molecular absorption spectra with SCIAMACHY pre-flight model: instrument characterization and reference data for atmospheric remote-sensing in the 230–2380 nm region, *J. Photochem. photobiol.*, *157*, 167–184, 2003.

Bojkov, R. D., and V. E. Fioletov, Estimating the global ozone characteristics during the last 30 years, *J. Geophys. Res.*, *100*, 16,537–16,551, 1995b.

Bojkov, R. D., C. Mateer, and A. Hanson, Comparison of ground-based and Total Ozone Mapping Spectrometer measurements used in assessing the performance of the global ozone observing system, *J. Geophys. Res.*, *93*, 9525–9533, 1988.

Bojkov, R. D., V. E. Fioletov, and A. M. Shalamjansky, Total ozone changes over Eurasia since 1973 based on reevaluated filter ozonometer data, *J. Geophys. Res.*, *99*, 22,985–22,999, 1994.

Bojkov, R. D., V. E. Fioletov, and S. B. Diaz, The relationship between solar UV irradiance and total ozone from observations over southern Argentina, *Geophys. Res. Lett.*, *22*, 1249–1252, 1995a.

Bovensmann, H., J. P. Burrows, M. Buchwitz, J. Frerick, S. Noël, V. V. Rozanov, K. V. Chance, and A. H. P. Goede, SCIAMACHY - Mission objectives and measurement modes, *J. Atmos. Sci.*, *56*, 127–150, 1999.

Bracher, A., M. Weber, K. Bramstedt, A. Richter, A. Rozanov, C. von Savigny, M. von König, and J. P. Burrows, Validation of ENVISAT trace gas data products by comparison with GOME/ERS-2 and other satellite sensors, in *Proceeding of ENVISAT validation workshop*, edited by H. Lacoste, pp. SP–531, ESA Publications Division, Nordwijk, the Netherlands, 2002.

Bracher, A., K. Bramstedt, A. Richter, A. Sinnhuber, M. Weber, and J. P. Burrows, Validation of GOMOS (GOPR 6.0a) and SCIAMACHY (V5.1/2.1) O_3 and NO_2 products with GOME (V3.0), HALOE (V19) and SAGE II (6.2), in *Proceeding of the Second Workshop on the Atmospheric Chemistry Validation of ENVISAT (ACVE-2), 3-7 May 2004*, edited by D. Danesy, pp. 397–405, ESA Publications Division, Nordwijk, the Netherlands, 2004.

Bracher, A., L. N. Lamsal, M. Weber, K. Bramstedt, M. Coldewey-Egbers, and J. P. Burrows, Global satellite validation of SCIAMACHY O_3 column with GOME WF-DOAS, *Atmos. Chem. Phys.*, *5*, 2357–2368, 2005.

Bramstedt, K., J. Gleason, D. Loyola, W. Thomas, A. Bracher, M. Weber, and J. P. Burrows, Comparison of total ozone from the satellite instruments GOME and TOMS with measurements from the Dobson network, *Atmos. Chem. Phys.*, *3*, 1409–1419, 2003.

Brasseur, G., and S. Solomon, Aeronomy of the middle atmosphere, *J. Atmos. Sci.*, *56*, 127–150, 1984.

Brewer, A. W., and J. R. Milford, The Oxford-kew ozonesonde, *Proc. R. Soc. London Ser. A*, *256*, 470–495, 1960.

Buchwitz, M., V. V. Rozanov, and J. P. Burrows, A correlated-k distribution scheme for overlapping gases suitable for retrieval of atmospheric constituents from moderate resolution radiance measurements in the visible/near-infrared spectral region, *J. Geophys. Res.*, *105*, 15,247–15,261, 2000a.

Buchwitz, M., V. V. Rozanov, and J. P. Burrows, A near-infrared optimized DOAS method for the fast global retrieval of atmospheric CH_4, CO, CO_2, H_2O, and N_2O

total column amounts from SCIAMACHY Envisat-1 nadir radiances, *J. Geophys. Res.*, *105*, 15,231–15,245, 2000b.

Burrows, J. P., E. Hölzle, A. P. H. Geode, H. Visser, and W. Fricke, SCIAMACHY: SCanning Imaging Absorption spectroMeter for Atmospheric CHartographY, *Acta Astronautica*, *35*, 445–451, 1995.

Burrows, J. P., et al., The Global Ozone Monitoring Experiment (GOME): Mission concept and first scientific results, *J. Atmos. Sci.*, *56*, 151–175, 1999a.

Burrows, J. P., et al., Atmospheric remote sensing reference data from GOME-2, temperature dependent absorption cross-sections of O_3 in the 231-794 nm range, *J. Quant. Spectrosc. Rad. Transfer*, *61*, 509–517, 1999b.

Callies, J., E. Corpaccioli, M. Eisinger, et al., GOME-2- METOP second generation sensor for operational ozone monitoring, *ESA bulletin*, *102*, 28–36, 2000.

Callis, L. B., M. Natarajan, J. D. Lambeth, and R. E. Boughner, On the origin of mid latitude ozone changes: Data analysis and simulations for 1979-1993, *J. Geophys. Res.*, *102*, 1215–1228, 1997.

Casper, C., and K. Chance, GOME wavelength calibration using solar and atmospheric spectra, in *Third ERS symposium on space at the service of our environment*, edited by T. D. Guyenne and D. Danesy, p. 609, European Space Agency, Florence, Italy, 1997.

Caudill, T. R., D. E. Flittner, O. Torres, and R. D. McPeters, Evaluation of the pseudo-spherical approximation for backscattered ultraviolate radiances and ozone retrieval, *J. Geophys. Res.*, *102*, 3881–3890, 1997.

Chance, K., and R. J. D. Spurr, Ring effect studies: Reyleigh scattering including molecular parameters for rotational Raman scattering, and the Fraunhofer spectrum, *Appl. Opt.*, *36*, 5224–5230, 1997.

Chance, K., P. Palmer, R. J. D. Spurr, R. V. Martin, T. P. Kurosu, and D. J. Jacob, Satellite observation of formaldehyde over North America from GOME, *Geophys. Res. Lett.*, *27*, 3461–3464, 2000.

Chandra, S., Changes in stratospheric ozone and temperature due to the eruptions of Mt. Pinatubo, *Geophys. Res. Lett.*, *20*, 33–36, 1993.

Chanin, M. L., The intercomparison ozone campaign held in France in June 1981 - Description of the campaign, *Planetary and Space Science*, *31*, 707–713, 1983.

Chanin, M. L., D. Ehhalt, P. F. ad J. F. Frederick, J. C. Gille, M. P. McCormick, G. Megie, and M. Schoeberl, Global trends, chapter 2 in scientific assessment of stratospheric ozone:1989, World Meteorological Organization, Report No. 20, Gobal Ozone Research and Monitoring Project, Geneva, 1998.

Chipperfield, M. P., Multiannual simulations with a three dimensional chemical transport model, *J. Geophys. Res.*, *104*, 1781–1805, 1999.

Chu, W. P., M. P. McCormick, J. Lenoble, C. Brogniez, and P. Pruvost, SAGE II inversion algorithm, *J. Geophys. Res.*, *94*, 8339–8351, 1989.

Coe, H., B. J. Allan, and J. M. C. Plane, Retrieval of vertical profiles of NO_3 from zenith sky measurements using an optimal estimation method, *J. Geophys. Res.*, *107*, doi: 10.1029/2002JD0002111, 2002.

Coldewey-Egbers, M., M. Weber, M. Buchwitz, and J. P. Burrows, Application of a modified DOAS method for ozone retrieval from GOME data at high polar latitude, *Adv. Space Res.*, in press, 2004.

Coldewey-Egbers, M., M. Weber, L. N. Lamsal, R. de Beek, M. Buchwitz, and J. P. Burrows, Total ozone retrieval from GOME UV spectral data using the weighting function DOAS approach, *Atmos. Chem. Phys.*, *5*, 1015–1025, SRef-ID: 1680-7324/acp/2005-5-1015, 2005.

Crutzen, P. J., and C. Brühl, A model study of atmospheric temperatures and the concentrations of ozone, hydroxyl, and some other photochemically active gases during the glacial, the pre-industrial holocene and the present, *Geophys. Res. Lett.*, *20*, 1047–1050, 1993.

Cunnold, D. M., W. P. Chu, R. A. Barnes, M. P. McCormick, and R. E. Veiga, Validation of SAGE II ozone measurements, *J. Geophys. Res.*, *94*, 8447–8460, 1989.

Danilin, M. Y., et al., Comparison of ER-2 aircraft and POAM III, MLS, and SAGE II satellite measurements during SOLVE using traditional correlative analysis and trajectory hunting technique, *J. Geophys. Res.*, *108*, doi: 10.1029/2001JD000781, 2002.

Darmawan, A., Improved dynamical climatology of ozone for use in optimal estimation retrieval, Master's thesis, University of Bremen, 2002.

De Backer, H., D. De Muer, and G. De Sadelaer, Comparison of ozone profiles obtained with Brewer-Mast and Z-ECC sensors during simultaneous ascents, *J. Geophys. Res.*, *103*, 19,641–19,648, 1989.

De Backer, H., E. Schoubs, and M. Allaart, Comparison of Brewer Mast and ECC ozonesonde profiles at Uccle and De Bilt, in *The third European workshop on polar stratospheric ozone*, edited by J. A. Pyle, N. R. P. Harris, and G. T. Amanatidis, pp. 512–515, 1995.

de Beek, R., and H. Bovensmann, Impact of SCIAMACHY diffuser spectral characteristics on level 1-2 DOAS products, *Tech. rep.*, Tech. rep., IfE, 2000.

de Beek, R., M. Vountas, V. V. Rozanov, A. Richter, and J. P. Burrows, The Ring effect in the cloudy atmosphere, *Geophys. Res. Lett.*, *28*, 721–724, 2001.

de Beek, R., M. Weber, V. V. Rozanov, A. Rozanov, A. Richter, and J. P. Burrows, Trace gas column retrieval - an error study for GOME-2, *Adv. Space Res.*, *34*, 727–733, 2004.

de F. Forster, P. M., and K. P. Shine, Radiative forcing and temperature trends from stratospheric ozone trends, *J. Geophys. Res.*, *102*, 10,841–10,855, 1997.

DeMore, W. B., S. P. Sander, D. M. Golden, R. F. Hampson, M. J. Kurylo, C. J. Howard, A. R. Ravishankara, C. E. Kolb, and M. J. Molina, Chemical kinetics and photochemical data for use in stratospheric modeling: Evaluation number 12, JPL publication 97-4, Jet Propulsion Laboratory, Pasadena, Calif, 1997.

DeMuer, D., and H. DeBacker, Revision of 20 years of Dobson total ozone data at Uccle (Belgium): Fictitious Dobson total ozone trends induced by sulfur dioxide trends, *J. Geophys. Res.*, *97*, 5921–5937, 1992.

Dhomse, S., M. Weber, J. Burrows, I. Wohltmann, and M. Rex, On the possible cause of recent increases in NH total ozone from a statistical analysis of satellite data from 1979 to 2003, *Atmos. Chem. Phys.*, *6*, 1165–1180, sRef-ID: 1680-7324/acp/2006-6-1165, 2006.

Dobber, M. R., Wavelength and slit function calibration of the SCIAMACHY PFM, *Tech. rep.*, TN-SCIA-1000TP/189, Issue 1, 15.02.1999, TPD-TNO, 1999.

Dobson, G. M. B., A photo-electric spectrometer for measuring the amount of atmospheric ozone, in *Proc. Phys. Soc.*, pp. 324–339, 1931.

Dobson, G. M. B., Forty year's research on atmospheric ozone at Oxford: a history, *Appl. Opt.*, *7*, 387–405, 1968.

Eck, T. F., P. K. Bhartia, and J. B. Kerr, Satellite estimation of spectral UVB irradiance using TOMS-derived total ozone and UV reflectivity, *Geophys. Res. Lett.*, *22*, 661–664, 1995.

Eder, B. K., and S. K. LeDuc, A climatology of Total Ozone Mapping Spectrometer data using rotated principal component analysis, *J. Geophys. Res.*, *104*, 3691–3709, 1999.

Eisinger, M., and J. P. Burrows, Tropospheric sulfur dioxide observed by the ESR-2 GOME instrument, *Geophys. Res. Lett.*, *25*, 4177–4180, 1998.

Eskes, H. J., and A. Dethof, SCIAMACHY column ozone validation with models and assimilation, in *Proceeding of the Second Workshop on the Atmospheric Chemistry Validation of ENVISAT (ACVE-2), 3-7 May 2004*, edited by D. Danesy, pp. 51–58, ESA ESRIN, Frascati, Italy, ESA Publications Division, Nordwijk, the Nederlands, 2004.

Eskes, H. J., R. J. van der A, E. J. Brinksma, J. P. Veefkind, J. F. de Haan, and P. J. M. Valks, Retrieval and validation of ozone columns derived from measurements of SCIAMACHY on ENVISAT, *Atmos. Chem. Phys. Discuss.*, *5*, 4429–4475, 2005.

Farman, J. C., B. G. Gardiner, and J. D. Shanklin, Large losses of total ozone in antarctica reveal seasonal ClO_x/NO_x interaction, *Nature*, *315*, 207–210, 1985.

Fels, S. B., A parameterization of scale-dependent radiative damping rates in the middle atmosphere, *J. Atmos. Sci.*, *39*, 1141–1152, 1982.

Fioletov, V. E., J. B. Kerr, E. W. Hare, G. J. Labow, and R. D. McPeters, An assessment of the world ground-based total ozone network performance from the comparison with satellite data, *J. Geophys. Res.*, *104*, 1737–1748, 1999.

Fioletov, V. E., G. E. Bodeker, A. J. Miller, R. D. McPeters, and R. Stolarski, Global and zonal total ozone variations estimated from ground-based and satellite measurements: 1964–2000, *J. Geophys. Res.*, *107*, doi:10.1029/2001JD001350, 2002.

Fish, J. D., and R. L. Jones, Rotational Raman scattering and the Ring effect in zenith-sky spectra, *Geophys. Res. Lett.*, *22*, 811–814, 1995.

Fishman, J., C. E. Watson, J. C. Larsen, and J. A. Logan, Distribution of tropospheric ozone determined from satellite data, *J. Geophys. Res.*, *95*, 3599–3617, 1990.

Fleming, E. L., S. Chandra, M. R. Shoeberl, and J. J. Barnett, Monthly mean global climatology of temperature, wind, geopotential height and pressure for 0-120 km, National Aeronautics and Space Administration, Technical Memorandum 100697, Washington, D.C., see also: http://modelweb.gsfc.nasa.gov/atmos/cospar1.html, 1988.

Fortuin, J. P., and H. Kelder, Possible links between ozone and temperature profiles, *Geophys. Res. Lett.*, *23*, 1517–1520, 1996.

Fortuin, J. P., and H. Kelder, An ozone climatology based on ozonesondes and satellite measurements, *J. Geophys. Res.*, *103*, 709–31, 1998.

Fournier, N., P. Stammes, M. de Graaf, R. van der A, A. Piters, R. Koelemeijer, and A. Kokhanovsky, Improving cloud information over deserts from SCIAMACHY O_2 A-band, *Atmos. Chem. Phys. Discuss.*, *5*, 6013–6039, 2005.

Frerick, J., SCIAMACHY L0/1b verification- data description, *Tech. rep.*, European Space Agency, Technical Report PE-TN-ESASCI- 102, 2005.

Fusco, A. C., and M. L. Salby, Interannual variation of total ozone and their relationship to variations of planetary wave activity, *J. Clim.*, *12*, 1619–1629, 1999.

Garcia, R. R., and B. A. Boville, "downward control" of the mean meridional circulation and temperature distribution of the polar winter stratosphere, *J. Atmos. Sci.*, *51*, 2238–2245, 1994.

Grainger, J. F., and J. Ring, Anomalous Fraunhofer line profiles, *Nature, 193*, 762–762, 1962.

Grzegorski, M., Determination of cloud parameters for GOME with broadband spectrometer and from absorption bands of oxygen dimer, Diplomarbiet, Univ. Heidelberg, 2003.

Gushchin, G. P., S. A. Sokolenko, and V. A. Kovalyov, Total-ozone measuring instruments used at the USSR station network, in *Atmospheric Ozone Proc. Quadr. Ozone Symp. Halkidiki, Greece*, edited by C. Zerefos and A. Ghazi, pp. 543–546, 1985.

Hare, E., and V. Fioletov, An examination of the total ozone data in the World Ozone and Ultraviolet Radiation Data Center, in *Atmospheric Ozone - Proc. 18th Quadrennial Ozone Symposium, L'Aquila, Italy*, edited by R. Bojkov and G. Visconti, pp. 45–48, 1998.

Hasekamp, O. P., and J. Landgraf, Ozone profile retrieval from backscattered ultraviolet radiances: The inverse problem solved by regularization, *J. Geophys. Res.*, *106*, 8077–8088, 2001.

Heath, D. F., and H. Park, The Solar Backscatter Ultraviolet (SBUV) and Total Ozone Mapping Spectrometer (TOMS) experiment, in *The Nimbus-7 Users'Guide*, edited by R. C. Madrid, NASA Goddard Space Flight Center, Greenbelt, Maryland, 1978.

Heath, D. F., A. J. Krueger, H. A. Roeder, and B. D. Henderson, The Solar Backscatter Ultraviolet and Total Ozone Mapping Spectrometer (SBUV/TOMS) for NIMBUS G, *Opt. Eng.*, *14*, 323–331, 1975.

Herman, J. R., and E. A. Celarier, Earth surface reflectivity climatology at 340–380 nm from TOMS data, *J. Geophys. Res.*, *102*, 28 003–28 011, 1997.

Highwood, E. J., and B. J. Hoskins, The tropical tropopause, *Quart. J. Roy. Meteorol. Soc.*, *124*, 1579–1604, 1998.

Hilsenrath, E., et al., Results from the balloon ozone comparison campaign (BOIC), *J. Geophys. Res.*, *91*, 137–13, 1986.

Hilsenrath, E., P. K. Bhartia, R. P. Cebula, V. A. Mohnen, and C. G. Wellemeyer, BUV ozone data: An example of calibration and validation needed for detecting trends from satellite observations, *SPARC Newsletter*, *10*, http://www.aero.jussieu.fr/~sparc/News10/index.html, 1998.

Hilsenrath, E., B. Bojkov, G. Labow, and A. Bracher, SCIAMACHY column ozone validation, in *Proceeding of the Second Workshop on the Atmospheric Chemistry Validation of ENVISAT (ACVE-2), 3-7 May 2004*, edited by D. Danesy, pp. 39–46, ESA ESRIN, Frascati, Italy, ESA Publications Division, Nordwijk, the Nethelands, 2004.

Hoinka, K. P., Statistics of the global tropopause pressure, *Mon. Weather Rev., 126*, 3303–3325, 1998.

Hoinka, K. P., H. Claude, and U. K. ohler, On the correlation between tropospheric pressure and ozone above central Europe, *Geophys. Res. Lett., 23*, 1753–1756, 1996.

Holton, J. R., P. H. Haynes, M. E. McIntyre, A. R. Douglass, R. B. Rood, and L. Pfister, Stratosphere-troposphere exchange, *Rev. Geophys., 33*, 403–439, 1995.

Hoogen, R., V. V. Rozanov, and J. P. Burrows, Ozone profiles from GOME satellite data: Algorithm description and first validation, *J. Geophys. Res., 104*, 8263–8280, 1999a.

Hoogen, R., V. V. Rozanov, and J. P. Burrows, O_3 profiles from GOME satellite data-I: Comparison with ozonesonde measurements, *Phys. Chem. Earth, 24*, 447–452, 1999b.

Hudson, R. D., A. D. Frolov, M. F. Andrade, and M. B. Follette, The total ozone field separated into meteorological regimes. part I: Defining the regimes, *J. Atmos. Sci., 60*, 1669–1677, 2003.

Jackman, C., E. Fleming, and F. Vitt, Influence of extremely large solar proton events in a changing stratosphere, *J. Geophys. Res., 105*, 11,659–11,670, 2000.

Joiner, J., and P. K. Bhartia, Rotational Raman scattering (Ring effect) in satellite backscatter ultraviolet measurements, *Appl. Opt., 34*, 4513–4525, 1995.

Joiner, J., A. P. Vasilkov, D. E. Flittner, J. F. Gleason, and P. K. Bhartia, Retrieval of cloud pressure and oceanic chlorophyll content using Raman scattering in GOME ultraviolet spectra, *J. Geophys. Res., 109*, doi:10.1029/2003JD003698, 2004.

Kamp, A., and M. Dobber, SCIAMACHY, ready for launch, *Acta Astronautica, 47*, 289–296, 2000.

Kattawar, G. W., A. T. Young, and T. J. Humphries, Inelastic scattering in planetary atmospheres, I, the Ring effect without aerosols, *Astrophys. J., 243*, 1049–1057, 1981.

Kerr, J. B., New methodology for deriving total ozone and other atmospheric variables from Brewer spectrometer direct sun spectra, *J. Geophys. Res., 107*, doi:10.1029/2001JD001227, 2002.

Kerr, J. B., and C. T. McElroy, Evidence for large upward trends of ultraviolet-B radiation linked to ozone depletion, *Science, 262*, 1032–1034, 1993.

Kerr, J. B., and C. T. McElroy, Total ozone measurements made with the Brewer ozone spectrometer during STOIC 1989, *J. Geophys. Res., 100*, 9225–9230, 1995.

Kerr, J. B., C. T. McElroy, and R. A. Olafson, Measurements of ozone with the Brewer spectrophotometer, in *Proceedings of the Quadrennial International Ozone Symposium, Natl. Cent. for Atmos. Res., Boulder, Colorado, USA*, edited by J. London, pp. 74–79, 1981.

Kerr, J. B., C. T. McElroy, D. I. Wardle, R. A. Olafson, and W. P. J. Evans, The automated Brewer spectrophotometer, in *Atmospheric Ozone Proc. Quadr. Ozone Symp. Halkidiki, Greece*, edited by C. Zerefos and A. Ghazi, pp. 543–546, 1985.

Kerr, J. B., I. A. Asbridge, and W. F. J. Evans, Intercomparison of total ozone measured by the Brewer and Dobson spectrophotometers at Toronto, *J. Geophys. Res.*, *93*, 11 129–11 140, 1988.

Klenk, K. F., P. K. Bhartia, E. Hilsenrath, and A. J. Fleig, Standard ozone profiles from balloon and satellite data sets, *J. Climate Appl. Meteor.*, *22*, 2012–2022, 1983.

Knudsen, B. M., J. M. Rosen, N. T. Kjome, and A. T. Whitten, Comparison of analyzed stratospheric temperatures and calculated trajectories with long-duration balloon data, *J. Geophys. Res.*, *101*, 19,137–19,146, 1996.

Koelemeijer, R. B. A., and P. Stammes, Validation of Global Ozone Monitoring Experiment cloud fractions relevant for accurate ozone column retrieval, *J. Geophys. Res.*, *104*, 18,801–18,814, 1999.

Koelemeijer, R. B. A., P. Stammes, J. W. Hovenier, and J. F. de Haan, A fast method for retrieval of cloud parameters using oxygen A-band measurements from the Global Ozone Monitoring Experiment, *J. Geophys. Res.*, *106*, 3475–3496, 2001.

Kokhanovsky, A. A., and V. V. Rozanov, The physical parameterization of the top-of-atmosphere reflection function for a cloudy atmosphere-underlying surface system: the oxygen A-band case study, *J. Quant. Spectrosc. Rad. Transfer*, *85*, 35–55, 2004.

Kokhanovsky, A. A., V. V. Rozanov, E. P. Zege, H. Bovensmann, and J. P. Burrows, A semi-analytical cloud retrieval algorithm using backscattered radiation in 0.4-2.4 μm spectral region, *J. Geophys. Res.*, *108*, doi:10.1029/2001JD001543, 2003.

Komhyr, W. D., A carbon-iodide ozone sensor for atmospheric soundings, in *paper presented at the Ozone Symposium World Meteorol. Organ.*, pp. 74–79, Albuquerque, N. Mex., 1964.

Komhyr, W. D., Electrochemical concentration cells for gas analysis, *Ann. Geophys.*, *25*, 203–210, 1969.

Komhyr, W. D., Operation handbook: Ozone observation with a Dobson spectrophotometer, WMO Ozone Rep. 6, World Meteorological Organization, Geneva, 1980.

Komhyr, W. D., C. L. Mateer, and R. D. Hudson, Effective Bass-Paur 1985 ozone absorption coefficients for use with Dobson ozone spectrophotometers, *J. Geophys. Res.*, *98*, 20,451–20,465, 1993.

Krzyścin, J. W., M. Degórska, and B. R. Więch, Seasonal acceleration of the rate of the total ozone decreases over central Europe: impact of tropopause height changes, *J. Atmos. Solar-Terr. Phys.*, *60*, 1755–1762, 1998.

Kurosu, T., V. V. Rozanov, and J. P. Burrows, Parameterization schemes for terrestrial water clouds in the radiative transfer model GOMETRAN, *J. Geophys. Res.*, *102*, 21,809–21,823, 1997.

Kurucz, R. L., I. Furenlid, J. Brault, and L. Testerman, *Solar flux atlas from 296 nm to 1300 nm*, National Solar Observatory, Sunspot, New Mexico, 1984.

Kusmierczyk-Michulec, J., and G. de Leeuw, Aerosol optical thickness retrieval over land and water using Global Ozone Monitoring Experiment (GOME) data, *J. Geophys. Res.*, *110*, doi:10.1029/2004JD004780, 2005.

Kuze, A., and K. V. Chance, Analysis of cloud top height and cloud fraction from satellites using the O_2 A- and B-bands, *J. Geophys. Res.*, *99*, 14,482–14,491, 1994.

Laan, E., J. de Vries, B. Kruizinga, H. Visser, P. Levelt, G. H. J. van den Oord, A. Maelkki, G. Leppelmeier, and E. Hilsenrath, Ozone monitoring with the OMI instrument, in *the SPIE's 45th Annual Meeting – The International Symposium on Optical Science and Technology*, vol. 4132-41, pp. 563–569, 2000.

Lambert, J. C., M. van Roozendael, M. De Maziére, P. C. Simon, J. P. Pommereau, F. Gourtail, A. Sarkissian, and J. F. Gleason, Investigation of pole-to-pole performances of spaceborne atmospheric chemistry sensors with the NDSC, *J. Atmos. Sci.*, *56*, 176–193, 1999.

Lambert, J. C., D. S. Balis, P. Gerard, J. Granville, Y. Livschitz, D. Loyola, R. Spurr, P. Valks, and M. Van Roozendael, Delta validation report for ERS-2 GOME Data Processor upgrade to version 4.0, Technical Note ERSE-CLVL-EOPG-TN-04-0001, Issue 1.0, December 2004, ed. J.–C. Lambert and Dimitris S. Balis, see also: http://wdc.dlr.de:8082/sensors/gome/gdp4.html, 2004.

Lambert, J.-C., et al., GDP V3 VALREPORT, 2002: ERS-2 GOME GDP 3.0 Implementation and Delta Validation Report, http://earth.esrin.esa.it/pub/ESA_DOC/GOME/gdp3/gdp3.htm, Technical Note ERSE-DTEX-EOAD-TN-02-0006, Issue 1.0, 2002a.

Lambert, J. C., et al., ERS-2 GOME GDP 3.0 implementation and delta validation report, Technical Note ERSE-DTEX-EOAD-TN-02-0006, Issue 1.0, November 2002, ed. J.–C. Lambert, see also: http://earth.esrin.esa.it/pub/ESA_DOC/GOME/gdp3/gdp3.htm, 2002b.

Lambert, J. C., et al., First ground-based validation of SCIAMACHY V5.01 ozone column, in *Proceeding of the Second Workshop on the Atmospheric Chemistry Validation of ENVISAT (ACVE-2), 3-7 May 2004*, edited by D. Danesy, pp. 39–46, ESA ESRIN, Frascati, Italy, ESA Publications Division, Nordwijk, the Netherlands, 2004b.

Lamsal, L. N., M. Weber, S. Tellmann, and J. P. Burrows, Ozone column classified climatology of ozone and temperature profiles based on ozonesonde and satellite data, *J. Geophys. Res.*, *109*, doi:10.1029/2004JD004680, 2004.

Lamsal, L. N., M. Weber, G. Labow, and J. P. Burrows, Influence of ozone and temperature climatology on the accuracy of satellite total ozone retrieval, *J. Geophys. Res.*, in press, 2006.

Lang, R., J. E. Williams, W. J. van der Zande, and A. N. Maurellis, Application of the spectral structure parameterization technique: retrieval of total water vapor columns from GOME, *Atmos. Chem. Phys.*, *3*, 145–160, 2003.

Leblanc, T., I. S. McDermid, P. Keckhut, A. Hauchecorne, C. Y. She, and D. A. Krueger, Temperature climatology of the middle atmosphere from longterm lidar measurements at middle and low latitudes, *J. Geophys. Res.*, *103*, 17,191–17,204, 1998.

Liang, X. Z., W. C. Wang, and J. R. Boyle, Atmospheric ozone climatology for use in general circulation models, Program for Climate Model Diagnosis and Intercomparison (PCMDI) , Report No. 43, University of California, 1997.

Lichtenberg, G., et al., SCIAMACHY Level1 data: Calibration concept and in-flight calibration, *Atmos. Chem. Phys. Discuss.*, *5*, 8925–8977, 2005.

Logan, J. A., Tropospheric ozone: Seasonal behaviour, trends, and anthropogenic influence, *J. Geophys. Res.*, *90*, 463–10, 1985.

Logan, J. A., An analysis of ozonesonde data for the troposphere: Recommendations for testing 3-D models and development of a gridded climatology for tropospheric ozone, *J. Geophys. Res.*, *104*, 115–16, 1999a.

Logan, J. A., An analysis of ozonesonde data for the lower stratosphere, *J. Geophys. Res.*, *104*, 151–16, 1999b.

Loyola, D., A new cloud recognition algorithm for optical sensors, in *IEEE International Geoscience and Remote Sensing Symposium*, pp. 572–574, Seattle, volume 2 of IGARSS 1998 Digest, 1999.

Lucke, R. L., et al., The Polar Ozone and Aerosol Measurement (POAM) III instrument and early validation results, *J. Geophys. Res.*, *104*, 18,785–18,799, 1999.

Lumpe, J. D., et al., Comparison of POAM III ozone measurements with correlative aircraft and balloon data during SOLVE, *J. Geophys. Res.*, *108*, 2002.

Martin, R. V., et al., An improved retrieval of tropospheric nitrogen dioxide from GOME, *J. Geophys. Res.*, *107*, 2002.

Mayer, B., I3RC phase 1 results from the MYSTIC Monte Carlo model, in *I3RC Workshop Proc.*, Tucson, Arizona, 1999.

Mayer, B., I3RC phase 2 results from the MYSTIC Monte Carlo model, in *I3RC Workshop Proc.*, Tucson, Arizona, 2000.

McCormick, M. P., SAGE II - An overview, *Adv. Space Res.*, *7*, 219–226, 1987.

McPeters, R., P. K. Bhartia, A. Krueger, and J. Herman, Earth Probe Total Ozone Mapping Spectrometer (TOMS) Data Products User's Guide, NASA Technical Publication 1998-206895, 1998.

McPeters, R. D., and G. J. Labow, An assessment of the accuracy of 14.5 years of Nimbus 7 TOMS Version 7 ozone data by comparison with the Dobson Network, *Geophys. Res. Lett.*, *23*, 3695–3698, 1996.

McPeters, R. D., G. J. Labow, and B. J. Johnson, A satellite-derived ozone climatology for balloonsonde extimation of total column ozone, *J. Geophys. Res.*, *102*, 8875–8885, 1997.

Meijer, Y. J., R. J. van der A, R. F. van Oss, D. P. J. Swart, and H. M. Kelder, Global Ozone Monitoring Experiment ozone profile characterization using interpretation tools and lidar measurements for intercomparison, *J. Geophys. Res.*, *108*, 2003.

Menkhaus, A., M. Weber, C. Haite, and J. P. Burrows, Surface UV modelling using GOME data, in *European symposium on atmospheric measurements from space, proc. ESAMS'99*, pp. 325–332, European Space Agency, ESA-WPP-161, 1999.

Miller, A. J., R. M. Nagatani, G. C. Tiao, X. F. Niu, G. C. Reinsel, D. J. Wuebbles, and K. Grant, Comparison of observed ozone and temperature trends in the lower stratosphere, *Geophys. Res. Lett.*, *19*, 929–932, 1992.

Miller, A. J., et al., A cohesive total data set from the SBUV2) satellite system, *J. Geophys. Res.*, *107*, doi:10.1029/2001JD000853, 2002.

Munro, R., R. Siddans, W. J. Reburn, and B. J. Kerridge, Direct measurement of tropospheric ozone distributions from space, *Nature*, *392*, 168–171, 1998.

Newchurch, M. J., E. S. Yang, D. M. Cunnold, G. C. Reinsel, J. M. Zawodny, and J. M. Russell, Evidence for slowdown in stratospheric ozone loss: First stage of ozone recovery, *J. Geophys. Res.*, *108*, 2003.

Noël, S., M. Buchwitz, H. Bovensmann, R. Hoogen, and J. P. Burrows, Atmospheric water vapor amounts retrieved from GOME satellite data, *Geophys. Res. Lett.*, *26*, 1841–1844, 1999.

Noxon, J. F., Nitrogen dioxide in the stratosphere and troposphere measured by ground-based absorption spectroscopy, *Science*, *187*, 547–549, 1975.

Orphal, J., A critical review of the absorption cross-sections of O_3 and NO_2 in the 240-790 nm region. Part I: Ozone, *Tech. rep.*, Technical Note MO-TN-ESA-GO-0302, 2002.

Orphal, J., A critical review of the absorption cross-sections of O_3 and NO_2 in the 240-790 nm region, *J. Photochem. photobiol., A 157*, 185–209, 2003.

Paur, R. J., and A. M. Bass, The ultraviolet cross-sections of ozone, II, The measurements, in *Atmospheric Ozone Proc. Quadr. Ozone Symp. Halkidiki, Greece*, edited by C. Zerefos and A. Ghazi, pp. 611–616, 1985.

Pérez, A., E. Crino, I. Aguirre de Cárcer, and F. Jaque, Low-ozone events and three-dimensional transport at mid latitudes of South America during springs of 1996 and 1997, *J. Geophys. Res.*, *105*, 4553–4561, 2000.

Petropavlovskikh, I., A. Changwoo, P. K. Bhartia, and L. E. Flynn, Comparison and covalidation of ozone anomalies and variability observed in (SBUV2) and Umkehr northern mid latitude ozone profile estimates, *Geophys. Res. Lett.*, *32*, doi:10.1029/2004GL022002, 2005.

Petzoldt, K., B. Naujokat, and K. Neugebohren, Correlation between stratospheric temperature, total ozone, and tropospheric weather systems, *Geophys. Res. Lett.*, *21*, 1203–1206, 1994.

Piters, A. J. M., K. Bramstedt, J. C. Lambert, and B. Kirchhoff, Overview of SCIAMACHY validation: 2002–2004, *Atmos. Chem. Phys. Discuss.*, *5*, 7769–7828, SRef-ID: 1680-7375/acpd/2005-5-7769, 2005.

Planet, W. G., A. J. Miller, K. Horvath, R. Nagatani, L. E. Flynn, E. Hilsenrath, S. Kondragunta, R. P. Cebula, and M. T. DeLand, Total ozone determinations from National Oceanic and Atmospheric Administration operational Solar Backscatterd Ultraviolet 2 instrument observations: An update, *J. Geophys. Res.*, *106*, 17,471–17,478, 2001.

Platt, U., Differential optical absorption spectroscopy (DOAS), in *Air monitoring by spectroscopic techniques*, edited by M. Sigrist, pp. 27–84, John Wiley & Sons Inc., 1994.

Platt, U., D. Perner, and H. W. Patz, Simultaneous measurements of atmospheric CH_2O, O_3, NO_2 by differential optical absorption, *J. Geophys. Res.*, *84*, 6329–6335, 1979.

Plumb, R. A., A "tropical pipe" model of stratospheric transport, *J. Geophys. Res.*, *101*, 3957–3972, 1996.

Pommereau, J. P., and F. Goutail, O_3 and NO_2 ground-based measurements by visible spectrometry during arctic winter and spring 1988, *Geophys. Res. Lett.*, *15*, 891–894, 1988.

Pullen, S., and R. L. Jones, Accuracy of temperatures from UKMO analysis of 1994/95 in the arctic winter stratosphere, *Geophys. Res. Lett.*, *24*, 845–848, 1997.

Randall, C. E., et al., Validation of POAM III ozone: Comparisons with ozonesonde and satellite data, *J. Geophys. Res.*, *108*, 2003.

Randel, W. J., and F. Wu, TOMS total ozone trends in potential vorticity coordinates, *Geophys. Res. Lett.*, *22*, 683–686, 1995.

Randel, W. J., F. Wu, and R. Stolarsky, Changes in column ozone correlated with EP flux, *J. Meteor. Soc. Jpn.*, *80*, 849–862, 2002.

Randel, W. J., F. Wu, and R. R. Waleska, Thermal variability of tropical tropopause region derived from GPS/MET observations, *J. Geophys. Res.*, *108*, 2003.

Rawcliffe, R. D., and D. D. Elliot, Latitude distributions of ozone at high altitudes deduced from satellite measurements of the earth's radiance at 2840 å, *J. Geophys. Res.*, *71*, 5077–5089, 1966.

Reck, R. A., B. L. Weinberg, R. M. Bornick, G. Wen, and J. E. Frederick, A new approach to the characterization of long-term changes in total atmospheric ozone: determination and application of frequency distributions, *Atmospheric Environment*, *30*, 2627–2636, 1996.

Richter, A., and J. P. Burrows, Tropospheric NO_2 from GOME measurements, *Adv. Space Res.*, *29*, 1673–1683, 2002.

Richter, A., and T. Wagner, Diffuser plate spectral structures and their influence on GOME slant columns, *Tech. rep.*, University of Bremen, www.iup.uni-bremen.de/gome/data/diffuser_gome.pdf, 2001.

Rodgers, C. D., Retrieval of atmospheric temperature and composition from remote measurements of thermal radiation, *Rev. Geophys.*, *14*, 607–624, 1976.

Rodgers, C. D. (Ed.), *Inverse methods for atmospheric sounding: Theory and practice, Ser. Atmos. Ocean. Planet. Phys.*, World Sci., River Edge, N. J., 2000.

Ronnebeck, R., and J. R. Milford, Eine weiterentwicklte electrochemische Ozonradiosonde, *Z. Meteorol*, *26*, 15–19, 1976.

Rood, R. B., and A. R. Douglass, Interpretation of ozone temperature correlations 1. theory, *J. Geophys. Res.*, *90*, 5733–5743, 1985.

Roozendael, M. V., V. Soebijanta, C. Fayt, and J. C. Lambert, Investigation of DOAS issues affecting the accuracy of the GDP version 3.0 total ozone product, unpublished manuscript, see Chapter VI of http://earth.esrin.esa.it/pub/ESA_DOC/GOME/gdp3/gdp3.htm, 2003.

Roozendael, M. V., et al., Reprocessing the 10-year GOME/ERS-2 total ozone record: the new GOME Data Processor Version 4.0, Paper 1: Algorithm Description, *J. Geophys. Res.*, in press, 2006.

Rozanov, A., V. V. Rozanov, and J. P. Burrows, Combined differential-integral approach for the radiation field computation in a spherical shell atmosphere: Non-limb geometry, *J. Geophys. Res.*, *105*, 22,937–22,943, 2000.

Rozanov, A., V. V. Rozanov, and J. P. Burrows, A numerical radiative transfer model for a spherical planetary atmosphere: combined differential-integral approach involving the picard iterative approximation, *J. Quant. Spectrosc. Rad. Transfer*, *69*, 491–512, 2001.

Rozanov, A., V. V. Rozanov, M. Buchwitz, A. Kokhanovsky, and J. P. Burrows, SCIATRAN 2.0: A new radiative transfer model for geophysical application in the 175–2400 nm spectral region, *Adv. Space Res.*, *36*, 1015–1019, 2005a.

Rozanov, V. V., and A. A. Kokhanovsky, Semianalytical cloud retrieval algorithm as applied to the cloud top altitude and the cloud geometrical thickness determination from top-of-atmosphere reflectance measurements in the oxygen A band, *J. Geophys. Res.*, *109*, doi:10.1029/2003JD004104, 2004.

Rozanov, V. V., D. Diebel, R. J. D. Spurr, and J. P. Burrows, GOMETRAN: A radiative transfer model for the satellite project GOME - The plane paralllel version, *J. Geophys. Res.*, *102*, 16,683–16,695, 1997.

Rozanov, V. V., T. Kurosu, and J. P. Burrows, Retrieval of atmospheric constituents in the UV-visible: A new quasi-analytical approach for the calculation of weighting functins, *J. Quant. Spectrosc. Rad. Transfer, 60*, 277–299, 1998.

Rozanov, V. V., M. Buchwitz, K. U. Eichmann, R. de Beek, and J. P. Burrows, SCIATRAN: A new radiative transfer model for geophysical application in the 240–2400 nm spectral region: The pseudo-spherical version, *Adv. Space Res.*, *29*, 1831–1835, 2002.

Rozanov, V. V., A. A. Kokhanovsky, and J. P. Burrows, The determination of cloud altitudes using GOME reflection spectra: Multilayered cloud systems, *IEEE Transactions on Geoscience and Remote Sensing*, *42*, 1009–1017, 2004.

Rozanov, V. V., A. A. Kokhanovsky, D. Loyola, R. Siddans, B. Latter, A. Stevens, and J. P. Burrows, Intercomparison of cloud top altitudes as derived using GOME and ATSR-2 instruments onboard ERS-2, *Rem. Sens. of Env.*, in press, 2005.

Runeckles, V. C., and S. Krupa, The impact of UV-B radiation and ozone on terretrial vegetation, *Environ. Pollut.*, *83*, 191–213, 1994.

Salby, M. L., and P. F. Callaghan, Fluctuations of total ozone and their relationship to stratospheric air motions, *J. Geophys. Res.*, *98*, 2715–2728, 1993.

Salomonson, V., W. L. Barnes, X. Xiong, S. Kempler, and E. Masuoka, An overview of the earth observing system MODIS instrument and associated data systems performance, in *Proceedings of the International Geoscience and Remote Sensing Symposium (IGARSS 02)*, Sydney, Australia, 2002.

Santer, B. D., et al., Behavior of tropopause height and atmospheric temperature in models, reanalyses, and observations, *J. Geophys. Res.*, *108*, 2003.

Shepherd, T. G., K. Semeniuk, and J. N. Koshyk, Sponge-layer feedbacks in middle atmosphere models, *J. Geophys. Res.*, *101*, 23,447–23,464, 1996.

Shiotani, M., Annual Quasi-Biennial, and El Nino-Southern Oscillation (ENSO) time-scale variations in equatorial ozone, *J. Geophys. Res.*, *97*, 7625–7633, 1992.

Sioris, C. E., and W. F. J. Evans, Filling in of Fraunhofer and gas absorption lines in sky spectra as caused by rotational Raman scattering, *Appl. Opt.*, *38*, 2706–2713, 1999.

Skupin, J., An alternative etalon correction for SCIAMACHY, *Tech. rep.*, University of Bremen, IFE-SCIA-JS-20050805_EtalonCorrections, Issue 3, 2005.

Slijkhuis, S., A. von Bargen, W. Thomas, and K. Chance, Calculation of undersampling correction spectra for DOAS spectral fitting, in *ESAM'99 - European Symposium on Atmospheric Measurements from Space*, pp. 563–569, ESA, Noordwijk, the Netherlands, WPP-161, 1999.

Smit, H. G. J., et al., JOSIE: The 1969 WMO international intercomparison of ozonesondes under quasi flight conditions in the environmental simulation chamber, in *Proc. Quadr. Ozone Symp.*, edited by R. D. Bojkov and G. Visconti, Parco Scientifics and Technologies, D'Abruzzo, Italy, 1997.

Smith, A. K., Numerical simulation of global variations of temperature, ozone, and trace species in the stratosphere, *J. Geophys. Res.*, *100*, 1253–1269, 1995.

Smith, W. H. F., and D. T. Sandwell, Global sea floor topography from satellite altimetry and ship depth soundings, *Science*, *277*, 1956–1962, 1997.

Solomon, S., A. L. Schmeltekopf, and R. W. Sanders, On the interpretation of zenith-sky absorption measurements, *J. Geophys. Res.*, *92*, 8311–8319, 1987.

Spurr, R., M. V. Roozendael, and D. Loyola, Algorithm Theoretical Basis Document for GOME total column densities of ozone and nitrogen dioxide, UPAS/GDOAS: GDP 4.0, Doc. No.: ERSE-DTEX-EOPG-TN-04-0007, Issue 1/A, December 2004, see also: http://wdc.dlr.de:8082/sensors/gome/gdp4.html, 2004.

Spurr, R., et al., GOME level 1-to-2 data processor version 3.0: A major upgrade of the GOME/ERS-2 total ozone retrieval algorithm, *Appl. Opt.*, *44*, 7196–7209, 2005.

Staehelin, J., A. Renaud, J. Bader, R. McPeters, P. Viatte, B. Hoegger, V. Bugnion, M. Giroud, and H. Schill, Total ozone series at Arosa (Switzerland): Homogenization and data comparison, *J. Geophys. Res.*, *103*, 5827–5841, 1998.

Staehelin, J., N. R. P. Harris, C. Appenzeller, and J. Eberhard, Ozone trends: A review, *Rev. Geophys.*, *39*, 231–290, 2001.

Staehelin, J., J. Kerr, R. Evans, and K. Vanicek, Comparison of total ozone measurements of Dobson and Brewer spectrophotometers and recommended transfer functions, *Tech. Rep. Report 149*, WMO, World Meteorological Organization Global Atmosphere Watch (WMO-GAW), 2003.

Stammes, P., P. Levelt, J. de Vries, H. Visser, B. Kruizinga, C. Smorenburg, G. Leppelmeier, and E. Hilsenrath, Scientific requirements and optical design of the Ozone Monitoring Instrument on EOS-CHEM, in *Proceedings of SPIE Conference on Earth Observing Systems IV, July 1999, Denver, Colorado, USA*, vol. SPIE 3750, pp. 221–232, 1999.

Stamnes, K., J. Slusser, and M. Bowen, Derivation of total ozone abundance and cloud effects from spectral irradiance measurements, *Appl. Opt., 30*, 4418–4426, 1991.

Stanford, J. L., J. R. Ziemke, R. D. McPeters, A. J. Krueger, and P. K. Bhartia, Spectral analyses, climatology, and interannual variability of Nimbus 7 TOMS version 6 total column ozone, *NASA Ref. Publ., 1360*, 1995.

Steele, H. M., and R. P. Turco, Separation of aerosol and gas components in the Halogen Occultation Experiment and the Stratospheric Aerosol and Gas Experiment (SAGE) II, extinction measurements: Implications for SAGE II ozone concentrations and trends, *J. Geophys. Res., 102*, 19,665–19,682, 1997.

Steinbrecht, W., H. Claude, U. Köhler, and K. P. Hoinka, correlation between tropopause height and total ozone: Implications for long-term changes, *J. Geophys. Res., 103*, 19,183–19,192, 1998.

Steinbrecht, W., B. Hassler, H. C. P. Winkler, and R. Stolarski, Global distribution of total ozone and lower stratospheric temperature variations, *Atmos. Chem. Phys., 3*, 3411–3449, 2003.

Stolarski, R. S., R. D. McPeters, J. R. Herman, and P. Bloomfield, Total ozone trends deduced from Nimbus 7 TOMS data, *Geophys. Res. Lett., 18*, 1015–1018, 1991.

Tanzi, C. P., R. Snel, O. Hasekamp, and I. Aben, Degradation of UV earth albedo observations by GOME, in *ERS-ENVISAT Symposium, Gothenburg, 16–20 October 2000*, pp. 81–84, ESA special publication SP-461 (CD-ROM), 2001.

Thompson, A. M., et al., Southern Hemisphere Additional Ozonesondes (SHADOZ) 1998-2000 tropical ozone climatology, 1, comparison with Total Ozone Mapping Spectrometer (TOMS) and ground-based measurements, *J. Geophys. Res., 108*, 2003a.

Thompson, A. M., et al., Southern Hemisphere Additional Ozonesondes (SHADOZ) 1998-2000 tropical ozone climatology, 2, tropospheric variability and the zonal wave-one, *J. Geophys. Res., 108*, 2003b.

Tiao, G. C., G. C. Reinsel, J. H. Pedrick, G. M. Allenby, C. L. Mateer, A. J. Miller, and J. J. DeLuisi, A statistical trend analysis of ozonesonde data, *J. Geophys. Res., 91*, 13,121–13,136, 1986.

Tuinder, O. N. E., R. de Winter-Sorkina, and P. J. H. Builtjes, Retrieval methods of effective cloud cover from the GOME instruments: an intercomparison, *Atmos. Chem. Phys., 4*, 255–273, 2004.

Valks, P. J. M., A. J. M. Piters, J. C. Lambert, C. Zehner, and H. M. Kelder, A fast delivery system for the retrieval of near-real time ozone columns from GOME data, *Int. J. Remote Sensing*, *24*, 423–436, 2002.

van der A, R. J., R. F. van Oss, A. J. M. Piters, J. P. F. Fortuin, Y. J. Meijer, and H. M. Kelder, Ozone profile retrieval from recalibrated Global Ozone Monitoring Experiment data, *J. Geophys. Res.*, *107*, 2002.

van der Leun, J. C., and F. R. de Gruijl, Influences of ozone depletion on human and animal health, in *UV-B Radiation and Ozone Depletion: Effects on humans, animals, plants, microorganisms, and materials*, edited by M. Tevini, pp. 95–123, Boca Raton, Lewis, 1993.

van Soest, G., L. G. Tilstra, and P. Stammes, Large-scale validation of SCIAMACHY reflectance in the ultraviolet, *Atmos. Chem. Phys.*, *5*, 2171–2180, 2005.

Vanicek, K., Differences between Dobson and Brewer observations of total ozone at Hradec-Kralove, in *Atmospheric Ozone - Proc. 18th Quadrennial Ozone Symposium, L'Aquila, Italy*, edited by R. Bojkov and G. Visconti, pp. 81–84, 1998.

Veefkind, J. P., and J. F. Haan, OMI algorithm Theoretical Basis Document, DOAS total ozone algorithm, ATBD-OMI-02, version 2.0, August 2002, http://www.knmi.nl/omi/documents/data/OMI ATBD volume 2 V2.pdf, 2002.

Voigt, S., J. Orphal, K. Bogumil, and J. P. Burrows, The temperature dependence (203-293 K) of the absorption cross-sections of O_3 in the 230-850 nm region measured by Fourier-transform spectroscopy, *J. Photochem. photobiol., A143*, 1–9, 2001.

Vountas, M., V. V. Rozanov, and J. P. Burrows, Ring effect: Impact of rotational Raman scattering on radiative transfer in earth's atmosphere, *J. Quant. Spectrosc. Rad. Transfer*, *60*, 943–961, 1998.

Wagner, T., and U. Platt, Satellite mapping of enhanced BrO concentrations in the troposphere, *Nature*, *395*, 486–490, 1998.

Wang, H. J., D. M. Cunnold, L. W. Thomason, J. M. Zawodny, and G. E. Bodeker, Assessment of SAGE version 6.1 ozone data quality, *J. Geophys. Res.*, *107*, 2002.

Wang, P. H., M. P. McCormick, W. P. Chu, J. Lenoble, R. M. Nagatani, M. L. Chanin, R. A. Barnes, F. Schmidlin, and M. Rowland, SAGE II stratospheric density and temperature retrieval experiment, *J. Geophys. Res.*, *97*, 843–863, 1992.

Wang, W. C., X. Z. Liang, M. P. Dudek, D. Pollard, and S. L. Thompson, Atmospheric ozone as a climate gas, *Atmospheric Environment*, *37*, 247–256, 1995.

Wayne, R. P. (Ed.), *Chemistry of atmosphere*, Oxford University press, Great Clarendon Street, Oxford, UK, 2000.

Weber, M., K.-U. Eichmann, F. Wittrock, L. Hild, K. Bramstedt, A. Richter, J. P. Burrows, and R. Müller, The cold Arctic winter 1995/96 as observed by the Global Ozone Monitoring Experiment GOME and HALOE: Tropospheric wave activity and chemical ozone loss, *Quart. J. Roy. Meteorol. Soc.*, 2002.

Weber, M., S. Dhomse, F. Wittrock, A. Richter, B. M. Sinnhuber, and J. P. Burrows, Dynamical control of NH and SH winter/spring total ozone from GOME observations in 1995-2002, *Geophys. Res. Lett.*, *31*, 2003.

Weber, M., L. N. Lamsal, M. Coldewey-Egbers, K. Bramstedt, and J. P. Burrows, Pole-to-pole validation of GOME WFDOAS total ozone with groundbased data, *Atmos. Chem. Phys.*, *5*, 1341–1355, SRef-ID: 1680-7324/acp/2005-5-1341, 2005.

Wellemeyer, C. G., S. L. Taylor, C. J. Seftor, R. D. McPeters, and P. K. Bhartia, A correlation for the total ozone mapping spectrometer profile shape errors at high latitude, *J. Geophys. Res.*, *102*, 9029–9038, 1997.

White, E., C. S. Kirkpatrick, and J. A. H. Lee, Case-control study of malignant melanoma in Washington State I: Constitutional factors and sun exposure, *Amer. J. Epidemiol.*, *139*, 857–868, 1994.

Williamson, C. E., P. C. Schulze, B. R. Hargreaves, and J. Seva, The impact of short-term exposure to UV-B radiation on zooplankton communities in northern temperate lakes, *J. Plankton. Res.*, *16*, 205–218, 1994.

Wirth, V., Quasi-stationary planetary waves in total ozone and their correlation with lower stratospheric temperature, *J. Geophys. Res.*, *98*, 8873–8882, 1993.

Wittrock, F., A. Richter, and J. P. Burrows, Validation of GOME BrO and OClO observations in the Northern Hemisphere, in *ESAM'99 - European Symposium on Atmospheric Measurements from Space*, pp. 735–738, ESA, Noordwijk, the Netherlands, WPP-161, 1999.

WMO, Definition of the tropopause, WMO Bulletin, 6, 136, 1957.

WMO, Assessment of trends in the vertical distribution of ozone, World Meteorological Organization, Report No. 43, Gobal Ozone Research and Monitoring Project, Geneva, 1998.

WMO, Scientific Assessment of Ozone Depletion: 1998, World Meteorological Organization, Gobal Ozone Research and Monitoring Project, Report No. 44, 1999.

WMO, Scientific Assessment of Ozone Depletion: 2002, World Meteorological Organization, Gobal Ozone Research and Monitoring Project, Report No. 47, 2003.

Yonemura, S., H. Tsuruta, S. Kawashima, S. Sudo, L. C. Peng, L. S. Fook, Z. Johar, and M. Hayashi, Tropospheric ozone climatology over peninsular Malaysia from 1992 to 1999, *J. Geophys. Res.*, *107*, 2002.

Zängl, G., and V. Wirth, Synoptic-scale variability of the polar and subpolar tropopause: Data analysis and idealized PV inversions, *Quart. J. Roy. Meteorol. Soc.*, *126*, 2000.

Zerefos, C. S., K. Tourpali, R. Bojkov, D. Balis, B. Rognerund, and I. Isaksen, Solar acticity - total ozone relationships: observations and model studies with heterogeneous chemistry, *J. Geophys. Res.*, *102*, 1561–1569, 1997.